12-2014

Reverse Genetics Approach to Examine Myosin XI Functions in Pollen Tube Growth

Stephanie Lin Madison
University of Tennessee - Knoxville, smadiso2@vols.utk.edu

To the Graduate Council:

I am submitting herewith a dissertation written by Stephanie Lin Madison entitled "Reverse Genetics Approach to Examine Myosin XI Functions in Pollen Tube Growth." I have examined the final electronic copy of this dissertation for form and content and recommend that it be accepted in partial fulfillment of the requirements for the degree of Doctor of Philosophy, with a major in Biochemistry and Cellular and Molecular Biology.

Andreas Nebenführ, Major Professor

We have read this dissertation and recommend its acceptance:

Bruce D. McKee, Beth Mullin, Albrecht G. von Arnim, Joseph Williams

Accepted for the Council:

Carolyn R. Hodges

Vice Provost and Dean of the Graduate School

(Original signatures are on file with official student records.)

Reverse Genetics Approach to Examine Myosin XI Functions in Pollen Tube Growth

A Dissertation Presented for the

Doctor of Philosophy

Degree

The University of Tennessee, Knoxville

Stephanie Lin Madison

December 2014

Dedication

This dissertation is dedicated to

my husband

Joseph Ballard

and

my parents

Robin and **Christopher Madison**

for all of the love and support

they have given me along the way.

Acknowledgements

First, I would like to acknowledge the professors in the department of Biology at Lock Haven University of Pennsylvania. Not only did my professors deepen my interest in biology, but they also influenced my career goals. They are the reason I decided to apply to graduate school and pursue a teaching career at a small primarily undergraduate institution.

I am extremely grateful for my advisor, Dr. Andreas Nebenführ, for helping me develop into an independent scientist. I am most thankful for his understanding, support, and advice for my life outside of lab. I would like to express my appreciation to my committee members, Dr. Albrecht von Arnim, Dr. Beth Mullin, Dr. Bruce McKee, and Dr. Joe Williams, for all of their advice over the years. I also would not have been able to complete my dissertation without the help of undergraduate students who assisted with various experiments in this dissertation. I am deeply appreciative of the time and effort Tarah, Whitnee, Jeremiah, Matt, Lauren, Tanner, Kenneth, and Ryan have given.

Finally, I want to thank my family for being so supportive during this long journey. I am deeply grateful to my parents for always encouraging me in everything that I do. I also want to thank my husband, Joseph. Without his support, I would not have been able to finish my dissertation while being the mother that I want to be.

Abstract

Pollen tube growth is an essential aspect of plant reproduction because it is the mechanism through which non-motile sperm cells are delivered to ovules thus allowing fertilization to occur. A pollen tube is a single cell that only grows at the tip, and this tip growth depends on actin filaments. Plants encode class VIII and class XI myosins as actin-based motor proteins, of which class XI myosins are required for cell expansion in vegetative tissues.

In *Arabidopsis thaliana*, 6 of 13 myosin XI genes are expressed in pollen: *XIA*, *XIB*, *XIC*, *XID*, *XIE*, and *XIJ*. Initially, two artificial microRNA constructs were designed to target multiple class XI myosins; however, plants expressing the artificial microRNAs had no reduction in overall fertility and only a slight reduction in root hair elongation. Therefore, to explore the functions of individual pollen myosins, homozygous T-DNA insertion mutants were isolated for all six pollen myosin genes. Single mutants had little or no reduction in overall fertility, whereas double mutants of highly similar pollen myosins had greater defects in pollen tube growth. In particular, *xic xie* pollen tubes grew more slowly than *WT* pollen tubes, which resulted in reduced fitness compared to *WT* and a drastic reduction in seed set. Organelle motility was significantly reduced in *xic xie* pollen tubes; however, vesicle accumulation and actin filament dynamics were not altered in the double mutant. Thus, it remains unclear how reduced organelle motility in *xic xie* pollen tubes leads to a slower growth rate.

A novel role of myosin XI in pollen germination was also revealed in this study. Pollen from mutants of *XIJ*, the only short-tailed myosin XI in *Arabidopsis*, germinated poorly *in vitro*. This *in vitro* pollen germination defect was rescued by the addition of diffusible components from female tissues. Interestingly in pollen grains, YFP-XIJ and YFP-XIA localized to the future site of germination, suggesting a role in pollen germination for multiple myosin XI isoforms. In

summary, this study provided the first direct evidence that class XI myosins are involved in pollen tube growth and pollen germination.

Table of Contents

List of Tables

List of Figures

List of Attachments

Chapter 1: Introduction – Myosins and Pollen Tubes

- *Section 1 of this chapter is revised from a review published by Stephanie L Madison and Andreas Nebenführ.*

  Madison SL, Nebenführ A (2013) Understanding myosin functions in plants: are we there yet? Current Opinion in Plant Biology. 16: 710-717

1.1: Plant myosins

Myosins form a large family of motor proteins that convert the energy released by ATP hydrolysis into mechanical force to move cargo along actin filaments. Myosin genes are found in almost all eukaryotes and can be grouped into 35 different classes, of which class VIII and class XI are found in plants (Odronitz and Kollmar, 2007). A recent comprehensive analysis of all known plant myosins has provided a definitive picture of myosin evolution in plants (Mühlhausen and Kollmar, 2013). On the basis of this analysis a new, unified myosin nomenclature was proposed (Mühlhausen and Kollmar, 2013) which removes previous inconsistencies and makes interspecies comparisons easier by clearly identifying orthologs. Class XI myosins were divided into five subgroups (Myo11A, Myo11C, Myo11E, Myo11G, and Myo11H) with three subgroups being further divided into subtypes (Myo11A/B, Myo11C/D, and Myo11E/F; **Table 1.1**). Subtypes Myo11B, Myo11D, and Myo11F are the result of a relatively recent genome duplication and are only present in eudicots.

Both classes of plant myosins have similar domain architecture (**Figure 1.1**) that is related to class V myosins in animals and fungi (Hammer and Sellers, 2012), with which they share a common ancestry (Odronitz and Kollmar, 2007). The motor domain binds actin and hydrolyzes ATP (Tominaga et al., 2003) and is preceded by an N-terminal SH3-like domain of unknown function. The neck domain, containing IQ motifs, acts as a lever arm and is bound by calmodulin-like proteins (Kinkema and Schiefelbein, 1994; Tominaga et al., 2012). The coiled-coil domain facilitates dimerization (Li and Nebenführ, 2008a), and the globular tail functions as the cargo binding domain (Li and Nebenführ, 2007). Class VIII myosins also contain an N-terminal extension, MyTH8 (Mühlhausen and Kollmar, 2013), and class XI myosins contain a dilute domain in the C-terminal globular tail (Odronitz and Kollmar, 2007). Interestingly, there is a subtype of myosin XI, Myo11D, which is only present in eudicots and is mostly comprised of

Table 1.1: New nomenclature of myosin XI genes based on their phylogenetic relationships

	Arabidopsis thaliana		*Oryza sativa*	
Subgroup/type	**New**	**Old**	**New**	**Old**
Myo11A	*Myo11A1*	*XIA*	*Myo11A1*	*OsMyoXID*
	Myo11A2	*XID*	*Myo11A2*	*OsMyoXIG*
			Myo11A3	*OsMyoXIB*
Myo11B	*Myo11B1*	*XIB*		
	Myo11B2	*MYA2*		
	Myo11B3	*XIH*		
	Myo11B4	*XIG*		
Myo11C	*Myo11C1*	*XIC*	*Myo11C*	*OsMyoXIJ*
	Myo11C2	*XIE*		
Myo11D	*Myo11D*	*XIJ*		
Myo11E	*Myo11E1*	*XIK*	*Myo11E1*	*OsMyoXIH*
	Myo11E2	*HDK**	*Myo11E2*	*OsMyoXIA*
			Myo11E3	*OsMyoXIF*
			Myo11E4	(pseudogene)
Myo11F	*Myo11F*	*MYA1*		
Myo11G	*Myo11G*	*XI-I*	*Myo11G1a*	*OsMyoXIC*
			Myo11G1b	*OsMyoXIK*
			Myo11G2	*OsMyoXIL*
Myo11H	*Myo11H*	*XIF*	*Myo11H*	*OsMyoXIE*

* *HDK* is a headless derivative of *XIK* that lacks the motor and IQ domains.

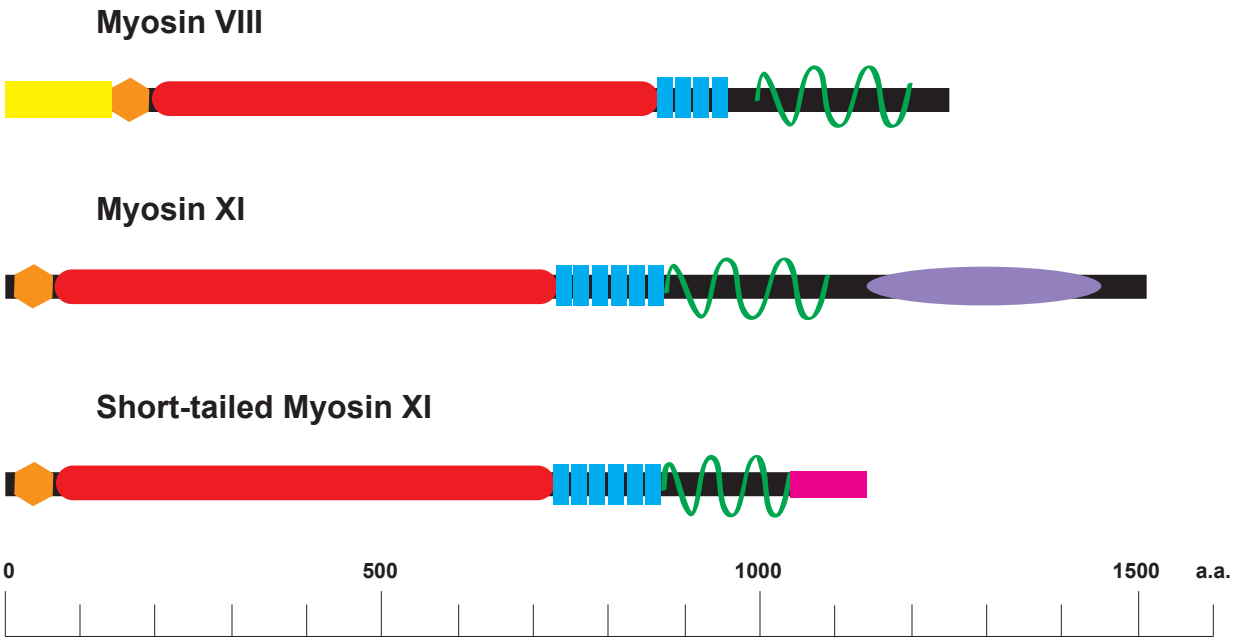

Figure 1.1: Myosin domain structures

Consensus domain structures for myosin VIII, myosin XI, and short-tailed myosin XI as described by Mühlhausen and Kollmar (2013). An SH3-like domain (orange), a motor domain (red), IQ motifs (blue), and a coiled-coil region (green) are found in all three types of myosins. The dilute domain (purple) normally found in myosin XI is lacking in short-tailed myosins, but is replaced by ~100 a.a. conserved sequence (pink) in short-tailed myosins. Myosin VIII also includes an N-terminal MyTH8 domain (yellow).

short-tailed myosins (Mühlhausen and Kollmar, 2013). Short-tailed myosins lack the normal myosin XI C-terminus that follows the coiled-coil domain, but instead contain a conserved C-terminal sequence which encodes ~100 amino acids (Mühlhausen and Kollmar, 2013). The function of this domain is not known.

The cellular function of myosins is generally assumed to be the movement of cellular components along actin filaments, which in the case of flowering plants takes the form of cytoplasmic streaming, that is, the rapid movement of organelles and cytosol throughout the cell (Shimmen, 2007). The biological function of this energetically very expensive process is largely unknown, although it has been proposed that the large size of plant cells necessitates a constant 'mixing' of cytoplasm to ensure rapid distribution of metabolites (Shimmen and Yokota, 1994). Comparisons with the related class V myosins in animals and fungi, which are involved in establishing and maintaining cell polarity (Hammer and Sellers, 2012), suggest that plant myosins may also participate in other cellular processes, but evidence for such activities has been slow to emerge. Recent progress, primarily in the model species *Arabidopsis thaliana* and *Physcomitrella patens*, has shed new light on these questions and allows us to draw preliminary conclusions about myosin functions in plants.

1.1.1: Loss of myosin VIII leads to growth defects in moss

Relatively little is known about class VIII myosins. Myosin VIII localization to the cell surface, endosomes, plasmodesmata, and the forming cell plate, as determined by immunolocalization and expression of fluorescently labeled tail constructs, implicated these motors in endocytosis, cell-cell communication/transport, and cell division (Reichelt et al., 1999; Van Damme et al., 2004; Avisar et al., 2008a; Golomb et al., 2008; Sattarzadeh et al., 2008; Yuan et al., 2011). The myosin VIII gene family in angiosperms is relatively small with typically two to four paralogs (Mühlhausen and Kollmar, 2013), but a genetic analysis has not been

described so far, making it difficult to assess the relevance of myosin VIII activity to any of these processes. By contrast, all five myosin VIII genes in the moss, *Physcomitrella patens*, have recently been disrupted to test the effect of these genes on gametophyte growth (Wu et al., 2011). Interestingly, the resulting quintuple mutant was found to be viable although of smaller size than wild-type. This implies that this class of myosins modulates growth by facilitating a process that is limiting for cell expansion.

Curiously, the smaller size and slower growth of the quintuple mutants was accompanied by developmental defects such as increased branching and earlier gametophore development. Additional experiments also revealed defects in hormone responses and nutrient utilization, suggesting that class VIII myosins can have pleiotropic effects on the physiology of plants (Wu et al., 2011). It remains to be seen whether these development defects are indirect effects of the reduced cell growth in the quintuple mutants, or whether a fundamental problem in hormone homeostasis in the mutants causes all the observed phenotypes. The excellent genetic tools available in *P. patens* (Bezanilla et al., 2005; Vidali et al., 2009a) will be instrumental in resolving this problem.

1.1.2: Myosins are involved in transporting proteins to plasmodesmata

Class VIII and class XI myosins have been implicated in transporting plant and viral proteins to plasmodesmata (PD) in *Nicotiana benthamiana*. Overexpression of dominant-negative myosin tail fragments reduced the PD dependent spread of several viruses. Myosin VIII tails blocked transport of *Beet yellows virus* Hsp70h and *Rice stripe virus* NSvc4 to the PD whereas myosin XI tails blocked the PD dependent spread of *Grapevine fanleaf virus* and *Tobacco mosaic virus* (Avisar et al., 2008a; Harries et al., 2009; Amari et al., 2011; Yuan et al., 2011). Interestingly, both class VIII and XI tail fragments inhibited the transport of endogenous Plasmodesmata Located Protein 1 (PDLP1) through the secretory pathway to PD (Yuan et al.,

2011). Another recent study contradicted this result showing PDLP1 transport to PD was only class XI myosin-dependent (Amari et al., 2011). Perhaps differences between the two studies were a result of different growth conditions. Overall, viruses have evolved various mechanisms for spreading through PD with each relying on specific myosins from either class of plant myosins.

1.1.3: Myosin XI activity is required for expansion of many different cell types

Most of the effort towards understanding myosin function in plants has been directed at class XI myosins since it is generally assumed that these motors are responsible for cytoplasmic streaming (Shimmen, 2007). Even though cytoplasmic streaming is absent from moss gametophytes, *P. patens* again demonstrated its usefulness as a model organism since the myosin XI gene family is very small in this species with only two expressed paralogs, compared to around 10 genes in angiosperms (Reddy and Day, 2001; Vidali et al., 2010; Mühlhausen and Kollmar, 2013). Targeted silencing of both myosin XI transcripts in *P. patens* resulted in small round cells that failed to undergo polarization or initiate tip growth. The resulting plants were severely stunted, emphasizing that myosin XI is required for setting up or maintaining proper cell polarity and growth (Vidali et al., 2010).

It is not known whether a similar situation exists for class XI myosins in angiosperms since the large size of the gene family, typically 7 to 13 (Mühlhausen and Kollmar, 2013), has so far prevented elimination of all myosin XI function from these plants. However, several publications have examined the effects of T-DNA insertions in highly expressed genes of *Arabidopsis thaliana*, primarily *XIK* and *MYA2* (Ojangu et al., 2007; Peremyslov et al., 2008; Prokhnevsky et al., 2008; Peremyslov et al., 2010; Ueda et al., 2010; Ojangu et al., 2012). A common theme that emerged from these studies is that myosin XI genes seem to act redundantly to enhance cell expansion in many different tissues. This is most readily visible in root hairs,

where single mutants of *XIK* and *MYA2* genes already show an effect (Ojangu et al., 2007; Peremyslov et al., 2008). Higher order mutants involving these and other genes show progressively more stunting that coincides with reduced cell expansion in leaves (Prokhnevsky et al., 2008; Peremyslov et al., 2010; Ojangu et al., 2012) and trichomes (Ojangu et al., 2012). A recently published detailed study on the *mya1 mya2 xik* triple mutant revealed that pavement cells in the epidermis of leaves are not only smaller than in wild-type but also showed reduced lobing (Ojangu et al., 2012), again emphasizing the function of myosin XI in normal cell growth. Interestingly, this study also demonstrated that the placement of trichome branches is altered in the *mya1 mya2 xik* triple mutant, suggesting that myosin function is also required for normal branch point selection.

In addition to these cell expansion defects, it was also found that fertility was reduced in the *mya1 mya2 xik* triple mutant (Peremyslov et al., 2010; Ojangu et al., 2012). Reciprocal crosses revealed that the reduced number of seeds per silique resulted from a female defect (Ojangu et al., 2012) which was consistent with the mutated genes showing very low expression levels in pollen but high levels in the stigma (Hruz et al., 2008). Scanning electron microscopy demonstrated that the low fertility rate of the triple mutant correlated with delayed elongation of stigmatic papillae, which in turn resulted in poor pollination (Ojangu et al., 2012). Thus, the reduced fertility of higher order mutants could also be traced back to a cell expansion defect. The mechanism(s) by which class XI myosins mediate their effects on cell growth are still largely unknown, although recent research has identified several aspects of cell physiology that are affected in myosin XI mutants.

1.1.4: Subcellular defects linked to myosin XI function

Myosin XI motors have been thoroughly examined for their effect on organelle motility and cytoskeletal elements by employing two different approaches. In the first approach, various

fluorescent markers were expressed in myosin knockout mutants. This demonstrated that Golgi stacks (Peremyslov et al., 2008; Prokhnevsky et al., 2008; Peremyslov et al., 2010; Avisar et al., 2012), peroxisomes (Peremyslov et al., 2008; Prokhnevsky et al., 2008; Peremyslov et al., 2010), mitochondria (Peremyslov et al., 2008; Prokhnevsky et al., 2008), and the endoplasmic reticulum (Ueda et al., 2010) move at reduced speeds in *Arabidopsis* mutants of class XI myosins. The second approach employed by several groups was to overexpress the tail portion of myosins in cells expressing various organelle markers. These dominant-negative tail fragments resulted in reduced motility of Golgi stacks (Avisar et al., 2008b; Sparkes et al., 2008; Avisar et al., 2009; Avisar et al., 2012), peroxisomes (Avisar et al., 2008b; Sparkes et al., 2008), mitochondria (Avisar et al., 2008b; Sparkes et al., 2008; Avisar et al., 2009), endoplasmic reticulum (Sparkes et al., 2009; Yokota et al., 2011; Wang et al., 2012; Griffing et al., 2014), *trans*-Golgi network (Avisar et al., 2012), pre-vacuolar compartment (Avisar et al., 2012), endosomes (Avisar et al., 2012), and exocytic vesicles (Avisar et al., 2012).

Interestingly, these results did not reveal a simple one-to-one relationship between myosin isoforms and specific organelles. While assigning unique functions to individual myosin XI genes is inherently difficult with the dominant-negative approach due to potential off-target effects (Vick and Nebenfuhr, 2012), this also proved to be difficult for knockout mutants. Single class XI myosin mutants have been shown to influence the motility of multiple organelles, and the motility of a particular organelle was affected by more than one myosin mutant, for example *mya2* and *xik* (Peremyslov et al., 2008). It is not clear how this apparent promiscuity arises since various tail constructs of the different myosin XI isoforms were shown to localize to different organelles (Li and Nebenführ, 2007; Reisen and Hanson, 2007; Sparkes et al., 2008; Avisar et al., 2009; Sattarzadeh et al., 2011) and hence are expected to move only those subcellular compartments. It is possible that at least some organelle movements observed in wild-type occur

passively, that is, as a result of the general hydrodynamic flow caused by movement of other organelles (Esseling-Ozdoba et al., 2008). A reduction of this hydrodynamic flow in a given myosin mutant would then cause all organelles to display reduced movements even though they are not directly moved by this myosin. Alternatively, myosin XI mutations may affect other, more general aspects of intracellular dynamics that then lead to an overall reduction in organelle movement. A candidate for such a 'common factor' has emerged recently in the form of the actin cytoskeleton.

Actin filaments are well established as the tracks along which myosin motors move (Tominaga et al., 2003; Shimmen, 2007), but interestingly, these filaments can also be moved by myosins. This feedback effect became evident from work in *P. patens* where loss of all myosin XI activity resulted in a complete disorganization of the normally highly polarized actin array (Vidali et al., 2010). Similarly in *A. thaliana*, triple *mya1 mya2 xik* and quadruple *mya1 mya2 xik xi-i* myosin XI mutants displayed actin cables that were oriented more transversely while cables in equivalent wild-type cells were primarily longitudinal (Peremyslov et al., 2010). This latter result was later expanded to the *mya2 xik* double mutant that showed a subtle phenotype of more skewed actin filaments that did not align as well with the long axis of the cell (Ueda et al., 2010). Recently, a reduction in actin filament dynamics was described in the *xik* single mutant that did not show a difference in actin organization (Park and Nebenführ, 2013), thus confirming a direct effect of myosin motors on actin filaments that had previously been inferred from inhibitor treatments (Staiger et al., 2009). Presumably, the movement of myosin motors along actin filaments introduces tension in the filament network, which ultimately leads to alignment of the filaments with the long axis of the cell. It should be noted that actin dynamics do not appear to be affected by the near total loss of myosin XI activity in *P. patens* (Vidali et al., 2010). In this case, an interdependence of myosin and actin localization at the tip was found that again highlights the

mutual regulation of tracks and motors (Furt et al., 2013). Thus, the situation in plants is similar to yeast and mammalian cells where myosin V has been found to influence actin organization and thereby influence cell polarity (Lo Presti et al., 2012).

An exciting addition to the repertoire of myosin functions was described in *Zea mays*. Cloning of the *Opaque1* gene revealed it to be one of two close homologs of *XI-I* in *A. thaliana* (Wang et al., 2012). The *opaque1* phenotype of non-translucent seed kernels was caused by accumulation of abnormally small, non-spherical protein bodies in the endosperm. These protein bodies are subdomains of the endoplasmic reticulum. Interestingly, Opaque1 myosin appears to be associated with ER membranes based on cell fractionation studies, and ER dynamics are reduced in *opaque1* mutants (Wang et al., 2012). Similar effects on ER dynamics and organization have also been described for myosin mutants in *A. thaliana* (Peremyslov et al., 2010; Ueda et al., 2010). How these myosin driven movements of the ER lead to the formation of appropriately sized zein protein bodies in the lumen of the ER is still not clear, but this discovery highlights the variety of myosin functions that go beyond classical cytoplasmic streaming.

Another example of 'alternative' myosin functions was revealed when a mutant screen for abnormal nuclear shape in *A. thaliana* identified a defect in *XI-I* (Tamura et al., 2013). Loss of this myosin also resulted in greatly reduced nuclear motility, which is consistent with the subcellular localization of this motor to the nuclear envelope (Avisar et al., 2009; Tamura et al., 2013). Other myosin single mutants did not affect nuclear shape, thus demonstrating a unique functional specialization of this myosin in *A. thaliana*. At the same time, *XI-I* appears to contribute to overall growth since loss of this gene in the *mya1 mya2 xik* triple mutant background exacerbates the phenotype (Peremyslov et al., 2010). Whether this effect depends on redundant functions of the involved myosins or on separate contributions of the myosins to

different growth-limiting processes is currently not known. It is also noteworthy that two closely related myosins appear to perform vastly different functions in *Z. mays* and *A. thaliana* (Wang et al., 2012; Tamura et al., 2013). Apparently, the simple assumption that orthologous genes perform the same or similar functions is not always correct.

1.1.5: Myosin localization and interacting partners provide further insight

A crucial aspect to understanding how myosins exert their function is to identify their molecular interactions inside cells. While binding of the myosin motor domain to actin filaments is often considered a given and hence rarely investigated (Walter and Holweg, 2008), it is the interaction of the tail domain with myosin cargo that is of central importance in this respect (Li and Nebenführ, 2008b). Considerable effort has been extended towards identification of the subcellular localization of various tail constructs tagged with fluorescent proteins (Li and Nebenführ, 2007; Reisen and Hanson, 2007; Sparkes et al., 2008; Avisar et al., 2009; Sattarzadeh et al., 2011). Unfortunately, the functional relevance of these localizations cannot be assessed since the tail constructs appear to exert their dominant-negative effect on organelle movements non-selectively. In other words, a given tail construct either inhibits movement of all tested organelles, as is the case for XIK (Avisar et al., 2009; Avisar et al., 2012), or of none, as is the case for XIA (Avisar et al., 2009). It is therefore necessary to create full-length fusion constructs that can functionally complement well-documented mutant phenotypes.

This was first accomplished in *P. patens* (Vidali et al., 2010), but recently two groups succeeded in this endeavor in *A. thaliana* and rescued the mutant phenotypes with YFP-tagged transgenes. In the first case, a XIK-YFP construct driven by the native *XIK* promoter was transformed into the *mya1 mya2 xik* triple mutant (Peremyslov et al., 2012), while in the second case, the YFP tag was fused to the N-terminus of XIK and introduced into the *xik* single mutant, again under control of the native promoter (Park and Nebenführ, 2013). Interestingly, both *A.*

thaliana constructs localized to the tip of growing root hairs as well as to motile vesicles in the shank of root hairs and leaf midrib epidermal cells (Peremyslov et al., 2012; Park and Nebenführ, 2013). The identity of the small vesicles or the nature of the accumulation at the root hair tip could not be identified, but it is tempting to speculate that they correspond to secretory vesicles as suggested by cell fractionation studies (Peremyslov et al., 2012), even though their distribution at the tip does not overlap completely with that of XIK (Park and Nebenführ, 2013).

The pool of XIK at the root hair tip depends on actin filaments (Park and Nebenführ, 2013) and is constantly replenished from other sources in the cell (Peremyslov et al., 2012). This situation is similar to that described for myoXIa in *P. patens* which also accumulated at the tip of caulonemal cells during growth (Vidali et al., 2010; Furt et al., 2013). It remains to be seen whether this pattern is found for all myosin XI motors or whether some of the isoforms function far away from the growing tip. Importantly, the ability to complement mutant phenotypes will also allow new experimental manipulations that take advantage of targeted alterations of myosin sequences.

Another approach to determine the functions of individual myosins is to identify interacting partners for each myosin. An earlier study using a yeast two-hybrid screen identified RabC2a and RabD1 as interacting partners for *Arabidopsis* MYA2 (Hashimoto et al., 2008). RabC2a was shown to localize to peroxisomes suggesting it may recruit MYA2 to peroxisomes (Hashimoto et al., 2008). A second yeast two-hybrid screen identified HSP70-interacting protein (HIP) as an interacting partner for *Z. mays* Opaque1 (Wang et al., 2012). The C-terminus of HIP bound Opaque1 while the N-terminus of HIP contains a tetratricopeptide repeat domain that could be involved in other protein-protein interactions (Wang et al., 2012), raising the possibility that HIP could act as an adaptor between Opaque1 and the ER. Further studies are necessary to confirm the biological relevance of these interactions and their regulation.

A recent study identified, also by a yeast two-hybrid screen, a family of plant-specific proteins containing the DUF593, domain of unknown function, as interacting partners of several myosin XI isoforms in *A. thaliana* (Peremyslov et al., 2013). These proteins appear to localize to a previously unidentified class of small vesicles that cannot be distinguished from the ER in density gradients, some of which co-localized with XIK-YFP (Peremyslov et al., 2013). In addition, different myosin XI isoforms showed various levels of selectivity for different members of the DUF593 family (Peremyslov et al., 2013), thus possibly explaining the observed mixture of genetic redundancy and specificity among myosin mutants. The detected genetic interaction with *xik* (Peremyslov et al., 2013) furthermore is compatible with the concept that DUF593 proteins act in the same pathway as myosins. Curiously, the DUF593 domain was previously identified as responsible for zein binding in the maize protein Floury1 (Holding et al., 2007). While these two findings are clearly incompatible with each other, it is tempting to speculate that the similarity of the *opaque1* and *floury1* phenotypes actually results from the direct interaction of the Opaque1 motor with its cognate DUF593 receptor on the ER membrane.

Another type of myosin interactor was discovered in *Arabidopsis* using a biochemical approach of immunoprecipitating plant expressed XI-I tails and identifying co-precipitated proteins by mass spectrometry (Tamura et al., 2013). In this case, a WPP domain-interacting tail-anchored protein (WIT2) was identified that localizes to the nuclear envelope. Importantly, loss of WIT2 and the related WIT1 in the *wit1 wit2* double mutant resulted in mislocalization of YFP-XI-I tails, thus demonstrating that WIT1 and WIT2 are required for attachment of this myosin motor to the nuclear envelope (Tamura et al., 2013). Furthermore, the *wit1 wit2* double mutant resulted in the same phenotype of immobile round nuclei as the *xi-i* mutant, again confirming the close functional interaction of the two proteins. Finally, it could be shown by pull-down from plant extracts that WIT1/2 interacts with WIP, which in turn links to SUN proteins that anchor

the inner nuclear membrane to the nuclear lamina (Tamura et al., 2013), thus beautifully explaining how the forces exerted by XI-I on the nuclear surface lead to a different shape of the nucleus.

1.1.6: Conclusions

Recent years have seen major progress in our understanding of myosin function in plant cells. It is now firmly established that myosin motors are responsible for the rapid organelle movements that lead to cytoplasmic streaming. It is also clear that these movements are required for normal rapid expansion of cells. In addition, other effects of myosins on cell polarity as well as actin/ER organization and nuclear shape have been described, raising the possibility that the biological functions of these important motors are broader than the previously envisioned 'mixing' role. The distribution of these functions between myosin VIII and myosin XI is beginning to come into focus with recent progress in *P. patens*.

Deeper understanding of the mechanisms by which myosins exert these functions will require identification of the cargo molecules that are being moved by these motors. Knowledge of these interacting partners combined with the availability of functional full-length constructs will enable us to perform more specific experiments as nicely illustrated in the identification of myosin receptors on the nuclear surface (Tamura et al., 2013). Additional progress along these lines should help us to overcome the apparent redundancy of myosin genes and establish the biological functions of all myosins in plants.

1.2: Pollen germination

Pollination is the first step in flowering plant reproduction when pollen is transferred from the anther to the stigma. Unlike a majority of angiosperm species that require cross-pollination to occur with the aid of various animal species or the wind (Glover, 2014),

Arabidopsis thaliana self-fertilizes 97% of the time (Platt et al., 2010). Pollen is directly transferred to the stigma due to the close proximity of the anthers to the stigma (Glover, 2014). Once on the stigma, pollen grains adhere to the stigmatic papillae, hydrate, and germinate (**Figure 1.2**).

1.2.1: A dry stigma allows selective adhesion and hydration of *Arabidopsis* pollen

Arabidopsis thaliana has a dry stigma, which allows for selective adhesion to pollen grains, a selection process that occurs within 30 seconds following pollination (Zinkl et al., 1999). Foreign pollen can adhere to *Arabidopsis* stigmas, albeit to a much lower extent than *Arabidopsis* pollen (Zinkl et al., 1999). The pollen surface is comprised of three layers: an inner intine composed of cellulose, an outer exine made of sporopollenin, and a pollen coat consisting of lipids and proteins that fills the cavities in the exine (Edlund et al., 2004). The pollen coat is not required for the initial adhesion to stigmatic papillae because *cer6* pollen lacking the coat and pollen with the coat removed with cyclohexane were able to adhere to the stigma with a similar affinity as wild-type pollen within the first few minutes following pollination (Zinkl et al., 1999). In contrast, the exine is required for normal pollen adhesion, as mutants with abnormal exine patterning have reduced adhesion to stigmatic papillae (Zinkl and Preuss, 2000; Dobritsa et al., 2009; Dobritsa et al., 2010). The exine is composed of sporopollenin, which is extremely resistant to degradation thus making it impossible to fully characterize its chemical composition (Ariizumi and Toriyama, 2011). Even though the exact chemical composition of sporopollenin remains unknown, detailed chemical analyses suggested that it is a polymer comprised of both aliphatic and aromatic components (de Leeuw et al., 2006; Fraser et al., 2012). A recent study was able to show that the general composition of sporopollenin has remained largely unchanged for over 300 million years and only varies slightly between extant species (Fraser et al., 2012). Thus, it is possibly the exine patterning, which varies widely between species (Edlund et al.,

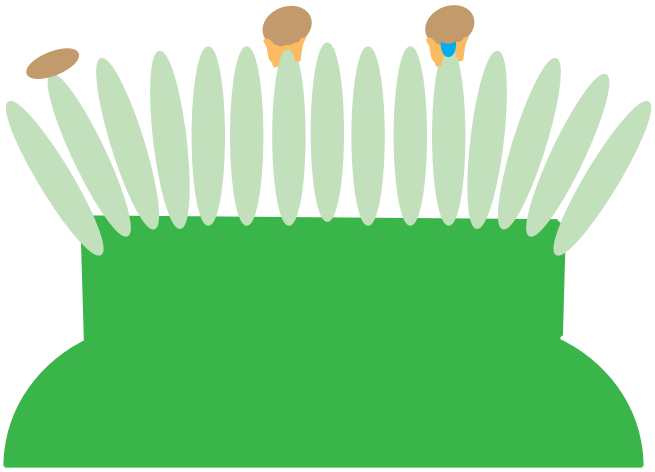

Figure 1.2: Pollen adhesion, hydration, and germination on a dry stigma

On the left, a desiccated pollen grain (brown) adheres to a stigmatic papilla (light green). In the center, an adhered pollen grain hydrates and the 'foot' (orange) forms. On the right, a hydrated pollen grain germinates, and the pollen tube (blue) passes through the 'foot' before penetrating the cell wall of the stigmatic papilla.

2004), that is important for the observed species-specific selection during initial pollen adhesion on *Arabidopsis* stigmas (Zinkl et al., 1999). It remains unclear how exine patterning could confer species-specific adhesion. Further chemical studies on the nature of sporopollenin and detailed genetic and microscopy analyses of exine patterning should shed light on the adhesion specificity observed in *Arabidopsis*.

Once adhered to the stigmatic papillae, *Arabidopsis* pollen grains begin to hydrate within a few minutes (Preuss et al., 1993). Depending on the species, some foreign pollen has been shown to be able to hydrate and germinate on *Arabidopsis* stigmas (Hiscock and Dickinson, 1993; Hülskamp et al., 1995), while pollen from certain species failed to hydrate and germinate despite adhesion (Hiscock and Dickinson, 1993; Hülskamp et al., 1995; Zinkl et al., 1999). This indicates that a regulatory step exists between pollen-stigma adhesion and the start of pollen hydration, which helps confer mating specificity. Interestingly, the failure of *Petunia* pollen to hydrate and germinate on *Arabidopsis* stigmas could be rescued by the addition of exogenous lipids (Zinkl and Preuss, 2000) suggesting that the mechanism regulating species-specific hydration can be bypassed by providing a lipid-rich environment.

Hydration is preceded by "foot" formation, an interface of the pollen coat and stigma surface (Elleman et al., 1992). Interestingly, the adhesion between pollen grains and the stigma has been shown to increase during pollen hydration (Zinkl et al., 1999). This suggests that either "foot" formation or something released from hydrated pollen grains might provide additional adhesives. Since the "foot" is partially composed of the pollen coat, it will be necessary to closely examine the lipid and protein components of the pollen coat.

Hydration experiments with the *eceriferum* (*cer*) mutants provided strong evidence for the requirement of pollen coat lipids during hydration on dry stigmas. The absence of long-chain lipids in a strong allele of *cer6* resulted in the lack of a pollen coat and prevented *cer6* pollen

from hydrating on *Arabidopsis* stigmas (Preuss et al., 1993). Additionally, pollen from *cer1* and a weaker allele of *cer6* had fewer or smaller, respectively, lipid droplets on the pollen coat, and both failed to hydrate on stigmas (Hülskamp et al., 1995). Interestingly, the failure of pollen to hydrate from the stronger *cer6* mutant could be rescued by the addition of exogenous lipids to the stigma or by growing the plants in a more humid environment (Preuss et al., 1993; Zinkl and Preuss, 2000). Pollen from *cer1* and the weaker *cer6* mutant were able to hydrate on *Arabidopsis* stigmas when mixed with wild-type pollen (Hülskamp et al., 1995).

Ten proteins have been isolated from *Arabidopsis* pollen coats: a potential calcium binding protein, 2 putative receptor kinases with extracellular domains, 2 extracellular lipases (EXLs), and 5 glycine-rich proteins (GRPs) each containing an oleosin domain (Mayfield et al., 2001). The EXLs and GRPs made up more than 90% of the detectable pollen coat proteins (Mayfield et al., 2001). The genes encoding the five detected GRPs along with three other *GRP* genes are clustered in a 30 kb section of chromosome 5 (Fiebig et al., 2004). Even between closely related species, the *GRP* genes have diverged greatly compared to neighboring genes (Fiebig et al., 2004; Schein et al., 2004). Therefore, GRPs could be the key to species-selective pollen hydration on dry stigmas. GRP17 is the most abundant pollen coat protein comprising 21% of the total isolated proteins (Mayfield and Preuss, 2000). Importantly, *grp17* pollen had the appearance of a normal pollen coat; however, it took more than twice as long to initiate hydration on a stigma compared to wild-type pollen (Mayfield and Preuss, 2000). Interestingly, *grp17 exl4* double mutant pollen showed an even longer delay in pollen hydration (Updegraff et al., 2009). The *exl4* single mutant did not show a delay in pollen hydration initiation; however, *exl4* pollen took three times as long to complete hydration than wild-type pollen (Updegraff et al., 2009). The duration of pollen hydration for the double mutant was the same as *exl4* (Updegraff et al., 2009). Thus, lack or reduction of lipids in the pollen coat resulted in pollen

unable to hydrate on dry stigmas, whereas, pollen lacking abundant pollen coat proteins resulted in either a delay or lengthening of the hydration process. This suggests that pollen coat lipids are required for pollen hydration while pollen coat proteins might be more involved in the timing of hydration. It is important to note that stigma lipids and proteins are also required for pollen hydration to occur on dry stigmas (Samuel et al., 2009; Chapman and Goring, 2011).

1.2.2: Pollen germination requires a complete intracellular reorganization

In *Arabidopsis*, a pollen tube usually grows through the foot and penetrates a stigmatic papilla within 20 minutes following pollination (Elleman et al., 1992; Kandasamy et al., 1994). *Arabidopsis* pollen tubes can even emerge through the exine wall in between apertures if that is where the pollen-stigma interface is located (Edlund et al., 2004). Studies have suggested that localized lipid-mediated uptake of water during pollen hydration determines the site of germination (Lush et al., 1998; Wolters-Arts et al., 1998). Even though signal origin and perception is unknown, many studies have examined the distribution of cytoskeletal elements, vesicles/organelles, and ions preceding pollen germination. Pollen hydration changes the uniform pollen grain into a highly polarized cell (Kandasamy et al., 1994). Vesicles accumulate at the future germination site (Kandasamy et al., 1994) while the vegetative nucleus and the two sperm cells move from the center of the pollen grain to the wall opposite of the site of germination (Lalanne and Twell, 2002). Actin filaments also orient towards the potential germination site (Heslop-Harrison and Heslop-Harrison, 1992b).

The role of specific cytoskeletal elements in pollen germination has been examined using various drug treatments that affect either actin filaments or microtubules. Colchicine or oryzalin treatment of pollen grains resulted in the complete disappearance of microtubules, yet pollen germination was unaffected (Franke et al., 1972; Heslop-Harrison et al., 1988; Gossot and Geitmann, 2007). Treatments of cytochalasin B, cytochalasin D, and latrunculin B each resulted

in pollen germination inhibition indicating that actin filaments are required for pollen germination (Franke et al., 1972; Tiwari and Polito, 1990; Gibbon et al., 1999). FIMBRIN5 (FIM5) is an actin bundling protein, and *fim5* mutants were shown to have reduced pollen germination compared to wild-type (Wu et al., 2010). Actin filaments in germinating *fim5* pollen formed thicker bundles and lacked the typically orientation of actin filaments converging on the germination site (Wu et al., 2010). This suggests that altering the germination site focused actin arrangement will prevent or delay pollen germination.

Rho GTPases and their interacting proteins have also been implicated in pollen germination. Expression of a constitutively active ROP1, a pollen-specific Rho GTPase, resulted in the formation of bulbous cells instead of normal polarized pollen tubes (Li et al., 1999). This study indicated that the local activation of ROP1 at the site of germination might be required for the initiation of tip-focused growth. Activated ROP6 was shown to be S-acylated, which possibly means other active ROPs are also S-acylated (Sorek et al., 2007). S-acylation of active ROPs has been proposed to increase the binding of active ROPs to the plasma membrane (Payne and Grierson, 2009; Sorek et al., 2010). TIP GROWTH DEFECTIVE1 (TIP1) is an S-acyl transferase (Hemsley et al., 2005), and *tip1* pollen was shown to germinate poorly both *in vivo* and *in vitro* (Ryan et al., 1998). It is possible that TIP1 S-acylates active ROP1 in hydrated pollen grains, stabilizing active ROP1 at the future germination site. Confirmation of S-acylation of active ROP1 in pollen will be crucial before future experiments utilizing ROP1 lacking S-acylation sites can be used to determine the importance of ROP1 S-acylation in pollen germination.

Interestingly, a GFP-labeled ROP interactive partner, GFP-RIP1, was shown to initially label the three nuclei in pollen grains; however, after incubation on pollen germination medium, GFP-RIP localized to the future site of germination (Li et al., 2008). RIP1 was shown to interact

with inactive and active ROP1making it difficult to predict the functional importance of this interaction (Lavy et al., 2007; Li et al., 2008). The localization of RIP1 to the future germination site could imply that RIP1 has a role in establishing polarized growth; however, future studies focusing on *rip1* mutants will be needed to elucidate the role of RIP1 in pollen germination and the significance of its interaction with ROP1.

Influx of calcium has been shown to be crucial for pollen germination. The addition of calcium improved *in vitro* pollen germination (Brewbaker and Kwack, 1963), and the addition of calcium channel blockers inhibited pollen germination (Heslop-Harrison and Heslop-Harrison, 1992a; Iwano et al., 2004; Wang et al., 2004). Furthermore, the cytoplasmic concentration of calcium was shown to increase at the future germination site *in vivo* (Iwano et al., 2004). Interestingly, calcium concentrations sometimes increased at another site, in addition to the future germination site, for pollen grains placed on pollen germination medium (Iwano et al., 2004). Germination was never observed in pollen grains with uniform calcium concentrations (Iwano et al., 2004) suggesting the calcium gradient is a prerequisite of germination.

1.2.3: Pollen germination *in vitro* can be stimulated by pistil extracts

Multiple variations of *Arabidopsis* pollen germination medium have been published (Azarov et al., 1990; Thorsness et al., 1993; Li et al., 1999; Fan et al., 2001; Derksen et al., 2002; Mouline et al., 2002; Hicks et al., 2004; Boavida and McCormick, 2007; Bou Daher et al., 2009). Pollen hydrates instantaneously on germination medium (Iwano et al., 2004); however, pollen germination takes longer *in vitro* than *in vivo* (Kandasamy et al., 1994; Iwano et al., 2004). The pistil must provide a pollen germination stimulant. Indeed, pistil-derived germination stimulants have been isolated from a few species. Some studies have shown that pistil extracts can stimulate germination of orchid, *Chrysanthemum*, and *Polygonatum odoratum* pollen; however, the stimulants have not been identified (Sanford et al., 1964; Tsukamoto and Matsubara, 1968;

Takagi et al., 1995). Kaempferol, a flavonol extracted from *Petunia hybrida* V26 stigmas (Mo et al., 1992), has been shown to stimulate *Petunia hybrida* and *Nicotiana tabacum* pollen germination (Ylstra et al., 1992). More recently, N-methanesulfinyl 1-azadecalin and N-methanesulfinyl 2-azadecalin were synthesized to mimic the diffusible chemical present in *A. thaliana* pistils that stimulates *A. thaliana* pollen germination (Qin et al., 2011). Interestingly, these synthesized chemicals also stimulated pollen germination of the closely related species *Olimarabidopsis pumila* and *Capsella rubella*, but they did not stimulate *Sisymbrium irio* and *Nicotiana tabacum* pollen germination (Qin et al., 2011). This study suggests that pistil-derived pollen germination stimulants are quite divergent, even among species within the same family such as *A. thaliana* and *S. irio*.

1.2.4: Conclusions

Arabidopsis pollen grains adhere, hydrate, and germinate within 20 minutes of making contact with the stigmatic papillae. Since these processes occur in a quick succession, it has been difficult to clearly identify the mechanism behind each process. In recent years, the processes of pollen adhesion and hydration have received very little attention. Although pollen tube growth is heavily studied, the steps leading up to germination are hardly examined. Most recently, two reports provided evidence for the possible roles of nitric oxide regulation (Sirova et al., 2011) and lysophosphatidylethanolamine production (Kim et al., 2011) in pollen germination. It is clear that pollen germination is preceded by the reorientation of the cytoskeleton, redistribution of vesicles, repositioning of the three nuclei, and establishment of a calcium gradient (**Figure 1.3**). What remains unclear is the relative timing of these events and how these events affect each other. Utilizing various fluorescent markers, detailed time-lapse imaging of pollen grains during their transition to a highly polarized cell that ultimately germinates will finally answer many of the questions that still remain about pollen germination.

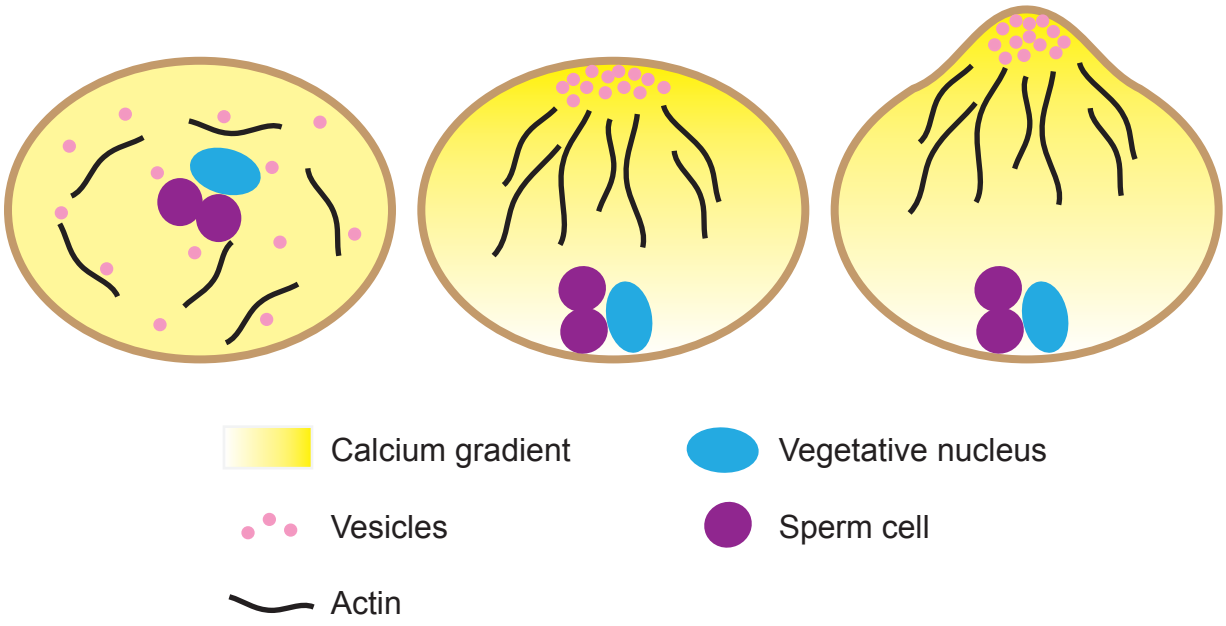

Figure 1.3: Intracellular reorganization leading to pollen germination

Following hydration, a tricellular pollen grain (**left**) will transition into a highly polarized cell (**center**) before the pollen tube emerges (**right**). Actin filaments reorient towards the future site of germination where vesicles start to accumulate. The vegetative nucleus and the two sperm cells relocate from the center of the cell to the wall opposite of the future germination site. A calcium gradient is also established.

1.3: Pollen tube growth

After pollen germination, a pollen tube grows through the stigma and style to the ovary. A pollen tube is a single cell that transports two sperm cells to an ovule where it will penetrate the female gametophyte and rupture. When the pollen tube ruptures, both sperm cells are released allowing double fertilization to occur. One sperm cell fertilizes the egg cell which then develops into the embryo, and the other sperm cell fuses with the central cell which then develops into the endosperm.

Pollen tubes are only 5-20 μm in diameter, but they have to grow to great lengths to reach the ovules. For an extreme example, *Zea mays* pollen tubes have to grow as long as 50 cm to reach the first ovule (Williams, 2008). Pollen tube growth rates range from as slow as 0.31 μm/h for *Ginkgo biloba* pollen to as fast as 40,000 μm/h for *Cichorium intybus* pollen (Williams, 2008). *Arabidopsis thaliana* pollen tube growth rates have been measured at 5-6 μm/min (300-360 μm/h) on stigmatic papilla and 2-3 μm/min (120-180 μm/h) growing through the style (Cheung et al., 2010). This highly regulated tip growth is supported by rapid membrane trafficking and a dynamic cytoskeleton.

1.3.1: Intracellular organization of growing pollen tubes

A pollen tube is a cylindrical cell with a cell wall composed of an outer cellulosic layer and an inner callose layer. The cell wall at the pollen tube tip is very thin and mostly comprised of pectin, and the inner callose wall is completely absent (Derksen et al., 2002). To maintain tip growth, cell wall components must be constantly delivered to the tip of the pollen tube. The cytoplasmic streaming in pollen tubes forms a ‘reverse fountain’ because organelles moving towards the tip travel along the cell membrane while organelles moving away from the tip travel through the center of the tube (Heslop-Harrison and Heslop-Harrison, 1990; Derksen et al., 2002). Despite vigorous cytoplasmic streaming, pollen tubes maintain a characteristic

organelle/vesicle organization (**Figure 1.4**). A pollen tube can be divided into three regions from the tip to the grain: apical, subapical, and shank regions. Small vesicles accumulate forming an inverted cone in the apical region of growing pollen tubes (Lancelle and Hepler, 1992; Derksen et al., 2002). In contrast, larger organelles, such as mitochondria, peroxisomes, and Golgi stacks, are only present in the subapical and shank regions (Pierson et al., 1990; Derksen et al., 2002). Actin filaments and microtubules have an axial orientation in the shank; however, irregular orientations of short actin filaments in the subapical region form a mesh (Derksen et al., 2002; Cheung and Wu, 2008).

1.3.2: The actin cytoskeleton is vital for pollen tube growth

In the past decade, multiple attempts have been made to accurately label all of the actin in living pollen tubes without affecting actin architecture or pollen tube growth rates. The localization of GFP-labeled actin binding proteins were usually compared to fixed pollen tubes labeled with actin antibodies. Immunolabeling revealed fine longitudinal actin cables in the shank and a dense actin fringe in the subapical region (Derksen et al., 2002; Wilsen et al., 2006). GFP-mTalin, GFP fused to the actin-binding domain of mouse talin, labeled actin filaments in the shank and weakly labeled a band in the subapical region (Kost et al., 1998; Wilsen et al., 2006). This weak band most likely represented the actin fringe revealed by immunolabeling; however, individual filaments in the fringe could not be distinguished with GFP-mTalin (Wilsen et al., 2006). GFP-mTalin also frequently labeled a thick central actin bundle and occasionally labeled coils of actin near the tip, which were considered to be artifacts of GFP-mTalin expression (Wilsen et al., 2006). Expression of GFP-mTalin also reduced tip growth (Ketelaar et al., 2004; Wilsen et al., 2006). GFP-ADF1, GFP fused to actin depolymerizing factor 1 from either *N. tabacum* or *L. longiflorum*, labeled the actin fringe, but it rarely labeled distinct actin filaments in the shank (Chen et al., 2002; Wilsen et al., 2006; Cheung et al., 2008). *GFP-ADF1*

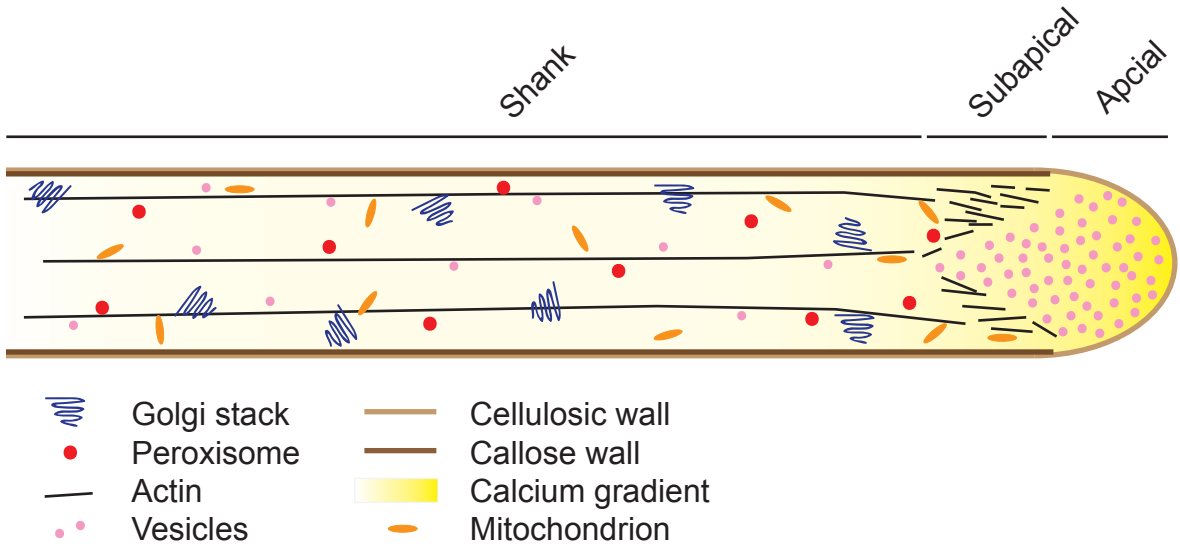

Figure 1.4: Growing angiosperm pollen tubes have a distinct intracellular organization

The pollen tube cell wall has an outer cellulosic layer and an inner callose layer that is absent at the tip. There is a cytoplasmic calcium gradient with the highest concentration of calcium at the tip where vesicles also accumulate. Organelles are excluded from the apical region. Long actin filaments stretch the length of the shank while a fine actin mesh is present in the subapical region. Note that the vegetative nucleus and sperm cells followed by the vacuole are usually located 30 – 40 μm behind the tip; therefore, they are not depicted in this diagram.

expression also resulted in a diffuse fluorescence throughout the cytosol (Chen et al., 2002; Wilsen et al., 2006; Cheung et al., 2008). GFP-FABD2, GFP fused to the second actin-binding domain of *A. thaliana* fimbrin1, only labeled actin filaments in the shank of growing pollen tubes (Wilsen et al., 2006). Expression of *GFP-FABD2* resulted in reduced pollen tube growth and frequently actin filaments were seen to form aggregates in the shank (Wilsen et al., 2006). PLIM2b-GFP, a pollen-expressed LIM protein from *N. tabacum* fused to GFP, clearly labeled actin filaments in the shank and sometimes labeled the subapical actin mesh (Cheung et al., 2008). Expression of *PLIM2b-GFP* reduced pollen tube growth and occasionally resulted in fluorescent intertwining donut-shaped structures near the tip (Cheung et al., 2008). Recently Lifeact-mEGFP, the first 17 amino acids from *Saccharomyces cerevisiae* ABP-140 fused to GFP with a 7 amino acid linker, was shown to label actin filaments in pollen tubes without causing any alterations in actin architecture or pollen tube growth defects (Vidali et al., 2009b). Importantly, Lifeact-mEGFP labeled actin filaments in the shank and in the subapical actin fringe (Vidali et al., 2009b). Unlike previous GFP fusions to actin binding proteins/domains, Lifeact-mEGFP will allow researchers to visualize actin in living pollen tubes under various experimental conditions with less concern about negative effects from expression of the GFP fusion itself.

Indeed, Lifeact-mEGFP has been used to visualize the disruption of the actin fringe during a low dose latrunculin B (latB) treatment of lily pollen tubes (Vidali et al., 2009b). Drug treatments that disrupt actin filaments have provided the strongest evidence for the important role of actin filaments in pollen tube growth. Pollen tubes treated with latB, cytochalasin B, and cytochalasin D stopped growing, lost the accumulation of vesicles at the tip, and organelles stopped moving (Franke et al., 1972; Mascarenhas and Lafountain, 1972; Heslop-Harrison and Heslop-Harrison, 1989a; Parton et al., 2001; Vidali et al., 2001). Interestingly at very low

concentrations of latB, pollen tube tip growth can be inhibited without stopping organelle movements in the shank (Vidali et al., 2001). Utilizing Lifeact-mEGFP, Vidali et al. (2009) were able to show that the low dose of latB that inhibits growth but does not stop organelle movements in the shank resulted in the disappearance of the actin fringe while actin cables in the shank remained. These results suggest that the fragile actin fringe is more important for tip growth than the more stable actin filaments in the shank. Additional evidence for the crucial role of actin during pollen tube growth comes from investigations of myosins, actin-based motor proteins. An antibody for animal myosins was used to isolate a 175 kDa myosin from *Nicotiana* (Tang et al., 1989). Additional myosin antibodies were shown to label vesicles, organelles, and the male germ unit (MGU) in pollen tubes (Heslop-Harrison and Heslop-Harrison, 1989b; Tang et al., 1989; Miller et al., 1995; Tirlapur et al., 1996). It is important to note that it is still unclear whether or not these antibodies really bind to plant myosins. Furthermore 2,3-butanedione monoxime, commonly used as a myosin inhibitor, inhibited growth and organelle motility in lily pollen tubes (Tominaga et al., 2000). These results indicate that myosins might localize to various organelles and vesicles in pollen tubes and could potentially be required for normal tube growth.

1.3.3: The role of microtubules in pollen tube growth is still up for debate

In growing pollen tubes, complete disruption of microtubules with either colchicine or oryzalin did not inhibit tip growth, stop cytoplasmic streaming, or completely arrest the movement of the MGU (Franke et al., 1972; Heslop-Harrison et al., 1988; Astrom et al., 1995; Gossot and Geitmann, 2007). When microtubules were disrupted, movement of the MGU into the pollen tube was delayed (Astrom et al., 1995). Also in the absence of microtubules, the vegetative nucleus and the generative cell were not located as close to the tip compared to untreated pollen tubes (Heslop-Harrison et al., 1988; Laitiainen et al., 2002). Heslop-Harrison et

al. (1988) also showed that upon microtubule disruption, the vegetative nucleus and the generative cell tended to be further apart than in untreated pollen tubes. Overall, these results suggest that microtubules are not solely responsible for but do contribute to the movement of the MGU into and through the pollen tube. Another piece of evidence suggesting that microtubules may be involved in intracellular transport in pollen tubes comes from immunological studies. Using antibodies against animal kinesins, 100 kDa proteins have been isolated from *Nicotiana tabacum* and *Corylus avellana* pollen (Tiezzi et al., 1992; Cai et al., 1993; Liu et al., 1994). The kinesin-like protein from *C. avellana* was identified from a fraction enriched in Golgi-derived vesicles (Liu et al., 1994). The kinesin(s) from *N. tabacum* localized to the subapical and apical regions of pollen tubes (Tiezzi et al., 1992; Cai et al., 1993). With the lack of an effect on tube growth by disrupting microtubules, it is unclear what these kinesins may be doing in the tip of growing pollen tubes. So far, microtubules seem to only be important for transport of the MGU; however, myosin antibodies not kinesin antibodies labeled the MGU in pollen tubes (Tang et al., 1989; Tiezzi et al., 1992; Cai et al., 1993; Miller et al., 1995).

Recently, Idilli et al. (2013) suggested that microtubules are involved in endocytosis and exocytosis in the tip of growing tobacco pollen tubes; however, all of their experiments used nocodazole to partially depolymerize microtubules. Nocodazole depolymerized microtubules closer to the tip, while leaving the microtubules far back in the shank unaffected, yet pollen tube growth was reduced between 15 and 45 minutes after the start of the drug treatment (Idilli et al., 2013). On the other hand, low concentrations of oryzalin completely depolymerized the microtubules throughout the pollen tube and did not inhibit pollen tube growth (Idilli et al., 2013). This suggests that nocodazole might be affecting something besides microtubules that results in growth inhibition. Therefore at this moment, it is difficult to draw any conclusions about the role of microtubules in endocytosis and exocytosis. Future experiments to investigate

this possibility will be necessary to be able to conclusively state the role of microtubules in pollen tube growth.

1.3.4: Membrane trafficking and regulation of tip growth

In order for the pollen tube to elongate, membrane and cell wall materials must be delivered to and secreted at the tip. In addition to secretion, endocytosis actively occurs in growing pollen tubes to retrieve excess membrane materials. Endocytosis occurs at the extreme apex of tube, while exocytosis occurs adjacent to the apical dome (Zonia and Munnik, 2008). Vesicle accumulation at the tip can be visualized by fusing a fluorescent protein to RabA4d, a small pollen-expressed GTPase (Lee et al., 2008; Szumlanski and Nielsen, 2009). RabA4d is predicted to associate with post-Golgi vesicles (Vernoud et al., 2003) and is closely related to RabA4b which is expressed in vegetative tissues (Preuss et al., 2004). RabA4b has been shown to be associated with secretory vesicles from the *trans*-Golgi network (Kang et al., 2011). *raba4d* pollen tubes are wider and have swollen tips compared to *WT* pollen tubes, and these phenotypes can only be partially rescued by expressing YFP-RabA4b in pollen, suggesting there is only partial functional overlap between RabA4d and RabA4b (Szumlanski and Nielsen, 2009).

Rho-GTPases are common regulators of tip growth. ROP1, a small Rho-GTPase expressed in pollen (Li et al., 1998) is not only required for pollen germination, but it also has a vital role in pollen tube growth (Lin and Yang, 1997; Li et al., 1999). ROP1 localizes to the apical plasma membrane of growing pollen tubes (Lin et al., 1996; Hwang et al., 2008), and is required for the polarized growth of pollen tubes (Li et al., 1999). Comparable to ROP1 overexpression lines, expression of fluorescently tagged ROP1 in *Arabidopsis* pollen tubes resulted in short, wide pollen tubes with slight swelling of the tip (Hwang et al., 2008) suggesting tight regulation of the level of ROP1 present in the pollen tube is necessary for normal tip growth. Two types of negative regulators of ROP1 are guanine dissociation factors

(GDI) and GTPase activating proteins (GAP). GDI sequesters ROP1 in the cytoplasm, which prevents ROP1 from localizes to the plasma membrane (Klahre et al., 2006; Hwang et al., 2010). GAPs, ROPGAPs and ROP Enhancer 1 (REN1), promote GTP hydrolysis thus inactivating ROP1 (Hwang et al., 2010). Furthermore, REN1 localization depends on ROP1-regulated exocytosis, which indicates the existence of a feedback loop that contributes towards the oscillation of ROP1 at the tip of growing pollen tubes (Hwang et al., 2008).

Two ROP1 effectors, RIC3 and RIC4, have been shown to regulate tip growth by affecting F-actin dynamics. ROP1 mediated regulation of actin filaments further emphasizes the importance of actin filaments in pollen tube growth. RIC, ROP-interactive CRIB motif-containing, proteins interact with active ROP1, and similar to ROP1 overexpression, when either RIC3 or RIC4 was overexpressed, the pollen tubes became partially depolarized (Wu et al., 2001). Interestingly, co-overexpression of RIC3 and RIC4 results in normal vesicle accumulation and pollen tube growth, suggesting RIC3 and RIC4 expression levels also must be tightly regulated to maintain normal tip growth (Gu et al., 2005; Lee et al., 2008). At the tip of growing pollen tubes, RIC4 promotes F-actin assembly while RIC3 promotes the disassembly of F-actin by increasing calcium influx (Gu et al., 2005). The cytoplasmic concentration of calcium forms a gradient in growing pollen tubes with the highest concentration in the apical region (Iwano et al., 2004). The calcium concentration at the tip oscillates with a maximum concentration of approximately 2 μM (Iwano et al., 2004).

1.3.5: Differences found in gymnosperm pollen tubes

Gymnosperm pollen tubes grow more slowly than angiosperm pollen tubes. Besides growth rate, gymnosperm pollen tubes also have a different intracellular organization compared to angiosperm pollen tubes. Gymnosperm pollen tubes have a crescent-shaped accumulation of vesicles at the tip (de Win et al., 1996; Wang et al., 2005; Wang et al., 2006) instead of the

inverted cone shape observed in angiosperm pollen tubes (Lancelle and Hepler, 1992; Derksen et al., 2002). In addition to the shape of vesicle accumulation, gymnosperm pollen tubes exhibit organelle movements that form a fountain-like cytoplasmic streaming pattern (de Win et al., 1996) instead of the reverse fountain pattern found in angiosperm pollen tubes (Heslop-Harrison and Heslop-Harrison, 1990; Derksen et al., 2002). It has been proposed that the reversal of actin filament orientation could result in the different vesicle accumulation and cytoplasmic streaming patterns observed in gymnosperm pollen tubes (Kroeger et al., 2009). In angiosperm pollen tubes, actin filaments near the cell membrane are oriented with the plus end pointing towards the tip, while filaments in the center of the cell are oriented with the plus end pointing towards the pollen grain (Lenartowska and Michalska, 2008). Since myosins are plus end directed motors, it is clear why cytoplasmic streaming occurs in a reverse fountain pattern in angiosperm pollen tubes. Unfortunately, actin filament orientation has yet to be determined in gymnosperm pollen tubes; however, computer modeling suggests that a reversal in actin filament orientation would explain the observed differences in gymnosperm pollen tubes (Kroeger et al., 2009). Another important difference between angiosperm and gymnosperm pollen tubes is the role of microtubules in pollen tube growth. When either actin or microtubule-disrupting drugs were applied to gymnosperm pollen tubes, growth was inhibited (Anderhag et al., 2000) suggesting that both microtubules and actin filaments are required for the normal growth of gymnosperm pollen tubes. Perhaps these intracellular differences contribute to the slower growth rate observed for gymnosperm pollen tubes.

1.3.6: Conclusions

In angiosperms, actin filaments, but not microtubules, play an essential role in pollen tube growth. Tip growth requires the continual delivery of secretory vesicles to the apex, and this accumulation depends on actin filaments, particularly in the subapical actin fringe. Even though

pollen tube growth has been frequently studied, the complex regulation of pollen tube growth is still not fully understood. ROP1 regulation of pollen tube growth is complicated and not all of the steps in this process have been clarified. Some ROP1 effectors are known; however, not much is known about the how ROP1 activation is regulated during pollen tube growth. Recently, studies in *Arabidopsis* have shown that AtPRK2, a receptor-like protein kinase, may activate RopGEF1, a Rho guanine nucleotide exchange factor, which in turn activates ROP1 (Gu et al., 2006; Zhang and McCormick, 2007; Chang et al., 2013). Further studies are necessary to not only clarify the ROP1-mediated regulation of pollen tube growth, but also other signaling pathways (Guan et al., 2013). In particular, it will be important to determine what initiates the oscillations in ROP1, growth, and cytoplasmic calcium concentration.

1.4: Rationale of this study

Pollen tubes grow exclusively at the tip, and in some species, pollen tubes can grow as fast as 40 mm/h (Williams, 2008). In angiosperms, this rapid pollen tube growth is dependent on the acto-myosin network (Franke et al., 1972; Mascarenhas and Lafountain, 1972; Heslop-Harrison and Heslop-Harrison, 1989a; Tominaga et al., 2000). To date, myosin mutants have not been examined for defects in pollen tube growth; however, by examining vegetative tissues, class XI myosins have been shown to be required for the expansion of various cell types including root hairs, trichomes, stigmatic papillae, and leaf epidermal cells (Ojangu et al., 2007; Peremyslov et al., 2008; Prokhnevsky et al., 2008; Peremyslov et al., 2010; Ojangu et al., 2012). Therefore, class XI myosins are predicted to be involved in pollen tube growth. Interestingly, pollen of an *Oryza sativa* myosin mutant developed abnormally under short-day conditions (Jiang et al., 2007) suggesting a possible role for myosins outside of cell expansion.

In *A. thaliana*, 6 out of the 13 myosin XI genes are expressed in pollen (Peremyslow et al., 2011; Sparkes, 2011). With multiple pollen-expressed myosins, there probably will be some redundancy similar to what has been shown for the vegetative myosins (Prokhnevsky et al., 2008; Peremyslov et al., 2010; Ojangu et al., 2012). Since myosin mutants have defects in cell expansion, it is quite probable that at least higher order pollen myosin mutants will have reduced pollen tube growth. In this study, pollen myosin mutants, T-DNA insertion lines for pollen myosin genes and lines expressing artificial microRNAs designed to silence multiple myosins, will be examined for defects in overall pollen tube growth and fertility. A closer look at organelle trafficking, vesicle accumulation, actin dynamics, and myosin localization will also help clarify the role of each pollen myosin in intracellular transport and overall pollen tube growth.

Chapter 2: Silencing Multiple Class XI Myosins

- *Eunsook Park, a former graduate student in the lab, performed the initial steps for this project. Lauren Swientoniewski, an undergraduate student who earned research credit in this lab, contributed to the results in this chapter. She assisted with replacing the* 35S *promoter with the* SYP22 *and* XIJ *promoters and then helped screen T1 and T2 plants. She also measured all of the root hairs for the dexamethasone-inducible lines.*

2.1: Introduction

In *Arabidopsis thaliana*, there are 13 class XI myosins, and myosin XI mutants have been shown to have defects in cell elongation. In particular, single mutants of *MYA2* and *XIK* have shorter root hairs than *WT*, and *xik* has reduced trichome elongation (Ojangu et al., 2007; Peremyslov et al., 2008; Park and Nebenführ, 2013). Furthermore, double, triple, and quadruple mutants, consisting of various combinations of *mya1*, *mya2*, *xib*, *xi-i*, and *xik*, have more drastic defects in cell elongation (Prokhnevsky et al., 2008; Peremyslov et al., 2010; Ojangu et al., 2012). These higher order mutants have reduced elongation of root hairs, trichomes, stigmatic papillae, and various types of leaf cells (Prokhnevsky et al., 2008; Peremyslov et al., 2010; Ojangu et al., 2012). Since single myosin XI mutants either exhibit a mild phenotype or have no detectable phenotype, there is functional redundancy among the 13 class XI myosins.

Surprisingly, eight of the *Arabidopsis* class XI myosins have not been examined as part of higher order mutants. Of these eight, five are predominately expressed in pollen: *XIA*, *XIC*, *XID*, *XIE*, and *XIJ* (Peremyslow et al., 2011; Sparkes, 2011). *XIB* is expressed in pollen but also in vegetative tissues such as root hairs (Peremyslow et al., 2011; Sparkes, 2011). Since pollen tubes undergo rapid cell elongation, it is quite plausible that higher order mutants of the pollen myosins will have reduced fertility due to reduced pollen tube growth. Indeed, myosins have been implicated in pollen tube growth, as disruption of actin filaments inhibits pollen tube growth (Franke et al., 1972; Mascarenhas and Lafountain, 1972; Heslop-Harrison and Heslop-Harrison, 1989a). Since generating higher order mutants from single T-DNA insertion mutants takes a long time, an alternative approach utilizing artificial microRNA could provide insights into the functions of class XI myosins in pollen tube growth faster than the traditional approach.

microRNAs are small, noncoding RNAs that negatively affect gene expression. Mature microRNAs are usually 19-24 nucleotides in length and are produced from a precursor

microRNA that forms a hairpin. In plants, Dicer-like I cleaves the hairpin precursor into smaller fragments (Kurihara and Watanabe, 2004). The mature microRNA binds to the RNA-induced silencing complex (RISC), and one strand of the microRNA serves as a probe to link RISC to the target mRNA. Binding of target mRNA to RISC usually leads to cleavage followed by degradation of the target mRNA; however, in a few cases, the target mRNA undergoes translational repression (Naqvi et al., 2012). Plant microRNAs have only a few mismatches to their target mRNAs, so each microRNA can only target a small number of closely related mRNAs (Schwab et al., 2005). Since sequence parameters determining native microRNA target recognition have been identified (Schwab et al., 2005), artificial microRNAs can be designed to target specific mRNAs (Schwab et al., 2006).

The motor domain is highly conserved among class XI myosins, raising the possibility of designing artificial microRNAs that target multiple class XI myosins. Since the quadruple myosin XI mutants exhibited reduced growth and were smaller in size (Peremyslov et al., 2010), it was hypothesized that silencing a majority of the class XI myosins would severely affect plant growth. Therefore, a dexamethasone-inducible system (Craft et al., 2005) was used to express the artificial microRNAs. Since some myosin XI mutants have shorter root hairs than *WT* (Ojangu et al., 2007; Peremyslov et al., 2008; Prokhnevsky et al., 2008; Park and Nebenführ, 2013), it was predicted that expression of the artificial microRNAs in *WT* would result in shorter root hairs. In addition, reduced expression of the pollen myosins was predicted to decrease pollen tube growth, thus reduce overall fertility.

2.2: Methods

2.2.1: Plant lines, constructs, and plant transformations

Arabidopsis thaliana Col-0 was used as wild-type (*WT*). T-DNA insertion mutants, *mya1* (SALK_022140) and *xik* (SALK_018764) were obtained from the Arabidopsis Biological Resource Center and confirmed to be knockout mutants by Eunsook Park in this lab. Eunsook Park also generated the *mya1 xik* double mutant. Dr. Xue Cai, a former post-doc in this lab, transformed *WT* with the *35Spro:GUS* construct to use as a positive control for GUS staining.

Eunsook Park used the Web MicroRNA Designer (Schwab et al., 2006) to design two artificial microRNAs, *R1* (TAACATGCAAGCTTCGTCGAG) and *R2* (TACATGCTGATTAAAGTGCTG), to target multiple class XI myosins. The mature artificial microRNA sequences were cloned into the endogenous *miR319a* precursor by performing PCR on pRS300 with three different primer sets and then combining the products in a fourth PCR (**Tables 2.1 and 2.2**). pRS300 was kindly provided by Dr. Detlef Weigel (Max Planck Institute, Tübingen, Germany). The resulting PCR products were cloned into pBS using blunt end ligation. The artificial microRNA precursors were moved into the multiple cloning site of the binary plasmid pV-TOP, which was kindly provided by Dr. Ian Moore (University of Oxford, Oxford, UK). pV-TOP contains a six-operator array flanked by two divergent TATA boxes with the GUS reporter gene on one side and the multiple cloning site on the other side (Craft et al., 2005). pV-TOP + R1 was transformed into *WT* and *xik*, and pV-TOP + R2 was transformed into *WT*, *xik*, *mya1*, and *mya1 xik*, all by the *Arabidopsis* floral dip method (Weigel and Glazebrook, 2002). *35Spro:LhGR* was moved from pBIN-LhGR-N (Craft et al., 2005) into another binary plasmid, pFGC19 (Nelson et al., 2007). pBIN-LhGR-N was kindly provided by Dr. Ian Moore (University of Oxford, Oxford, UK). Eunsook Park left the project at this stage. The new *35Spro:LhGR* construct was transformed into the inducible artificial microRNA lines by the *Arabidopsis* floral

Table 2.1: Construction of artificial microRNAs, R1 and R2

Template	Primers	Product
pRS300	OLIGO-F & A14	A
pRS300	A12 & A13	B
pRS300	A11 & OLIGO-R	C
A, B, C	OLIGO-F & OLIGO-R	R1
pRS300	OLIGO-F & A24	1
pRS300	A22 & A23	2
pRS300	A21 & OLIGO-R	3
1, 2, 3	OLIGO-F & OLIGO-R	R2

Table 2.2: List of primers

Primer name	Primer sequence (5' to 3')
A11	GATAACATGCAAGCTTCGTCGAGTCTCTCTTTTGTATTCC
A12	GACTCGACGAAGCTTGCATGTTATCAAAGAGAATCAATGA
A13	GACTAGACGAAGCTTCCATGTTTTCACAGGTCGTGATATG
A14	GAAAACATGGAAGCTTCGTCTAGTCTACATATATATTCCT
A21	GATACATGCTGATTAAAGTGCTGTCTCTCTTTTGTATTCC
A22	GACAGCACTTTAATCAGCATGTATCAAAGAGAATCAATGA
A23	GACAACACTTTAATCTGCATGTTTCACAGGTCGTGATATG
A24	GAAACATGCAGATTAAAGTGTTGTCTACATATATATTCCT
OLIGO-F	CTGCAAGGCGATTAAGTTGGGTAAC
OLIGO-R	GCGGATAACAATTTCACACAGGAAACAG
SEQ-35S-F	CGCACAATCCCACTATCCTTCGCA
SYP22pro-F3	CGAGAATTCATCAACCACTATCTGTCGTCC
M11.J-pro-F1	ACGTCCGGAGGTCTGCTGAACTAGAGACT
DT6-LP	ATACCATCAAGAAGGTTCGGG
DT6-RP	CTTTTCCGGTGGATTCTCTTC
JT3-LP2	CTCACCTTGCAAAGTGGAGTC
JT3-RP2	CTCAACTTGCAATAAGGCCTG

dip method (Weigel and Glazebrook, 2002). To simplify the naming of plant lines containing both the artificial microRNA/GUS reporter gene construct and the *35Spro:LhGR* construct, lines were referred to as *R1X* and *R2X*. X indicates the background: C – *WT*, M – *mya1*, K – *xik*, and D – *mya1 xik*.

For constitutive expression, *R1* and *R2* were expressed by the *CaMV 35S*, *SYP22*, and *XIJ* promoters. The native *SYP22* promoter extended 1,357 base pairs upstream of the *SYP22* start codon and included the first 20 base pairs of the *SYP22* coding sequence (19,013,796-19,015,171 based on TAIR10). The native *XIJ* promoter extended 757 base pairs upstream of the *XIJ* start codon and included the first 9 base pairs of the *XIJ* coding sequence (21,534,040-21,534,805 based on TAIR10). *35Spro:R1* and *35Spro:R2* were moved into the binary plasmid pFGC19 (Nelson et al., 2007). *SYP22pro:R1*, *SYP22pro:R2*, *XIJpro:R1*, and *XIJpro:R2* were moved into the binary plasmid pPZP221 (Hajdukiewicz et al., 1994). All constructs were transformed into *WT* by the *Arabidopsis* floral dip method (Weigel and Glazebrook, 2002).

2.2.2: Seed sterilization and plant growth conditions

Seeds were incubated at -80°C for a minimum of 15 minutes to kill pests and then surface sterilized with 30% bleach and 0.1% TritonX-100. Sterilized seeds were washed 3 – 5 times with sterile dH_2O and unless otherwise noted, plated on ½X Murashige and Skoog medium with 1% sucrose (pH 6.0) solidified with 0.2% phytagel. For selection of transgenic lines, glufosinate (Basta), hygromycin B, or gentamicin was added to a final concentration of 10 μg/ml, 37.5 μg/ml, or 25 μg/ml, respectively. Note that 0.6% plant agar was used instead of phytagel when gentamicin was included. Plates were incubated at 4°C for 2 days to stratify the seeds and then transferred to 22°C with 16 hours of light and 8 hours of dark. 10 -14 day-old seedlings were transferred to soil (Fafard Superfine Germinating Mix) and grown in 60% humidity at 22°C in 16 hours of light and at 20°C in 8 hours of dark.

2.2.3: Dexamethasone induction

The first induction method was only used to check for the expression of the GUS reporter gene. Leaves were removed and soaked in 500 μM dexamethasone overnight. The 500 μM dexamethasone solution was a dilution from a 100 mM dexamethasone in 95% ethanol stock solution. Ethanol was added to the dH_2O used to soak the control leaves. The second induction method was used for screening for homozygous mutants and for the root hair and gravitropism experiments. Seeds were germinated and grown on MS medium containing 0 μM, 10 μM, or 200 μM dexamethasone. Dexamethasone was added to the medium from a 100 mM dexamethasone in DMSO stock solution. Dexamethasone or DMSO was added to the medium after autoclaving.

2.2.4: GUS staining

After dexamethasone induction, the leaves or seedlings were transferred to 24-well plates with staining buffer containing 50 mM sodium phosphate buffer (pH 7.2), 0.2% Triton X-100, 0.2 mM potassium ferrocyanide, 0.2 mM potassium ferricyanide, and 1 mM X-Gluc (5-bromo-4-chloro-3-indolyl-β-glucuronide). The samples were incubated at 37°C overnight. Leaves and seedlings were washed three times with 70% ethanol and three times with 95% ethanol. Root hairs were imaged in 95% ethanol using a Zeiss SteREO Discovery.V8 stereomicroscope equipped with a Canon EOS Rebel XS digital camera. Leaves were transferred to dH_2O by gradually reducing the concentration of ethanol and then transferred to a 50% glycerol solution before imaging. Leaves were imaged using a Leica MZ16 FA stereomicroscope equipped with a Leica DFC420 digital camera.

2.2.5: Root hair analysis

For all root hair analysis experiments, 24 seeds were plated in two rows on square plates containing ¼X MS medium with 1% sucrose (pH 5.7) solidified with 0.5% phytagel. Plates were placed in a vertical orientation in the growth chamber. Five-day-old seedlings were imaged using

a Zeiss SteREO Discovery.V8 stereomicroscope equipped with a Canon EOS Rebel XS digital camera. The lengths of all in focus mature root hairs were measured in ImageJ. Mutants that were statistically different from the control were identified by a Mann-Whitney unpaired t-test using Prism 6 software (GraphPad).

For the dexamethasone-inducible lines, each line was plated along with the *35Spro:GUS* line and the corresponding control (*WT*, *mya1*, *xik*, or *mya1 xik*) on MS medium containing 0 μM, 10 μM, or 200 μM dexamethasone. GUS staining was performed on each seedling, and the root hairs were examined for positive GUS staining. Root hair measurements were combined by genotype and dexamethasone concentration.

For the constitutively expressed artificial microRNA lines, T2 seeds from 5 *35Spro:R1* lines and 5 *35Spro:R2* lines were plated with one plant line per plate. Genomic DNA (gDNA) was extracted from each 15-day-old seedling, and PCR was used to amplify the construct in order to determine which seedlings contained the artificial microRNA and which did not (**Tables 2.2 and 2.3**). JT3-LP2 and JT3-RP2 were used as control primers to check for the presence of gDNA. For each plate, root hair measurements were combined into two groups, one from seedlings containing the artificial microRNA and one from *WT* seedlings.

2.2.6: Gravitropism analysis

Seeds were plated on MS medium with 0.8% plant agar and either 10 μM dexamethasone in DMSO or DMSO only. Plates were incubated for two hours at 22°C in the light and then placed in a vertical orientation at 22°C in the dark for 48 hours. The plates were then moved to room temperature and rotated 90° to the left. Images were captured in the dark every 15 minutes for 24 hours using a Marlin CCD camera and infrared radiation. Angles of the hypocotyl and root were measured using ImageJ. 0° was horizontal and 90° was vertical (up for hypocotyls and down for roots).

Table 2.3: Primer pairs used for genotyping

Template	Gene/construct	Primers	PCR condition
gDNA	*35Spro:R1*	SEQ-35S-F & A12	A58E30C
	35Spro:R2	SEQ-35S-F & A22	A58E30C
	SYP22pro:R1	SYP22pro-F3 & A12	A58E120C
	SYP22pro:R2	SYP22pro-F3 & A22	A58E120C
	XIJpro:R1	M11.J-pro-F1 & A12	A58E90C
	XIJpro:R2	M11.J-pro-F1 & A22	A58E90C
	XID	DT6-LP & DT6-RP	A58E90C
	XIJ	JT3-LP2 & JT3-RP2	A60E90C

PCR conditions are identified by their annealing temperature (A##), extension time (E##), and number of cycles (letter code: A=20, B=25, C=30, D=35, E=40).

2.2.7: DNA extraction and genotyping

Genomic DNA (gDNA) was extracted from either a leaf or a seedling. Plant tissue was ground in a microcentrifuge tube with a small plastic pestle in 400 μl of extraction buffer (200 mM Tris-Cl pH 7.0, 250 mM NaCl, 25 mM EDTA, and 0.5% SDS). gDNA was precipitated with isopropanol and washed twice with 75% ethanol. Pellets were dissolved in 100 μl of dH_2O, and 1-2 μl of gDNA was used for PCR. PCR was performed using construct specific primers with the following conditions: initial denaturation at 94°C for 2 minutes, followed by multiple cycles with 94°C (15 s), an annealing temperature (15 s), 72°C (for a set time), and after the final cycle 5 minutes at 72°C (**Tables 2.2 and 2.3**). Note that for the pollen expressed artificial microRNA lines, DT6-LP and DT6-RP were used as control primers to check for the presence of gDNA.

A variation on the gDNA extraction protocol was utilized when there were hundreds of samples. Leaves were placed in microfuge tubes each containing one cleaned BB (a 4.5 mm zinc-plated steel pellet) and incubated at -80°C for at least 24 hours. Immediately after removing the tubes from the freezer, they were inverted and tapped repeatedly on a hard surface to break apart the leaves. 200 μl of extraction buffer was added and the remainder of the normal procedure was followed except the pellets were dissolved in 50 μl of dH_2O.

2.3: Results

2.3.1: Generation of artificial microRNAs

Since there is redundancy among class XI myosins in *Arabidopsis* (Prokhnevsky et al., 2008; Peremyslov et al., 2010; Ojangu et al., 2012), some defects might not be detected until a majority of the myosins are knocked out. Instead of generating higher order mutants by crossing single T-DNA insertion mutants, artificial microRNAs were designed to reduce the expression of

multiple class XI myosins at once. Web MicroRNA Designer (WMD), a web application for the automated design of artificial microRNAs (Schwab et al., 2006), was used to identify artificial microRNA sequences that could target as many of the 13 class XI myosins as possible. Of the multiple suggested sequences, two artificial microRNAs, *R1* (TAACATGCAAGCTTCGTCGAG) and *R2* (TACATGCTGATTAAAGTGCTG), were selected and cloned into an endogenous microRNA precursor, *miR319a*. In the time since the two artificial microRNAs were cloned, the web application was updated twice and is now on version 3, WMD3. Using WMD3 to design artificial microRNAs to target the 13 class XI myosins, *R1* and *R2* were not among the sequences recommended (data not shown). Therefore if this experiment were repeated today, the artificial microRNA sequences would be different. WMD3 also has a target search application to predict targets of native or artificial microRNAs based on criteria obtained from experiments with native and artificial microRNAs (Schwab et al., 2005; Schwab et al., 2006). Using the WMD3 target search application, *R1* and *R2* were predicted to target 9 and 6 out of the 13 class XI myosins, respectively (**Tables 2.4 and 2.5**). *R1* was also predicted to target *ILITYHIA* (At1g64790), a target that was not identified with the original version of WMD. *ILITYHIA* is expressed throughout the plant (Hruz et al., 2008) and encodes a protein involved in plant immunity (Monaghan and Li, 2010).

2.3.2: The GUS reporter gene was successfully induced with the addition of dexamethasone

Quadruple myosin XI mutants were the highest order of myosin mutants examined in *Arabidopsis*, and these mutants exhibited reduced growth (Peremyslov et al., 2010). Since *R1* and *R2* were predicted to target six or more myosins at once, there was concern that the seedlings expressing the constructs would not survive. Therefore, a dexamethasone-inducible system was used to drive the expression of the artificial microRNAs (Craft et al., 2005). This system involves transforming two constructs into plants. One construct contains the artificial microRNA

Table 2.4: Predicted targets of *R1*

Gene	Location (bp)*	Sequence (5' to 3')	Hybrid. energy (kcal/mol)
XIC	1,543-1,563	CTCGATGAAGCTTGCATGTTT	-40.66
XIE	1,528-1,548	CTTGATGAAGCTTGCATGTTT	-38.43
XIG	1,546-1,566	CTGGACGAGGCTTGCATGTTC	-37.62
XIA	1,516-1,536	CTAGACGAGGCTTGCATGTTT	-36.54
XID	1,567-1,587	CTTGATGAGGCTTGTATGTTC	-35.83
XIB	1,522-1,542	CTAGATGAAGCTTGCATGTTT	-34.84
XI-I	1,707-1,727	TTAGATGAAGCTTGCATGTTT	-34.84
MYA2	1,692-1,712	CTAGATGAAGCTTGCATGTTT	-34.84
ILITYHIA	2,795-2,815	CTTGGTGAAGCTTGCACGTTG	-31.99
XIH	1,798-1,818	CTGAATGAGGCTTGCATGTTC	-30.73

* Based on the TAIR9 cDNA sequence.
Red letters are mismatches.
Perfect match hybridization energy = -44.07 kcal/mol

Table 2.5: Predicted targets of *R2*

Gene	Location (bp)*	Sequence (5' to 3')	Hybrid. energy (kcal/mol)
MYA1	1,519-1,539	CAGCATTTTAATCAGCATGTC	-36.77
MYA2	1,551-1,571	CAGCATTTTAATCAGCATGTC	-36.77
XIB	1,381-1,401	CAGCACTTTAATCAGCACGTC	-34.42
XIF	1,378-1,398	CAGCATTTCAATCAGCATGTA	-33.82
XIJ	1,372-1,392	CAGCATTTCAATCAGCATGTA	-33.82
XID	1,426-1,446	CAGCATTTCAATCAGCATGTG	-33.51

* Based on the TAIR9 cDNA sequence.
Red letters are mismatches.
Perfect match hybridization energy = -40.82 kcal/mol

and a GUS reporter gene, separated by six *lac* operators. The other construct encodes LhGR under the control of the *CaMV 35S* promoter. LhGR is comprised of the ligand binding domain of the rat glucocorticoid receptor, the high affinity DNA binding domain of the *lac* repressor, and the GAL4 transcription activation domain II (Craft et al., 2005). In the absence of dexamethasone, LhGR remains bound to heat shock protein 90 (HSP90) in the cytoplasm (**Figure 2.1**). In the presence of dexamethasone, the interaction between LhGR and HSP90 is disrupted, allowing LhGR to enter the nucleus and induce expression of the artificial microRNA and the GUS reporter gene (**Figure 2.1**).

The dexamethasone-inducible system with *R1* was transformed into *WT* and *xik* and while a similar system with *R2* was transformed into *WT*, *mya1*, *xik*, and *mya1 xik*. All lines were initially screened for expression of the GUS reporter gene in the absence and presence of dexamethasone. Leaves were collected, soaked in dexamethasone, and then GUS staining was performed to determine whether or not the GUS reporter gene was expressed. In a few lines, the GUS reporter gene was expressed in the absence of dexamethasone (data not shown). These lines were not examined further. In most lines, leaves exhibited the expected result: no staining in the absence of dexamethasone and some degree of positive GUS staining in the presence of dexamethasone (**Figure 2.2A**). Lines with strong GUS staining were selected for in every generation following the transformation.

The inducible artificial microRNA lines were also germinated and grown on medium containing dexamethasone. The seeds germinated normally, and the seedlings appeared to grow as well as *WT* (data not shown). GUS staining revealed that when grown on dexamethasone, the GUS reporter gene was expressed throughout each seedling, including the root hairs (**Figure 2.2C**). This result indicated that induction of the GUS reporter gene and the inferred induction of either *R1* or *R2*, did not drastically affect seed germination or seedling growth.

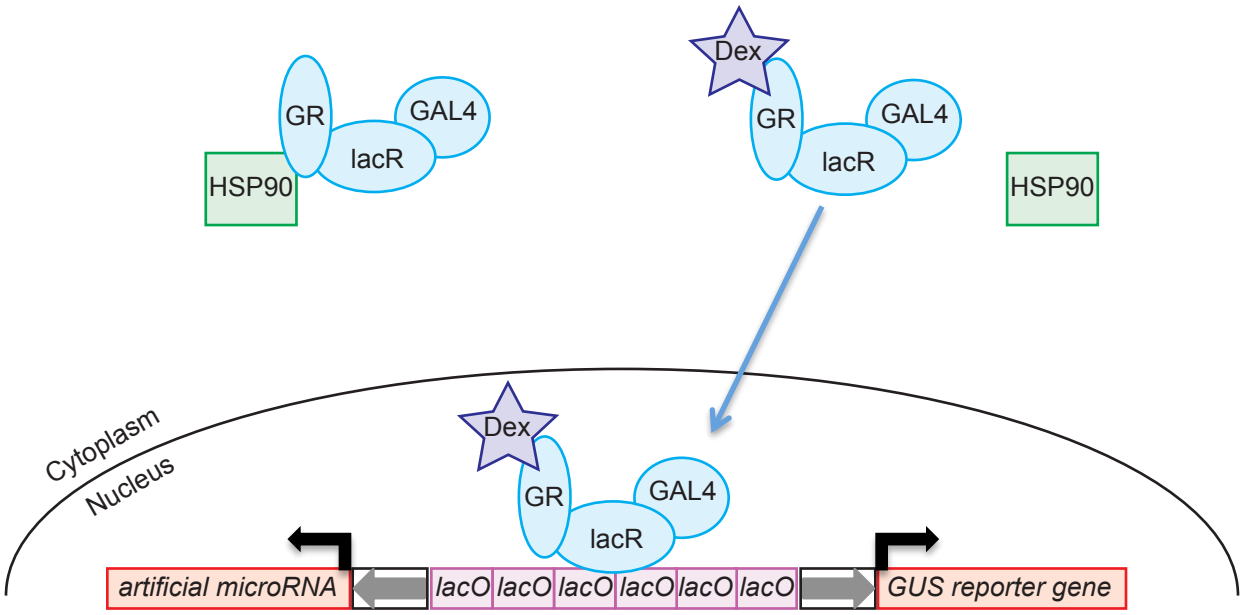

Figure 2.1: Dexamethasone-inducible system

In the absence of dexamethasone (**Left**), LhGR (light blue) remains bound to HSP90 (green) in the cytoplasm, so the artificial microRNA and the GUS reporter gene are not transcribed. When dexamethasone (dark blue) is present (**Right**), it binds to LhGR and disrupts its interaction with HSP90. Then LhGR can enter the nucleus, bind to the six *lac* operators (purple), and activate transcription of the artificial microRNA and the GUS reporter gene (red).

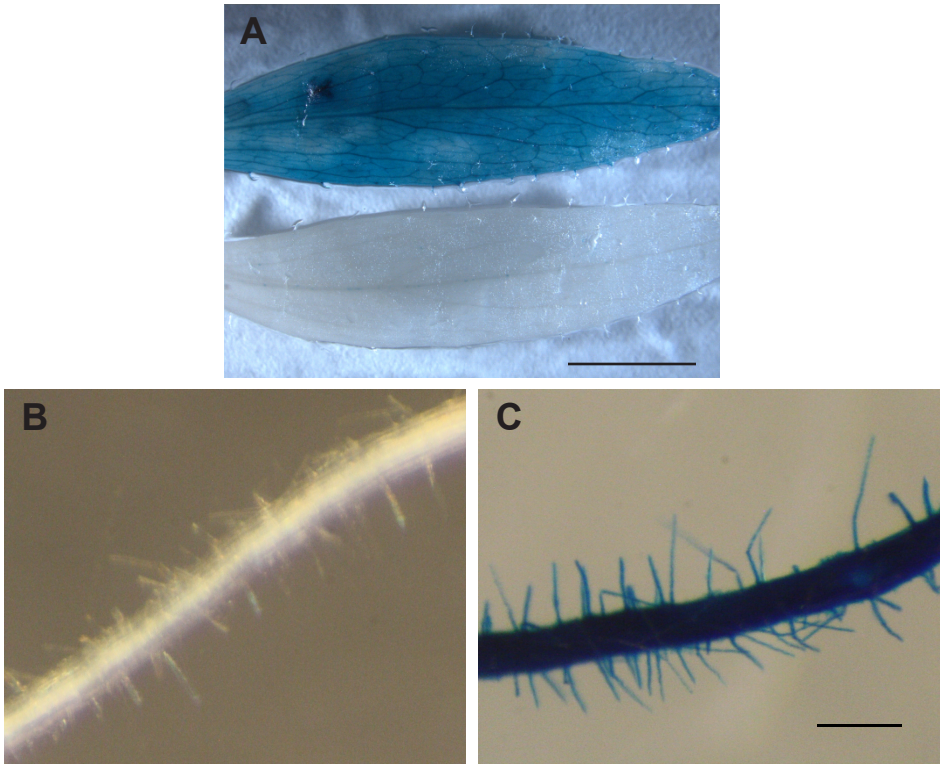

Figure 2.2: GUS staining results of inducible artificial microRNA lines

(**A**) Leaves from a *mya1* plant expressing the dexamethasone-inducible system with *R2*: Top = induced, Bottom = not induced. Positive GUS staining result was only obtained after induction with dexamethasone. Scale bar = 5 mm.

(**B**) *WT* seedling grown on 200 μM dexamethasone. No GUS staining observed in the root or root hairs.

(**C**) *WT* seedling expressing the dexamethasone-inducible system with *R2* grown on 200 μM dexamethasone. Positive GUS staining observed in the root and root hairs. Scale bar = 0.5 mm.

2.3.3: Induced expression of myosin XI artificial microRNAs did not shorten root hairs

The *mya2* single mutant has short root hairs, and the *mya2 xib* double mutant has even shorter root hairs (Peremyslov et al., 2008; Prokhnevsky et al., 2008). Since both *R1* and *R2* should target *MYA2* and *XIB* (**Tables 2.4 and 2.5**), the inducible artificial microRNA lines can be expected to have shorter root hairs when grown on dexamethasone. Two lines for each construct in every genetic background were grown on vertical plates along with *35Spro:GUS* seedlings and the corresponding control (*WT*, *mya1*, *xik*, *or mya1 xik*) on medium containing 0 μM, 10 μM, or 200 μM dexamethasone. Five-day-old seedlings were imaged, and the lengths of all in-focus, mature root hairs were measured (**Figure 2.3**). GUS staining was performed on all seedlings, and the root hairs were examined for the presence of staining. None of the controls (*WT*, *mya1*, *xik*, *or mya1 xik*) had positive GUS staining, and the *35Spro:GUS* seedlings always had positive GUS staining. Some artificial microRNA seedlings were omitted from the root hair analysis because they either had positive staining when grown on 0 μM dexamethasone or lacked positive staining when grown on 10 μM or 200 μM dexamethasone. All genotypes had shorter root hairs when grown on medium containing 200 μM dexamethasone (**Figure 2.3**). *35Spro:GUS* seedlings have a *WT* background, so they always had longer root hairs than seedlings with either the *xik* or the *mya1 xik* background (**Figure 2.3**). Five of the 12 artificial microRNA lines were statistically shorter or longer than the control when grown on 0 μM dexamethasone (**Figure 2.3**; $p < 0.01$). This difference was most likely due to variation and sample size. Six of the 12 artificial microRNA lines were not statistically different from the control when grown on dexamethasone (**Figure 2.3**; $p > 0.01$). Four of the 12 artificial microRNA lines were statistically longer than the control when grown on either 10 μM or 200 μM dexamethasone (**Figure 2.3**; $p < 0.01$). This was the opposite of the expected result. *R2C-2* and *R2M-2* were statistically shorter than the control when grown on 10 μM but not on 200 μM

Figure 2.3: Inducible artificial microRNA lines do not have shorter root hairs

The inducible artificial microRNA lines (*R1* and *R2*) were grown on vertical plates along with *35Spro:GUS* and control seedlings at three concentrations of dexamethasone. The controls were *WT*, *mya1*, *xik*, and *mya1 xik* depending on the background of *R1*/*R2*: C = *WT*, M = *mya1*, K = *xik*, and D = *mya1 xik*. The length of every in focus mature root hair was measured (Mean ± SD; n = 12 to 218). Overall, the inducible artificial microRNA lines did not have shorter root hairs than the control when grown on medium containing dexamethasone (* $p < 0.01$, Mann-Whitney test). Note, *R2K-1* was not grown on 200 μM dexamethasone, and statistics were not performed on the *35Spro:GUS* line.

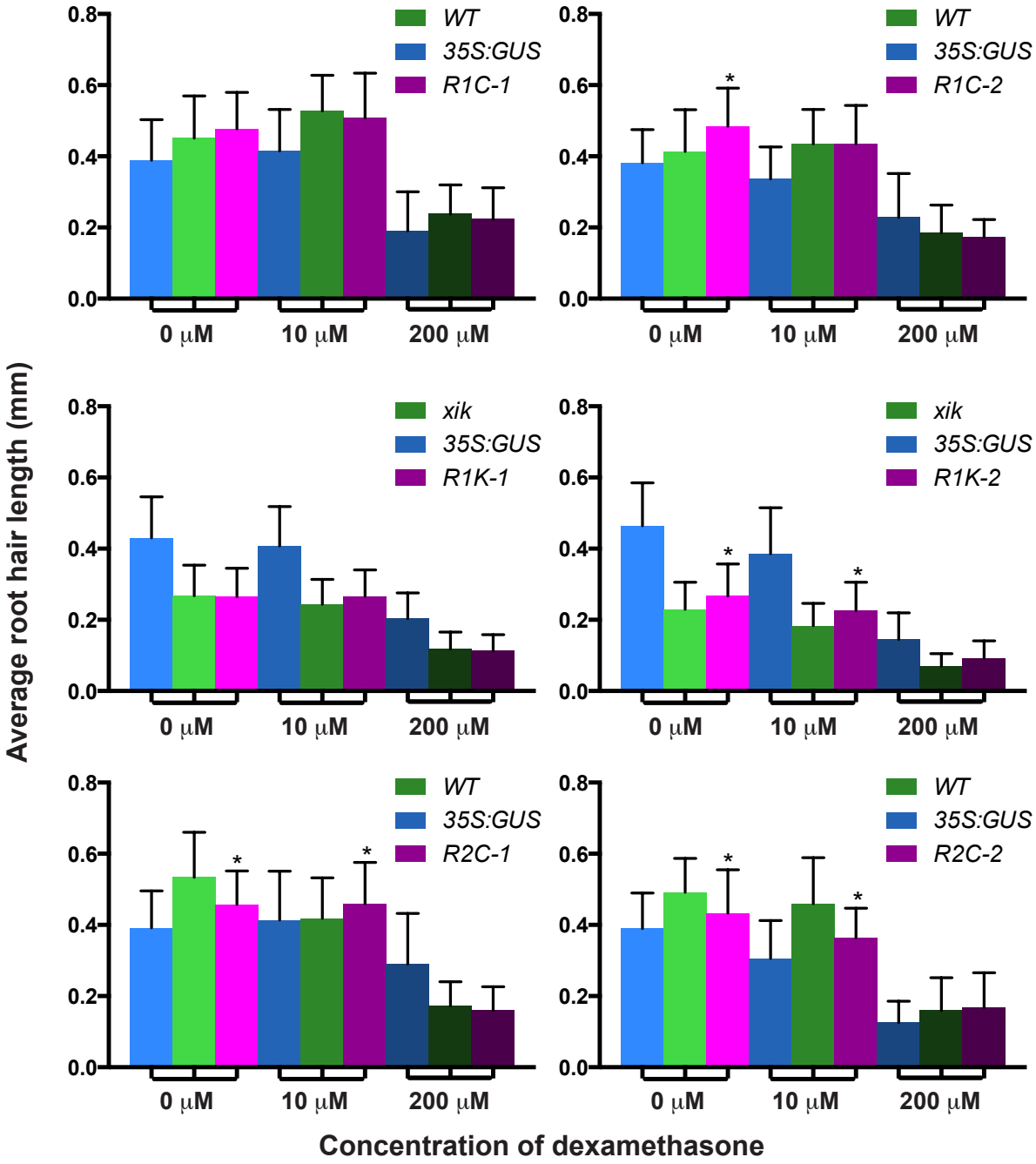
Average root hair length (mm)
0.8
0.6
0.4
0.2
0.0
WT
35S:GUS
R1C-1
R1C-2
xik
R1K-1
R1K-2
R2C-1
R2C-2
*
0 μM
10 μM
200 μM
Concentration of dexamethasone

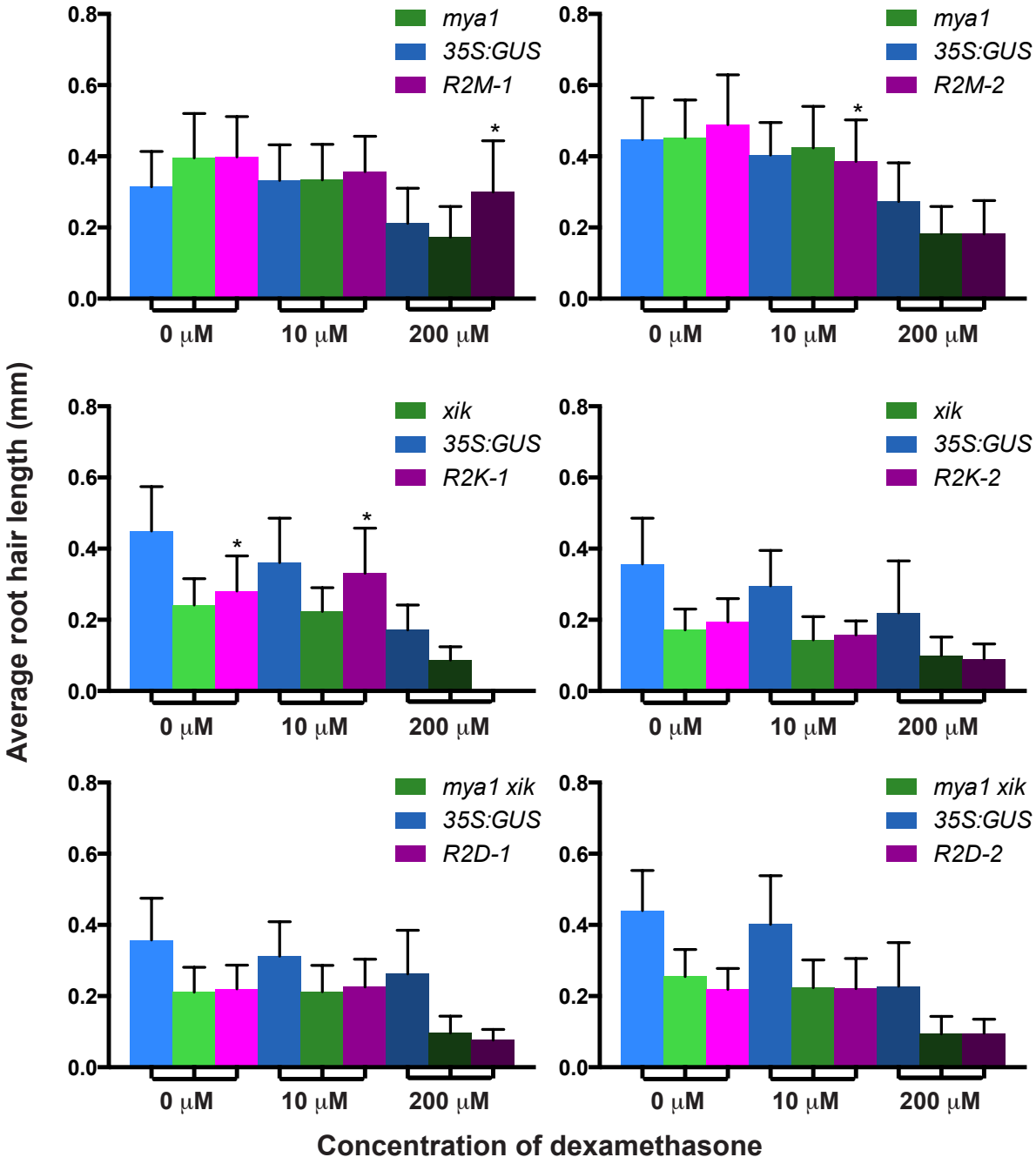

Figure 2.3: Continued

dexamethasone (**Figure 2.3**; $p < 0.01$). Overall, the addition of dexamethasone resulted in the expression of the GUS reporter gene, but it did not reliably result in shortened root hairs in the artificial microRNA lines. This means that the expression levels of *MYA2* and *XIB* probably were not reduced at all or not reduced enough to detect a defect in root hair growth. This suggests that the artificial microRNAs were not expressed, not expressed at a high enough level, or *MYA2* and *XIB* were not targeted by *R1* and *R2*.

2.3.4: The gravitropic response was unaffected when *R2M* was grown on dexamethasone

Gravitropism is the response of plants to the direction of gravity. Roots grow downward, and shoots grow upward. Myosin XI mutants have not been examined for defects in gravitropism; however, the gravitropic response is dependent on differential cellular elongation (Toyota and Gilroy, 2013). Since class XI myosins are involved in the elongation of various cell types (Ojangu et al., 2007; Peremyslov et al., 2008; Prokhnevsky et al., 2008; Peremyslov et al., 2010; Ojangu et al., 2012), myosin XI might be involved in gravitropic responses. Therefore, the inducible artificial microRNA lines might have a delayed gravitropic response when grown on dexamethasone.

R2M seedlings were germinated and grown in the dark for 48 hours on vertical plates containing either 0 μM or 10 μM dexamethasone. The plates were rotated 90° and imaged in the dark every 15 minutes for 24 hours (**Movie 2.1**). The angles of the roots and hypocotyls were measured as they reoriented from 0° to 90°. There was a large degree of variation in the reorientation rate for roots and hypocotyls among seedlings, and no difference was detected between seedlings grown on 0 μM and 10 μM dexamethasone (**Figure 2.4**). Therefore, induction of the GUS reporter gene and the possible induction of *R2*, did not affect the root or hypocotyl gravitropic response. Since myosin XI mutants have not been tested for delays in gravitropic responses, the effectiveness of *R2* could not be evaluated from this experiment.

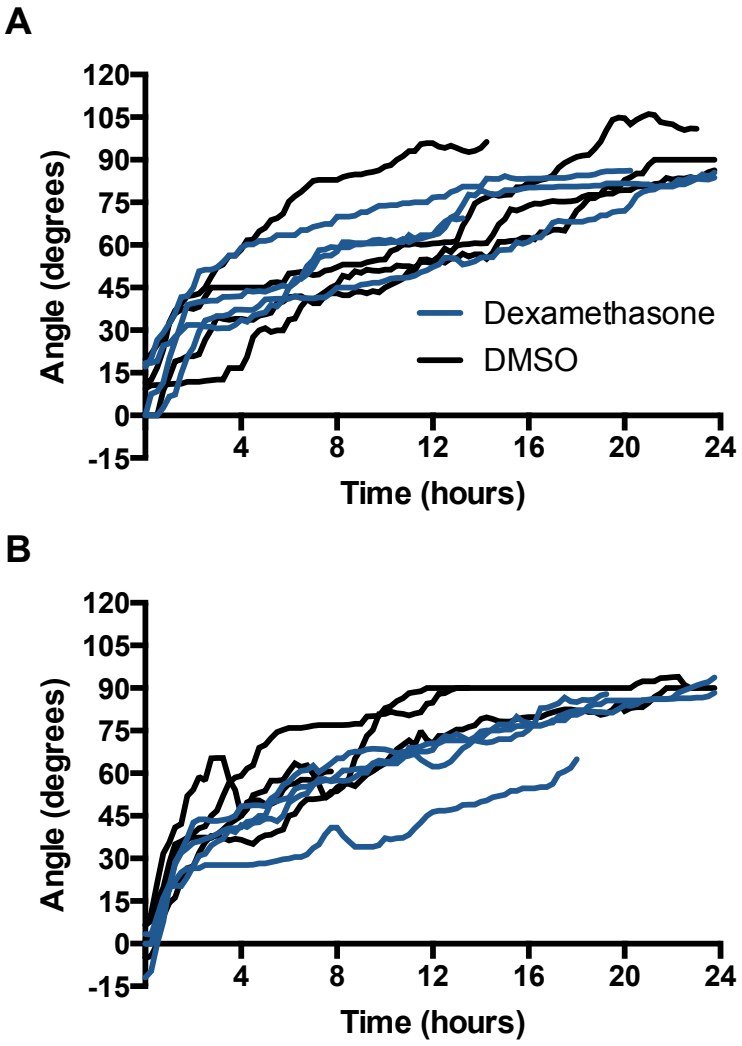

Figure 2.4: Gravitropism was unaffected in the *R2M* line grown on dexamethasone

Gravitropism was examined in *R2M*, the inducible *R2* line in the *mya1* background, grown on 0 μM (black) or 10 μM (blue) dexamethasone. Two-day-old seedlings were grown and imaged in the dark. The reorientation rate of the root (**A**) and hypocotyl (**B**) remained unchanged between the absence and the presence of dexamethasone.

2.3.5: Constitutively expressed myosin XI artificial microRNAs shortened root hairs

Even though the inducible artificial microRNA lines did not have defects in root hair elongation or gravitropic response (**Figures 2.3 and 2.4**), it was still possible that the artificial microRNAs were able to target the myosin XI mRNAs, but were not expressed at a high enough level to result in growth defects. To test the effectiveness of *R1* and *R2*, they were constitutively expressed in *WT* under control of the strong *CaMV 35S* promoter. *MYA2* and *XIB* are involved in root hair elongation (Peremyslov et al., 2008; Prokhnevsky et al., 2008), and both *R1* and *R2* should target *MYA2* and *XIB* (**Tables 2.4 and 2.5**). Therefore, root hair lengths of five *35Spro:R1* and five *35Spro:R2* lines were examined. T2 seedlings were grown on vertical plates, imaged five days post-germination, and genotyped to determine which seedlings contained the artificial microRNA constructs. Seedlings not containing *R1* or *R2* were considered to be *WT*. *R2-2*, *R2-3*, and *R2-5* probably contained multiple insertions of the *35Spro:R2* construct because none of the T2 seedlings tested were *WT* (**Figure 2.5**).

All five *R1* lines and *R2-1* had shorter root hairs than their *WT* siblings grown on the same plate (**Figure 2.5**; $p < 0.01$). *R2-4* did not have shorter root hairs than *WT*, and *R2-5* appeared to have root hairs similar in length to WT seedlings grown on other plates (**Figure 2.5**), suggesting that *R2* might have been silenced in those lines. *R2-2* and *R2-3* appeared to have shorter root hairs than *WT* on other plates (**Figure 2.5**). Overall, constitutive expression of *R1* or *R2* resulted in shortened root hairs. This was most likely due to the reduced expression of myosin XI genes, in particular *MYA2* and *XIB*, suggesting that *R1* and *R2* were able to silence myosin XI gene expression.

2.3.6: Constitutively expressed myosin XI artificial microRNAs did not affect fertility

R1 and *R2* should target five and three out of the six myosin XI genes expressed in pollen, respectively. Pollen tube growth has not been examined in myosin XI mutants; however,

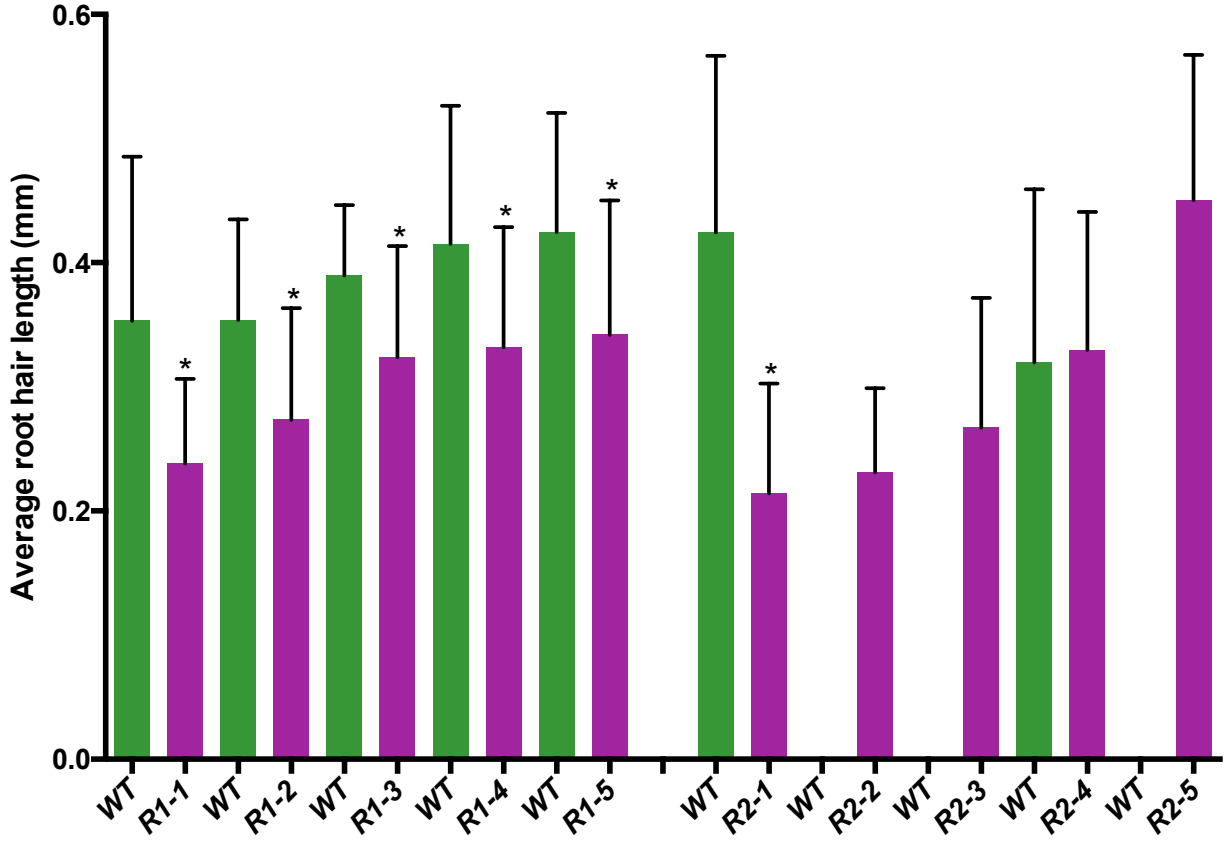

Figure 2.5: Constitutively expressed artificial microRNA lines have shorter root hairs

Five-day-old T2 *35Spro:R1* and *35Spro:R2* vertically grown seedlings were imaged, and the length of every in-focus mature root hair was measured. All seedlings were genotyped to determine which ones contained the artificial microRNA construct and which ones did not (*WT*). All *R1* lines and some *R2* lines had shorter root hairs than *WT* (Mean ± SD; n = 11 to 546; * $p < 0.01$). Note, *R2-2*, *R2-3*, and *R2-5* lines most likely contained multiple insertions, so there were not any *WT* seedlings to compare to those *R2* lines.

actin disrupting drug treatments have implicated myosins in angiosperm pollen tube growth (Franke et al., 1972; Mascarenhas and Lafountain, 1972; Heslop-Harrison and Heslop-Harrison, 1989a). Since the *35S* promoter does not function in pollen, it was exchanged for the *SYP22* and *XIJ* promoters. *SYP22* is expressed throughout the plant, including pollen, and *XIJ* is predominately expressed in pollen (Hruz et al., 2008). If pollen tube growth is affected by silencing of myosin genes, there could be a reduction in the number of ovules being fertilized that would reduce the number of seeds per silique. If pollen tube growth was drastically reduced or inhibited, the plants would be male-sterile. Male sterility is easily observed in *Arabidopsis* because siliques will not be formed, meaning the pistils will not elongate.

SYP22pro:R1, *SYP22pro:R2*, *XIJpro:R1*, and *XIJpro:R2* were transformed into *WT*. T1 plants were selected by antibiotic resistance and confirmed by genotyping (**Table 2.6**). No obvious defects were observed for any of the T1 plants (data not shown). T2 seeds were germinated on selection medium and lines with a resistant : sensitive ratio larger than 3 : 1 were not tested any further because they likely contained multiple insertions. Surprisingly, multiple lines had resistant : sensitive ratios lower than 3 :1, such as 2 : 1 or 1 : 3. This segregation pattern could only occur if the antibiotic resistance gene was silenced in those lines. These lines were examined for fertility defects along with lines that exhibited the expected 3 : 1 ratio (**Table 2.6**).

Twelve T2 seedlings from each line that was screened further were transferred to soil, and then 8-week-old plants were examined for fertility defects. One *SYP22pro:R1*, one *XIJpro:R1*, and six *XIJpro:R2* lines exhibited some degree of sterility (**Table 2.6**). In most of the lines with fertility defects, not all 12 T2 plants were sterile. *SYP22pro:R1* had the weakest phenotype; all flower structures appeared normal; however, siliques were not always formed (**Figure 2.6**). *XIJpro:R1* had the most severe phenotype; all of the plants transferred to soil were completely sterile. The plants had lancet-shaped rosette leaves and abnormally small flowers

Table 2.6: Plant lines generated for the pollen artificial microRNA experiment

Construct	# of independent lines	# of lines examined	# of lines with fertility defect
SYP22pro:R1	27	14	1
SYP22pro:R2	11	7	0
XIJpro:R1	24	12	1
XIJpro:R2	17	8	6

Figure 2.6: Subtle phenotypes detected in a *SYP22pro:R1* line.

One *SYP22pro:R1* line exhibited a slight fertility defect. The majority of siliques on some plants were shorter than normal (**A**) while some plants appeared completely normal (**B**). Flowers from plants with reduced fertility appeared normal and had numerous pollen grains (**C**).

with short filaments (**Figure 2.7**). Interestingly, the anthers appeared normal; however, mature flowers lacked free pollen. The observation that *XIJpro:R1* plants had defects in vegetative tissues was not consistent with the *XIJ* promoter being primarily active in pollen (Hruz et al., 2008). However, the transgene could have inserted immediately downstream of a promoter that is active throughout the plant. Sterile *XIJpro:R2* plants appeared normal except no siliques were formed and the anthers appeared shriveled and brown, suggesting a sporophytic defect (**Figure 2.8**). In one *XIJpro:R2* line, the plants with reduced fertility were completely sterile. In the other five lines, only certain branches were affected on the plants with reduced fertility.

T2 seeds from all eight lines with fertility defects were grown up again; however, this time without selection to determine if the fertility defects segregated with the transgene. 45 to 60 seedlings per line were transferred to soil, and 8-week-old plants were examined for the fertility defects. Sterile or partially sterile plants were not observed in the five weaker lines of *XIJpro:R2*, so these lines were not examined further. For the remaining three lines, each T2 plant was genotyped to determine whether or not the artificial microRNA construct was present and examined for the sterility phenotype (**Table 2.7**). For *SYP22pro:R1*, not all of the partially sterile plants contained the artificial microRNA construct, so reduced expression of class XI myosins could not be responsible for this phenotype. For *XIJpro:R1*, all of the plants contained the artificial microRNA (**Table 2.7**), indicating multiple insertions were likely present. However, only ~25% of the plants exhibited the strong phenotype (**Table 2.7** and **Figure 2.7**). This could be due to the copy number of the transgene, meaning there is a level of artificial microRNA expression that has to be reached before growth and fertility defects are detectable. An alternative explanation would be that one of the insertions occurred within a gene that when both copies are mutated results in the observed phenotype. The *XIJpro:R2* line also might have contained multiple insertions due to the deviation from a 3 : 1 ratio (**Table 2.7**). Similarly to the

Figure 2.7: Strong defects observed in an *XIJpro:R1* line.

(**A**) When grown without selection, some *XIJpro:R1* plants were reduced in size and completely sterile (left), while some plants were fertile and normal in appearance (right). (**B**) Sterile *XIJpro:R1* flowers were smaller in size, had short filaments with yellow anthers, and lacked free pollen.

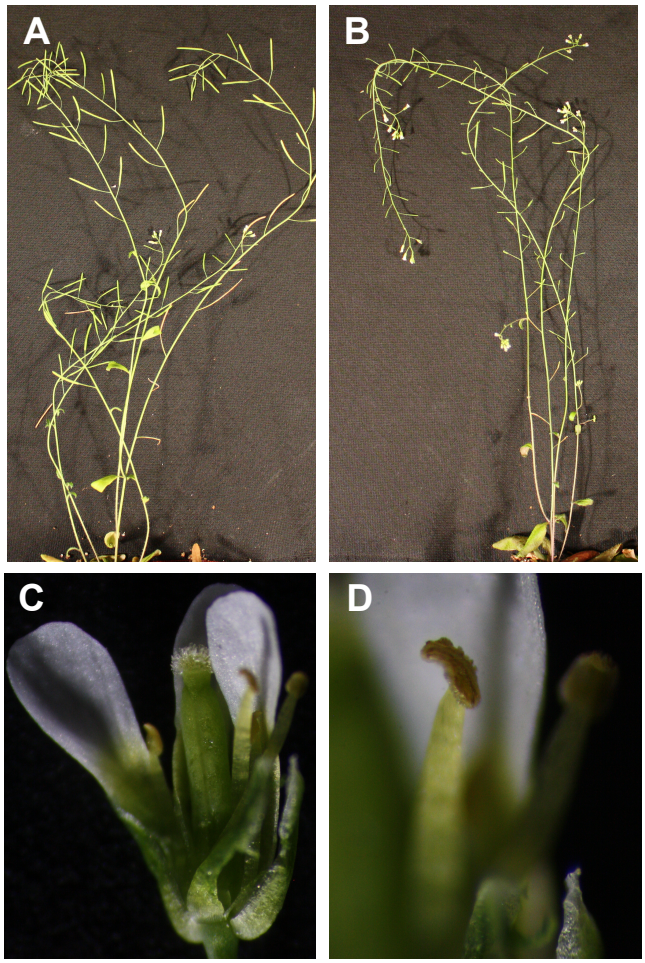

Figure 2.8: Abnormal anthers present in an *XIJpro:R2* line.

The *XIJpro:R2* line with the strongest phenotype had some plants that appeared normal (**A)**, while some plants were completely sterile (**B**). For sterile plants, stigmas from open flowers lacked pollen (**C**), and the anthers were brown and shriveled (**D**).

Table 2.7: T2 plants grown without selection were genotyped and examined for defects.

Construct	Total # of plants	# of plants with construct	# of sterile plants
SYP22pro:R1	47	26	10
XIJpro:R1	60	60	16
XIJpro:R2	53	47	14

XIJpro:R1 line, only ~25% of the plants that contained R2 were sterile.

To determine whether or not the phenotypes in *XIJpro:R1* and *XIJpro:R2* were due to a mutation caused by the insertion of the transgene, both lines were crossed to *WT*. The F1 plants were grown up and examined for fertility defects (**Table 2.8**). F1 seeds were formed from using sterile *XIJpro:R1* and *XIJpro:R2* plants as the female in crosses with non-sterile plants. This supported the hypothesis that the sterility was a result from defects in either the male gametophyte or sporophytic tissues involved in pollen development. If the sterility phenotype was due to the construct being inserted into a sporophytic gene that when homozygous recessive the plants were sterile, all of the F1 plants would be fertile from a cross with *WT*. This was observed for both *XIJpro:R1* and *XIJpro:R2* lines (**Table 2.8**). The single sterile plant from *WT* x *XIJpro:R2* could have been from a contamination. Since sterile plants were grown in the same pots as non-sterile siblings, a pollen grain from the non-sterile sibling could have landed on the stigma of the sterile plant used in the cross. Obtaining only fertile F1 plants from backcrossing to *WT* does not completely rule out the possibility that the sterility phenotypes were related to the number of copies of the artificial microRNA construct. F1 plants could have been fertile because the number of copies of the artificial microRNA was drastically reduced from the backcross to *WT*. Therefore, a sterile *XIJpro:R2* plant was also crossed to a non-sterile sibling. If the sterility phenotype was due to the transgene being inserted into a gene required for anther development that when homozygous recessive the plants were sterile, fertile siblings would either be heterozygous for the mutation or *WT*. If a homozygous recessive mutant (sterile) was crossed to a heterozygous mutant (fertile), F1 plants would have a 1 : 1 ratio of sterile : fertile plants. This was observed for the sibling cross (**Table 2.8**; $\chi^2 = 0.81$, $p = 0.37$). A 1 : 1 ratio most likely would not have been observed if the sterility phenotype was a result of the number of copies of the artificial microRNA. Given the cross results (**Table 2.8**) and that approximately only ¼ of

Table 2.8: Phenotypes of F1 plants resulting from crosses with the sterile lines.

Male parent	Female parent	# of sterile F1 plants	# of fertile F1 plants
WT	*XIJpro:R1* (sterile)	0	27
WT	*XIJpro:R2* (sterile)	1	41
XIJpro:R2 (fertile)	*XIJpro:R2* (sterile)	18	13

the T2 plants were sterile (**Table 2.7**), the sterility phenotypes in the *XIJpro:R1* and *XIJpro:R2* lines were almost certainly a result from a single gene, recessive mutation caused from the insertion of the transgene. Although the drastic fertility defects were not due to the artificial microRNAs, these lines could still have slight defects in pollen tube growth that could be identified by performing *in vitro* pollen tube growth experiments.

2.4: Discussion

There are 13 class XI myosins in *Arabidopsis thaliana*, and analysis of higher order mutants has revealed that there is redundancy among some of the myosins (Prokhnevsky et al., 2008; Peremyslov et al., 2010). Some myosin XI genes have not been studied as much as the more highly expressed genes in vegetative tissues, such as *XIK*, *MYA2*, and *XI-I*. In particular, little attention has been given to the myosin XI genes expressed in pollen: *XIA*, *XIB*, *XIC*, *XID*, *XIE*, and *XIJ* (Peremyslow et al., 2011; Sparkes, 2011). Since it takes years to generate different combinations of higher order mutants, a faster approach would be to generate artificial microRNAs that would target multiple class XI myosins at once (Schwab et al., 2006). Therefore, two artificial microRNAs were designed to target 9 and 6 out of the 13 class XI myosins.

Constitutive expression of myosin XI artificial microRNAs resulted in shorter root hairs

Initially, we expressed the two artificial microRNAs using a dexamethasone-inducible system that also included a GUS reporter gene (Craft et al., 2005). Both the artificial microRNA and the GUS reporter gene should be expressed when dexamethasone is present. In all of the lines tested, the GUS reporter gene was expressed in the presence of dexamethasone. It is important to note that the expression of the GUS reporter gene and the artificial microRNA were most likely poorly correlated (Craft et al., 2005). Selection of lines with strong positive GUS

staining ensured that the plants examined contained a functional LhGR; however, it did not guarantee that the artificial microRNA was highly expressed in those lines. Both artificial microRNAs, *R1* and *R2*, should target *MYA2* and *XIB*. *mya2* and *mya2 xib* mutants have shorter root hairs than *WT* (Peremyslov et al., 2008; Prokhnevsky et al., 2008), so when *R1* and *R2* were expressed, they should have had shortened root hairs. Only constitutive expression of the artificial microRNAs resulted in shortened root hairs. This suggests that the artificial microRNAs were probably not expressed well using the dexamethasone-inducible system. RNA was extracted and cDNAs were generated from the roots of *35Spro:R1* and *35Spro:R2* lines; however, there were problems with the RT-PCR, so the reduced expression of the targeted myosin XI genes was not confirmed. In the future, quantitative RT-PCR could be performed on these lines to determine which myosins were effectively target by *R1* and *R2*. Besides having shorter root hairs than *WT*, the *35Spro:R1* and *35Spro:R2* lines had no other obvious phenotypes.

Expression of myosin XI artificial microRNAs in pollen did not drastically reduce fertility

R1 and *R2* should target 5 and 3, respectively, of the pollen myosins when expressed from the native *SYP22* and *XIJ* promoters, which are both active in pollen (Hruz et al., 2008). If silencing of the pollen myosins reduced pollen tube growth, a reduction in overall fertility would have been expected. Drastic fertility defects resulting from the artificial microRNA constructs were not detected. It is possible that the pollen expressed artificial microRNAs do slightly reduce pollen tube growth; however, to detect a subtle pollen tube growth defect, multiple lines for each construct would have to be thoroughly examined. The number of seeds per silique could be counted, or *in vitro* pollen tube growth experiments could be performed. However, the amount of work required to possibly detect a slight defect would have to be considered before examining these lines further. An alternative approach could be to express the artificial microRNAs in pollen using a stronger promoter, such as the LAT52 promoter (Twell et al., 1990). It is possible

that expressing the artificial microRNAs at a higher level would result in an easily detectable reduction in fertility.

Conclusions

The dexamethasone-inducible system did not work well with the artificial microRNAs. The artificial microRNAs were either not expressed or not expressed at a high enough level in the presence of dexamethasone. Expression of the artificial microRNAs could be tested by performing real-time PCR on cDNA samples from the inducible lines (Shi and Chiang, 2005). *R1* and *R2* most likely can reduce the expression of some myosin XI genes. When the artificial microRNAs were constitutively expressed, the seedlings had shorter root hairs than *WT*. This was a phenotype that had been observed in single and double myosin XI mutants (Ojangu et al., 2007; Peremyslov et al., 2008; Prokhnevsky et al., 2008). It will be important to confirm which myosin XI genes were efficiently targeted by *R1* and *R2*. As for expressing *R1* and *R2* in pollen, there was no drastic decrease in fertility, which could have been due to a few reasons. The artificial microRNAs might not have been expressed at a high enough level; the pollen myosins might not have been targeted well; or reducing the expression of multiple pollen myosins does not result in a drastic decrease in fertility (but see Chapter 3).

Overall, *R1* and *R2* might not have been the best artificial microRNAs to use in this experiment. Using the latest version of the web application used to design *R1* and *R2*, these sequences are no longer recommended for silencing multiple class XI myosins. Recently, it has also been shown that artificial microRNAs expressed using the *miR390a* precursor are expressed at significantly higher levels than the same artificial microRNAs expressed using the *miR319a* precursor (Carbonell et al., 2014), which was used in this study. Ultimately, if this experiment were started over today, it would be designed differently. There are also a number of tools available now that make design and testing of artificial microRNAs much more efficient. For

example, a method for testing the effectiveness of artificial microRNAs using transient expression in protoplasts has been developed (Li et al., 2013). Using this approach, only optimal artificial microRNAs would be transformed into plants, thus drastically reducing the time required to obtain transgenic plants with artificial microRNAs that efficiently silence their target mRNAs. It should be noted that even if a novel phenotype were detected using a single artificial microRNA that reduces the expression of multiple myosins, it would still be necessary to examine other mutant lines. A single artificial microRNA line cannot be used to determine exactly which myosins are required for a particular function. Either higher order myosin XI mutants using T-DNA insertion lines or a collection of specific artificial microRNA lines would have to be examined.

Chapter 3: Phenotype Survey of Pollen Myosin Mutants Using a Reverse Genetics Approach

- *Undergraduate students who earned research credit in this lab contributed to the results in this chapter. Whitnee Ferari assisted in genotyping the new T-DNA lines for* XIJ *and in making the* XIJpro:YFP-XIJ *construct. Tarah McClain, Matt Buchanan, and Kenneth Hoang helped count seeds, and Jeremiah Glass observed the offspring from the* XIB *pollen competition experiment. Matt Buchanan imaged and analyzed a majority of the pollen tubes grown* in vitro *and observed the offspring from the* XIA *pollen competition experiment. Tanner Beard assisted in the* in vivo *pollen tube growth experiment.*

3.1: Introduction

Class XI myosins have been shown to be required for the expansion of various cell types in *Arabidopsis thaliana*. Single mutants of *MYA2* and *XIK* have shorter roots hairs (Ojangu et al., 2007; Peremyslov et al., 2008), while higher order mutants involving these and other genes show progressively more stunting that coincides with reduced cell expansion in leaves (Prokhnevsky et al., 2008; Peremyslov et al., 2010; Ojangu et al., 2012). MYA1, MYA2, and XIK are also involved in trichome branch and stigmatic papillae elongation (Ojangu et al., 2007; Ojangu et al., 2012). Additionally, root hairs of the *xik* mutant were shown to have a slower growth rate than wild-type root hairs (Park and Nebenführ, 2013). Even though class XI myosin mutants have been studied extensively in various vegetative cell types, no studies have examined pollen tube growth in myosin mutants.

Pollen tubes undergo rapid tip growth making them an ideal cell type to study cell expansion. Drug treatments to disrupt microtubules or actin filaments or to inhibit myosins have been used to suggest which cytoskeletal elements play an important role in pollen tube growth. In gymnosperm pollen, both microtubules and the acto-myosin network are required for tube elongation (Anderhag et al., 2000). On the other hand, the acto-myosin network, and not microtubules, is required for pollen tube elongation in angiosperms (Franke et al., 1972; Mascarenhas and Lafountain, 1972; Heslop-Harrison and Heslop-Harrison, 1989a; Tominaga et al., 2000). Although class XI myosins have been suggested to be involved in angiosperm pollen tube growth for over a decade, direct evidence linking class XI myosins to pollen tube growth is still missing. There is one study that suggested class XI myosins are involved in pollen development where *Oryza sativa XIB* was shown to be required for normal pollen development under short-day conditions (Jiang et al., 2007).

In *Arabidopsis thaliana*, there are 13 class XI myosin genes of which *XIA*, *XIB*, *XIC*, *XID*, *XIE*, and *XIJ* are preferentially expressed in pollen (Peremyslow et al., 2011; Sparkes, 2011). Some functional redundancy among the pollen myosins is predicted since vegetative myosins have been shown to have partially overlapping roles in growth and development (Prokhnevsky et al., 2008; Peremyslov et al., 2010; Ojangu et al., 2012). Recently, a phylogenetic analysis based on myosin motor domains was used to divide class XI myosins into five subgroups with three subgroups being further divided into subtypes. *XIA* and *XID* are members of subtype Myo11A while *XIC* and *XIE* are in subtype Myo11C (Mühlhausen and Kollmar, 2013). This means that of the six pollen myosins, XIA and XID, as well as XIC and XIE, are most likely to have overlapping functions based on sequence similarity. It is important to note that *XIJ* belongs to subtype Myo11D which is only present in eudicots and contains mostly short-tailed myosins (Mühlhausen and Kollmar, 2013). Short-tailed myosins, including *XIJ*, lack the normal class XI myosin domains that follow the coiled-coil domain (Kinkema and Schiefelbein, 1994; Li and Nebenführ, 2007), but instead contain a conserved C-terminal sequence which encodes ~100 amino acids (Mühlhausen and Kollmar, 2013).

To address the question as to which pollen myosins are responsible for normal pollen tube growth in *Arabidopsis thaliana*, we isolated T-DNA insertion mutants for all six pollen myosins and examined them for defects in overall fertility, pollen fitness, and pollen tube growth. Myosin mutants have reduced cell expansion in various cell types. Since pollen tubes undergo rapid tip growth, we hypothesized that pollen myosin mutants would exhibit reduced pollen tube growth and therefore have reduced pollen fitness and overall fertility.

3.2: Methods

3.2.1: Mutant lines

T-DNA insertion lines for myosin genes were ordered from the Arabidopsis Biological Resource Center (**Table 3.1**). Homozygous T-DNA insertion lines were identified by genomic PCR using three different primer pairs: 1) XT#-LP and XT#-RP to identify the wild-type allele, 2) XT#-LP and TP to test for the insertion, and 3) XT#-RP and TP to test for the insertion. X refers to the gene letter, # refers to the allele number. For example, *AT2* genomic DNA was tested with AT2-LP and AT2-RP primers to detect the wild-type allele. The TP primers used were T-LBa-1 for SALK lines, SAIL-LB1 for SAIL lines, and GABI-LB for GABI-Kat lines (**Table 3.2**).

Several crosses were made to obtain double mutants, and potential F1 seeds were collected and grown up. Potential F1 plants were genotyped for presence of both T-DNA insertions. F2 seeds were collected from verified double heterozygous plants. F2 plants for 3 *xia xid* and 3 *xic xie* lines were genotyped, and double homozygous mutant plants were identified.

3.2.2: RNA extraction and RT-PCR

For each T-DNA insertion mutant, the presence/absence of the full-length transcript encoded by the disrupted gene was tested by RT-PCR on flower cDNA using gene specific primers (**Tables 3.2 and 3.3**). RNA was isolated from whole flowers. At least 100 mg of flowers was collected for each genotype and froze in liquid nitrogen. The flowers were ground slightly before the addition of 500 μl of Trizol (Sigma). The tissue was ground completely, and another 500 μl of Trizol was added. After 200 μl of chloroform was added, the samples were centrifuged at 11,000 rpm for 15 minutes at 4°C. The top aqueous layer was transferred to a new microfuge tube, and the RNA was precipitated with isopropanol and washed with 75% ethanol in DEPC dH_2O. Pellets were dissolved in 50 μl of dH_2O, and cDNAs were generated using Superscript III

Table 3.1: List of T-DNA insertion lines

Gene	Stock name	Local name	Allele name	Primer used[#]
XIA	SALK_086989*	*AT2*	*xia-1*	LP
	SALK_117717*	*AT4*	*xia-2*	LP
XIB	SALK_113062*	*BT2*	*xib-1*	LP
	SALK_016579*	*BT3*	*xib-2*	Not tested
	SALK_087951*	*BT5*	-	Not tested
XIC	SALK_097302*	*CT1*	-	Not tested
	SALK_002170*	*CT2*	-	Not tested
	SALK_104026*	*CT5*	-	Not tested
	SALK_129231C	*CT6*	*xic-1*	RP
	GABI_262B03	*CT7*	-	RP
	SAIL_905_C08	*CT8*	*xic-2*	RP
	SALK_051582	*CT9*	-	No T-DNA
XID	SALK_082078*	*DT2*	-	Not tested
	SALK_029987*	*DT3*	-	Not tested
	SALK_029988	*DT4*	-	No T-DNA
	SALK_033198	*DT6*	*xid-2*	RP
	SALK_033208	*DT7*	-	No T-DNA
	SAIL_607_G06	*DT8*	*xid-1*	LP or RP
XIE	SALK_122989*	*ET1*	-	Not tested
	SALK_119881*	*ET2*	-	Not tested
	SALK_044890*	*ET4*	-	Not tested
	SALK_089338C	*ET6*	*xie-2*	LP or RP
	SALK_025293C	*ET7*	*xie-3*	LP or RP
	SALK_072023	*ET8*	*xie-1*	RP
	SALK_072025	*ET9*	-	No T-DNA
XIJ	SALK_026367*	*JT1*	-	Not tested
	SALK_048730	*JT2*	-	No T-DNA
	SALK_063159	*JT3*	*xij-2*	LP or RP
	SAIL_341_F05	*JT6*	*xij-3*	LP or RP
	SALK_005198C	*JT7*	*xij-1*	RP

* Homozygous T-DNA insertion lines were identified by Eunsook Park.

[#] Primer used to detect the T-DNA insertion.

Table 3.2: List of primers

Gene	Primer name	Primer sequence (5' to 3')
SALK T-DNA	T-LBa-1	TGGTTCACGTAGTGGGCCATCG
SAIL T-DNA	SAIL-LB1	CAGAAATGGATAAATAGCCTTGCTTCC
GABI-Kat T-DNA	GABI-LB	ATATTGACCATCATACTCATTGC
RuBisCO	Rbs-F	CATCCACCGTGCAATGCACGCTG
	Rbs-R	AGCAGCAGCTAGTTCAGGACTCC
NIP4;1	NIP4;1-F	GGAAGATCTATGTCTTCGCATAGTGAT
	NIP4;1-R	GGAAGATCTTTAAGTCTTAGAACTAGA
XIA	AT2-LP	TGCAACAACATTTCAACCAGG
	AT2-RP	TCCGTGGTGCTCAAACTCTCC
	AT4-LP	CGTTCAACCTCTTCCCCGAAT
	AT4-RP	GGATCCTACGAACTGCATTCAAGA
	M11.A-F1	GGAGTCATCGGGAGATAAG
	M11.A-R1	GAAGCTGACTTTACATTCGC
	M11.A-F2	GCTCCGGAATGGCGCTTCAGCCAAAG
	M11.A-R2	CTCGTCTAGAAGGGCAATG
	M11.A-F3	GCTCTAGACGAGGCTTGCATG
	M11.A-R3	CTCCATGGAACTTACCAATG
	M11.A-F4	GTTCCATGGAGGAGAAAATC
	M11.A-R4	CGGCGGCCGCGGAATGTTATACCAAG
XIB	BT2-LP	TTCCAGTGGCCTAGATTGGCTT
	BT2-RP	TTTACATGAGAAGCTCGGCGG
	M11.B-D-F1	ACGGGATCCCCGAGAATTTCAAAAGG
	M11.B-Stop-R1	GCAGCGGCCGCTTGCAAGAAAGAAACAACCC
XIC	M11.C-D-F1	ACGTCCGGACCAAGAACATCGAGGG
	M11.C-Stop-R1	GCAGCGGCCGCAGAATCACTCAGAGA
	CT5-RP	GGCAGCCTTTGTTTGCTTCCT
	CT6-LP	GGAGCTGGAAAAACTGAAACC
	CT6-RP	TTGATAACTTCCTCGGGTGTG
	CT7-LP	TTATGATCACACCCGAGGAAG
	CT7-RP	AAAGACCCACAACAAAGGGAC
	CT8-LP	TGGTTTGCATTTGGGTTAATC
	CT8-RP	AGTCAACCCACGAAACATTTG
	CT9-LP	GTTCGAGGGTATTTGCCCTAG
	CT9-RP	TGGTTAATCGAATGGCTATGC
XID	11.D-GSP-F	AACAGGAGGTTCCCGTCA
	11.D-GSP-R	AGAGGTTAGTCGTTAGATCA
	DT4-LP2	CTGCATCAACTTAGGTGTGGG
	DT4-RP2	AGCCACATTGAGTGGTAATCG
	DT6-LP	ATACCATCAAGAAGGTTCGGG
	DT6-RP	CTTTTCCGGTGGATTCTCTTC
	DT7-LP	ATGCAGGAATTTGTTGACGTC
	DT7-RP	TGGGTGAATTCTCCTCAGATG
	DT8-LP	GGTGTGCAACTTTCACTCTCC

Underlined sequences are restriction sites used in cloning.

Table 3.2: Continued

Gene	Primer name	Primer sequence (5' to 3')
XID	DT8-RP	GAGGCAACGGAGAGAAGGTAG
XIE	M11.E-F1	CTTAAGGCAAGTTGAGGCG
	M11.E-R1	CATCTCCGATCTCTATCCG
	ET2-RP	AGGTTCAAGCCACAAACGGAA
	ET4-RP	CAGATTTCTGATCCAGAGCGCA
	ET5-RP	GGGTCATCCCAAGACGTTTCA
	ET6-LP	GCAGAGGTGAACCATCTGATTC
	ET6-RP	ATCTGATCGCCAATGAATACG
	ET7-LP	TGCTGCAACTTCTCATTTGTG
	ET7-RP	GCTGCACCACAGGAGGTATAC
	ET8-LP*	TTGGGATGACCCAACTTGTAC
	ET8-RP*	GCCTGGAATACACTGAAGCTG
XIJ	M11.J-F1	GCACTAGTATGGCTGAAAACATAATGGTGG
	M11.J-R1	GAGTCTAGAGTATATTGTCTTTG
	M11.J-F2	TATACTCTAGACTCTTTGATTGG
	M11.J-R2	CGGGATCCTCAAAAGTAATCTTCGAAGCCC
	JT2-LP2	TACACTCAAGGGGTCAGGTTG
	JT2-RP2	ACTTCTTCTGGGGTGACCATC
	JT3-LP2	CTCACCTTGCAAAGTGGAGTC
	JT3-RP2	CTCAACTTGCAATAAGGCCTG
	JT4-LP	TCCCTCACTGCAGAAGTTGAGATG
	JT4-RP	TCGAAGCCCCCTTCCTTATCA
	JT6-LP	GCTTCAGCACATTTTCTTTCG
	JT6-RP	AATCAACTTGCAGGCGTATTG
	JT7-LP	GTCGTAGCTCTCAGTTCCTGC
	JT7-RP	TTCCATCGAATCAGAAGATGG

* Primers were also used for *ET9*.
Underlined sequences are restriction sites used in cloning.

Table 3.3: Primer pairs used for RT-PCR

Gene	Primers used	Product size (bp)	PCR condition
RuBisCO	Rbs-F & Rbs-R	499	Varied
NIP4;1	NIP4;1-F & NIP4;1-R	870	A54E60C
XIA	M11.A-F1 & M11.A-R1	678	A58E60C
	M11.A-F2 & M11.A-R2	1,524	A58E120D
	M11.A-F3 & M11.A-R3	1,681	A58E120D
	M11.A-F4 & M11.A-R4	2,026	A58E120D
XIB	M11.B-D-F1 & M11.B-Stop-R1	825	A60E90D
XIC	M11.C-D-F1 & M11.C-Stop-R1	711	A58E90D
	CT6-LP & CT6-RP	679	A58E90D
	CT7-LP & CT7-RP	640	A58E90D
	CT8-RP & CT5-RP	961	A58E90D
XID	11.D-GSP-F & 11.D-GSP-R	1,953	A56E120E
	DT4-LP2 & DT6-RP	2,520	A60E180D
XIE	M11.E-F1 & M11.E-R1	787	A56E60D
	ET4-RP & ET7-LP	644	A58E60E
	ET2-RP & ET8-LP	724	A58E60E
XIJ	JT4-LP & JT4-RP	467	A62E30C
	JT3-LP2 & JT6-LP	916	A58E90D

Reverse Transcriptase following the manufacturer's instructions (Invitrogen). 1-2 μl of cDNA was used for PCR.

3.2.3: Constructs and plant transformations

The native *XIJ* promoter, which extended 757 base pairs upstream of the *XIJ* start codon and included the first 9 base pairs of the *XIJ* coding sequence (21,534,040-21,534,805 based on TAIR10), was used to drive expression of the YFP peroxisome marker (Nelson et al., 2007) and *XIJ* complementation constructs. The YFP peroxisome construct was moved into the binary plasmid pVKH18 (Batoko et al., 2000) and transformed into *WT* (then referred to as *WT**) by the *Arabidopsis* floral dip method (Weigel and Glazebrook, 2002). For the *XIJ* complementation construct, the promoter was followed by *YFP*, a linker sequence that encodes GGPGGSG, and the full-length *XIJ* coding sequence. This construct was moved into the binary plasmid pPZP221 (Hajdukiewicz et al., 1994) and transformed into *xij-1* by the *Arabidopsis* floral dip method (Weigel and Glazebrook, 2002). The full-length *XIJ* cDNA was obtained by overlapping PCR from flower cDNA with the primers M11.J-F1, M11.J-R1, M11.J-F2, and M11.J-R2 (**Table 3.2**).

The native *XIA* promoter, which extended 709 base pairs upstream of the *XIA* start codon and included the first exon, first intron, and first 8 base pairs of the second exon of *XIA* (1,261,414-1,262,561 based on TAIR10), was used to drive expression of the *XIA* complementation construct. The promoter was followed by *YFP*, a linker sequence that encodes GGPGGSG, and the full-length *XIA* coding sequence including 38 base pairs of the 3'UTR. The construct was moved into the binary plasmid pFGC19 (Nelson et al., 2007) and transformed into *WT* and *xia-2* by the *Arabidopsis* floral dip method (Weigel and Glazebrook, 2002). The full-length *XIA* cDNA was obtained by overlapping PCR from flower cDNA with the primers M11.A-F2, M11.A-R2, M11.A-F3, M11.A-R3, M11.A-F4, and M11.A-R4 (**Table 3.2**).

3.2.4: Seeds per silique analysis

Plants were grown, as described in Chapter 2, in individual 6 cm circular pots (except the *WT* and *xid-2* set with 4 plants per 8 cm square pots) until maturity, and individual dry siliques were collected. The silique length was measured to an accuracy of 0.5 mm. Unopened siliques were manually opened, and the seeds were counted. Mutants that were statistically different from *WT* were identified by a Mann-Whitney unpaired t-test using Prism 6 software (GraphPad). Which genotypes were grown and which siliques were collected varied between experiments. In one experiment, the plants were fertilized (MiracleGro, ¼ tsp/gallon) once every two weeks. In all other experiments, no fertilizer was used.

3.2.5: Pollen competition experiment

Seeds for FTL 1285 and FTL 2217 were graciously donated by Dr. Greg Copenhaver (University of North Carolina, Chapel Hill, NC). FTL 1285 and FTL 2217 are fluorescently tagged lines that have pollen specific cytoplasmic DSRed2 or AmCyan markers inserted at positions 80,614 or 2,007,280 on chromosome 1, respectively(Francis et al., 2007). *XIA* (1,262,123-1,272,376) and *XIB* (1,086,495-1,096,146) are located nearby these insertion sites on chromosome 1. Positions are based on TAIR10.

WT, *xia-1*, and *xib-1* were each crossed to FTL 1285, and *WT*, *xia-1*, and *xia-2* were each crossed to FTL 2217. Pollen from the F1 plants was used to pollinate *ms1* plants. Seeds for *ms1* (Wilson et al., 2001) were kindly provided by Dr. Ravi Palanivelu (University of Arizona, Tucson, AZ). Pollen from the resulting offspring was examined using an AxioObserver.Z1 microscope (Zeiss) equipped with filters for RFP and CFP fluorescence (63 HE and 47 HE, Zeiss). If fluorescence was present in half of the pollen grains, the offspring was counted as a *WT* offspring; if fluorescence was not present, the offspring was counted as a test offspring. The observed segregation ratio was tested against the expected 1:1 ratio using a chi-square analysis.

Before some of the hand pollinations, the F1 and *ms1* plants were watered with fertilizer (MiracleGro, ¼ tsp/gallon).

3.2.6: *in vitro* pollen tube growth, pollen germination efficiency, and pollen hydration

WT or mutant flowers were brushed together with *WT** flowers onto solid pollen germination medium (PGM; 0.01% H_3BO_3, 5 mM $CaCl_2$, 1 mM $MgSO_4$, 5 mM KCl, 10% sucrose, 1% SeaPlaque GTG Agarose, pH 7.75) on a microscope slide and incubated in a dark, humid chamber at 22°C (Boavida and McCormick, 2007). Incubation times were 3 hours for pollen tube growth experiments and 1-4.5 hours for pollen germination efficiency experiments. Pollen tubes were observed on an AxioObserver.Z1 microscope (Zeiss) equipped with filters for YFP fluorescence (46 HE, Zeiss). Images were captured using a digital camera (Orca ER; Hamamatsu Photonics) operated by OpenLab5 software (Improvision/Perkin Elmer). For pollen tube length measurements, DIC images were captured using a 10X objective, and tube lengths were measured using OpenLab5 software. For pollen tube growth rate measurements, DIC time-lapse images were taken at 10-second intervals for 1.5 minutes using a 40X objective. Growth rate was calculated by measuring the amount of elongation that occurred within 1 minute using OpenLab5 software. *WT* and mutant measurements for tube length and growth rate were adjusted to the *WT** measurements for each slide. Specifically, the average of all *WT** measurements was divided by the average *WT** measurements from each slide to obtain the correction factor for the test sample on each slide. The *WT* or mutant measurements for each slide were multiplied by the corresponding correction factor. This correction factor allowed for measurements from multiple trials of the same genotype to be combined for the analysis. Mutants that were statistically different from *WT* were identified by a Mann-Whitney unpaired t-test using Prism 6 software (GraphPad). For determining percentage of pollen germination, DIC and YFP images, covering the entire area of PGM where pollen grains were present, were captured using a 10X objective.

The numbers of pollen grains and pollen tubes for mutant and *WT** were manually counted, and the germination percentages were calculated. For the pollen hydration experiment, *WT** and *xij-1* flowers were dabbed onto a coverslip. DIC and YFP images of the pollen grains were captured using a 10X objective. 10 µl of dH_2O was added to the coverslip, and the pollen grains were immediately re-imaged. Pollen grain widths were measured using OpenLab5 software.

3.2.7: Germination efficiency in the presence of 'cut pistil' exudate

'Cut pistil' exudate was obtained by soaking 36 'cut pistils' overnight in 120 µl of PGM lacking agarose (Qin et al., 2011). Cut pistils included the stigma and style of *ms1* pistils. 5 µl of either liquid PGM or PGM with exudate was pipetted onto the center of solid PGM. Two flowers of either *WT* or *xij-1* were dipped into the droplet before incubating the slide for 5 hours in a dark, humid chamber at 22°C. For determining percentage of pollen germination, DIC images, covering the entire area of PGM where pollen grains were present, were captured using a 10X objective. Pollen grains and tubes were counted, and the germination percentages were calculated.

3.2.8: *in vivo* pollen tube growth

Pollen tube growth *in vivo* was visualized by staining callose with aniline blue (Mori et al., 2006). *WT* or mutant pollen was used to pollinate *ms1* flowers. Pollinated pistils were removed at various time points following pollination and placed in a fixing solution (3:1, ethanol : acetic acid). The pistils were aspirated and left in the fixing solution overnight. The fixed pistils were rehydrated by soaking for 10 minutes in each of the following solutions: 70% ethanol, 50% ethanol, 30% ethanol, and dH_20. The pistils were softened overnight in 8 M NaOH and washed for 10 minutes in dH_20. Aniline blue solution (0.11% aniline blue in 0.1 M K_2HPO_4, pH ~11) was added, and the samples were covered with aluminum foil for two hours. The aniline blue solution was made 1-3 days prior to use and was stored at 4°C. Immediately before use, glycerol

was added to the aniline blue solution to a final concentration of 2%. After the two-hour incubation, the pistils were transferred to microscope slides. A small amount of aniline blue solution was added to each slide before placing a coverslip on it.

The pollen tubes in the pistils were observed using a 20X objective on an Axiovert 200 M microscope (Zeiss) equipped with filters for DAPI fluorescence (62002, Chroma). Images covering the length of each pistil were captured using a digital camera (Orca ER; Hamamatsu Photonics) using OpenLab5 software (Improvision/Perkin Elmer). Using OpenLab5 software, the furthest distance traveled by a pollen tube was measured for each pistil. This was the distance from the highest (furthest from the style) pollen grain on the stigma to the lowest (furthest from the style) pollen tube tip in the ovary (**Figure 3.1**). Pollen tubes were not clearly visible in the style; therefore, if the pollen tube tips had not emerged from the style for a given pistil, the distance from the highest pollen grain on the stigma to halfway through the style was used for that measurement. Only pistils with more than 5 pollen grains on the stigma were used in the analysis since low pollen density negatively affected pollen germination and growth (data not shown). Statistically significant differences were calculated by a Mann-Whitney unpaired t-test using Prism 6 software (GraphPad).

3.3: Results

3.3.1: Identification of knockout mutants

To investigate the function of class XI myosins during pollen tube growth, a total of 14 T-DNA insertion lines for *XIA* (At1g04600), *XIB* (At1g04160), *XIC* (At1g08730), *XID* (At2g33240), *XIE* (At1g54560), and *XIJ* (At3g58160) were previously isolated by Eunsook Park (Table 3.1). Four additional T-DNA insertion lines were ordered from the *Arabidopsis* Biological Resource Center for each *XIC*, *XID*, *XIE*, and *XIJ* (**Table 3.1**). Presence of the T-DNA insertion

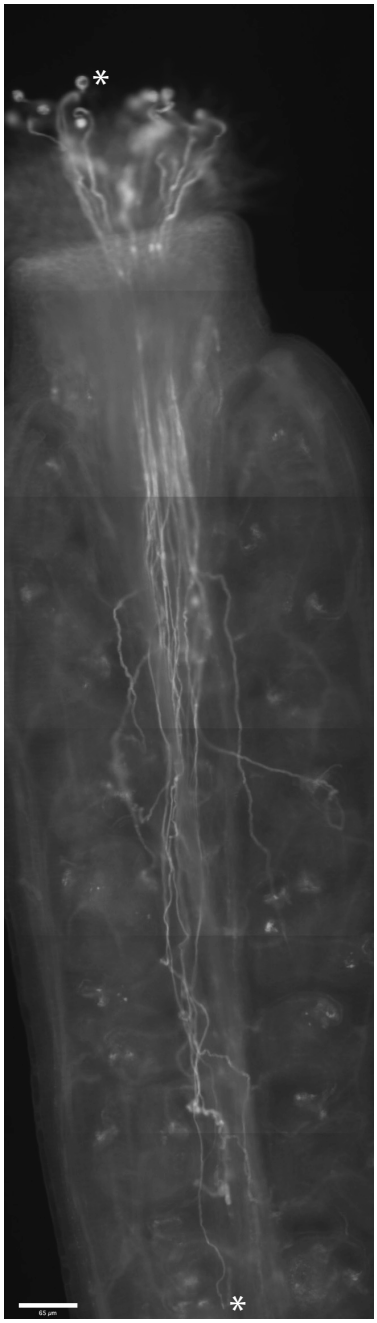

Figure 3.1: An *Arabidopsis* pistil stained with aniline blue.

Overlapping images covering the length of the pistil were captured, and the furthest distance traveled by a pollen tube was measured in a straight-line between the asterisks. To simplify visualization in this figure, individual images were stitched together using Adobe Photoshop CS3. Scale bar = 65 μm.

was confirmed by PCR using primers specific for each insertion line (**Table 3.2**). The expected T-DNA insertion was not detected in 5 out of the 16 new lines while homozygous mutants were identified for the remaining 11 lines (**Table 3.4**).

The 25 homozygous mutants were then checked for gene expression by RT-PCR using gene specific primers (**Tables 3.2 and 3.3** and **Figure 3.2**). Only 6 out of the 25 lines lacked transcript downstream of the insertion site while 13 out of the 25 either had no normal transcript or a low level of transcript detected when primers spanned the insertion site (**Table 3.5**). When a decreased amount of transcript was detected for a mutant by RT-PCR (see *CT6* and *CT7* **Figure 3.2H**), the PCR product was re-amplified by PCR and then digested with various restriction enzymes. For *CT6*, the PCR product from using primers *CT6-LP* and *CT6-RP* was only digested by restriction enzymes specific for *XIE* not *XIC* transcript indicating that *CT6* was a knockout for *XIC*. On the other hand for *CT7*, the PCR product from using primers *CT7-LP* and *CT7-RP* was digested by restriction enzymes specific for both *XIC* and *XIE* suggesting that expression of *XIC* is just extremely knocked-down in *CT7*. It is also important to note that for 10 lines, primers were only used downstream of the insertion site where transcript was detected. Those lines might have also been classified as knockout mutants if primers had been used that spanned the insertion site. For example, *BT5* had normal transcript downstream of the insertion site; however, *BT5* seedlings were shown by Eunsook Park to have slightly shorter root hairs than wild-type, a phenotype also seen in *BT2* and *BT3* which lacked transcript at the 3' end (**Figure 3.2B**). Interestingly, an increase in transcript was occasionally detected when using primers downstream of the insertion site. This was most strikingly seen for *BT5* (**Figure 3.2B**), *DT2* (**Figure 3.2D**), and *ET8* (**Figure 3.2G**). In summary, *AT2*, *AT4*, *BT2*, *BT3*, *CT6*, *CT8*, *DT6*, *DT8*, *ET6*, *ET7*, *ET8*, *JT3*, *JT6*, and *JT7* were confirmed as knockout mutants while *CT7*, was confirmed as a knockdown mutant. All of the knockout mutants were examined further and given allele names

Table 3.4: Isolation of T-DNA insertion lines

Gene	Local name	Genotype
XIC	*CT6*	Homozygous
	CT7	Homozygous
	CT8	Homozygous
	CT9	No T-DNA found
XID	*DT4*	No T-DNA found
	DT6	Homozygous
	DT7	No T-DNA found
	DT8	Homozygous
XIE	*ET6*	Homozygous
	ET7	Homozygous
	ET8	Homozygous
	ET9	No T-DNA found
XIJ	*JT2*	No T-DNA found
	JT3	Homozygous
	JT6	Homozygous
	JT7	Homozygous

Figure 3.2: Confirmation of knockout and knockdown mutants by RT-PCR

Small white letters indicate whether the primers amplified transcript upstream of (U), across (A) , or downstream of (D) the insertion site.

(**A**) Lack of *XIA* transcript for *AT2* and *AT4* using M11.A-F1 & M11.A-R1 confirmed both are knockout mutants. Rbs-F & Rbs-R were control primers.

(**B**) Lack of *XIB* transcript for *BT2* and *BT3* using M11.B-D-F1 & M11.B-Stop-R1 confirmed both are knockout mutants. JT4-LP & JT4-RP were control primers. *BT5* was not confirmed as a knockout mutant.

(**C**) Presence of *XIC* transcript using M11.C-D-F1 & M11.C-Stop-R1. *CT1*, *CT2*, and *CT5* were not confirmed as knockout mutants.

(**D**) Presence of *XID* transcript using 11.D-GSP-F & 11.D-GSP-R. *DT2* and *DT3* were not confirmed as knockout mutants.

(**E**) Presence of *XIE* transcript using M11.E-F1 & M11.E-R1. *ET1*, *ET2*, and *ET4* were not confirmed as knockout mutants.

(**F**) Presence of *XIJ* transcript using JT4-LP & JT4-RP. *JT1* was not confirmed as a knockout mutant.

(**G**) Lack of *XIE* transcript for *ET6* and *ET8* using ET2-RP & ET8-LP, lack of *XIE* transcript for *ET6* and *ET7* using ET4-RP & ET7-LP, and lack of *XIE* transcript for *ET6* using M11.E-F1 & M11.E-R1 confirmed all three as knockout mutants. Rbs-F & Rbs-R were control primers.

(**H**) Lack of *XIC* transcript for *CT6* (faint product was confirmed to be *XIE*) using CT6-LP & CT6-RP, extremely decreased *XIC* transcript for *CT7* using CT7-LP & CT7-RP, and lack of *XIC* transcript for *CT8* using CT8-RP & CT5-RP and M11.C-D-F1 & M11.C-Stop-R1 confirmed *CT6* and *CT8* as knockout mutants and *CT7* as a knockdown mutant.

Rbs-F & Rbs-R were control primers.

(**I**) Lack of *XID* transcript for *DT6* and *DT8* using DT4-LP2 & DT6-RP confirmed both are knockout mutants. Rbs-F & Rbs-R were control primers.

(**J**) Lack of *XIJ* transcript for *JT3* and *JT6* using JT3-LP2 & JT6-LP and for *JT7* using JT4-RP & JT4-RP confirmed all three were knockout mutants. NIP4;1-F & NIP4;1-R were control primers.

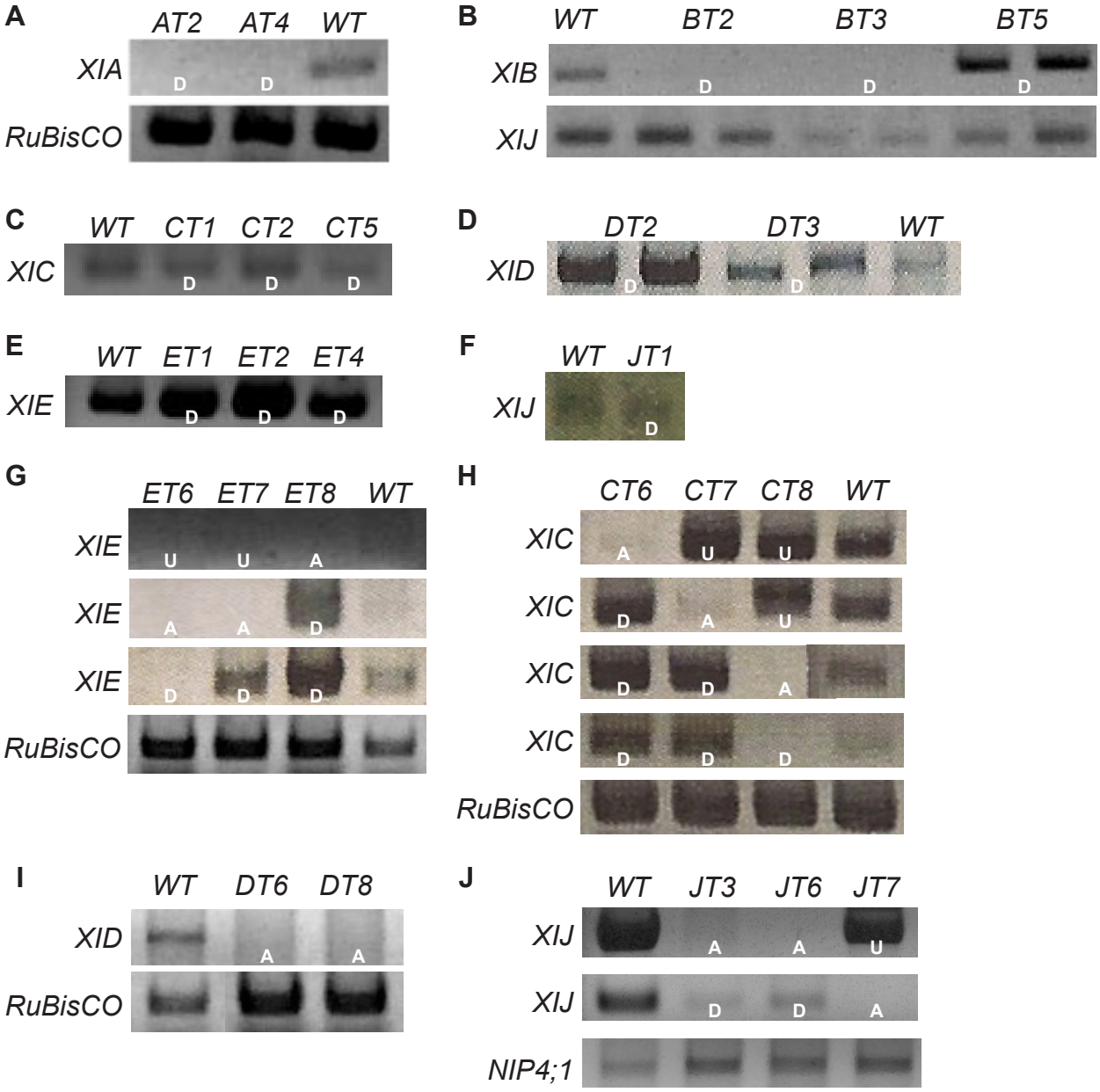
A
AT2
AT4
WT
XIA
D
D
RuBisCO
B
WT
BT2
BT3
BT5
XIB
D
D
D
XIJ
C
WT
CT1
CT2
CT5
XIC
D
D
D
D
DT2
DT3
WT
XID
D
D
E
WT
ET1
ET2
ET4
XIE
D
D
D
F
WT
JT1
XIJ
D
G
ET6
ET7
ET8
WT
XIE
U
U
A
XIE
A
A
D
XIE
D
D
D
RuBisCO
H
CT6
CT7
CT8
WT
XIC
A
U
U
XIC
D
A
U
XIC
D
D
A
XIC
D
D
D
RuBisCO
I
WT
DT6
DT8
XID
A
A
RuBisCO
J
WT
JT3
JT6
JT7
XIJ
A
A
U
XIJ
D
D
A
NIP4;1

Table 3.5: Identification of knockout mutants by RT-PCR

	Normal transcript present in relation to insertion site			
Local name	**Upstream**	**Across**	**Downstream**	**Knockout**
AT2	Yes	No	No	Yes
AT4	Yes	No	No	Yes
BT2	n.t.	n.t.	No	Yes
BT3	n.t.	n.t.	No	Yes
BT5	n.t.	n.t.	Yes	Maybe*
CT1	n.t.	n.t.	Yes	?
CT2	n.t.	n.t.	Yes	?
CT5	n.t.	n.t.	Yes	?
CT6	n.t.	No	Yes	Yes
CT7	Yes	Reduced	Yes	Knockdown
CT8	Yes	No	No	Yes
DT2	n.t.	n.t.	Yes	?
DT3	n.t.	n.t.	Yes	?
DT6	n.t.	No	n.t.	Yes
DT8	n.t.	No	Yes	Yes
ET1	n.t.	n.t.	Yes	?
ET2	n.t.	n.t.	Yes	?
ET4	n.t.	n.t.	Yes	?
ET6	No	No	No	Yes
ET7	Yes	No	Yes	Yes
ET8	n.t.	No	Yes	Yes
JT1	n.t.	n.t.	Yes	?
JT3	n.t.	No	Yes	Yes
JT6	n.t.	No	Yes	Yes
JT7	Yes	No	n.t.	Yes

* *BT5* was shown by Eunsook Park to have shorter root hairs similar to *BT2* and *BT3*.

for publication (**Table 3.6**). Meanwhile, *BT2*, *CT7*, *DT2*, *ET8*, and *JT3* were isolated as knockout mutants by another group; however, they never assigned allele numbers to those lines (Peremyslov et al., 2008).

3.3.2: Double mutant screening

Since six class XI myosins are expressed in pollen, it was predicted that there would be at least some redundancy among the pollen myosins. In case phenotypes were not detected in single mutants, several crosses were initiated to generate double mutants (**Table 3.7**). F1 plants were genotyped to confirm the presence of both T-DNA insertions, and F2 seeds were collected for all 11 lines. Of the pollen myosins, XIC and XIE are most similar to each other with 90.9% identity and 97.7% similarity (Pearson and Lipman, 1988). XIA and XID are also very similar to each other with 78.0% identity and 89.3% similarity (Pearson and Lipman, 1988). Therefore, it was hypothesized that XIC and XIE would have at least partial overlapping functions and that XIA and XID would also be partially redundant. Consequently, F2 plants for 3 *xic xie* and 3 *xia xid* lines were screened to obtain double homozygous mutants (**Table 3.7**). Double mutants were identified for *xia-1 xid-1*, *xia-2 xid-1*, *xia-2 xid-2*, and *xic-1 xie-1*. Out of 96 *xic-2 xie-2* and 103 *xic-2 xie-3* F2 plants, no double homozygous mutants were identified, so F3 seeds were collected, and double homozygous mutants were identified in the F3 generation. Interestingly when generating all three allele combinations for *xic xie*, significantly fewer double homozygous mutants were obtained in the F2 generation than expected ($\chi^2 > 4.8$; $p < 0.05$; **Table 3.7**). *XIC* and *XIE* are more than 17 Mb apart on chromosome 1 (TAIR10) and are likely to be unlinked (Koornneef et al., 1983). Therefore, the segregation distortion could have been due to a defect in the male gametophyte, female gametophyte, or embryo development; however, *XIC* and *XIE* are primarily expressed in pollen based on microarray experiments (Peremyslow et al., 2011; Sparkes, 2011). Segregation distortion was not observed for any of the allele combinations for

Table 3.6: Allele names for mutants analyzed further

Gene	Local name	Allele name
XIA	*AT2*	*xia-1*
	AT4	*xia-2*
XIB	*BT2*	*xib-1*
	BT3	*xib-2*
XIC	*CT6*	*xic-1*
	CT8	*xic-2*
XID	*DT8*	*xid-1*
	DT6	*xid-2*
XIE	*ET8*	*xie-1*
	ET6	*xie-2*
	ET7	*xie-3*
XIJ	*JT7*	*xij-1*
	JT3	*xij-2*
	JT6	*xij-3*

Table 3.7: List of double mutants generated

Genes	Alleles	# homozygous / total F2 screened	Homozygous
XIA XIB	*xia-2 xib-1*	n.t.	No
XIA XID	*xia-1 xid-1*	3 / 77	Yes
	xia-2 xid-1	1 / 22	Yes
	xia-2 xid-2	1 / 53	Yes
XIC XIE	*xic-1 xie-1*	1 / 101	Yes
	xic-2 xie-2	0 / 96	Yes
	xic-2 xie-3	0 / 103	Yes
XID XIJ	*xid-1 xij-1*	n.t.	No
	xid-2 xij-1	n.t.	No
XIE XIJ	*xie-2 xij-1*	n.t.	No
	xie-3 xij-1	n.t.	No

x*ia xid* ($\chi^2 > 4.8$; $p < 0.05$; **Table 3.7**).

3.3.3: Pollen myosins are required for normal seed set

If pollen myosin mutants had defects in pollen tube growth, a reasonable prediction would be that a reduction in overall fertility should be observed. It was possible to obtain homozygous single and double mutants, so any reduction in fertility compared to *WT* had to be very small. Pollen myosin mutant plants developed normally, produced seeds, and had no obvious phenotypes (data not shown). Even though mutant plants produced a normal amount of seeds, it was possible that a slight decrease in seed set could be detected by examining individual siliques. Therefore, the average number of seeds in 10 mm long siliques was determined for *WT*, *xia-1*, *xia-2*, and *xib-1* (**Figure 3.3**). Both *xia* mutants had significantly fewer seeds per silique than *WT* ($p < 0.01$). *xib-1* had fewer seeds than *WT*, but it was not statistically different from *WT*. To further examine the reduced seed set phenotype in *xia* mutants, every unopened silique on inflorescences initiating from the rosette were collected from 1 *WT*, 2 *xia-1*, and 3 *xia-2* plants. Collecting siliques of all lengths allowed for a more detailed analysis of seed set differences between *WT* and mutants compared to the previous experiment. Silique length and the number of seeds per silique were positively correlated for all three genotypes (**Figure 3.4A**). Instead of comparing the average number of seeds at each length, a method for combining all of the data into one comparison of the number of seeds per mm of silique was developed. Simply dividing the number of seeds by the silique length did not remove the effect of length on seed set because the x-intercepts of the linear regressions do not equal zero (**Figure 3.4B**). To adjust for length, the x-intercept from the *WT* linear regression (5.1 mm) was subtracted from each silique length, and then the new length values were used to divide the seed count values. The new seeds / mm values no longer correlated with silique length (**Figure 3.4C**). The *xia* mutants had significantly fewer seeds / mm than *WT* ($p < 0.0001$; **Figure 3.4D**). Interestingly, average silique length did

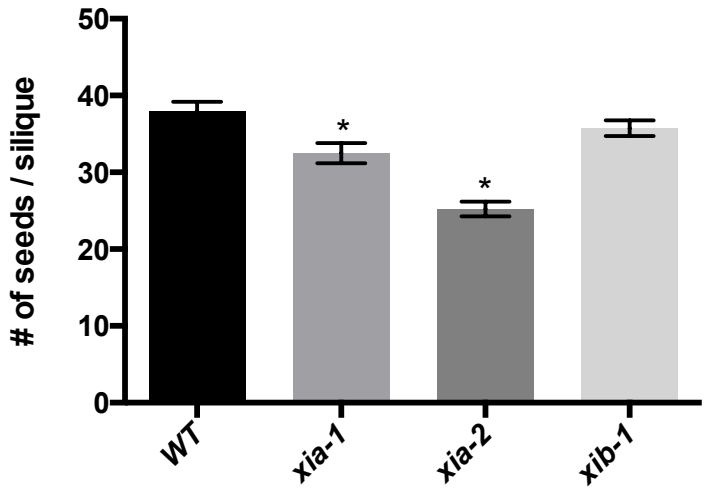

Figure 3.3: *xia* mutants had a reduced seed set in 10 mm siliques

10 mm long siliques were collected from *WT*, *xia-1*, *xia-2*, and *xib-1* plants, and the number of seeds in each silique were manually counted (Mean ± SEM; n = 50; * $p < 0.01$). *xia* mutants had significantly fewer seeds per silique than *WT*.

Figure 3.4: *xia* mutants had a reduced seed set

(**A**) Silique length and the number of seeds per silique had a positive correlation for *WT*, *xia-1*, and *xia-2*.

(**B**) Dividing the number of seeds by the length of the silique did not completely remove the effect of length on the number of seeds. Note the slight positive correlation between seeds/mm and silique length.

(**C**) Seeds / mm was calculated by dividing the number of seeds by the (length – 5.1). 5.1 was the x-intercept of the *WT* linear regression (black line) shown in **A**. Note the lack of correlation between seeds / mm and silique length.

(**D**) Average number of seeds / mm for *WT*, *xia-1*, and *xia-2* as calculated in **C** (Mean ± SEM; n = 84, 178, and 281; * $p < 0.0001$). *xia* mutants had significantly fewer seeds per silique than *WT*.

(**E**) Average silique length for *WT*, *xia-1*, and *xia-2* (Mean ± SEM; n = 84, 178, and 281; * $p < 0.0001$). There was no difference between *WT* and mutant siliques lengths.

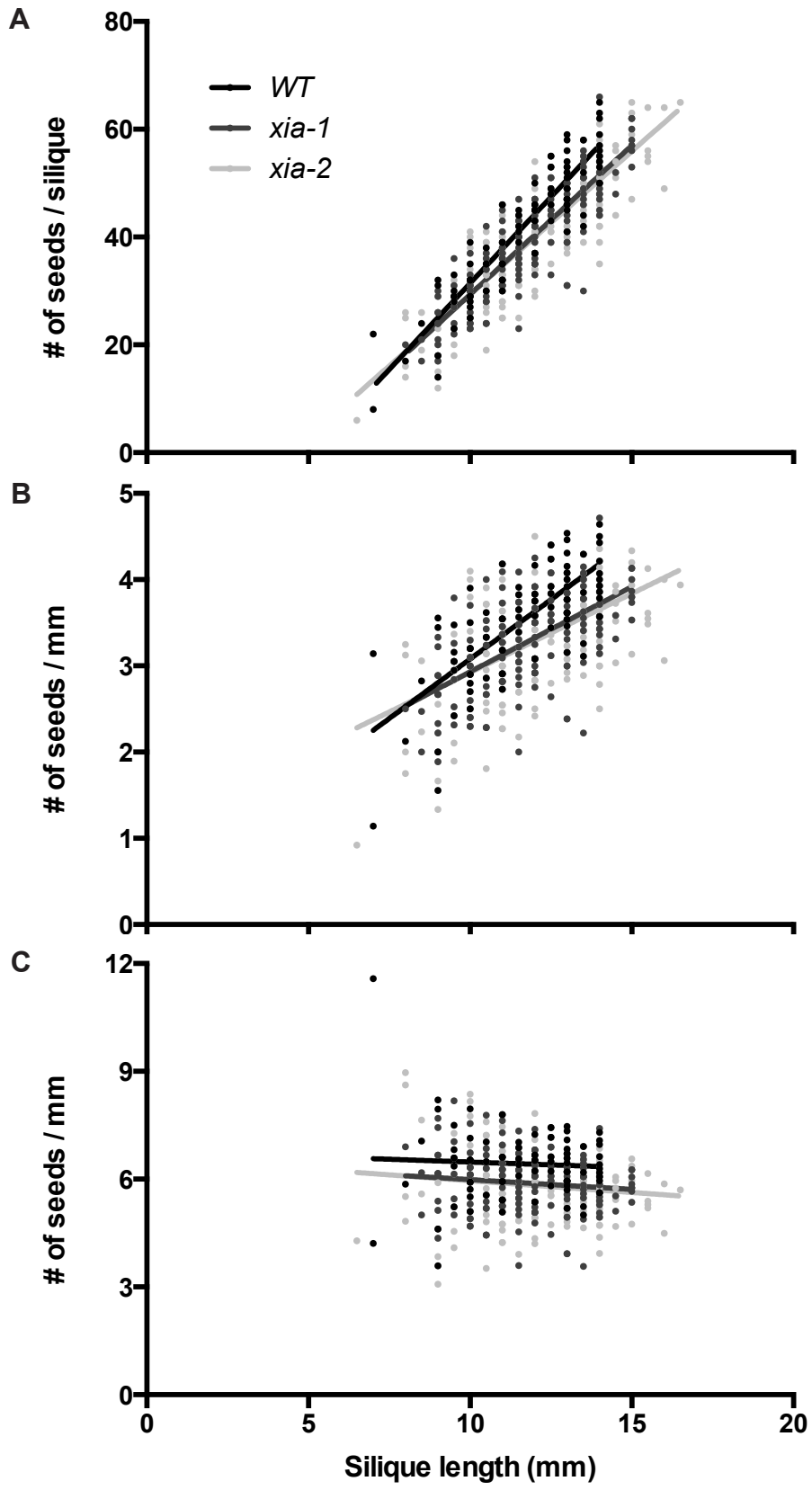
A
B
C
WT
xia-1
xia-2
# of seeds / silique
# of seeds / mm
# of seeds / mm
Silique length (mm)
0
20
40
60
80
1
2
3
4
5
3
6
9
12
0
5
10
15
20

D

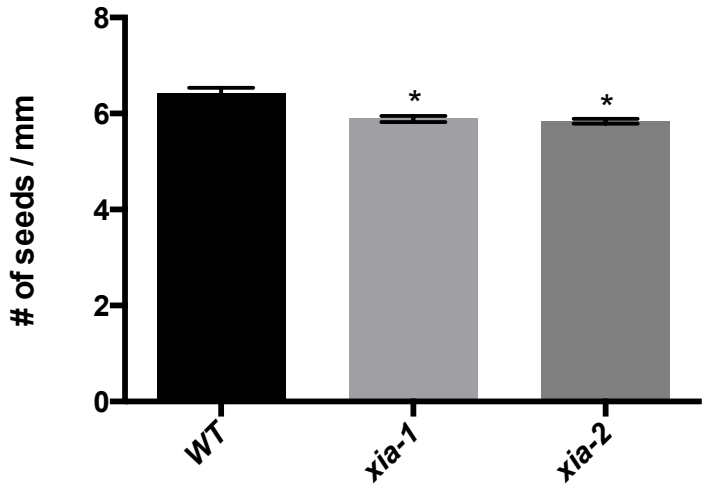

E

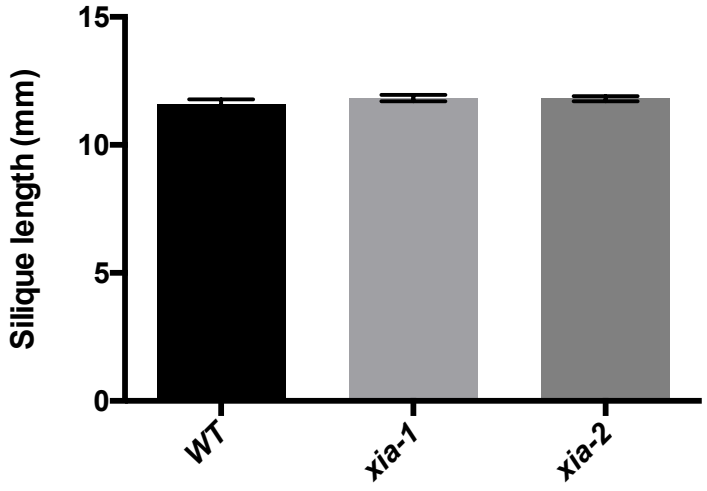

Figure 3.4: Continued

not vary between *WT* and the *xia* mutants (**Figure 3.4E**) suggesting that *XIA* is required for seed set and not silique length. If the loss of *XIA* had a drastic effect on seed set, an overall decrease in silique length would be expected. It is also important to note that the difference in seed set between *WT* and the *xia* mutants was so slight that there was not a visible difference between them. Thus, the decrease in the number of seeds / mm was small but detectable.

Following the slight fertility defect detected in the *xia* mutants, mutants for all of the pollen myosins were grown to collect siliques for analysis. In these experiments, unopened and opened siliques were collected from the primary inflorescence of multiple plants. Plants were grown in five sets, and mutants were always compared to the *WT* in their own set (**Figure 3.5**). In the first 3 sets (**Figure 3.5A-3.5F**), plants were grown in individual pots. In set 4 (**Figure 3.5G-3.5H**), plants were grown four to a pot. In set 5 (**Figure 3.5I-3.5J**), plants were grown in individual pots and fertilized once every two weeks.

All single and double mutants for *XIA*, *XIC*, *XID*, and *XIE* were examined within the first three sets (**Figure 3.5A-3.5F**). *xid-2* was excluded from **Figure 3.5A and 3.5B**. *xid-2* had visibly fewer seeds per silique with gaps visible throughout the length of the silique. Since this striking phenotype was not present in *xid-1*, *xid-2* was backcrossed to *WT*. F1 plants were allowed to self, and F2 plants were grown up. The F2 plants were genotyped using primers for *DT6* (**Table 3.2**), and the siliques were examined for the striking seeds per silique phenotype. Only 5 out of 9 homozygous plants had the striking phenotype in the F2 generation suggesting that the drastic phenotype was caused by a mutation in another gene other than *XID* which probably only displayed the striking phenotype when homozygous. 2 out of the 4 homozygous *xid-2* plants lacking the strong phenotype were used for set 4 of the seeds per silique analysis (**Figure 3.5G-3.5H**). Only 2 out of the 4 plants were used in the analysis because the other 2 plants were determined to be heterozygous for the additional mutation due to the presence of the strong

Figure 3.5: Pollen myosin mutants had reduced seed sets compared to *WT*

Mature siliques were collected, and the average silique lengths (**A, C, E, G, and I**) and seeds / mm values (**B, D, F, H, and J**) of the mutants were compared to *WT* (Mean ± SEM; * $p < 0.05$; * $p < 0.01$). When plants were grown without fertilizer (**A-H**), the most striking phenotype observed was that all three *xic xie* double mutants had shorter siliques and fewer seeds / mm than *WT* (**A-F**). When plants were fertilized (**I-J**), all single mutants had fewer seeds / mm than *WT* (**J**). Number in columns indicates the sample size.

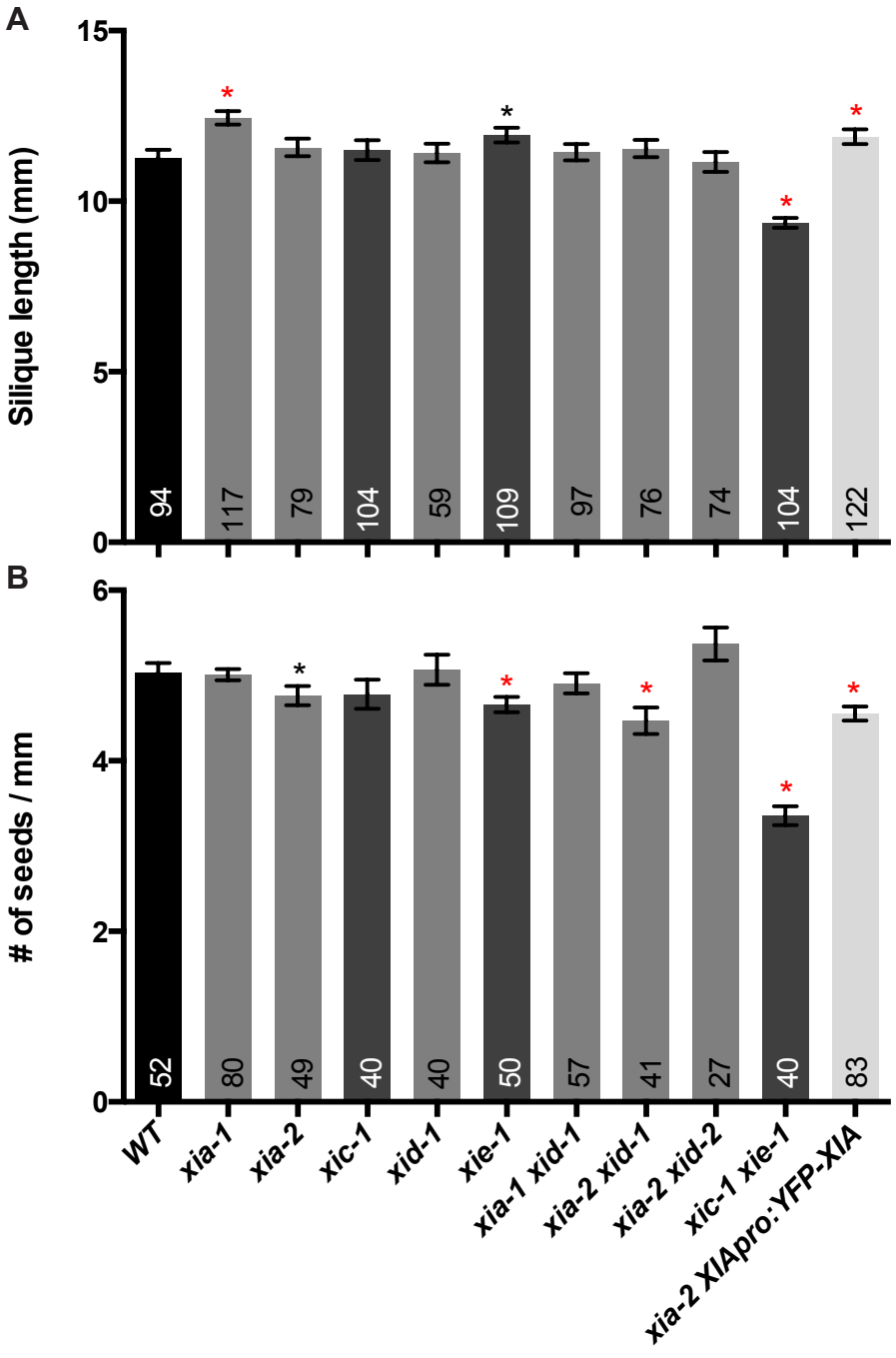
A
Silique length (mm)
15
10
5
0
94
117
79
104
59
109
97
76
74
104
122
B
# of seeds / mm
6
4
2
0
52
80
49
40
40
50
57
41
27
40
83
WT
xia-1
xia-2
xic-1
xid-1
xie-1
xia-1 xid-1
xia-2 xid-1
xia-2 xid-2
xic-1 xie-1
xia-2 XIApro:YFP-XIA

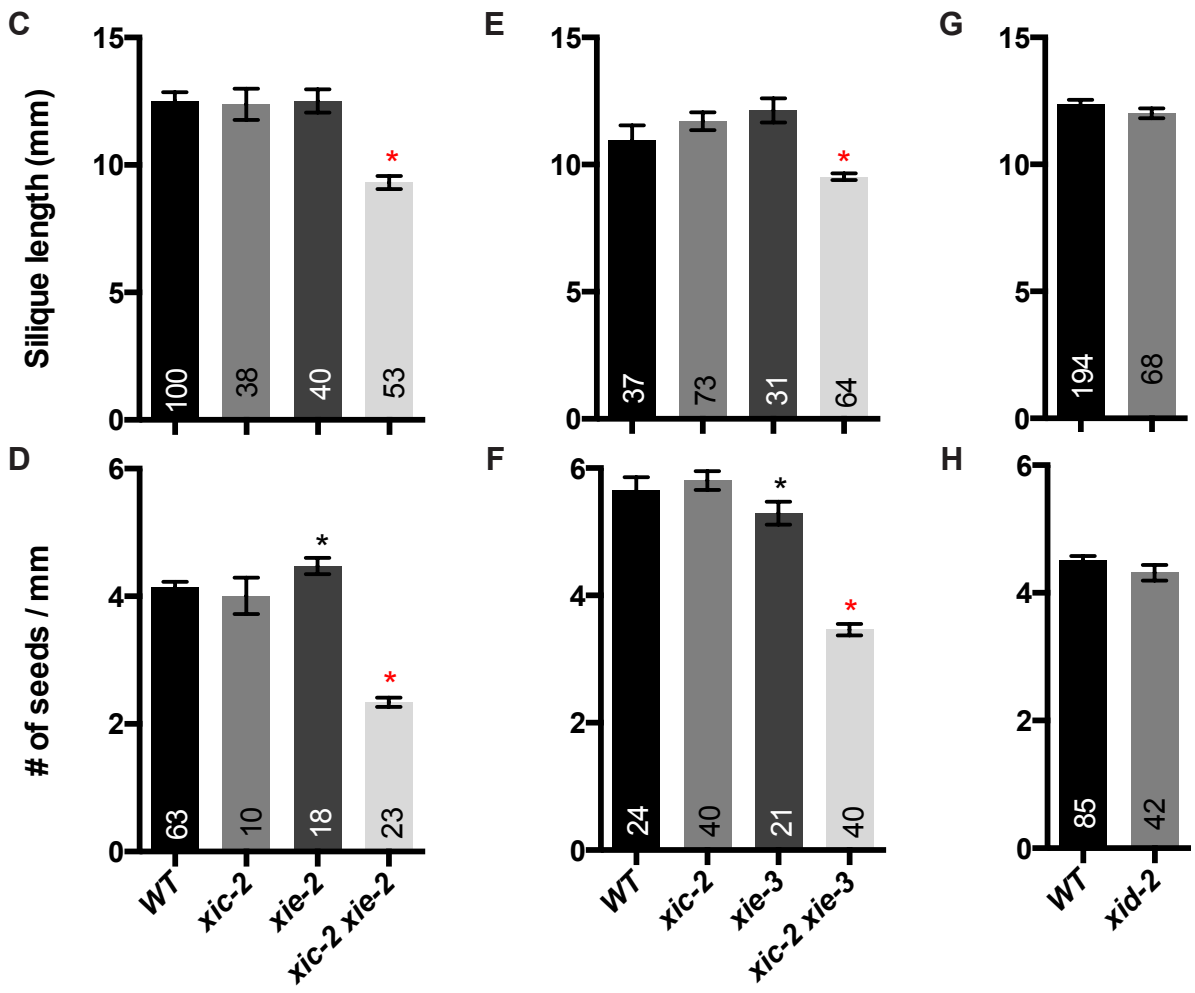

Figure 3.5: Continued

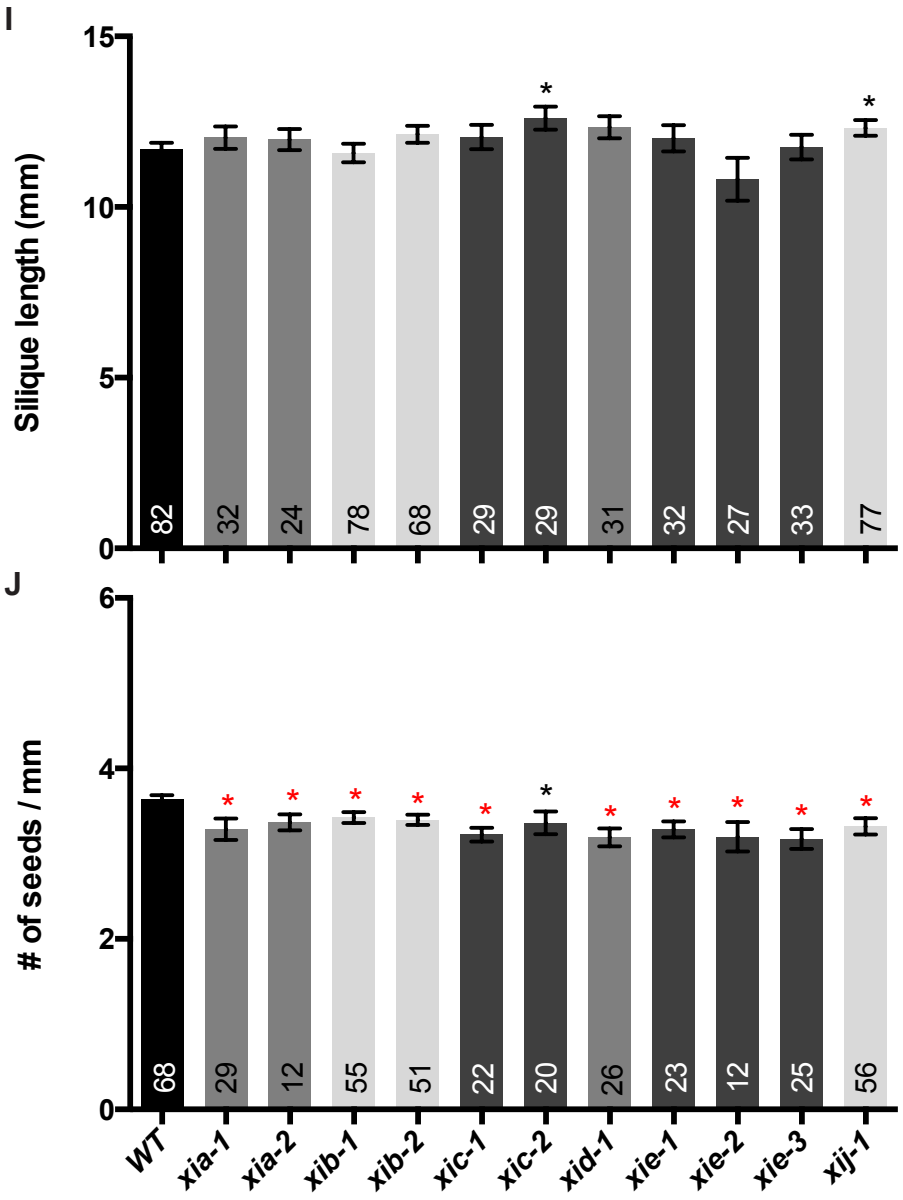

Figure 3.5: Continued

phenotype in ¼ of the next generation. The 2 plants heterozygous for the additional mutation did have slightly shorter siliques with fewer seeds / mm than *WT* (data not shown).

Other than *xid-2* before backcrossing, the most striking phenotype observed was for *xic xie*. All three double mutants had shorter siliques and fewer seeds / mm than *WT* (**Figure 3.5A-3.5F**; $p < 0.01$). Occasionally, other myosin mutants had fewer seeds / mm than *WT*; however, the *xic xie* mutants were the only mutants with visibly fewer seeds per silique than *WT* (**Figure 3.6**). Gaps were frequently observed at the bottom of the *xic xie* siliques (**Figure 3.6B**) suggesting that there was a defect in *xic xie* pollen tube growth. Single mutants of *XIC* never showed a difference in silique length or seed set compared to *WT* (**Figure 3.5A-3.5F**). On the other hand, 2 out of 3 *xie* mutants had fewer seeds / mm than *WT* while *xie-2* had more seeds / mm than *WT* (**Figure 3.5A-3.5F**). None of the *xie* mutants had shorter siliques or as few of seeds per silique as the *xic xie* double mutants. Therefore, XIC and XIE seem to function redundantly in their role in fertility. No differences from *WT* were detected for mutants of *XID* (**Figure 3.5A, 3.5B, 3.5G, and 3.5H**). As for mutants of *XIA*, *xia-2* had fewer seeds / mm than *WT* while x*ia-1* did not even though differences were previously detected for both alleles (**Figures 3.3, 3.4D, and 3.5B**). Both *xia-2* and *xia-2 XIApro:YFP-XIA* had fewer seeds / mm than *WT* suggesting that the *XIApro:YFP-XIA* construct did not rescue the *xia* mutant phenotype.

Single mutants for *XIA*, *XIB*, *XIC*, *XID*, *XIE*, and *XIJ* were examined in set 5 which included fertilization. In the previous seed set experiments, the plants were not as healthy as they could have been with the addition of fertilizer. Even *WT* did not always produce completely full siliques (data not shown). It was possible that a reduction in seed set for some of the single mutants was dependent on an overall nutrient deficiency. To remove the effect of nutrient deficiency on seed set, *WT* and the single mutants were grown with the regular addition of fertilizer. Interestingly, when plants were fertilized, all of the single mutants had fewer seeds /

Figure 3.6: *xic xie* mutants lacked seeds in the bottom half of siliques

xic xie mutants (**B**) had fewer seeds per silique than *WT* (**A**). There were fewer seeds in the bottom half of *xic xie* siliques. Scale bar = 1 mm.

mm than *WT* ($p < 0.05$; **Figure 3.5J**) suggesting that the addition of fertilizer increases the seed set for *WT* to a greater extent than for pollen myosin mutants. With the addition of fertilizer, significant differences were detected for *xib-1*, *xic-1*, *xic-2*, and *xid-1* that were not detected when plants were not fertilized (**Figures 3.3, 3.5B, 3.5D, and 3.5F**). By fertilizing plants, small decreases in seed set can be detected.

3.3.4: *XIB* is necessary in pollen for normal fertilization success

Decreased fertility in *xia* and *xib* mutants could be a result of a defect in the male gametophyte, female gametophyte, or embryo development; however, in reproductive tissues, *XIA* and *XIB* are primarily expressed in pollen (Peremyslow et al., 2011; Sparkes, 2011). In order to test the pollen fitness of *xia* and *xib*, mutants were crossed with fluorescently tagged lines (FTLs) containing pollen specific cytoplasmic markers expressed from genes that had inserted near the *XIA* and *XIB* loci. The number of offspring resulting from pollination of *ms1* plants with pollen from plants heterozygous for a marker gene near the *XIA* and *XIB* loci were counted (**Table 3.8**). Pollen carrying the *xib-1* allele had significantly reduced fertilization success than *WT* ($p = 0.011$) while the *xia* mutants were similar to *WT* (**Table 3.8**). This was surprising since the *xia* mutants showed more of a reduction in seed set than *xib* mutants (**Figures 3.3 and 3.5J**). Furthermore, the pollen competition experiment for the *xia* mutants was conducted with and without fertilizing the F1 and *ms1* plants prior to the hand pollinations. The addition of fertilizer did not affect pollen fitness (**Table 3.8**).

3.3.5: *XIC* and *XIE* function redundantly to sustain normal pollen tube growth *in vitro*

To directly examine the role of myosins in pollen tube growth, pollen from all single and double mutants were grown *in vitro* along with *WT**, *WT* expressing a YFP peroxisome marker, to control for experimental variation from slide to slide. Three hours after setup, pollen tube lengths and growth rates were measured, adjusted to *WT**, and compared to *WT* (**Figure 3.7**). *xij*

Table 3.8: Results from the pollen competition experiment

FTL	Test genotype	# of test offspring	# of *WT* offspring	p value	Fertilizer
1285	*WT*	670	664	0.87	No
	xib-1	188	241	0.011	No
	xia-1	712	751	0.31	Yes
2217	*WT*	280	282	0.93	Yes
	xia-2	188	194	0.76	Yes
	WT	378	355	0.40	No
	xia-1	271	315	0.069	No
	xia-2	342	349	0.79	No

Figure 3.7: *xic xie* mutants had reduced pollen tube growth *in vitro*

Three hours after incubation, the tube lengths (**A**) and growth rates (**B**) for *WT* and mutant pollen were measured and corrected based on the control (*WT**) included on each slide. All trials with the same genotypes were combined (Mean ± SEM; * $p < 0.05$). All three *xic xie* double mutants had shorter pollen tubes than *WT* pollen tubes while none of the other mutants' pollen were consistently different from *WT* pollen. The pollen tubes from double mutants tended to grow slower than *WT* pollen tubes, while whenever *XIApro:YFP-XIA* was expressed, the pollen tubes grew faster than *WT* pollen tubes. Sample size given at the bottom of columns.

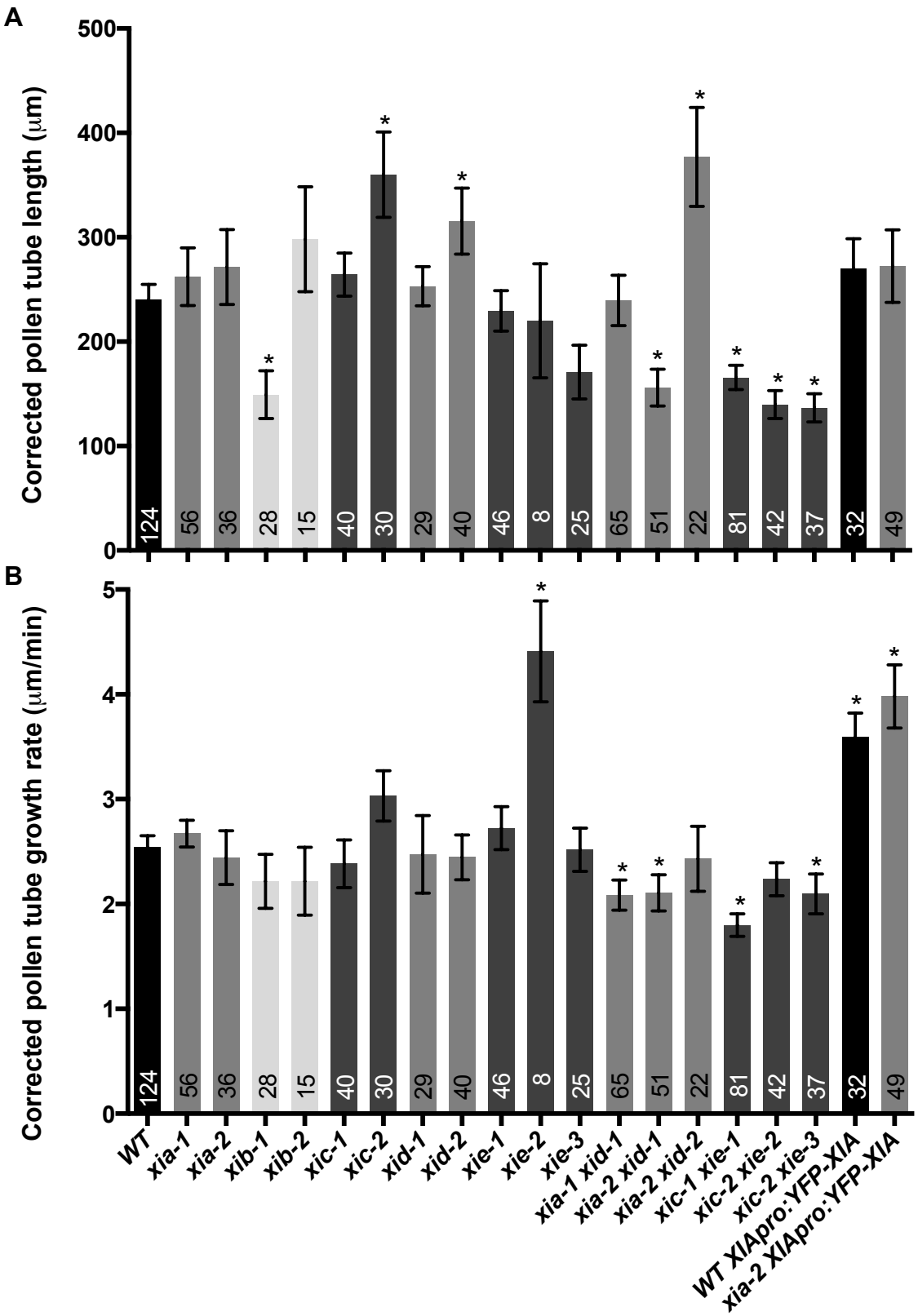
A
Corrected pollen tube length (μm)
500
400
300
200
100
0
124
56
36
28
15
40
30
29
40
46
8
25
65
51
22
81
42
37
32
49
B
Corrected pollen tube growth rate (μm/min)
5
4
3
2
1
0
WT
xia-1
xia-2
xib-1
xib-2
xic-1
xic-2
xid-1
xid-2
xie-1
xie-2
xie-3
xia-1 xid-1
xia-2 xid-1
xia-2 xid-2
xic-1 xie-1
xic-2 xie-2
xic-2 xie-3
WT XIApro:YFP-XIA
xia-2 XIApro:YFP-XIA

pollen germinated poorly *in vitro*, so it was not included in the analysis. All three allele combinations of the *xic xie* double mutants had shorter pollen tubes than *WT* ($p < 0.05$; **Figure 3.7A**) suggesting *xic xie* pollen tubes either grew slower than *WT* pollen tubes or *xic xie* pollen germinated later than *WT* pollen. There most likely was not a germination delay because all three *xic xie* double mutants had slower pollen tube growth rates than *WT* pollen tube growth rates, and 2 out of the 3 mutants had statistically slower pollen tube growth rates than *WT* (**Figure 3.7B**). *xib-1* pollen tubes were also shorter than *WT* pollen tubes ($p < 0.05$; **Figure 3.7A**) which supported results from the pollen competition experiment (**Table 3.8**). On the contrary, *xib-2* did not have shorter pollen tubes; however, the sample size for this genotype was small (**Figure 3.7A**). Variation in tube length between alleles was also seen for *xic*, *xid*, and *xia xid* (**Figure 3.7A**). One source of variation stems from not all of the pollen grains germinated at the same time, so pollen tube lengths following three hours of incubation varied greatly. There was also a lot of variation in pollen tube growth rates, so it was difficult to detect differences between *WT* and mutant pollen. All three *xia xid* double mutants had slower pollen tube growth rates than the growth rate of *WT* pollen tubes; however, only two mutants were statistically different from *WT* (**Figure 3.7B**). *xie-2* had a drastically faster pollen tube growth rate than *WT* pollen tubes ($p < 0.05$); however, the sample size for *xie-2* was extremely small (**Figure 3.7B**). Interestingly, whenever *XIApro:YFP-XIA* was present in either *WT* or *xia-2* pollen, the pollen tubes grew faster than *WT* pollen tubes ($p < 0.05$; **Figure 3.7B**) suggesting a role for *XIA* in pollen tube growth even though *xia* pollen showed no defects.

3.3.6: *XIJ* is essential for efficient pollen germination *in vitro*.

Since *xij* pollen germinated so poorly *in vitro*, *xij* pollen germination efficiency was examined. *xij* and *WT** pollen were germinated side by side on the same microscope slide, so germination efficiencies could be compared. *xij-1*, *xij-2*, and *xij-3* all had poor pollen

germination efficiencies compared to *WT**, always less than 10% of the *WT** pollen germination efficiency (**Table 3.9**). *JT1* pollen germinated normally further confirming that *JT1* was not a knockout mutant for *XIJ* (**Figure 3.2** and **Table 3.9**). *xij-1* pollen containing *XIJpro:YFP-XIJ* also germinated normally (**Table 3.9**) confirming the poor germination efficiency was due to the loss of *XIJ* and also confirming that YFP-XIJ was functional. *WT* pollen did not germinate very well, but it still germinated a lot better than *xij* pollen by germinating 25-36% of the corresponding *WT** pollen germination efficiencies (**Table 3.9**).

A delay in pollen germination could be due to a delay in hydration, so *xij-1* and *WT** pollen were examined before and after the addition of water. Before hydration, the average widths of *WT** and *xij-1* pollen grains were 14.7 ± 1.8 μm (n = 44) and 13.8 ± 1.8 μm (n = 253), respectively. Both *WT** and *xij-1* pollen grains hydrated within 30 seconds after the addition of water. Post-hydration, the *WT** and *xij-1* pollen grains were 23.0 ± 2.8 μm (n = 39) and 22.1 ± 3.4 μm (n = 356), respectively. Therefore, the poor *in vitro* germination efficiency of *xij* pollen was not a result of a defect in hydration. Once germinated, *xij-1* pollen tubes appeared to grow at a normal rate; however, the sample size was too small to do statistical analysis (data not shown).

3.3.7: Double mutants have slower pollen tube growth rates *in vivo*

To determine whether or not myosin mutants had defects in pollen tube growth *in vivo*, male sterile (*ms1*) plants were pollinated with one of the following genotypes: *WT*, *xij-1*, *xia-1 xid-1*, *xib-1*, or *xic-1 xie-1*. Pollinated pistils were fixed at various time points, and the pollen tubes were stained with aniline blue. For each pistil, the furthest distance traveled by a pollen tube was measured. The distance was measured in a straight-line, so the actual path taken by a given pollen tube was actually longer (Crawford and Yanofsky, 2011). The furthest distance traveled for the double mutant pollen, *xia-1 xid-1* and *xic-1 xie-1*, was significantly shorter than that for *WT* pollen at all four time points ($p < 0.01$; **Figure 3.8**) with the *xic-1 xie-1* mutant

Table 3.9: *xij* pollen germinated poorly *in vitro*

Percent pollen germination (%)											
*WT**	*WT*	*WT**	*xij-1*	*WT**	*xij-1*[#]	*WT**	*xij-2*	*WT**	*xij-3*	*WT**	*JT1*
3.4	0.84	7.0	0.37	9.3	4.4	3.6	0.079	4.4	0.31	5.6	3.6
1.6	0.46	8.5	0	1.1	2.4	14	0.81	5.0	0.091	15	7.4
1.8	0.64	9.6	0.29	0.78	0.99						
		4.2	0.081	0.55	2.3						
		0.52	0								
		2.8	0.13								

# indicates the presence of *XIJpro:YFP-XIJ*.

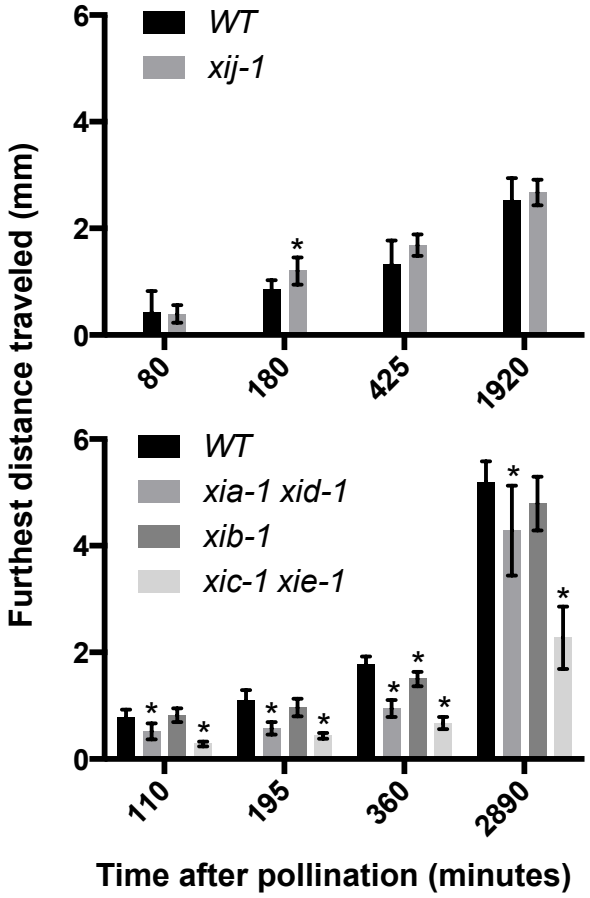

Figure 3.8: Some myosin mutants had slower pollen tube growth rates *in vivo*

WT or *xij-1* (**Top**) or *WT*, *xia-1 xid-1*, *xib-1*, or *xic-1 xie-1* (**Bottom**) pollen was used to pollinate *ms1* plants. Pollinated pistils were removed, fixed, and stained with aniline blue at various time points following pollination. For each pistil, the furthest distance traveled by a pollen tube was measured (Mean ± SD; n = 4 to 23; * $p < 0.01$). Pollen tubes of *xia-1 xid-1* and particularly *xic-1 xie-1* mutants grew more slowly than *WT* pollen while pollen tubes of *xij-1* and *xib-1* single mutants showed essentially no difference to *WT* pollen.

having the shortest pollen tubes. This suggests that within the first 48 hours following pollination, the double mutants' pollen tubes grew slower than *WT* pollen tubes. Another possible explanation for the shorter distances would be that the double mutant pollen germinated later than *WT* pollen; however, this was not observed during *in vitro* pollen germination experiments for these mutants. Starting at 195 minutes post-pollination, *xib-1* had shorter pollen tubes than *WT*; however, it was not always statistically different from *WT* pollen tubes (**Figure 3.8**). This result was consistent with *xib-1* pollen being less fit than *WT* pollen in the pollen competition experiment (**Table 3.8**) and having shorter tubes *in vitro* (**Figure 3.7A**). *xij-1* was tested separately from the other genotypes, so it could only be compared to its *WT* control. *xij-1* pollen tubes grew slightly further than *WT* pollen tubes by 180 minutes ($p < 0.01$; **Figure 3.8**); however, this difference was probably due to unusually poor pollen tube growth by *WT* for that time point. Surprisingly, these results suggest that *in vivo* pollen tube growth and pollen germination is not affected by the loss of *XIJ*.

3.3.8: Poor germination of *xij* pollen *in vitro* can be rescued with 'cut pistil' exudate

Since *xij* pollen germinated poorly *in vitro* but not *in vivo*, pistils were added to the solid PGM to test whether or not it improved germination efficiency for *xij* pollen. When whole pistils were added to the medium, more pollen grains for *WT** and *xij-1* germinated near the pistils. However, the germination efficiencies could not be calculated accurately due to difficulties imaging around large pistils. Next, a drop of 'cut pistil' exudate or liquid PGM was added to the solid PGM, and *WT* or *xij-1* flowers were dabbed directly onto the droplet. With the addition of liquid PGM, the pollen germination efficiencies for *WT* and *xij-1* were 5% and 0.4%, respectively. With the addition of 'cut pistil' exudate, the pollen germination efficiencies for *WT* and *xij-1* were 9.1% and 10.8%, respectively. The germination efficiency improved for both *WT* and *xij-1*, and *xij-1* even caught up to *WT* suggesting *XIJ* is only required for pollen germination

in the absence of female components.

3.4: Discussion

The vegetative tissues of class XI myosin mutants have been studied extensively, which revealed roles for class XI myosins in cell expansion, organelle motility, and actin dynamics (Ojangu et al., 2007; Peremyslov et al., 2008; Prokhnevsky et al., 2008; Peremyslov et al., 2010; Ojangu et al., 2012; Park and Nebenführ, 2013). On the other hand, very few studies have examined reproductive tissues of class XI myosin mutants. Recently, a triple mutant in *Arabidopsis thaliana* was shown to have fewer seeds per silique than *WT* due to reduced elongation of the stigmatic papillae (Ojangu et al., 2012), thus providing further evidence for the role of class XI myosins in cell expansion. Another recent study showed that a single myosin XI mutant in *Zea mays* had an accumulation of abnormally small protein bodies in the endosperm (Wang et al., 2012). It is unclear how myosin XI contributes to the formation of appropriately sized protein bodies; however, this result alludes to a possible role of myosins outside of moving organelles and contributing to cell expansion. Another study in *Oryza sativa* showed that *XIB* was required for normal pollen development under short-day conditions (Jiang et al., 2007) further suggesting a role for myosins outside of cell expansion.

Due to the known involvement of class XI myosins in trichome, stigmatic papillae, and root hair elongation (Ojangu et al., 2007; Peremyslov et al., 2008; Prokhnevsky et al., 2008; Peremyslov et al., 2010; Ojangu et al., 2012), it was very reasonable to predict that class XI myosins were also required for the rapid elongation of pollen tubes. Indeed, the acto-myosin network had been shown to be required for angiosperm pollen germination and tube growth (Franke et al., 1972; Mascarenhas and Lafountain, 1972; Heslop-Harrison and Heslop-Harrison, 1989a; Tiwari and Polito, 1990; Gibbon et al., 1999; Tominaga et al., 2000). Even though 6 out

of the 13 class XI myosins in *Arabidopsis* are predominately expressed in pollen (Peremyslow et al., 2011; Sparkes, 2011), no one has published any results describing pollen phenotypes. Pollen myosin mutants would be expected to have reduced pollen tube growth, which could lead to an overall reduction in fertility. The lack of publications describing *Arabidopsis* pollen myosin mutants is probably due to two reasons. First, redundancy among the pollen myosins makes it difficult to detect any phenotypes in single mutants. Secondly, most experiments to detect defects in pollen tube growth are tedious, have a large variation, and do not always provide consistent results.

A detailed seeds per silique analysis, a direct pollen competition experiment, and an examination of *in vitro* and *in vivo* pollen tube growth can provide crucial information for mutants that possibly have slight defects in pollen tube growth. Small differences in seed set can be detected if a large number of siliques are analyzed; however, this is an extremely tedious experiment that is dependent on growth conditions. I would only recommend counting the number of seeds per silique for genotypes that have a visible reduction in seed set as seen for the *xic xie* double mutants. Of course, this will miss weak effects such that any 'small contribution' gene will go undetected. The pollen competition experiment does take the longest from start to finish due to generation times, and a lot of materials are used to grow vast quantities of plants. However, this experiment does specifically test pollen fitness, and a small decrease in fitness can be detected as seen with *xib-1* pollen. It is important to note that the pollen competition experiment is only practical with single mutants. Examining pollen tube lengths and growth rates *in vitro* is fairly easy; however, there is a lot of variation within each genotype making it difficult to detect differences between *WT* and mutant pollen. The *in vivo* pollen tube growth experiment takes a week to perform and a long time to image all of the pistils; however, the analysis is quick. There also is very little variation within genotypes making comparisons between *WT* and

mutant pollen easier. When examining mutants for slight defects in pollen tube growth, I would recommend the *in vivo* pollen tube growth experiment. This experiment is very useful for detecting pollen tube growth defects *in vivo*, yet any '*in vitro* specific defects', as with *xij* pollen, would go undetected. Overall, each of these experiments can provide unique and useful information when trying to determine the role of a particular gene in pollen tube growth.

XIB *has a slight role in both root hairs and pollen tubes*

XIB has been shown to be involved in root hair elongation. The single mutant did not have a root hair phenotype; however, the *xib mya2* double mutant had drastically shorter root hairs than *WT*, even shorter than the *mya2* single mutant (Prokhnevsky et al., 2008). *XIB* is expressed in root hairs and pollen (Peremyslow et al., 2011; Sparkes, 2011) suggesting that this myosin may also affect pollen tube growth. After observing over 400 offspring from the pollen competition experiment, *xib-1* pollen was shown to be slightly less fit than *WT* pollen ($p = 0.011$). *xib-1* pollen tubes were also shown to not have grown quite as far as *WT* pollen tubes *in vivo*, and *xib-1* had shorter pollen tubes than *WT* pollen tubes *in vitro*. *xib-2* pollen tubes were not shorter than *WT* pollen tubes *in vitro*; however, both *xib-1* and *xib-2* had slightly reduced seed sets compared to *WT*. Overall, *XIB* is involved in both root hair and pollen tube growth; however, when other myosins are present, loss of *XIB* results in marginal defects. Due to the role of *XIB* in both pollen tube and root hair growth, it would be interesting to examine the localization of XIB by generating and then expressing an *XIBpro:YFP-XIB* construct in *xib* mutants. It would be interesting to determine whether or not YFP-XIB has a similar localization pattern in both tissue types.

XIA and XID may function redundantly in pollen tube growth

Comparing the amino acid sequences of XIA and XID, they have 78.0% identity and 89.3% similarity (Pearson and Lipman, 1988). The *xia-1 xid-1* double mutant showed slower

pollen tube growth *in vivo*; however, *xia* and *xid* single mutants were not tested. Therefore, it is unknown whether the defect is due to a loss of both closely related myosins or if one of the single mutants would have shown the same effect. One piece of evidence supporting at least partial redundancy is that neither single mutant showed a defect during *in vitro* growth; whereas, all three *xia xid* double mutants had slower pollen tube growth rates compared to *WT* pollen tubes, with 2 having significant differences. In some experiments, the single and double mutants showed reduced seed set compared to *WT* suggesting *XIA* and *XID* play either a minimal role in fertility or the other pollen myosins can compensate for the loss of both *XIA* and *XID*. Surprisingly, *xia* pollen was not less fit than *WT* pollen. Even though *XIA* is expressed primarily in pollen (Peremyslow et al., 2011; Sparkes, 2011), it is a possibility that the reduced seed set was a result of a defect in the female gametophyte, sporophytic tissues, or embryo development. Unfortunately, the *XIApro:YFP-XIA* construct did not rescue the reduced seed set phenotype of *xia-2* suggesting that YFP-XIA is either not fully functional or the reduced seed set is not due to the mutation in *XIA*. Currently, the *XIApro:YFP-XIA* construct is being tested for partial complementation of the *xia xid* reduced pollen tube growth phenotype observed *in vivo*. Interestingly when *YFP-XIA* was expressed in *WT* and *xia-2* pollen, the pollen tubes grew faster than *WT* pollen tubes *in vitro*. One explanation could be that either *YFP-XIA* was overexpressed compared to native *XIA* or YFP-XIA was more stable than native XIA which led to extra XIA in the pollen tube that somehow increased the overall growth rate. This could suggest a role for *XIA* in pollen tube growth under certain circumstances even though it normally is not required.

XIC and XIE function redundantly and are required for normal pollen tube growth

XIC and XIE have 90.9% amino acid sequence identity and 97.7% similarity (Pearson and Lipman, 1988). Double mutants have a reduced seed set with fewer seeds present in the bottom-half of siliques. This phenotype can be explained by the drastically slower pollen tube

growth *in vivo*. *xic xie* pollen tubes also grew slower than WT pollen tubes *in vitro*. Because single mutants of *XIC* and *XIE* had minimal defects, XIC and XIE clearly have overlapping roles in pollen tube growth. When one is absent, the other closely related myosin can compensate for the loss. Out of the pollen myosins, XIC and XIE seem to play the most important role in pollen tube growth. Future experiments should focus on determining exactly how XIC and XIE contribute to pollen tube elongation.

XIJ *is required for pollen germination in the absence of female components*

The most striking phenotype observed for a single pollen myosin mutant was for *xij*. *xij* pollen germinated very poorly *in vitro*; however, this drastic defect was absent *in vivo*. Interestingly, the poor pollen germination *in vitro* could be rescued by the addition of 'cut pistil' exudate. This suggests that *XIJ* is only required for germination in the absence of some unknown diffusible female component. It will be extremely important to determine the exact mechanisms behind *XIJ*-dependent and *XIJ*-independent pollen germination. The first step will be to identify the diffusible female component that rescued the *xij* pollen germination defect. The first chemicals to test would be N-methanesulfinyl 1-azadecalin and N-methanesulfinyl 2-azadecalin. These chemicals were synthesized to mimic the diffusible chemical present in 'cut pistil' exudate that stimulates *WT* pollen germination (Qin et al., 2011). If these chemicals do not rescue the *xij* pollen germination defect, the 'cut pistil' exudate will have to be examined further. It is possible that the 'mystery' component somehow stimulates the expression of certain pollen myosins, which are not expressed well *in vitro*. Indeed, *XIE* showed a three-fold increase in expression level during semi *in vivo* pollen tube growth compared to *in vitro* pollen tube growth (Qin et al., 2009). The other pollen myosins exhibited similar expression levels between the two pollen tube growth conditions (Qin et al., 2009). *XIE* and *XIC* are closely related to *XIJ* (Mühlhausen and Kollmar, 2013); however, it is hard to imagine that XIJ and XIE perform the same function since

XIJ has such a different C-terminus compared to the other pollen myosins (Mühlhausen and Kollmar, 2013).

Conclusions

Class XI myosins are involved in pollen tube growth and surprisingly, in *in vitro* pollen germination. The exact mechanisms of how pollen myosins contribute to these processes remain unknown. In the future, it will be important to identify what intracellular defects are present in mutant pollen tubes in order to elucidate the exact function of each pollen myosin. YFP-tagged complementation constructs will also shed light on this dilemma. There is definitely some redundancy among the pollen myosins because single mutants show minimal defects; therefore, it will also be crucial to identify the cargo of each pollen myosin in order to fully determine the level of functional redundancy among the pollen myosins.

Chapter 4: Examining the Subcellular Function of Pollen Myosins

- *Undergraduate students who earned research credit in this lab contributed to the results in this chapter. Tanner Beard assisted with imaging some of the marker lines. Tanner Beard and Ryan Wilson manually tracked peroxisomes and Golgi stacks in* WT *and mutant pollen tubes.*

4.1: Introduction

There are 13 class XI myosins in *Arabidopsis thaliana*, and examination of higher order mutants revealed that there is a degree of redundancy among the myosin XI genes expressed in vegetative tissues (Prokhnevsky et al., 2008; Peremyslov et al., 2010; Ojangu et al., 2012). One method to examine the degree of functional overlap among class XI myosins is to determine the subcellular function of each myosin. Two approaches have been employed to show that class XI myosins are required for normal organelle trafficking in vegetative cells. First, several groups overexpressed the tail portion of myosins in cells expressing various fluorescent markers. The dominant-negative tail fragments are predicted to saturate myosin binding sites on the cargo, thus preventing native myosins from binding to and transporting the organelle or vesicle. Expression of myosin XI tails resulted in reduced motility of peroxisomes, Golgi stacks, mitochondria, the endoplasmic reticulum (ER), trans-Golgi network, pre-vacuolar compartment, endosomes, and exocytic vesicles (Avisar et al., 2008b; Sparkes et al., 2008; Avisar et al., 2009; Yokota et al., 2011; Avisar et al., 2012; Wang et al., 2012). Unfortunately, tail constructs appear to exert their dominant-negative effect on organelle movements non-selectively. For example, XIK tails reduced the motility of all tested organelles despite not being localized to most of them (Avisar et al., 2009; Avisar et al., 2012). In the second approach, knockout mutants for class XI myosins have been examined for defects in organelle motility using various fluorescent markers. With this approach, myosin XI was implicated in moving peroxisomes, Golgi stacks, mitochondria, the ER, and the nucleus (Peremyslov et al., 2008; Prokhnevsky et al., 2008; Peremyslov et al., 2010; Ueda et al., 2010; Avisar et al., 2012; Tamura et al., 2013). In addition to organelle motility, myosin XI mutants have also been shown to have disorganized actin filaments and reduced actin filament dynamics (Peremyslov et al., 2010; Ueda et al., 2010; Vidali et al., 2010; Park and Nebenführ, 2013). Similarly to the dominant-negative approach, some single myosin

XI mutants have been shown to reduce motility of various organelles. Additionally, the movement of a particular organelle was reduced in more than one myosin mutant.

Another method to evaluate the level of overlapping functions among the class XI myosins is to determine the subcellular localization of each myosin. Myosins are predicted to function where they are localized. For instance, if a particular myosin was localized to Golgi stacks, it would be predicted to transport Golgi stacks throughout the cell. Therefore, it is necessary to create fluorescent protein tagged, full-length constructs that can complement well-documented mutant phenotypes. To date, this has been accomplished for myoXIa, a myosin XI in *Physcomitrella patens*, (Vidali et al., 2010) and XIK in *Arabidopsis thaliana* (Peremyslov et al., 2012; Park and Nebenführ, 2013). Interestingly, YFP-tagged XIK and myoXIa accumulated at the tips of growing root hairs and caulonemal cells, respectively (Vidali et al., 2010; Peremyslov et al., 2012; Park and Nebenführ, 2013). It will be interesting to determine whether or not all class XI myosins have a similar localization pattern.

In *A. thaliana*, 6 out of the 13 myosin XI genes are expressed in pollen (Peremyslow et al., 2011; Sparkes, 2011). Some pollen myosin knockout mutants exhibited a reduction in overall fertility (see Chapter 3). In particular, *xic xie* pollen tubes grew slowly which resulted in drastically shorter siliques with fewer seeds (see Chapter 3). The exact role of XIC and XIE in pollen tube growth is unclear. Pollen tubes undergo rapid tip growth that is dependent on the actin cytoskeleton, the accumulation of vesicles at the tip, and the balance of signaling pathways coordinating tip-focused growth (Guan et al., 2013). Determining the subcellular functions of XIC and XIE should indicate how XIC and XIE contribute overall pollen tube growth. Furthermore, pollen from mutants of *XIJ*, the short-tailed myosin XI (Mühlhausen and Kollmar, 2013), germinated poorly *in vitro* suggesting a role in of myosin XI in pollen germination (see Chapter 3). The first step to identify the role of XIJ during *in vitro* pollen germination is to

determine its localization during germination.

In this study, the subcellular function of the pollen myosins was examined. The localization of two pollen myosins, XIA and XIJ, was determined using YFP-tagged, full-length fusion constructs. Additionally, the *xic xie* double mutant and the *xij* single mutant were examined for defects in organelle motility, vesicle accumulation, and actin dynamics in growing pollen tubes using various fluorescent markers. Since myosin XI mutants that have reduced cell expansion in vegetative tissues also tend to have reduced organelle motility, *xic xie* pollen tubes were predicted to have reduced organelle motility.

4.2: Methods

4.2.1: Plant lines, constructs, and transformations

Arabidopsis thaliana plants were grown as described in Chapter 2, and Col-0 was used as *WT*. *xia-2 XIApro:YFP-XIA*, *xij-1 XIJpro:YFP-XIJ*, *xic-1 xie-1*, and *xij-1* were generated or identified as described in Chapter 3. Seeds for *LAT52pro:GFP* were kindly provided by Dr. Mark Johnson (Brown University, Providence, RI). All plant transformations were performed using the *Arabidopsis* floral dip method (Weigel and Glazebrook, 2002). The native *XIJ* promoter, which was described in Chapter 3, was used to drive expression of most markers. The native *XIA* promoter, which was described in Chapter 3, was used to drive expression of *YFP-XIA* and *mCherry-XIA*. *mCherry-XIA* was composed of *mCherry*, a linker sequence that encodes ELYGGPGGSGSA, and the full-length *XIA* coding sequence including 38 base pairs of the 3'UTR. The full-length *XIA* coding sequence was obtained as described in Chapter 3. The construct was moved into the binary plasmid pFGC19 (Nelson et al., 2007) and co-transformed into *WT* along with *XIJpro:YFP-XIJ*.

The YFP peroxisome marker, described in Chapter 3, was transformed into *xic-1 xie-1* and *xij-1*. The Golgi marker was the first 49 amino acids of soybean α-1,2 mannosidase I fused to YFP (Saint-Jore-Dupas et al., 2006). *YFP-FABD2* was reconstructed based on the *35Spro:GFP-FABD2* plasmid graciously donated by Dr. Carola Holweg (University of Freiburg, Germany). Full-length *RabA4d*, *ROP1*, *RIC3*, and *RIC4* coding sequences were amplified from *Arabidopsis* flower cDNA using specific primers (**Table 4.1**) and fused to the C-terminus of YFP. The *YFP-Golgi*, *YFP-RabA4d*, *YFP-ROP1*, *YFP-RIC3*, and *YFP-RIC4* constructs were moved into the binary plasmid pVKH18 (Batoko et al., 2000) and transformed into *WT*, *xic-1 xie-1*, and *xij-1*. The *YFP-FABD2* construct was moved into the binary plasmid pPZP221 (Hajdukiewicz et al., 1994) and transformed into *WT*, *xic-1 xie-1*, and *xij-1*.

4.2.2: *in vitro* pollen germination / growth and microscopy

Pollen was germinated and grown *in vitro* as described in Chapter 3. Unless otherwise noted, pollen tubes were observed using an Axiovert 200 M microscope (Zeiss). The microscope was equipped with filter sets for CFP, YFP, and mCherry fluorescence (52017 and 69308, Chroma). Images were captured using a CCD camera (Orca ER; Hamamatsu Photonics).

4.2.3: Fluorescence resonance energy transfer (FRET) analysis

xia-2 XIApro:YFP-XIA XIJpro:CFP-RabA4d and *xij-1 XIJpro:YFP-XIJ XIJpro:CFP-RabA4d* pollen tubes were grown *in vitro* and imaged using a 63X (1.4 NA) plan-apo oil immersion objective. Using OpenLab5 software (Improvision/Perkin Elmer), CFP and YFP images were captured sequentially for one minute with 2-s intervals. CFP (donor), YFP (acceptor), and FRET images were acquired using an image splitter (Dual-View; Optical Insights) to separate the emission wavelengths into two images that were projected side by side on the camera chip (dichroic filter 505dcxr; emission filters D465/30 for CFP and HQ535/30 for YFP; Chroma Technology). The CFP and YFP half-images were separated, and normalized

Table 4.1: List of primers

Gene	Primer name	Primer sequence (5' to 3')
RabA4d	RabA4d-F	GCGGATCCATGTCTAATTTGTATGGAGATTATA
	RabA4d-R	CGCTGCAGTTACGATTTGCCGCAACATCC
RIC3	RIC3-F	GCAGATCTATGGCGACCGTGAAAGGCC
	RIC3-R	CGCTGCAGTTACTCTTTGTCACTGATATTATTA
RIC4	RIC4-F	GCGGATCCATGAGAGATAGAATGGAGAGAC
	RIC4-R	CGCTGCAGTTATAAAGTTGGATGAAGATGAG
ROP1	ROP1-F	GCAGATCTATGAGCGCTTCGAGGTTCGTA
	ROP1-R	CGGCGGCCGCTCATAGAATGGAGCATGCCTTC

Underlined sequences are restriction sites used in cloning.

FRET (NFRET) values were calculated with the NFRET algorithm (Xia and Liu, 2001) using the FRET module in OpenLab5 software. The bleed-through constants used were 0.8 for the donor and 0.03 for the acceptor. NFRET images were colorized to represent the relative degree of normalized FRET within the pollen tubes.

4.2.4: Drug treatments

xia-2 XIApro:YFP-XIA and *xij-1 XIJpro:YFP-XIJ* pollen were germinated and grown *in vitro* as described in Chapter 3. Pollen tubes were observed using a 40X objective on an AxioObserver.Z1 microscope (Zeiss) equipped with filters for YFP fluorescence (46 HE, Zeiss). Inhibitors were diluted in liquid pollen germination medium (PGM) to final concentrations of 100 nM or 1 μM of latrunculin B (latB), from a 1 mM stock in DMSO, and 10 μg/ml (36 μM) brefeldin A (BFA) from a 5 mg/ml stock in ethanol. 5 μl of the diluted inhibitors or diluted DMSO or ethanol (mock treatment), was pipetted onto each sample immediately before imaging. Images were captured with 15-s intervals for at least 20 minutes for latB treatments and for 30 minutes for BFA treatments.

4.2.5: Analysis of RabA4d accumulation

Pollen expressing *YFP-RabA4d* were germinated and grown *in vitro*, as described above. Pollen tubes were observed 4 to 8 hours after setup using a 100X oil immersion objective. Using OpenLab5 software (Improvision/Perkin Elmer), images were captured for two minutes with 0.5-s intervals. For every frame, the mean YFP fluorescence intensity was measured in an oval area at the tip using a custom macro in ImageJ. Raw fluorescence intensity values were corrected for photo-bleaching by normalizing to an exponential decay that was obtained by linear regression of the log-transformed raw data. For each pollen tube, the coefficient of variation was calculated by multiplying 100 by the standard deviation divided by the mean of the normalized fluorescence intensity. Significant differences were calculated by a Mann-Whitney unpaired t-test using Prism

6 software (GraphPad).

4.2.6: Organelle movement analysis

Pollen expressing either the peroxisome marker or the Golgi marker were germinated and grown *in vitro*, as described above. Pollen tubes were observed 3 to 10 hours after setup using a 63X (1.4 NA) plan-apo oil immersion objective. Using OpenLab5 software (Improvision/Perkin Elmer), images were captured for two minutes at 0.5-s intervals. At least nine independent videos were analyzed per treatment, except only three were analyzed for *xij-1* expressing the peroxisome marker. Most time-lapse images included only one pollen tube; however, in a few cases, multiple pollen tubes were imaged together. Time-lapse images always included the pollen tube tip.

Image sequences were exported to ImageJ, and background subtraction was performed using the rolling ball radius that yielded the largest signal-to-noise ratio as calculated by a custom macro. Individual organelle velocities were measured using the Particle Tracker plug-in (Sabalzarini and Koumoutsakos, 2005) for ImageJ. For particle detection, the radius and cutoff were always set to 2 and 1, respectively, while the percentile was adjusted between 0.2% and 0.9% depending on the image sequence. For particle linking, the link range was always set to 1, and the displacement was set to 20 pixels for peroxisomes and 15 pixels for Golgi stacks, corresponding to a maximal velocity of 8 μm/s and 6 μm/s, respectively. The displacement values chosen were based on the maximum velocities measured for peroxisomes and Golgi stacks by manual tracking. For automated tracking, all measured velocities from one time-lapse were combined to examine the range of cumulative distributions observed for each genotype. Velocities were then combined by genotype, and significant differences in the cumulative distribution of velocities between *WT* and mutant were calculated by a Kolmogorov-Smirnov test using Prism 6 software (GraphPad).

Organelles were manually tracked using OpenLab5 software. Organelles visually identified as moving very fast were tracked in two pollen tubes for every treatment. For each pollen tube analyzed, ten organelles moving towards the tip and ten organelles moving away from the tip were tracked for as long as they were in focus. Significant differences in the cumulative distribution of velocities between *WT* and mutant or between towards the tip and away from the tip movement were calculated by a Kolmogorov-Smirnov test using Prism 6 software (GraphPad).

4.2.7: Actin analysis

Pollen expressing *YFP-FABD2* were germinated and grown *in vitro*, as described above. Pollen tubes were observed 2 to 5 hours after setup using a 63X (1.4 NA) plan-apo oil immersion objective. Using OpenLab5 software (Improvision/Perkin Elmer), images were captured for two minutes with 1-s intervals. Actin dynamics were quantified by determining the decay of image cross-correlation over time (Park and Nebenführ, 2013). Images were exported to ImageJ, and analyzed using a custom macro. The images were divided into 2 μm x 2 μm squares. The images were also divided into a second set of squares that were displaced by 1 μm from the original set of squares. For each square, cross-correlation was calculated for increasing intervals between all possible image frame pairs. An exponential decay was fitted to the data using Prism 6 software (GraphPad). The decay constants from the 10 squares with the largest range in the y-axis were plotted and their average was used to perform a Mann-Whitney unpaired t-test using Prism 6 software.

4.3: Results

4.3.1: YFP-XIA and YFP-XIJ localized to the tips of growing pollen tubes

One crucial piece of information for determining the function of a protein is to determine its localization. For a myosin, localization to a subcellular compartment suggests that particular myosin moves those organelles. Therefore, it was important to determine where the pollen myosins were localized within pollen grains and tubes. *XIJpro:YFP-XIJ* was shown to complement the *xij in vitro* pollen germination defect (see Chapter 3), while *XIApro:YFP-XIA* is currently being tested for its ability to at least partially complement the *xia xid in vivo* pollen tube growth defect. Nevertheless, YFP-XIJ and YFP-XIA localization was examined in *xij-1* and *xia-2* pollen grains, respectively, that were incubated on pollen germination medium.
YFP-XIJ usually was diffuse throughout the cytoplasm of pollen grains; however, in some grains, YFP-XIJ accumulated in a small region (**Figure 4.1**). Most pollen grains with the accumulation of YFP-XIJ were not observed germinating; however, some of the grains were observed bursting during germination (data not shown). In the rare cases where a pollen grain was observed from the start of accumulation of YFP-XIJ through germination, YFP-XIJ was observed to accumulate and then become diffuse again well before tube emergence although the distribution of YFP-XIJ fluorescence was uneven (**Figure 4.1**). The accumulation of YFP-XIJ appeared to be located near the future germination site (**Figure 4.1**), suggesting XIJ is involved in an early step of germination. As soon as the tube emerged, YFP-XIJ accumulated in the pollen tube (**Figure 4.1**).

Similar to YFP-XIJ, YFP-XIA appeared diffuse throughout the cytoplasm of most pollen grains, while accumulating in a small region in a few pollen grains. Interestingly, YFP-XIA accumulated at the future germination site (**Figure 4.2**). Pollen tubes only emerged at locations of YFP-accumulation, and as the tube emerged, YFP-XIA accumulated in the tube (**Figure 4.2**).

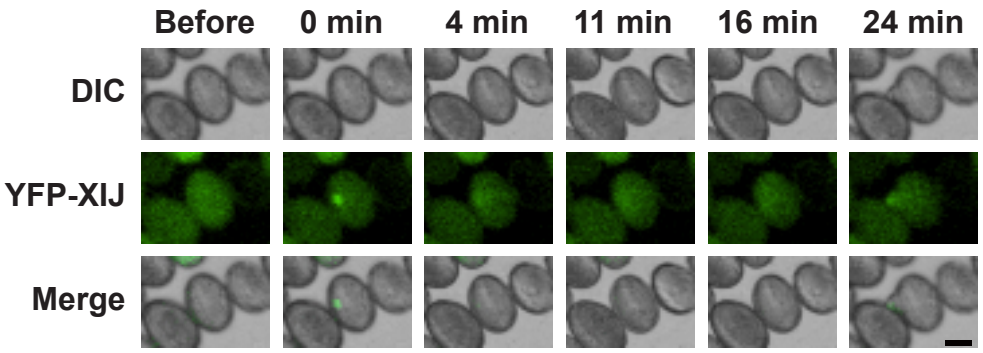

Figure 4.1: YFP-XIJ might localize to the future germination site

DIC (**Top**) and YFP fluorescence (**Center**) images of *xij-1 XIJpro:YFP-XIJ* pollen grains on pollen germination medium were captured and merged (**Bottom**) at various time points. Before YFP-XIJ accumulated in a small region, it appeared diffuse throughout the cytoplasm. YFP-XIJ became diffuse again over 10 minutes before germination, and once germinated YFP-XIJ accumulated in the newly emerged tube. Scale bar = 12.5 μm.

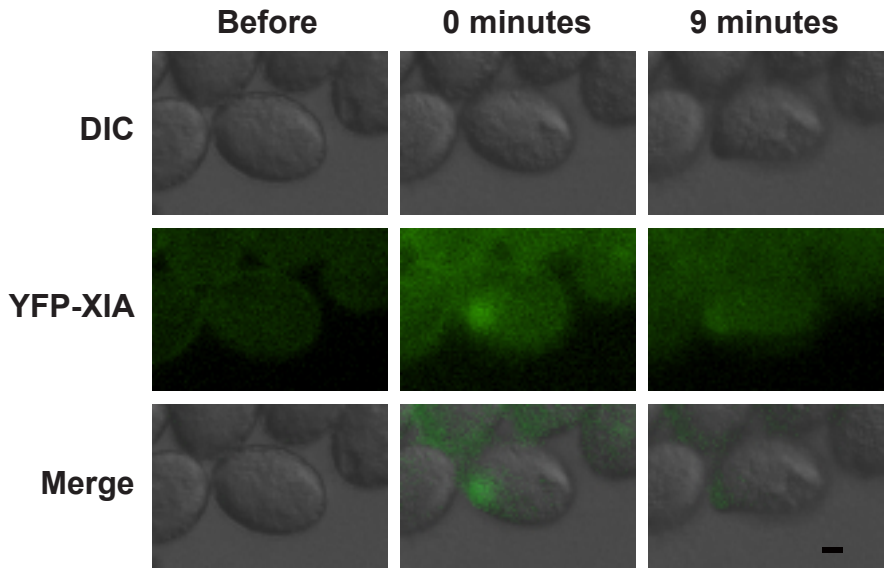

Figure 4.2: YFP-XIA localized to the future germination site

DIC (**Top**) and YFP fluorescence (**Center**) images of *xia-2 XIApro:YFP-XIA* pollen grains on pollen germination medium were captured and merged (**Bottom**) at various time points. YFP-XIA accumulated at the future germination site and in the newly emerged pollen tube. Scale bar = 5 μm.

This suggests that XIA might be involved in pollen germination; however, a pollen germination defect was not detected in *xia* or *xia xid* mutants. It is possible that XIA is only required for germination under certain environmental conditions or the other four pollen myosins compensate for the loss of *XIA* and *XID*.

The localization YFP-XIA and YFP-XIJ was also examined in growing pollen tubes. Both YFP-XIA and YFP-XIJ localized to the tip of growing pollen tubes (**Figures 4.3A and 4.3B** and **Movies 4.1 and 4.2**). *XIApro:mCherry-XIA* and *XIJpro:YFP-XIJ* were transformed into *WT*, and mCherry-XIA and YFP-XIJ co-localized at the tip of growing pollen tubes (**Figure 4.3D**). Sometimes mCherry-XIA appeared closer to the tip while other times YFP-XIJ was observed closer to the tip; however, this could have been a result of the delay in image capture. To confirm that YFP-XIA and YFP-XIJ were not freely diffusing throughout the cytoplasm and only appeared to accumulate at the tip as a result of the higher density of cytoplasm at the tip, *LAT52pro:GFP* pollen tubes were observed (**Figure 4.3C**). The cytoplasmic GFP appeared more evenly distributed throughout the pollen tube than YFP-XIA and YFP-XIJ. Interestingly, when pollen tubes stopped growing, YFP-XIA, mCherry-XIA, and YFP-XIJ were no longer concentrated at the pollen tube tip and only a weak fluorescence was observed throughout the pollen tube (data not shown). To confirm that the tip-localization of YFP-XIA and YFP-XIJ was a result of functional XIA and XIJ traveling along actin filaments, pollen tubes expressing either *YFP-XIA* or *YFP-XIJ* were treated with latrunculin B (latB), an inhibitor of actin polymerization. 1 μM latB, but not 100 nM latB, was sufficient to inhibit pollen tube growth within 10 minutes. 100 nM latB was the upper end of latB concentrations previously tested with *Arabidopsis* pollen (Zhang et al., 2010); however, since the latB was pipetted onto moist, solid medium, the concentration of latB could be diluted. Both latB concentrations resulted in the loss of YFP-XIA and YFP-XIJ accumulation at the tip (**Figure 4.4** and **Movies 4.3 - 4.6**). Mock treatment with

Figure 4.3: YFP-XIA and YFP-XIJ localized to the tips of growing pollen tubes

(**A**) 30-s intervals between images of *xia-2 XIApro:YFP-XIA* pollen tubes. YFP-XIA localized to the tip of growing pollen tubes.

(**B**) 1-min intervals between images of *xij-1 XIJpro:YFP-XIJ* pollen tubes. YFP-XIJ localized to the tip of growing pollen tubes.

(**C**) *LAT52pro:GFP* pollen tube had fluorescence throughout the cytoplasm.

(**D**) mCherry (**Top**) and YFP (**Center**) fluorescence images of a *WT* pollen tube with *XIApro:mCherry-XIA* and *XIJpro:YFP-XIJ* were captured and merged (**Bottom**). There was a 1.1-s delay between images. mCherry-XIA and YFP-XIJ co-localized at the tip of growing pollen tubes.

Scale bars = 2 μm.

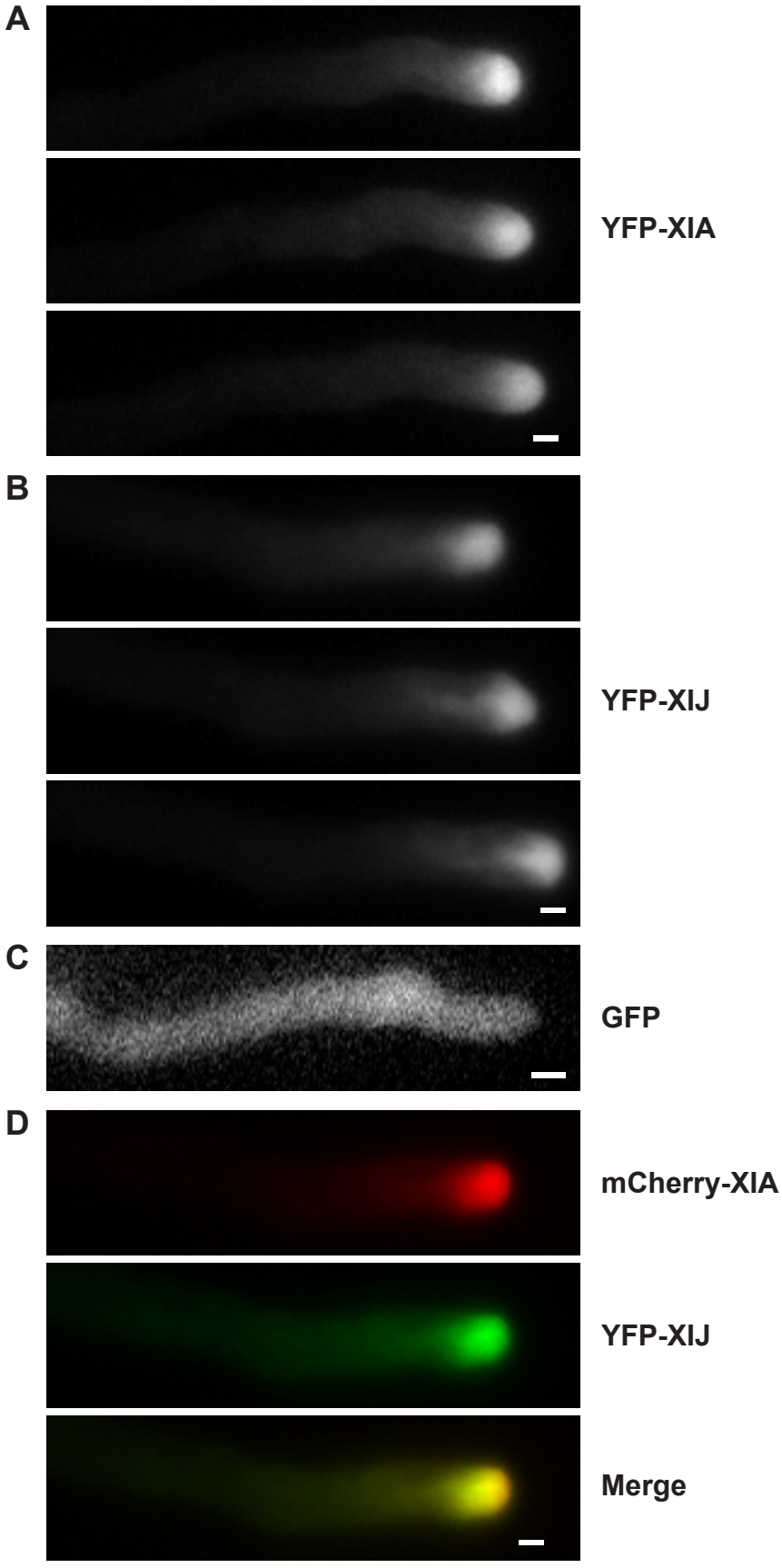
A
YFP-XIA
B
YFP-XIJ
C
GFP
D
mCherry-XIA
YFP-XIJ
Merge

Figure 4.4: Accumulation of YFP-XIA and YFP-XIJ at the tip was actin dependent

xia-2 XIApro:YFP-XIA (**A-C**) and *xij-1 XIJpro:YFP-XIJ* (**D-F**) pollen tubes were treated with 0 nM (**A,D**), 100 nM (**B,E**), or 1 μM (**C,F**) of latrunculin B (latB). Only 1 μM of latB was sufficient to completely inhibit pollen tube growth; however, both 100 nM and 1 μM latB resulted in the loss of YFP-XIA and YFP-XIJ accumulation at the pollen tube tip. Scale bar = 3 μm.

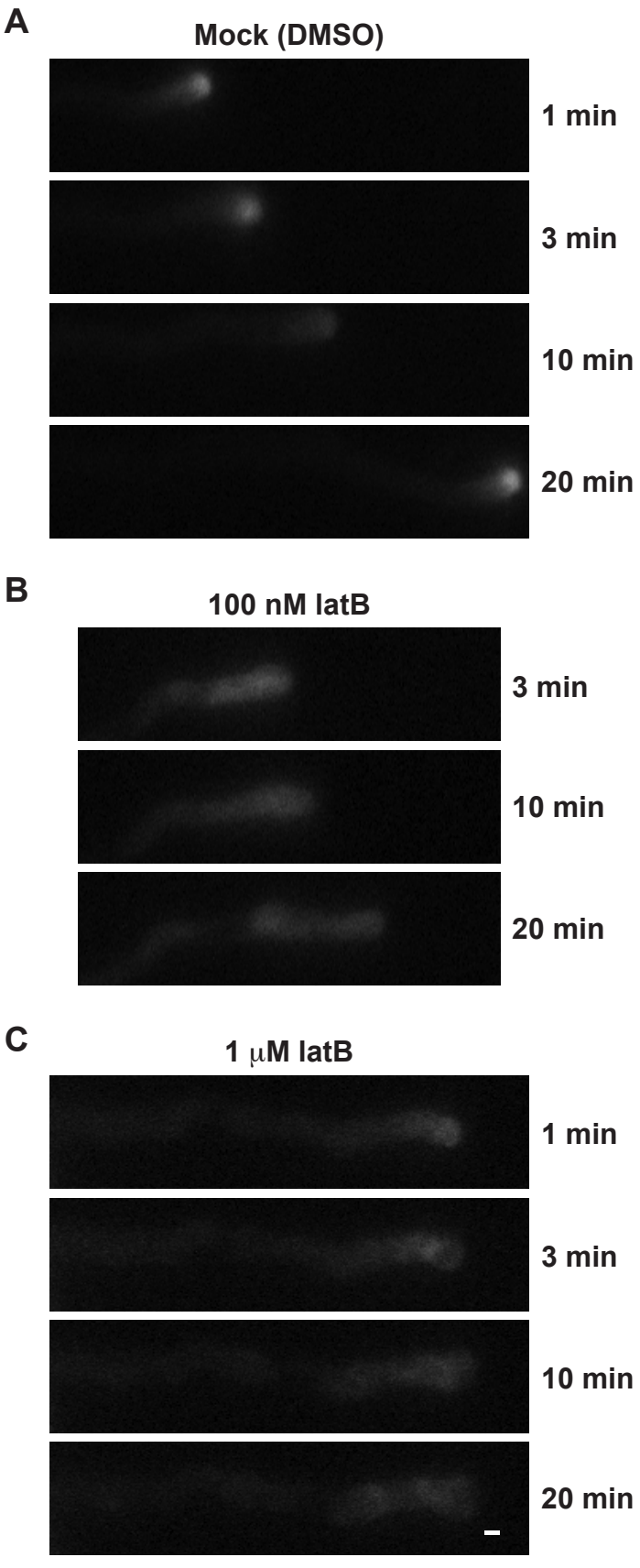
A
Mock (DMSO)
1 min
3 min
10 min
20 min
B
100 nM latB
3 min
10 min
20 min
C
1 μM latB
1 min
3 min
10 min
20 min

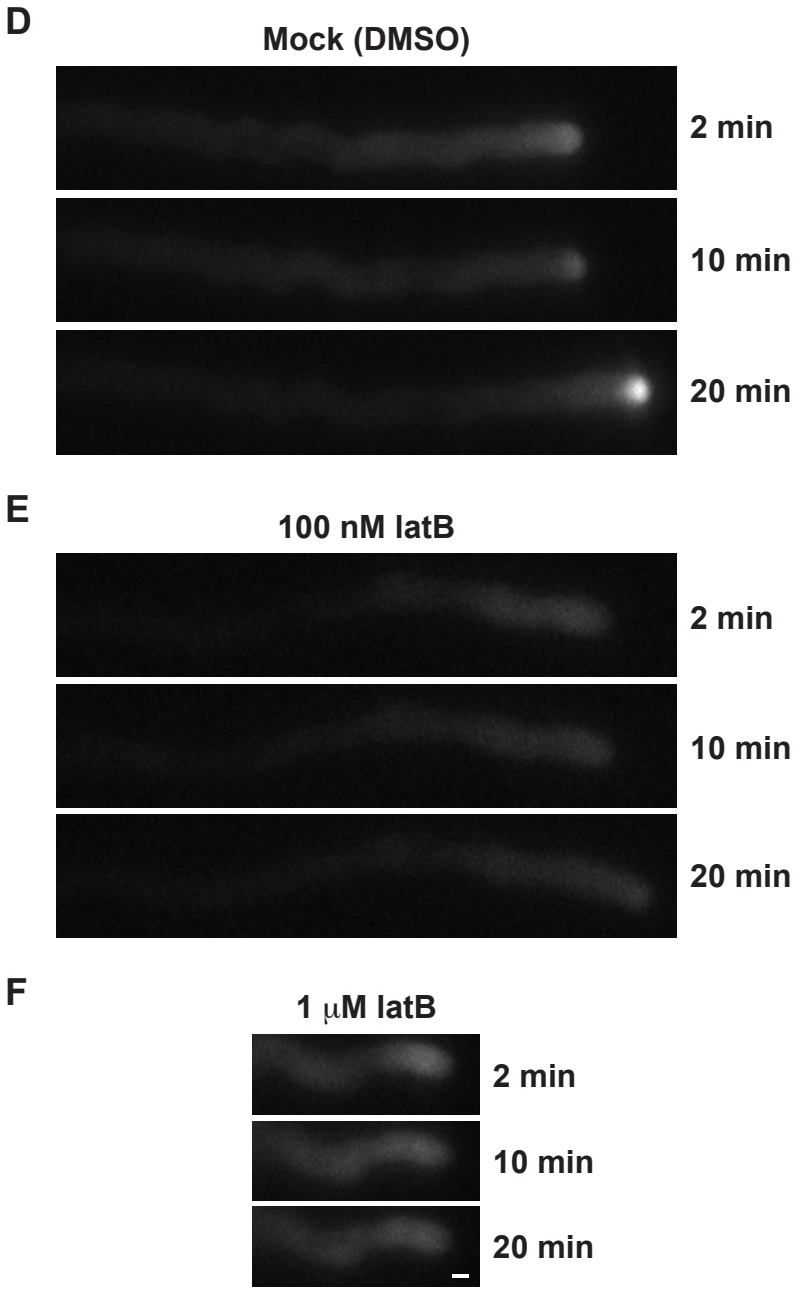

Figure 4.4: Continued

DMSO did not affect YFP-XIA accumulation or pollen tube growth (**Figure 4.4A** and **Movie 4.7**). Mock treatment with DMSO did initially retard the growth of *YFP-XIJ* pollen; however, the pollen tubes recovered within 15 minutes and accumulated YFP-XIJ at the tip (**Figure 4.4D** and **Movie 4.8**). In the mock treatment, YFP-XIJ was observed accumulated at the tip only during pollen tube growth. This correlation between growth and accumulation of YFP-XIJ was disrupted with 100 nM latB (**Figure 4.4E**). The pollen tube was still growing, but lost the accumulation of YFP-XIJ at the tip. Overall, these results suggest that the accumulation of YFP-XIA and YFP-XIJ at the pollen tube tip is dependent on the actin cytoskeleton.

Since YFP-XIA and YFP-XIJ accumulated at the tip of growing pollen tubes, these pollen myosins were predicted to transport the secretory vesicles that accumulate at the apex. Therefore, the degree of overlap between vesicle accumulation and myosin accumulation was determined. RabA4d is predicted to associate with post-Golgi vesicles (Vernoud et al., 2003), and the accumulation of YFP-RabA4d at the tip of growing pollen tubes is sensitive to brefeldin A, a secretion inhibitor (Lee et al., 2008; Szumlanski and Nielsen, 2009). Therefore, *XIJpro:CFP-RabA4d* was transformed into *xia-2 XIApro:YFP-XIA* and *xij-1 XIJpro:YFP-XIJ* plants. CFP and YFP images of growing pollen tubes were captured and merged. YFP-XIA and YFP-XIJ accumulation was confined to a small region in the apex of growing pollen tubes, whereas, CFP-RabA4d accumulation was not as consolidated (**Figure 4.5** and **Movies 4.9 and 4.10**). Interestingly, CFP-RabA4d in *xia-2 XIApro:YFP-XIA* pollen tubes was not as confined in the apical region as was observed in *WT* (see **Figure 4.7**) and *xij-1 XIJpro:YFP-XIJ* pollen tubes (**Figure 4.5**). It is possible that vesicle accumulation is altered either in the *xia* mutant or in the presence of YFP-XIA, so this will have to be investigated further. Since CFP-RabA4d accumulation partially overlapped with YFP-XIA and YFP-XIJ accumulation, a fluorescence resonance energy transfer (FRET) experiment was conducted using these lines to determine

Figure 4.5: YFP-XIA and YFP-XIJ do not co-localize or interact with CFP-RabA4d

xia-2 pollen tubes expressing *YFP-XIA* and *CFP-RabA4d* (**A**) and *xij-1* pollen tubes expressing *YFP-XIJ and CFP-RabA4d* (**B**) were grown *in vitro*. CFP (red), YFP (green), and FRET images were captured. Normalized FRET (NFRET) values were calculated and visualized using color to represent the relative degree of NFRET. Neither YFP-XIA nor YFP-XIJ produced a FRET signal with CFP-RabA4d. CFP and YFP images were also merged to compare the tip-localization of myosins and RabA4d. The accumulation of CFP-RabA4d only partially overlapped (yellow) with the accumulation of YFP-XIA and YFP-XIJ. Scale bar = 2 μm.

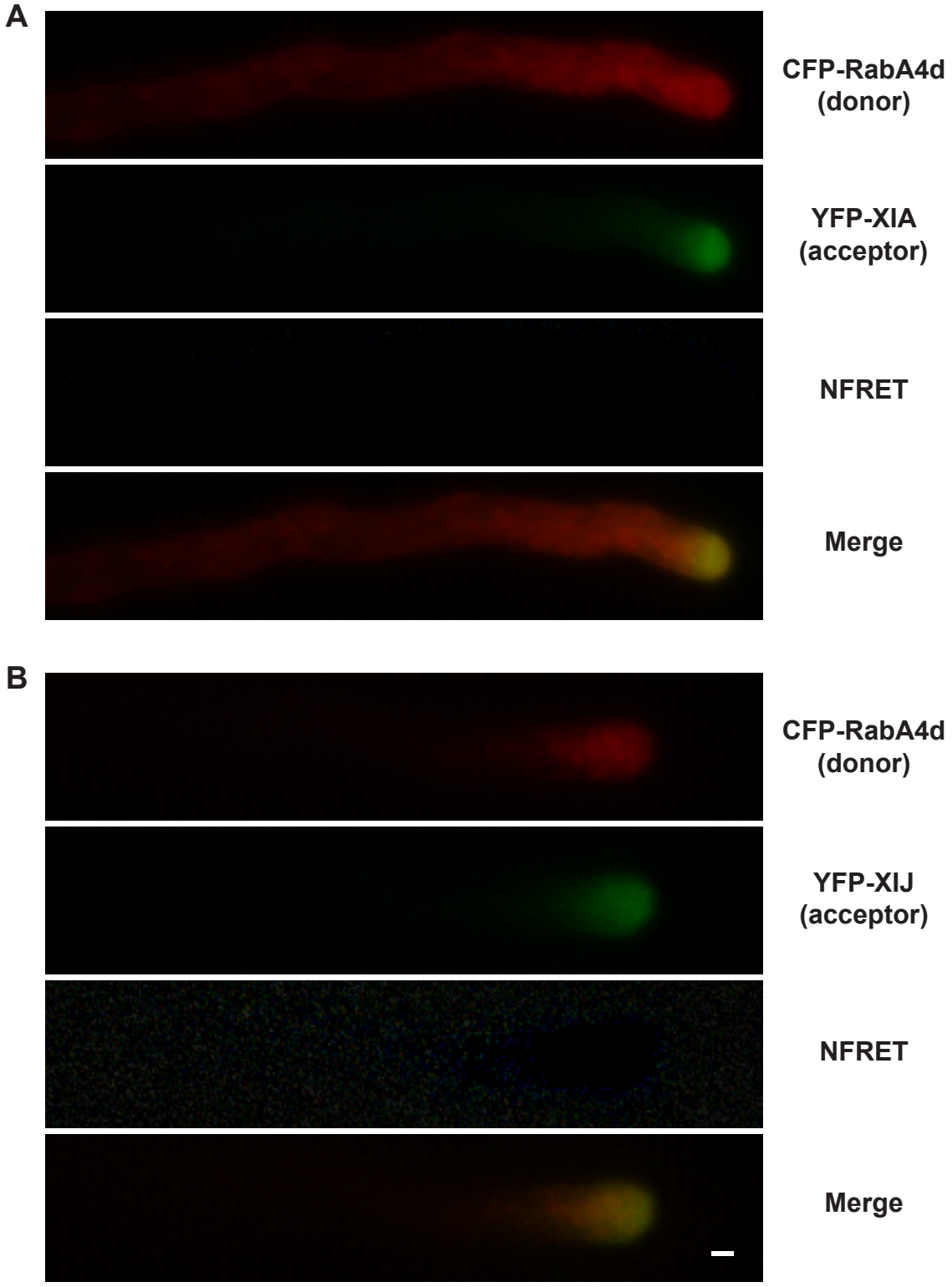
A
CFP-RabA4d
(donor)
YFP-XIA
(acceptor)
NFRET
Merge
B
CFP-RabA4d
(donor)
YFP-XIJ
(acceptor)
NFRET
Merge

whether or not RabA4d was closely associated with these pollen myosins. Pollen tubes expressing both *YFP-XIA* and *CFP-RabA4d* or *YFP-XIJ* and *CFP-RabA4d* did not produce a FRET signal (**Figure 4.5**). This suggests that RabA4d probably does not interact with XIA or XIJ. Even though YFP-XIA and YFP-XIJ do not interact with CFP-RabA4d, they could still be associated with the secretory vesicles at the tip.

To investigate the possible association of XIA and XIJ to secretory vesicles accumulated at the tip, pollen tubes expressing either *YFP-XIA* or *YFP-XIJ* were treated with 36 μM brefeldin A (BFA), a secretion inhibitor. BFA results in cessation of pollen tube growth, loss of vesicle accumulation at the tip, and aggregation of membranes from secretory vesicles in the subapical region (Parton et al., 2003). As expected, pollen tube growth ceased 10-15 minutes after the addition of BFA (**Figure 4.6B and 4.6D** and **Movies 4.11 and 4.12**). BFA also resulted in the gradual loss of YFP-XIA and YFP-XIJ accumulation at the pollen tube tip; however, aggregation was not observed (**Figure 4.6B and 4.6D** and **Movies 4.11 and 4.12**). Mock treatment with ethanol did not affect YFP-XIA accumulation or pollen tube growth (**Figure 4.6A** and **Movie 4.13**). Mock treatment with ethanol did initially inhibit the growth of *YFP-XIJ* pollen; however, the pollen tubes recovered within 25 minutes and accumulated YFP-XIJ at the tip (**Figure 4.6D** and **Movie 4.14**). These results suggest that YFP-XIA and YFP-XIJ may normally associate with secretory vesicles at the pollen tube tip; however, they do not stay associated after treatment with BFA.

4.3.2: RabA4d accumulation at the tip of growing pollen tubes was not altered

The accumulation of vesicles at the tip of growing pollen tubes is dependent on actin filaments (Parton et al., 2001), suggesting a role for myosins in vesicle accumulation. Fluorescently tagged RabA4d and XIJ accumulated at the tips of growing pollen tube; however, they did not completely co-localize or interact. Nevertheless, it was still possible that XIJ was

Figure 4.6: BFA treatment reduced the accumulation of YFP-XIA and YFP-XIJ at the tip

xia-2 XIApro:YFP-XIA (**A-B**) and *xij-1 XIJpro:YFP-XIJ* (**C-D**) pollen tubes were treated with 0 μM (**A,C**) or 36 μM (**B,D**) of brefeldin A (BFA). BFA completely inhibited pollen tube growth and resulted in the gradual loss of YFP-XIA and YFP-XIJ accumulation at the pollen tube tip. Scale bar = 3 μm.

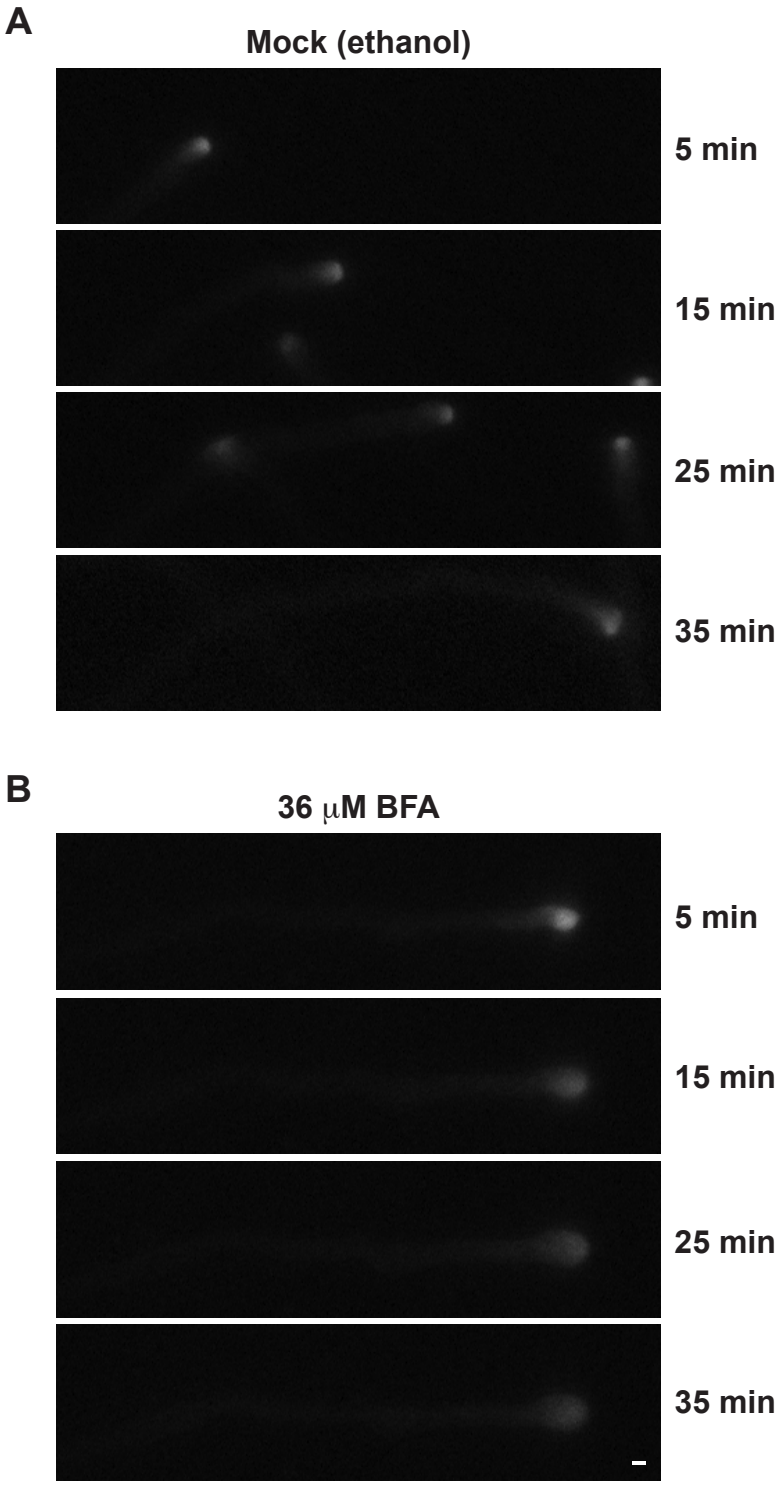
A
Mock (ethanol)
5 min
15 min
25 min
35 min
B
36 μM BFA
5 min
15 min
25 min
35 min

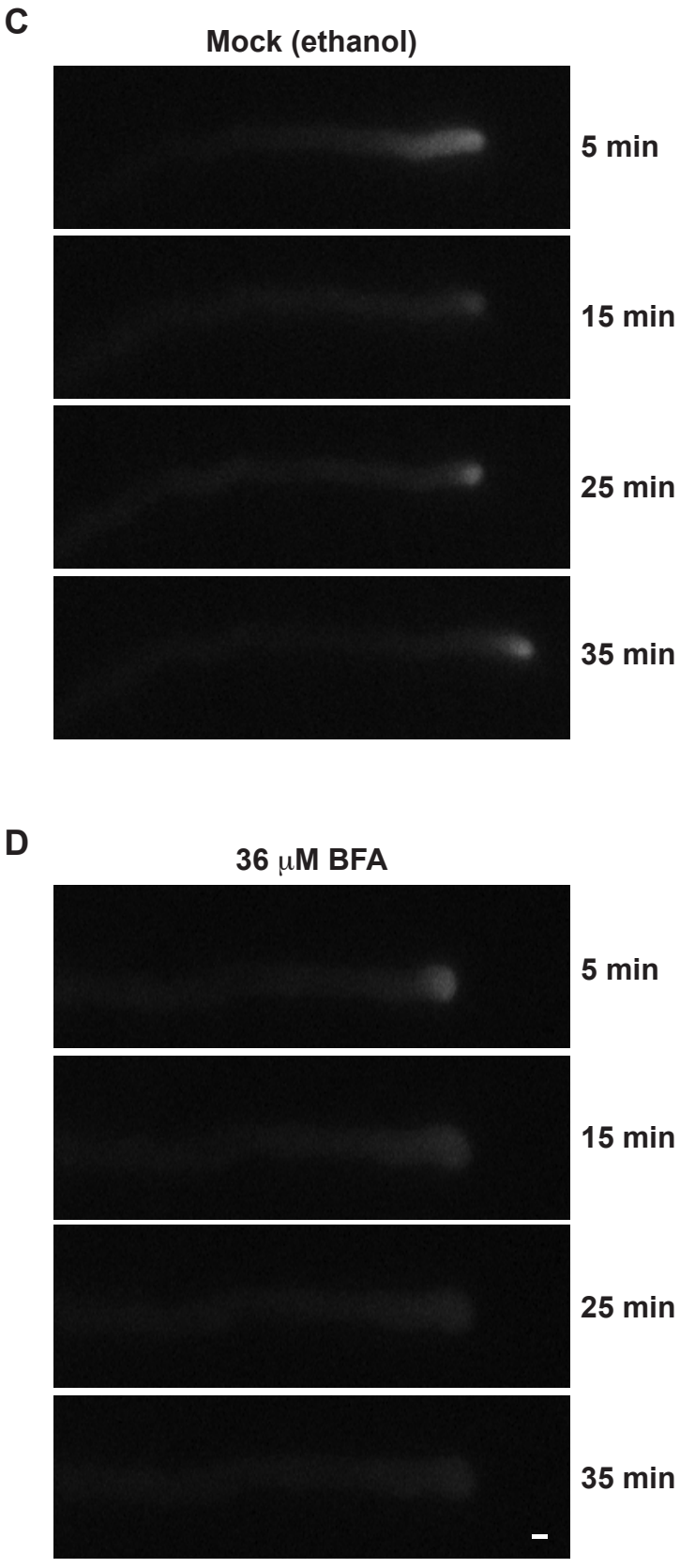

Figure 4.6: Continued

involved in the accumulation of RabA4d-associated vesicles. Furthermore, out of the remaining five pollen myosins, XIC and XIE might also have a role in the vesicle accumulation at the tip of growing pollen tubes because *xic xie* pollen tubes grew more slowly than *WT* pollen tubes (see Chapter 3). Therefore, YFP-RabA4d accumulation was examined in *WT*, *xic-1 xie-1*, and *xij-1* pollen tubes.

In *WT*, *xic-1 xie-1*, and *xij-1*, YFP-RabA4d accumulated at the tip of growing pollen tubes (**Figure 4.7A** and **Movies 4.15 - 4.17**). YFP fluorescence at the tip of pollen tubes was measured over time; however, a direct comparison of fluorescence intensity among the three genotypes was not possible because fluorescence intensity varied even among pollen from the same flower (data not shown). Mean fluorescence intensity at the tip fluctuated slightly over time in all three genotypes (**Figure 4.7B**). Coefficients of variation of YFP-RabA4d accumulation at the tip of *xic-1 xie-1* pollen tubes were slightly lower but not significantly different from those of *WT* and *xij-1* pollen tubes (**Figure 4.7C**; $p > 0.05$). Overall for *WT* and mutant pollen tubes, accumulation of YFP-RabA4d was stable with only slight fluctuations in intensity over time (**Figure 4.7**).

4.3.3: Golgi stacks and peroxisomes moved at reduced velocities in *xic xie* pollen tubes

Single and higher order myosin XI mutants have reduced organelle motility in vegetative tissues (Peremyslov et al., 2008; Prokhnevsky et al., 2008; Peremyslov et al., 2010; Ueda et al., 2010; Avisar et al., 2012). Furthermore, drug treatments that disrupt actin filaments have been shown to inhibit organelle movements in pollen tubes (Mascarenhas and Lafountain, 1972; Heslop-Harrison and Heslop-Harrison, 1989a; Vidali et al., 2001). Hence, pollen myosin mutants were predicted to have reduced organelle motility. Since *xic xie* pollen tubes exhibited the strongest growth defects and *xij* pollen had the unique pollen germination defect (see Chapter 3), peroxisome and Golgi stack movements were examined in *WT*, *xic-1 xie-1*, and *xij-1* pollen

Figure 4.7: RabA4d accumulation at the tip of growing pollen tubes was not altered

(**A**) *WT*, *xic-1 xie-1*, and *xij-1* pollen tubes expressing *YFP-RabA4d* were imaged for two minutes at 0.5-s intervals. YFP-RabA4d accumulated at the tip. Scale bar = 2 μm.

(**B**) Normalized fluorescence intensity of YFP-RabA4d fluctuated to the same degree in *WT* (black), *xic-1 xie-1* (blue), and *xij-1* (red) pollen tubes. Each line represents data from one pollen tube.

(**C**) Coefficients of variation of YFP-RabA4d accumulation at the tip of *WT*, *xic-1 xie-1*, and *xij-1* pollen tubes. Means ± SD were not significantly different ($p > 0.05$, Mann-Whitney test).

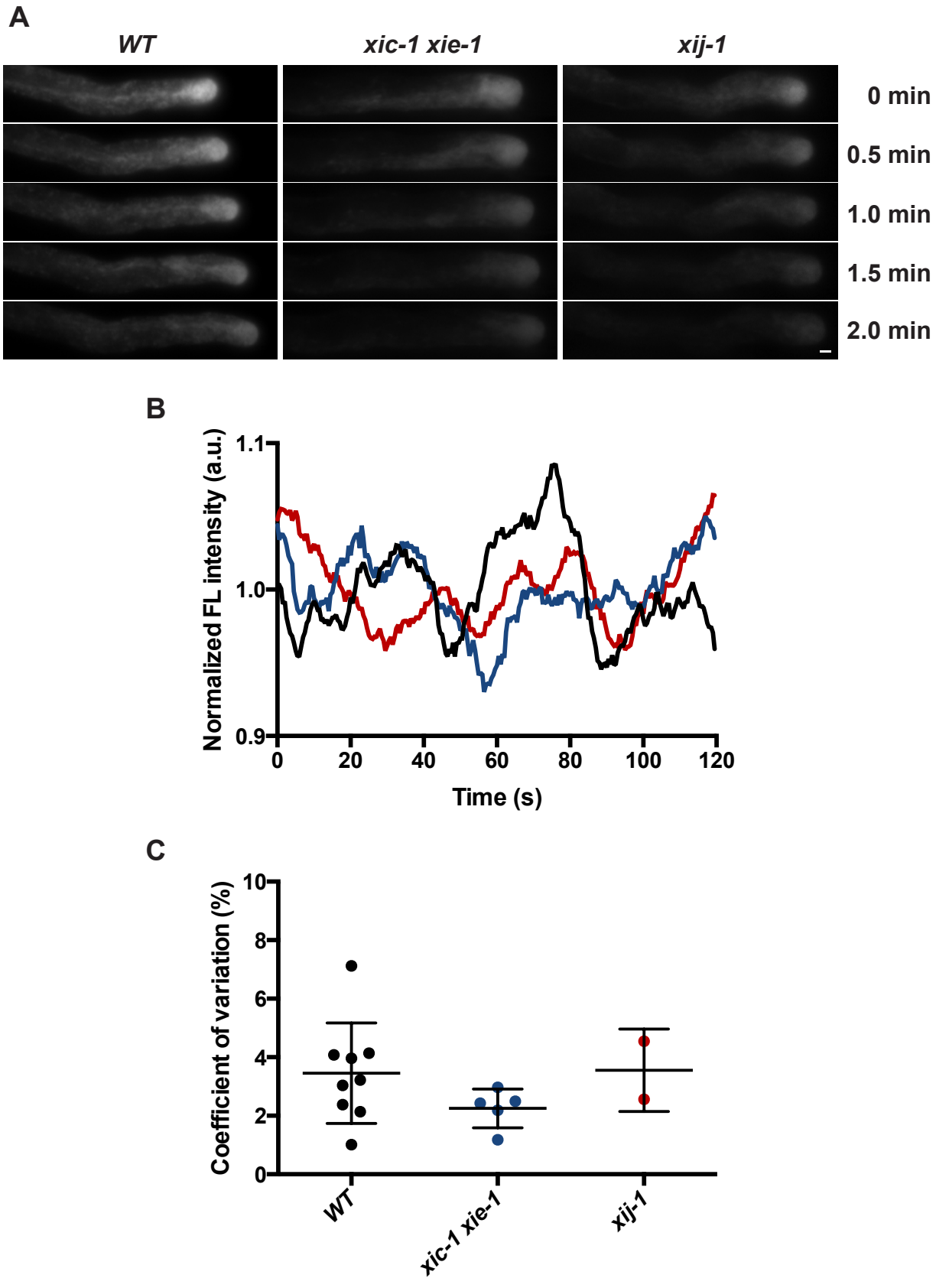
A
WT
xic-1 xie-1
xij-1
0 min
0.5 min
1.0 min
1.5 min
2.0 min
B
Normalized FL intensity (a.u.)
1.1
1.0
0.9
0
20
40
60
80
100
120
Time (s)
C
Coefficient of variation (%)
10
8
6
4
2
0
WT
xic-1 xie-1
xij-1

tubes.

Pollen tubes stably expressing either a YFP-peroxisome or YFP-Golgi marker were grown *in vitro* and examined using wide-field epifluorescence microscopy. *xic-1 xie-1* pollen tubes had visually reduced peroxisome and Golgi stack movements compared to *WT* pollen tubes (**Figure 4.8A** and **Movies 4.18 - 4.21**). There was not a visual difference in organelle velocities between *WT* and *xij-1* pollen tubes (**Figure 4.8A** and **Movies 4.18 - 4.19 and 4.22 - 4.23**). At least nine independent, two-minute time-lapse image sequences with 0.5-s intervals were captured for each treatment, except only 3 were captured for *xij-1* pollen tubes expressing the peroxisome marker. Organelles were detected and tracked automatically using the Particle Tracker plug-in (Sabalzarini and Koumoutsakos, 2005) for ImageJ. The cumulative frequency distribution of velocities was plotted for all measurements from individual time-lapse image sequences. The frequency distribution of Golgi stack and peroxisome velocities varied greatly between pollen tubes of the same genotype (**Figure 4.8B**). Despite this variation from cell to cell, the results from *WT* and *xic-1 xie-1* pollen tubes were clearly separated (**Figure 4.8B**). Velocities were then combined by genotype, and the cumulative frequency distribution of velocities between *WT* and *xic-1 xie-1* were significantly different from each other ($p < 0.0001$; **Figure 4.8B**). Organelle movements were not analyzed in the *xic* and *xie* single mutants; however, the lack of major fertility and growth defects in the single mutants would suggest that organelle motilities remain similar to *WT*. Interestingly in *xij-1* pollen tubes, peroxisomes moved significantly slower and Golgi stacks moved significantly faster than in *WT* pollen tubes ($p < 0.0001$; **Figure 4.8B**). Since there did not appear to be a difference visually (**Figure 4.8A** and **Movies 4.19 and 4.23**), perhaps the slight differences between *WT* and *xij-1* organelle velocities were exaggerated as a result of the large sample sizes (**Table 4.2**).

Figure 4.8: Golgi stacks and peroxisomes moved at reduced velocities in *xic xie* pollen tubes

WT (black), *xic-1 xie-1* (blue), and *xij-1* (red) pollen tubes expressing either a YFP peroxisome marker or a YFP Golgi marker were imaged for two minutes at 0.5-s intervals.

(**A**) For each genotype, the first frame (**Top**) was compared to the first 20 frames, representing 10 seconds, merged (**Bottom**). *xic-1 xie-1* pollen tubes had visually slower peroxisome and Golgi stack movements than *WT* and *xij-1* pollen tubes. Scale bar = 2 μm.

(**B-C**) Velocity measurements were plotted as cumulative frequency distribution graphs. Peroxisomes and Golgi stacks moved more slowly in *xic-1 xie-1* pollen tubes than *WT* pollen tubes. Peroxisomes moved slower and Golgi stacks moved faster in *xij-1* pollen tubes than *WT* pollen tubes.

(**B**) Organelles were automatically detected and velocities were measured for each frame. Velocity measurements were combined for each time-lapse (**Top**) and by genotype (**Bottom**).

(**C**) 20 organelles moving visually very fast were manually tracked for two pollen tubes per treatment. Velocity measurements were combined for each pollen tube (**Top**) and by genotype (**Bottom**).

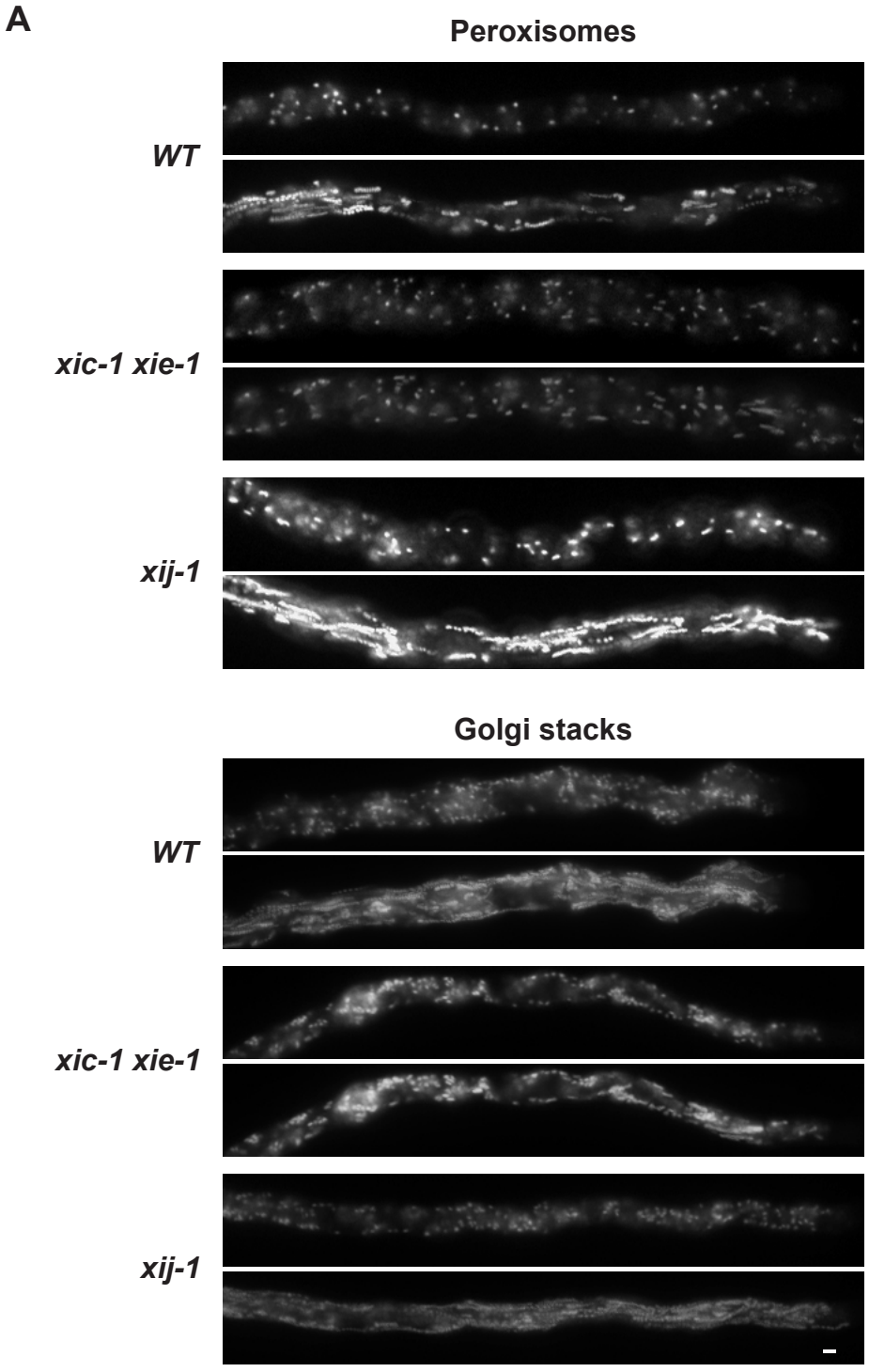
A
Peroxisomes
WT
xic-1 xie-1
xij-1
Golgi stacks
WT
xic-1 xie-1
xij-1

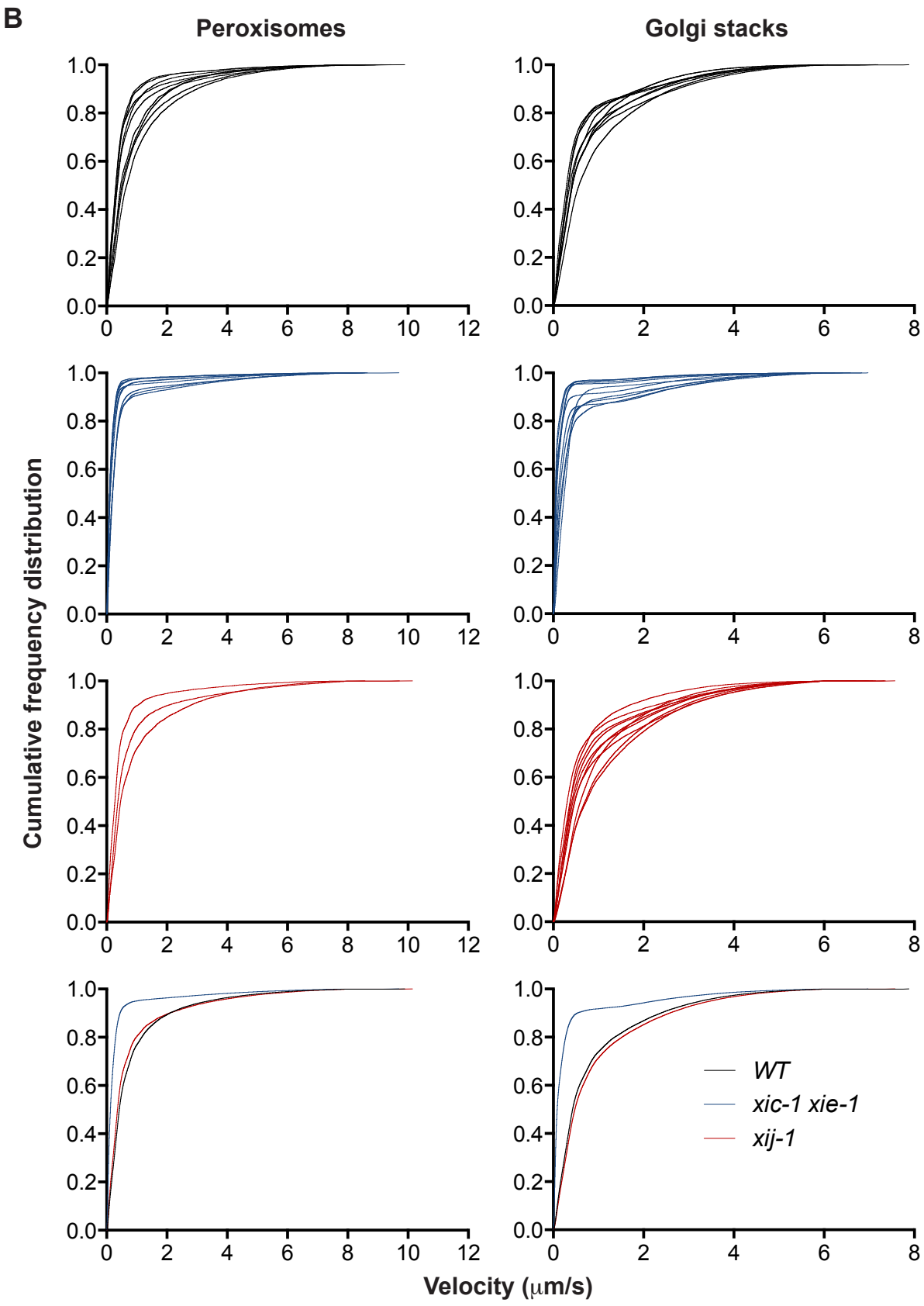

Figure 4.8: Continued

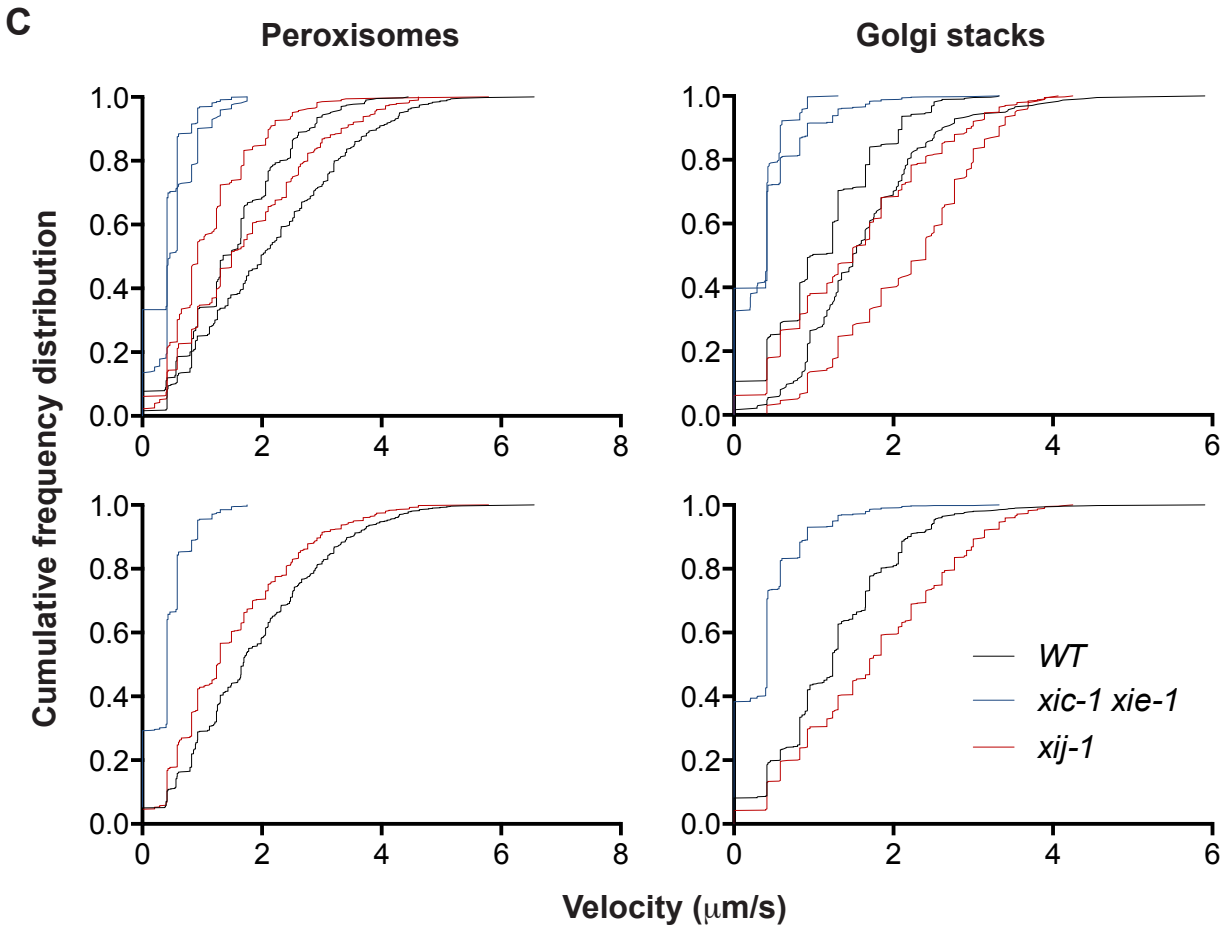

Figure 4.8: Continued

Table 4.2: Sample sizes for organelle movement analysis

Method	Organelle	Genotype	# of measurements	# of organelles
Automated	Peroxisomes	*WT*	108148	479
		xic-1 xie-1	144471	663
		xij-1	40650	183
	Golgi stacks	*WT*	270017	1190
		xic-1 xie-1	218766	949
		xij-1	250523	1110
Manual	Peroxisomes	*WT*	978	20
		xic-1 xie-1	1601	20
		xij-1	890	20
	Golgi stacks	*WT*	882	20
		xic-1 xie-1	1723	20
		xij-1	638	20

# of organelles for the automated method was calculated by adding the average # of particles detected per frame for each time-lapse sequence.

After examining the tracking results, it was apparent that the automated tracking program made some errors due to the high velocity and high density of the organelles in pollen tubes. Occasionally, an organelle in one frame would be incorrectly linked to a different organelle in the next frame, as has been described previously (Chenouard et al., 2014). This error in linkage often resulted in false high velocity measurements that affected the cumulative frequency distributions (**Figure 4.8B**). Therefore, the velocities of organelles that were visually identified as moving very fast were manually measured for two pollen tubes per genotype (**Figure 4.8C**). For *WT* pollen tubes, the maximum velocities for peroxisomes and Golgi stacks measured by manual tracking were 6.6 μm/s and 5.9 μm/s, respectively. For *xic-1 xie-1* pollen tubes, the maximum velocities measured for peroxisomes and Golgi stacks were 1.8 μm/s and 3.3 μm/s, respectively. For *xij-1* pollen tubes, the maximum velocities for peroxisomes and Golgi stacks measured were 5.8 μm/s and 4.2 μm/s, respectively. These maximal velocities were considerably slower than those determined by automatic tracking, particularly for the *xic-1 xie-1* pollen tubes suggesting the false high velocity measurements have a particular range regardless of the actual velocities within the pollen tube. Nevertheless, the clear difference in velocity distribution between *WT* and *xic-1 xie-1* detected by automatic tracking (**Figure 4.8B**) is still valid as the algorithm made only few mistakes at slower velocities (< 1 μm/s) that represent 65-95% of all measurements.

Even though the manual tracking of visually very fast organelles provided very different maximal velocities than the automated tracking of all organelles, the differences detected between genotypes were similar for the two methods. Manually tracked peroxisomes and Golgi stacks in *xic-1 xie-1* pollen tubes moved at significantly reduced velocities compared to organelles in *WT* pollen tubes ($p < 0.0001$; **Figure 4.8C**). Peroxisomes also moved significantly more slowly in *xij-1* pollen tubes than in *WT* pollen tubes ($p < 0.0001$; **Figure 4.8C**). Manually

tracked Golgi stacks were traveling faster in *xij-1* pollen tubes than in *WT* pollen tubes ($p < 0.0001$; **Figure 4.8C**), as had been observed with automated tracking ($p < 0.0001$; **Figure 4.8B**). For manual tracking, ten organelles moving towards and ten organelles moving away from the pollen tube tip were tracked. Interestingly, organelles in 8 out of the 12 pollen tubes moved faster when traveling away from the tip, while only in 2 pollen tubes organelles moved faster when traveling towards the tip ($p < 0.001$; **Figure 4.9**).

4.3.4: Actin filament dynamics were not altered in myosin XI mutant pollen tubes

The *mya2 xik* double mutant has altered actin filament organization that in higher order mutants becomes more skewed from the typical longitudinal orientation (Peremyslov et al., 2010; Ueda et al., 2010). Not only are class XI myosins required for normal actin organization, but they are also involved in the dynamic rearrangements of actin filaments. Recently, the *xik* single mutant was shown to have a reduction in actin filament dynamics compared to *WT* (Park and Nebenführ, 2013). To investigate the role of class XI myosins in actin filament organization and rearrangements in pollen tubes, actin filaments in *WT*, *xic-1 xie-1*, and *xij-1* pollen tubes were visualized with YFP-FABD2. YFP-FABD2, YFP fused to the second-actin binding domain of *A. thaliana* fimbrin1, only labels the actin filaments in the shank of growing pollen tubes and not the subapical actin mesh (Wilsen et al., 2006). Overall, the organization of actin filaments in the shank was similar for *WT*, *xic-1 xie-1*, and *xij-1* pollen tubes (**Figure 4.10A**). The rate of actin filament rearrangements also appeared similar in all three genotypes (**Movies 4.24 - 4.26**). Quantification of actin filament dynamics by measuring the decay of image cross-correlation over time confirmed that there was no significant difference between *WT* and mutant (**Figure 4.10B**; $p > 0.05$). Therefore, either XIC, XIE, and XIJ are not involved in actin filament organization and rearrangements, or their function is redundant with other pollen myosins.

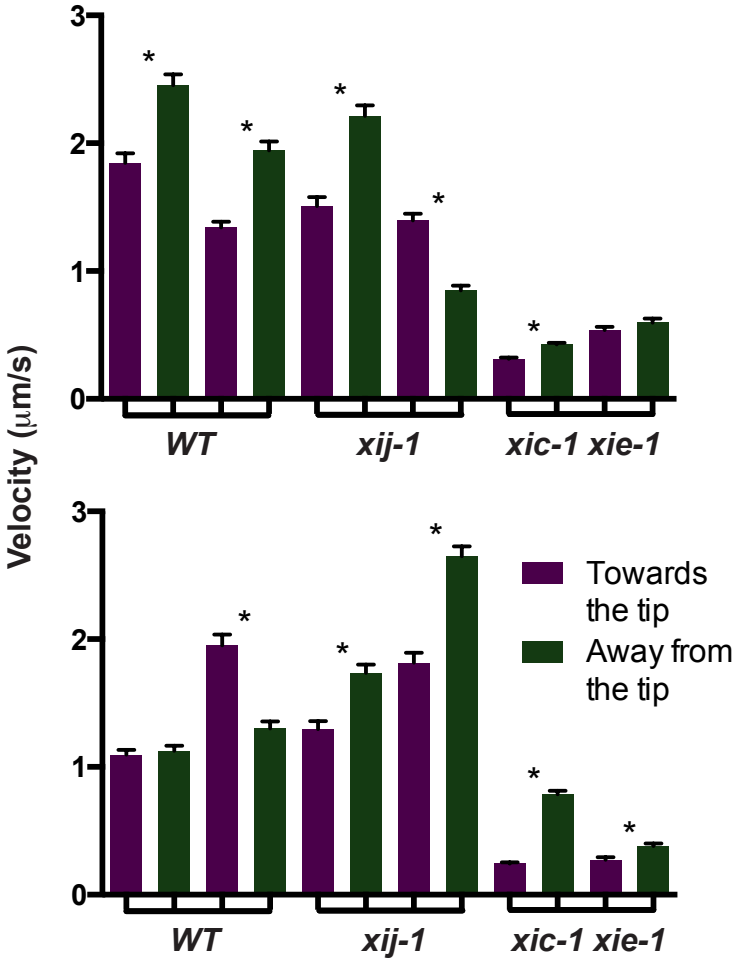

Figure 4.9: Organelles tended to move slowly traveling towards the pollen tube tip

WT, *xij-1*, and *xic-1 xie-1* pollen tubes expressing either a YFP peroxisome marker (**Top**) or a YFP Golgi marker (**Bottom**) were imaged for two minutes at 0.5-s intervals. 10 organelles traveling towards (purple) and 10 organelles traveling away from (green) the pollen tube tip were manually tracked (Mean ± SEM; * $p < 0.001$, Kolmogorov-Smirnov test). Peroxisomes and Golgi stacks traveling away from the pollen tube tip tended to move faster than organelles traveling towards the pollen tube tip.

Figure 4.10: Actin filament dynamics were similar in *WT* and mutant pollen tubes

(**A**) Actin filaments in the pollen tube shank were labeled with YFP-FABD2, and images are representative of actin filament organization 20 μm from the tip of growing pollen tubes. Actin filament organization in the shank was similar in *WT*, *xic-1 xie-1*, and *xij-1* pollen tubes. Scale bar = 2 μm.

(**B**) Actin filament dynamics in *WT* (black), *xic-1 xie-1* (blue), and *xij-1* (red) pollen tubes were measured by fitting an exponential decay curve to image cross-correlation data with increasing time intervals. Each box-and-whisker plot represents the minimum, 25th percentile, median, 75th percentile, and maximum decay constants from the 10 most active regions of a single pollen tube. Mean decay constants were compared, and there was no significant difference between *WT* and mutant actin dynamics ($p > 0.05$, Mann-Whitney test).

A

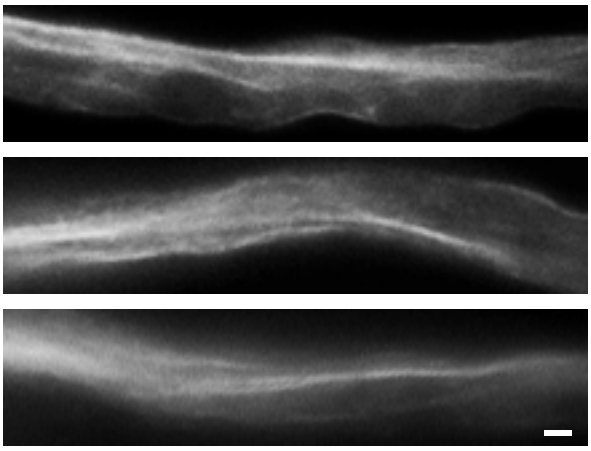
WT
xic-1 xie-1
xij-1

B

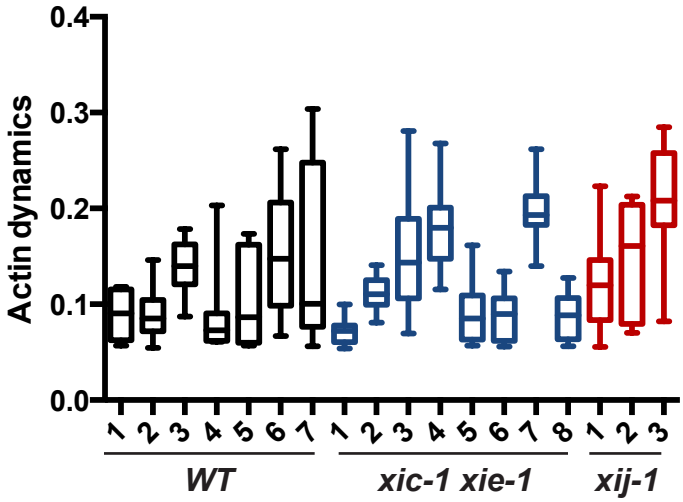
Actin dynamics
0.4
0.3
0.2
0.1
0.0
1 2 3 4 5 6 7 1 2 3 4 5 6 7 8 1 2 3
WT
xic-1 xie-1
xij-1

4.3.5: Localization of ROP1 and its effectors, RIC3 and RIC4, was unchanged in mutants

ROP1, a small Rho-GTPase, is predominately expressed in pollen (Li et al., 1998) and localizes to the apical plasma membrane of growing pollen tubes (Lin et al., 1996; Hwang et al., 2008). ROP1 is required for pollen tube growth (Lin and Yang, 1997; Li et al., 1999). Expression of constitutively active ROP1 resulted in the complete depolarization of pollen tubes while overexpression of ROP1 only resulted in partial depolarization (Li et al., 1999). Comparable to ROP1 overexpression lines, expression of fluorescently tagged ROP1 in *Arabidopsis* pollen tubes resulted in short, wide pollen tubes with slight swelling of the tip (Hwang et al., 2008). Furthermore, GFP-ROP1 localization was not restricted to the apical plasma membrane (Hwang et al., 2008). It was hypothesized that the reduction in pollen tube growth observed in some myosin XI mutants (see Chapter 3) was a result of the mislocalization of ROP1. To determine whether or not ROP1 localization was altered in pollen myosin mutants, *YFP-ROP1* was expressed in *WT*, *xic-1 xie-1*, and *xij-1* pollen tubes. In all three genotypes, YFP-ROP1 was observed throughout the pollen tube (**Figure 4.11A**). An alternative approach using antibodies to ROP might have provided clearer results since antibodies would have only labeled native ROP1 in the apical plasma membrane.

Two ROP1 effectors, RIC3 and RIC4, have been shown to regulate tip growth by affecting F-actin dynamics. RIC, ROP-interactive CRIB motif-containing, proteins interact with active ROP1, and overexpression of either RIC3 or RIC4 results in partial depolarization of pollen tube growth comparable to the overexpression of ROP1 (Wu et al., 2001). Furthermore, overexpression of either RIC3 or RIC4 alters the accumulation of vesicles at the tip of growing pollen tubes (Lee et al., 2008). Interestingly, co-overexpression of RIC3 and RIC4 results in normal vesicle accumulation and pollen tube growth, suggesting RIC3 and RIC4 expression levels must be balanced for normal growth to occur (Gu et al., 2005; Lee et al., 2008). RIC4

Figure 4.11: Localization of ROP1 and its effectors was unaffected by the loss of myosin XI

WT, *xic-1 xie-1*, and *xij-1* pollen tubes expressing *YFP-ROP1* (**A**), *YFP-RIC3* (**B**), or *YFP-RIC4* (**C**) were imaged. No differences in localization were observed between *WT* and mutant pollen tubes. Scale bar = 2 μm.

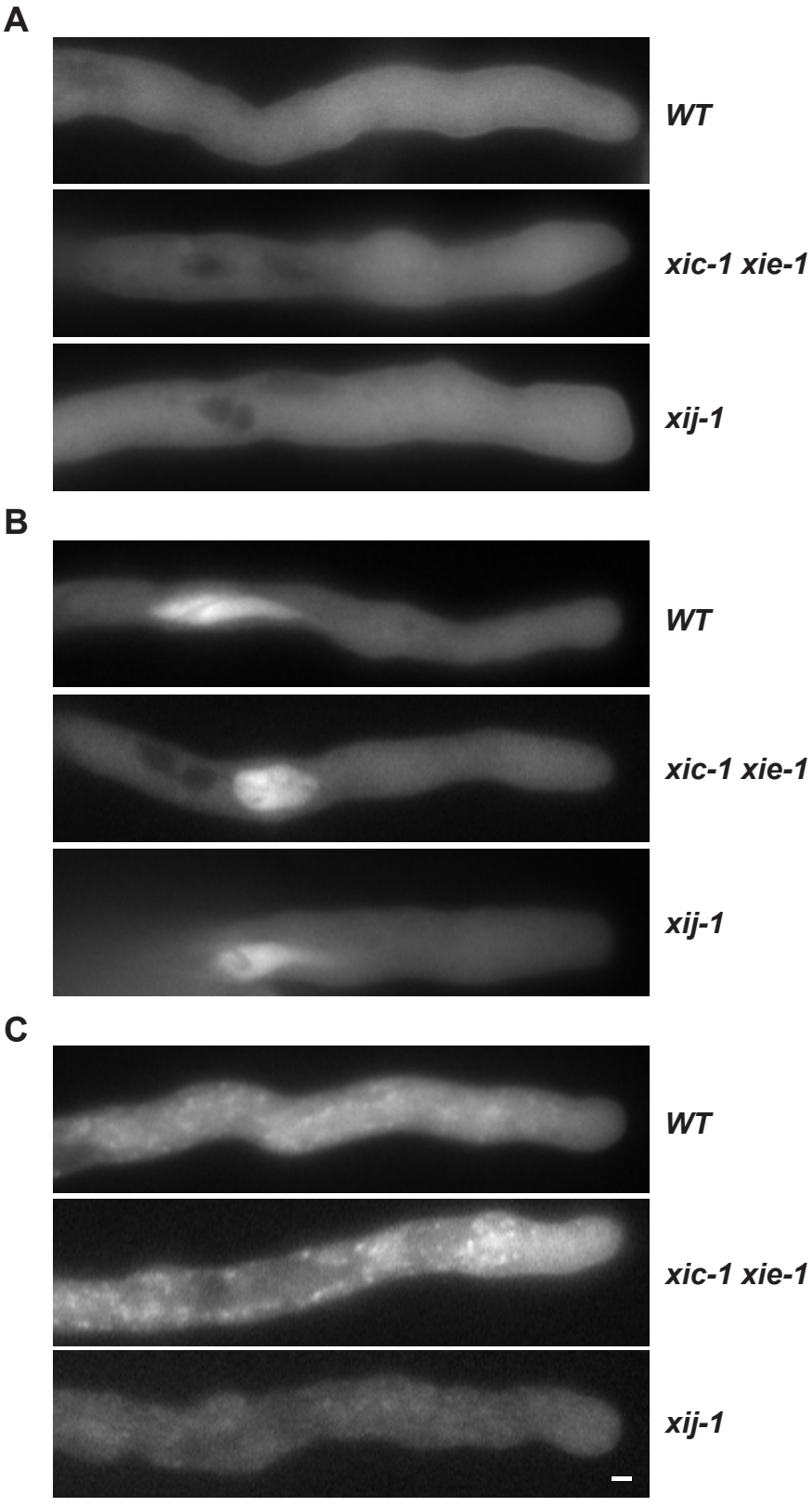
A
WT
xic-1 xie-1
xij-1
B
WT
xic-1 xie-1
xij-1
C
WT
xic-1 xie-1
xij-1

promotes the assembly of F-actin at the tip of growing pollen tubes while RIC3 promotes the disassembly of F-actin at the tip through regulating calcium influx (Gu et al., 2005). The localization of fluorescently tagged RIC3 and RIC4 had only been examined via transient expression in tobacco pollen tubes. When co-expressed with ROP1, GFP-RIC4 is predominately localized to the plasma membrane whereas GFP-RIC3 is diffuse throughout the cytoplasm (Wu et al., 2001). In addition, GFP-RIC3 accumulates in the vegetative nucleus (Wu et al., 2001). To examine the localization of ROP1 effectors in pollen myosin mutants, *YFP-RIC3* and *YFP-RIC4* were expressed in *WT*, *xic-1 xie-1*, and *xij-1* pollen tubes. In all three genotypes, YFP-RIC3 was diffuse throughout the pollen tube except for one region of accumulation that most likely represented the vegetative nucleus (**Figure 4.11B**). Plasma membrane localization of YFP-RIC4 was not observed in any pollen tubes, which could be a result of the YFP-RIC4 being overexpressed or the localization pattern in *Arabidopsis* differs from tobacco (**Figure 4.11C**). Instead YFP fluorescence was observed throughout the cytoplasm as well as in a punctate pattern that was only observed in the subapical and shank regions (**Figure 4.11C**).

4.4: Discussion

Class XI myosins are required for normal cell expansion, organelle motility, actin filament organization, and actin filament dynamics in vegetative cells. In Chapter 3, class XI myosins were shown to also be required for normal pollen tube growth and fertility. In order to determine the mechanism with which myosin XI contributes to pollen tube growth, various fluorescent markers were expressed in myosin XI mutant and *WT* pollen. In addition, the localization of two pollen myosins was examined.

Pollen myosins localize to the tips of growing pollen tubes

Both YFP-XIA and YFP-XIJ accumulated at the tip of growing pollen tubes, a localization pattern strikingly similar to YFP-XIK in growing root hairs (Peremyslov et al., 2012; Park and Nebenführ, 2013). Additionally, YFP-myoXIa in moss also accumulated at the tip of elongating cells (Vidali et al., 2010). This leads to the question of whether or not all myosin XI isoforms localize to the apex of tip growing cells. It also raises the question as to what is the functional relevance of this localization. Growing pollen tubes have a high concentration of calcium at the tip (Iwano et al., 2009), and myosin XI has been shown *in vitro* to take smaller steps and detach easily from actin filaments in the presence of 10 μM calcium (Tominaga et al., 2012). However, cytoplasmic calcium concentrations at the tip of growing *Arabidopsis* pollen tubes do not exceed 1 μM (Iwano et al., 2009), suggesting myosin XI at the tip of growing pollen tubes could still be actively transporting cargo on the short actin filaments in the actin fringe.

An even more striking observation was the accumulation of YFP-XIA and YFP-XIJ at the future germination site within pollen grains. Interestingly, YFP-XIA localized to the germination site immediately preceding tube emergence; however, *xia* mutant pollen did not have a reduction in germination efficiency. Since *xij* pollen germinated poorly *in vitro*, it was not surprising that YFP-XIJ appeared to accumulate at the future germination site. However, YFP-XIJ became diffuse again prior to tube emergence. These results suggest that XIA and XIJ are differentially regulated during pollen germination. It will be crucial to determine the order of the steps in the intracellular reorganization that occurs during pollen germination, in order to elucidate the roles of XIA and XIJ.

Myosin XI is required for normal organelle motility during pollen tube growth

In addition to the reduced growth of *xic xie* pollen tubes, peroxisomes and Golgi stacks moved at reduced speeds in the double mutant compared to *WT* pollen tubes. Organelle

movements were not examined in the single *xic* and *xie* mutants; however, given the high degree of similarity between XIC and XIE, these pollen myosins probably function redundantly to move peroxisomes and Golgi stacks. Interestingly, loss of *XIJ* resulted in slower peroxisome movements, but faster Golgi stack movements. It could be possible that XIJ normally inhibits Golgi stack movements either by binding to the unidentified receptors on the Golgi thus preventing faster isoforms from binding or possibly by directly inhibiting other myosins. Given that XIJ is the only short-tailed myosin XI in *Arabidopsis* (Mühlhausen and Kollmar, 2013), meaning it lacks the typical myosin XI globular tail involved in cargo binding (Li and Nebenführ, 2007), it is currently not clear how XIJ can contribute to organelle motility. It is also unclear how XIJ could regulate organelle movements in the shank, while it is primarily localized to the apex. This is not a unique dilemma to a short-tailed myosin. XIK predominately localizes to the tip of growing root hairs (Peremyslov et al., 2012; Park and Nebenführ, 2013); however, *xik* mutants also have reduced organelle motility. The exact mechanism of how one isoform can regulate the motility of multiple organelles without localizing to those organelles is still unknown; however, myosin effects on the actin cytoskeleton (Peremyslov et al., 2010; Ueda et al., 2010; Park and Nebenführ, 2013) might result in the overall reduction in organelle motility.

Pollen myosins are not involved in vesicle accumulation and actin dynamics

Fluctuations in vesicle accumulation at the tip of *WT*, *xij* and *xic xie* pollen tubes were similar. *xic xie* pollen tubes grow more slowly than *WT*, thus a reduction in the accumulation of secretory vesicles at the tip would be expected. Using YFP-RabA4d as a vesicle marker enables the analysis of fluctuations of accumulation at the tip. However, it cannot be used for quantification of vesicle number and density at the tip due to the inherent variation of YFP-RabA4d expression among pollen tubes. To answer this question, images of the apex using electron microscopy could be used to count the number of vesicles. *WT* and mutant pollen tubes

also had similar levels of actin dynamics and localization of ROP1 and its effectors, RIC3 and RIC4. These results suggest that XIC, XIE, and XIJ are either not involved in vesicle accumulation or actin dynamics, or the other pollen myosins can compensate for the loss of one or two myosins. In contrast, the loss of a single myosin, *XIK*, in root hairs resulted in the reduction of actin filament dynamics (Park and Nebenführ, 2013). This suggests that there may be a higher degree of redundancy among pollen myosins than among vegetative myosins.

Conclusions

Class XI myosins are involved in organelle motility during pollen tube growth; however, the direct link between myosin function and pollen tube growth has not been identified. It will be crucial to identify the interacting partners of pollen myosins in order to fill in the missing parts of the equation. The generation of functional, full-length fusion constructs also provided further insight into the role of XIA and XIJ. The localization of YFP-XIA and YFP-XIJ further implicated both myosins in tip growth, but also in pollen germination. The intracellular reorganization of pollen grains during germination is poorly understood. Detailed time-lapse imaging of pollen grains expressing an array of fluorescent markers will be necessary to tease out the process of pollen germination and the role of myosin XI during this process. Due to the auto-fluorescence of the pollen coat, a spinning-disk confocal microscope will be vital to this experiment. Additionally, electron microscopy could also be used to investigate the localization of pollen myosins during germination. However, this technique will be difficult because germination of pollen grains will have to be synchronized with a high percentage of the pollen grains germinating around the same time.

Chapter 5: Concluding Remarks

A pollen tube is a single cell that undergoes rapid tip growth for the sole purpose of delivering two non-motile sperm cells to an ovule. In some species, pollen tubes have to grow as long as 0.5 m to reach the first ovule (Williams, 2008). In order for a single cell to maintain tip-focused growth, secretory vesicles must be continually delivered to the apex of the pollen tube. Actin filaments are necessary for angiosperm pollen tube growth (Heslop-Harrison and Heslop-Harrison, 1989a); therefore, myosins, which are actin-based motor proteins, were predicted to also be required for normal pollen tube growth. Only two classes of myosins, class VIII and class XI, are found in plants (Odronitz and Kollmar, 2007). The localization of class VIII myosins, as determined by immunolocalization and expression of fluorescently labeled full-length or tail constructs, has implicated these myosins in cell-cell communication/transport, cell division, and endocytosis (Reichelt et al., 1999; Van Damme et al., 2004; Avisar et al., 2008a; Golomb et al., 2008; Sattarzadeh et al., 2008; Yuan et al., 2011; Haraguchi et al., 2014). On the other hand, genetic analysis has revealed that class XI myosins are required for normal cell expansion (Ojangu et al., 2007; Peremyslov et al., 2008; Prokhnevsky et al., 2008; Peremyslov et al., 2010; Ojangu et al., 2012). Thus, class XI and not class VIII myosins were hypothesized to be involved in pollen tube growth.

In *Arabidopsis thaliana*, six myosin XI genes are expressed in pollen (Peremyslow et al., 2011; Sparkes, 2011). To determine the levels of functional redundancy and specificity among the six pollen myosins, two approaches were employed. For the first approach, two artificial microRNAs were designed to silence multiple class XI myosins at once (**Tables 2.4 and 2.5**). Ultimately, the artificial microRNA lines only exhibited a slight reduction in root hair length that was not as severe as had been observed in double mutants (Prokhnevsky et al., 2008), and obvious fertility defects were not detected in any of the lines. The artificial microRNA constructs most likely did not efficiently target myosin mRNAs. Therefore, the functions of the six pollen

myosins were then investigated using single and double T-DNA insertion mutants.

As previously reported for the vegetative myosins, the pollen myosins were observed to have at least partially overlapping functions. Single pollen myosin mutants had either minor or no defects in pollen tube growth and overall fertility. This suggests that each isoform contributes only a little toward pollen tube growth or is redundant with the other pollen myosins. The latter was best exemplified with XIC and XIE, two pollen myosins with greater than 90% amino acid sequence identity. *XIC* and *XIE* have the strongest influence on pollen tube growth since we could see an effect on seed set, segregation distortion, *in vivo* pollen tube growth, and even for most *in vitro* pollen tube growth experiments (see Chapter 3). Furthermore, both XIA and XID together are needed for normal pollen tube growth *in vivo*, which was also seen in some of the *in vitro* pollen tube growth experiments (**Figures 3.7 and 3.8**). These results indicate that at least four of the six pollen-expressed myosins contribute to pollen tube growth; however, it is still unclear whether or not they contribute to growth through the same pathway or different pathways. Generation of triple and quadruple mutants of myosins from different subgroups will be essential for determining the degree of overlapping functions between subgroups Myo11A (*XIA*, *XID*, *XIB*) and Myo11C (*XIC*, *XIE*, *XIJ*). Additionally, the level of redundancy between myosins from different subgroups could be examined by exchanging the native promoters used to express full-length myosin constructs. For example, YFP-XIA could be expressed using the native *XIE* promoter in the *xic xie* mutant. Then it would be possible to determine whether or not XIA can functionally replace XIE if it is expressed at the same time and at the same level as the native XIE. If *XIEpro:YFP-XIA* cannot rescue the double mutant phenotype, chimeras of XIE and XIA could be generated in order to determine which region of XIE is required for its role in pollen tube growth.

Future experiments should also focus on illuminating the mechanisms by which myosins contribute to pollen tube growth. *xic xie* pollen tubes had drastically reduced organelle motility (**Figure 4.8**), yet no defects were detected in vesicle accumulation or actin organization and dynamics (**Figures 4.7 and 4.10**). Organelle movements are not sufficient for pollen tube growth (Vidali et al., 2001); therefore, it will be essential to find the causal link between organelle movements and cell growth. Pollen tube growth is proposed to be dependent on vesicle accumulation at the tip, so it is perplexing to have pollen tubes that grow slowly with a seemingly normal vesicle distribution. Similarly, *xik* root hairs grow more slowly than *WT*, have reduced organelle motility, but do not have an altered vesicle accumulation (Peremyslov et al., 2008; Prokhnevsky et al., 2008; Park and Nebenführ, 2013). Of course, vesicle accumulation in *xik* root hairs and *xic xie* pollen tubes was observed using YFP-tagged Rab GTPases that associate with secretory vesicles, which allowed for the analysis of fluctuations in accumulation but not quantification of vesicle accumulation. Therefore, electron microscopy would provide critical quantification of the number and density of vesicles at the tips of *WT* and myosin mutant root hairs or pollen tubes. Furthermore, actin organization and dynamics were only examined in the shank of *xic xie* pollen tubes, so it is possible that the double mutant pollen tubes have an altered actin fringe. Thus, *WT* and mutant pollen tubes expressing Lifeact-YFP will have to be thoroughly examined.

Furthermore, observing the localization of fluorescently tagged full-length myosins will also shed light on the role of class XI myosins during pollen tube growth. Even though YFP-XIA and YFP-XIJ were shown to accumulate at the apex of growing pollen tubes (**Figure 4.3**), the identity of their cargo remains unknown. It is also unclear how XIJ can affect organelle movements in the shank when it is localized to the tip of growing pollen tubes. Immunoprecipitation experiments using pollen expressing the YFP-tagged full-length myosins

could identify the cargo of individual pollen myosins and possibly provide critical insights into this dilemma. Interestingly, observation of YFP-XIJ and YFP-XIA prior to germination revealed that both pollen myosins localized to the future site of germination (**Figures 4.1 and 4.2**). However, YFP-XIA remained localized to the site of germination during tube emergence, whereas YFP-XIJ accumulated at the future germination site and then became diffuse again prior to tube emergence. This result is consistent with the hypothesis that myosin isoforms are differentially regulated and also indicates that there is some degree of functional specificity among the pollen myosins. This was also evident with the *in vitro* specific pollen germination defect of *xij* mutants (**Table 3.9**). Not only was this a novel phenotype for myosin mutants, but it was also the first phenotype described for a short-tailed myosin XI. In order to elucidate the mechanism for *XIJ*-dependent *in vitro* pollen germination, it will be critical to identify the diffusible female component that rescues the *xij* germination defect. It will also be important to closely examine the localization of YFP-XIJ during germination along with fluorescent markers for actin, vesicles, and various organelles. Not only will this provide additional information on the role of XIJ during pollen germination, but it will also clarify the order of the steps of the intracellular reorganization that occurs during pollen germination.

Overall, the study in this dissertation has provided the first direct evidence for the role of myosin XI in pollen tube growth and pollen germination. The techniques described in Chapter 3 will also be useful for examining higher order mutants as well as testing for the complementation of phenotypes using YFP-tagged full-length myosins. Finally, the results from this work will also help guide the direction of future experiments in this field.

References

Amari K, Lerich A, Schmitt-Keichinger C, Dolja VV, Ritzenthaler C (2011) Tubule-guided cell-to-cell movement of a plant virus requires class XI myosin motors. PLoS pathogens **7:** e1002327

Anderhag P, Hepler PK, Lazzaro MD (2000) Microtubules and microfilaments are both responsible for pollen tube elongaion in the confier *Picea abies* (Norway spruce). Protoplasma **214:** 141-157

Ariizumi T, Toriyama K (2011) Genetic regulation of sporopollenin synthesis and pollen exine development. Annual review of plant biology **62:** 437-460

Astrom H, Sorri O, Raudaskoski M (1995) Role of microtubules in the movement of the vegetative nucleus and generative cell in tobacco pollen tubes. Sexual plant reproduction **8**

Avisar D, Abu-Abied M, Belausov E, Sadot E (2012) Myosin XIK is a major player in cytoplasm dynamics and is regulated by two amino acids in its tail. Journal of experimental botany **63:** 241-249

Avisar D, Abu-Abied M, Belausov E, Sadot E, Hawes C, Sparkes IA (2009) A comparative study of the involvement of 17 Arabidopsis myosin family members on the motility of Golgi and other organellles. Plant Physiology **150:** 700-709

Avisar D, Prokhnevsky AI, Dolja VV (2008a) Class VIII myosins are required for plasmodesmatal localization of a closterovirus Hsp70 homolog. Journal of Virology **82:** 2836-2843

Avisar D, Prokhnevsky AI, Makarova KS, Koonin EV, Dolja VV (2008b) Myosin XI-K Is required for rapid trafficking of Golgi stacks, peroxisomes, and mitochondria in leaf cells of Nicotiana benthamiana. Plant Physiol **146:** 1098-1108

Azarov AS, Tokarev BI, Netchepurenko AE (1990) Effect of sodium chloride on pollen germination and pollen tube growth in vitro in Arabidopsis thaliana (L.) Heynh. Arabidopsis Inf. Serv. **27:** 9-12

Batoko H, Zheng H-Q, Hawes C, Moore I (2000) A Rab1 GTPase is required for transport between the endoplasmic reticulum and Golgi apparatus and for normal Golgi movement in plants. Plant Cell **12:** 2201-2218

Bezanilla M, Perroud PF, Pan A, Klueh P, Quatrano RS (2005) An RNAi system in Physcomitrella patens with an internal marker for silencing allows for rapid identification of loss of function phenotypes. Plant biology **7:** 251-257

Boavida L, McCormick S (2007) Temperature as a determinant factor for increased and reproducible *in vitro* pollen germination in *Arabidopsis thaliana*. The Plant Journal **52:** 570-582

Bou Daher F, Chebli Y, Geitmann A (2009) Optimization of conditions for germination of cold-stored Arabidopsis thaliana pollen. Plant cell reports **28:** 347-357

Brewbaker JL, Kwack BH (1963) The essential role of calcium ion in pollen germination and pollen tube growth. American Journal of Botany **50:** 859-865

Cai G, Bartalesi A, Del Casino C, Moscatelli A, Tiezzi A, Cresti M (1993) The kinesin-immunoreactive homologue from Nicotiana tabacum pollen tubes: biochemical properties and subcellular localization. Planta **191:** 496-506

Carbonell A, Takeda A, Fahlgren N, Johnson SC, Cuperus JT, Carrington JC (2014) New generation of artificial MicroRNA and synthetic trans-acting small interfering RNA vectors for efficient gene silencing in Arabidopsis. Plant physiology **165:** 15-29

Chang F, Gu Y, Ma H, Yang Z (2013) AtPRK2 promotes ROP1 activation via RopGEFs in the control of polarized pollen tube growth. Molecular plant **6:** 1187-1201

Chapman LA, Goring DR (2011) Misregulation of phosphoinositides in Arabidopsis thaliana decreases pollen hydration and maternal fertility. Sexual plant reproduction **24:** 319-326

Chen CY, Wong EI, Vidali L, Estavillo A, Hepler PK, Wu HM, Cheung AY (2002) The regulation of actin organization by actin-depolymerizing factor in elongating pollen tubes. The Plant cell **14:** 2175-2190

Chenouard N, Smal I, de Chaumont F, Maska M, Sbalzarini IF, Gong Y, Cardinale J, Carthel C, Coraluppi S, Winter M, Cohen AR, Godinez WJ, Rohr K, Kalaidzidis Y, Liang L, Duncan J, Shen H, Xu Y, Magnusson KE, Jalden J, Blau HM, Paul-Gilloteaux P, Roudot P, Kervrann C, Waharte F, Tinevez JY, Shorte SL, Willemse J, Celler K, van Wezel GP, Dan HW, Tsai YS, Ortiz de Solorzano C, Olivo-Marin JC, Meijering E (2014) Objective comparison of particle tracking methods. Nature Methods **11:** 281-289

Cheung A, Wu H (2008) Structural and signaling networks for the polar cell growth machinery in pollen tubes. Annual Review of Plant Biology **59:** 547-572

Cheung AY, Boavida LC, Aggarwal M, Wu HM, Feijo JA (2010) The pollen tube journey in the pistil and imaging the *in vivo* process by two-photon microscopy. Journal of Experimental Botany **61:** 1907-1915

Cheung AY, Duan QH, Costa SS, de Graaf BH, Di Stilio VS, Feijo J, Wu HM (2008) The dynamic pollen tube cytoskeleton: live cell studies using actin-binding and microtubule-binding reporter proteins. Molecular plant **1:** 686-702

Craft J, Samalova M, Baroux C, Townley H, Martinez A, Jepson I, Tsiantis M, Moore I (2005) New pOp/LhG4 vectors for stringent glucocorticoid-dependent transgene expression in Arabidopsis. The Plant journal : for cell and molecular biology **41:** 899-918

Crawford BC, Yanofsky MF (2011) *HALF FILLED* promotes reproductive tract development and fertilization efficiency in *Arabidopsis thaliana*. Development **138:** 2999-3009

de Leeuw JW, Versteegh GJM, van Bergen PF (2006) Biomacromolecules of algae and plants and their fossil analogues. Plant Ecology **182:** 209-233

de Win AHN, Knuiman B, Pierson ES, Geurts H, Kengen HMP, Derksen J (1996) Development and cellular organization of Pinus sylvestris pollen tubes. Sexual plant reproduction **9:** 93-101

Derksen J, Knuiman B, Hoedemaekers K, Guyon A, Bonhomme S, Pierson ES (2002) Growth and cellular organization of *Arabidopsis* pollen tubes *in vitro*. Sexual Plant Reproduction **15:** 133-139

Dobritsa AA, Lei Z, Nishikawa S, Urbanczyk-Wochniak E, Huhman DV, Preuss D, Sumner LW (2010) LAP5 and LAP6 encode anther-specific proteins with similarity to chalcone synthase essential for pollen exine development in Arabidopsis. Plant physiology **153:** 937-955

Dobritsa AA, Nishikawa S, Preuss D, Urbanczyk-Wochniak E, Sumner LW, Hammond A, Carlson AL, Swanson RJ (2009) LAP3, a novel plant protein required for pollen development, is essential for proper exine formation. Sexual plant reproduction **22:** 167-177

Edlund AF, Swanson R, Preuss D (2004) Pollen and stigma structure and function: the role of diversity in pollination. The Plant cell **16 Suppl:** S84-97

Elleman CJ, Franklin-Tong V, Dickinson HG (1992) Pollination in species with dry stigmas: the nature of the early stigmatic response and the pathway taken by pollen tubes. New Phytologist **121:** 413-424

Esseling-Ozdoba A, Houtman D, AA VANL, Eiser E, Emons AM (2008) Hydrodynamic flow in the cytoplasm of plant cells. Journal of microscopy **231:** 274-283

Fan LM, Wang YF, Wang H, Wu WH (2001) In vitro Arabidopsis pollen germination and characterization of the inward potassium currents in Arabidopsis pollen grain protoplasts. Journal of experimental botany **52:** 1603-1614
Fiebig A, Kimport R, Preuss D (2004) Comparisons of pollen coat genes across Brassicaceae species reveal rapid evolution by repeat expansion and diversification. Proceedings of the National Academy of Sciences of the United States of America **101:** 3286-3291
Francis KE, Lam SY, Harrison BD, Bey AL, Berchowitz LE, Copenhaver GP (2007) Pollen tetrad-based visual assay for meiotic recombination in *Arabidopsis*. Proceedings of the National Academy of Sciences of the United States of America **104:** 3913-3918
Franke WW, Herth W, VanDerWoude WJ, Morre DJ (1972) Tubular and Filamentous Structures in Pollen Tubes: Possible Involvement as Guide Elements in Protoplasmic Streaming and Vectorial Migration of Secretory Vesicles. Planta **105:** 317-341
Fraser WT, Scott AC, Forbes AE, Glasspool IJ, Plotnick RE, Kenig F, Lomax BH (2012) Evolutionary stasis of sporopollenin biochemistry revealed by unaltered Pennsylvanian spores. The New phytologist **196:** 397-401
Furt F, Liu YC, Bibeau JP, Tuzel E, Vidali L (2013) Apical myosin XI anticipates F-actin during polarized growth of Physcomitrella patens cells. The Plant journal : for cell and molecular biology **73:** 417-428
Gibbon BC, Kovar DR, Staiger CJ (1999) Latrunculin B has different effects on pollen germination and tube growth. The Plant cell **11:** 2349-2363
Glover BJ (2014) Understanding flowers and flowering : an integrated approach, Ed Second edition. Oxford University Press, Oxford
Golomb L, Abu-Abied M, Belausov E, Sadot E (2008) Different subcellular localizations and functions of *Arabidopsis* myosin VIII. BMC Plant Biology **8:** 3
Gossot O, Geitmann A (2007) Pollen tube growth: coping with mechanical obstacles involves the cytoskeleton. Planta **226:** 405-416
Griffing LR, Gao HT, Sparkes I (2014) ER network dynamics are differentially controlled by myosins XI-K, XI-C, XI-E, XI-I, XI-1, and XI-2. Frontiers in plant science **5:** 218
Gu Y, Fu Y, Dowd P, Li S, Vernoud V, Gilroy S, Yang Z (2005) A Rho family GTPase controls actin dynamics and tip growth via two counteracting downstream pathways in pollen tubes. Journal of Cell Biology **169:** 127-138
Gu Y, Li S, Lord EM, Yang Z (2006) Members of a novel class of Arabidopsis Rho guanine nucleotide exchange factors control Rho GTPase-dependent polar growth. The Plant cell **18:** 366-381
Guan Y, Guo J, Li H, Yang Z (2013) Signaling in pollen tube growth: crosstalk, feedback, and missing links. Molecular plant **6:** 1053-1064
Hajdukiewicz P, Svab Z, Maliga P (1994) The small, versatile pPZP family of *Agrobacterium* binary vectors for plant transformation. Plant Molecular Biology **25:** 989-994
Hammer JA, 3rd, Sellers JR (2012) Walking to work: roles for class V myosins as cargo transporters. Nature reviews. Molecular cell biology **13:** 13-26
Haraguchi T, Tominaga M, Matsumoto R, Sato K, Nakano A, Yamamoto K, Ito K (2014) Molecular characterization and subcellular localization of *Arabidopsis* class VIII myosin, ATM1. The Journal of Biological Chemistry **289:** 12343-12355
Harries PA, Park J-W, Sasaki N, Ballard KD, Maule AJ, Nelson RS (2009) Differing requirements for actin and myosin by plant viruses for sustained intercellular movement. Proceedings of the National Academy of Sciences, U.S.A. **106:** 17594-17599
Hashimoto K, Igarashi H, Mano S, Takenaka C, Shiina T, Yamaguchi M, Demura T, Nishimura M, Shimmen T, Yokota E (2008) An isoform of *Arabidopsis* myosin XI

interacts with small GTPases in its C-terminal tail region. Journal of Experimental Botany **59:** 3523-3531

Hemsley PA, Kemp AC, Grierson CS (2005) The TIP GROWTH DEFECTIVE1 S-Acyl Transferase Regulates Plant Cell Growth in Arabidopsis. Plant Cell **17:** 2554-2563

Heslop-Harrison J, Heslop-Harrison Y (1989a) Cytochalasin effects on structure and movement in the pollen tube of Iris. Sexual Plant Reproduction **2:** 27-37

Heslop-Harrison J, Heslop-Harrison Y (1989b) Myosin associated with the surface of organelles, vegetative nuclei and generative cells in angiosperm pollen grains and tubes. Journal of Cell Science **94:** 319-325

Heslop-Harrison J, Heslop-Harrison Y (1990) Dynamic aspects of the apical zonation in the angiosperm pollen tube. Sexual Plant Reproduction **3:** 187-194

Heslop-Harrison J, Heslop-Harrison Y (1992a) Germination of monocolpate angiosperm pollen: effects of inhibitory factors and the Ca2+-channel blocker, nifedipine. Annals of Botany **69:** 395-403

Heslop-Harrison J, Heslop-Harrison Y, Cresti M, Tiezzi A, Moscatelli A (1988) Cytoskeletal elements, cell shaping and movement in the angiosperm pollen tube. Journal of Cell Science **91:** 49-60

Heslop-Harrison Y, Heslop-Harrison J (1992b) Germination of monocolpate angiosperm pollen: evolution of the actin cytoskeleton and wall during hydration, activation and tube emergence. Annals of Botany **69:** 385-394

Hicks GR, Rojo E, Hong S, Carter DG, Raikhel NV (2004) Geminating pollen has tubular vacuoles, displays highly dynamic vacuole biogenesis, and requires VACUOLESS1 for proper function. Plant physiology **134:** 1227-1239

Hiscock SJ, Dickinson HG (1993) Unilateral incompatibility within the brassicaceae: further evidence for the involvement of the self-incompatibility (S)-locus. TAG. Theoretical and applied genetics. Theoretische und angewandte Genetik **86:** 744-753

Holding DR, Otegui MS, Li B, Meeley RB, Dam T, Hunter BG, Jung R, Larkins BA (2007) The maize floury1 gene encodes a novel endoplasmic reticulum protein involved in zein protein body formation. The Plant cell **19:** 2569-2582

Hruz T, Laule O, Szabo G, Wessendorp F, Bleuler S, Oertle L, Widmayer P, Gruissem W, Zimmermann P (2008) Genevestigator v3: a reference expression database for the meta-analysis of transcriptomes. Advances in bioinformatics **2008:** 420747

Hülskamp M, Kopczak SD, Horejsi TF, Kihl BK, Pruitt RE (1995) Identification of genes required for pollen-stigma recognition in *Arabidopsis thaliana*. The Plant Journal **8:** 703-714

Hwang JU, Vernoud V, Szumlanski A, Nielsen E, Yang Z (2008) A tip-localized RhoGAP controls cell polarity by globally inhibiting Rho GTPase at the cell apex. Current biology : CB **18:** 1907-1916

Hwang JU, Wu G, Yan A, Lee YJ, Grierson CS, Yang Z (2010) Pollen-tube tip growth requires a balance of lateral propagation and global inhibition of Rho-family GTPase activity. Journal of cell science **123:** 340-350

Idilli AI, Morandini P, Onelli E, Rodighiero S, Caccianiga M, Moscatelli A (2013) Microtubule depolymerization affects endocytosis and exocytosis in the tip and influences endosome movement in tobacco pollen tubes. Molecular plant **6:** 1109-1130

Iwano M, Entani T, Shiba H, Kakita M, Nagai T, Mizuno H, Miyawaki A, Shoji T, Kubu K, Isogai A, Takayama S (2009) Fine-tuning of the cytoplasmic Ca2+ concentration is essential for pollen tube growth. Plant Physiology **150:** 1322-1334

Iwano M, Shiba H, Miwa T, Che FS, Takayama S, Nagai T, Miyawaki A, Isogai A (2004) Ca2+ dynamics in a pollen grain and papilla cell during pollination of Arabidopsis. Plant physiology **136:** 3562-3571

Jiang S-Y, Cai M, Ramachandran S (2007) *ORYZA SATIVA MYOSIN XI B* controls pollen development by photoperiod-sensitive protein localizations. Developmental Biology **304:** 579-592

Kandasamy MK, Nasrallah JB, Nasrallah ME (1994) Pollen-pistil interactions and developmental regulation of pollen tube growth in Arabidopsis. Development **120:** 3405-3418

Kang B-H, Nielsen E, Preuss ML, Mastronarde D, Staehelin LA (2011) Electron tomography of RabA4b and PI-4Kb1-labeled *trans* Golgi network compartments in *Arabidopsis*. Traffic **12:** 313-329

Ketelaar T, Anthony RG, Hussey PJ (2004) Green fluorescent protein-mTalin causes defects in actin organization and cell expansion in Arabidopsis and inhibits actin depolymerizing factor's actin depolymerizing activity in vitro. Plant physiology **136:** 3990-3998

Kim HJ, Ok SH, Bahn SC, Jang J, Oh SA, Park SK, Twell D, Ryu SB, Shin JS (2011) Endoplasmic reticulum- and Golgi-localized phospholipase A2 plays critical roles in Arabidopsis pollen development and germination. The Plant cell **23:** 94-110

Kinkema M, Schiefelbein J (1994) A myosin from a higher plant has structural similarities to class V myosins. Journal of Molecular Biology **239:** 591-597

Klahre U, Becker C, Schmitt AC, Kost B (2006) Nt-RhoGDI2 regulates Rac/Rop signaling and polar cell growth in tobacco pollen tubes. The Plant Journal **46:** 1018-1031

Koornneef M, van Eden J, Hanhart CJ, Stam P, Braaksma FJ, Feenstra WJ (1983) Linkage map of *Arabidopsis thaliana*. The Journal of Heredity **74:** 265-272

Kost B, Spielhofer P, Chua N-H (1998) A GFP-mouse talin fusion protein labels plant actin filaments *in vivo* and visualizes the actin cytoskeleton in growing pollen tubules. Plant Journal **16:** 393-401

Kroeger JH, Daher FB, Grant M, Geitmann A (2009) Microfilament orientation constrains vesicle flow and spatial distribution in growing pollen tubes. Biophysical journal **97:** 1822-1831

Kurihara Y, Watanabe Y (2004) Arabidopsis micro-RNA biogenesis through Dicer-like 1 protein functions. Proceedings of the National Academy of Sciences of the United States of America **101:** 12753-12758

Laitiainen E, Nieminen KM, Vihinen H, Raudaskoski M (2002) Movement of generative cell and vegetative nucleus in tobacco pollen tubes is dependent on microtubule cytoskeleton but independent of the synthesis of callose plugs. Sexual plant reproduction **15:** 195-204

Lalanne E, Twell D (2002) Genetic control of male germ unit organization in Arabidopsis. Plant physiology **129:** 865-875

Lancelle S, Hepler PK (1992) Ultrastructure of freeze-substitued pollen tubes of Lilim longiflorum. Protoplasma **167:** 215-230

Lavy M, Bloch D, Hazak O, Gutman I, Poraty L, Sorek N, Sternberg H, Yalovsky S (2007) A Novel ROP/RAC effector links cell polarity, root-meristem maintenance, and vesicle trafficking. Current biology : CB **17:** 947-952

Lee Y, Szumlanski A, Nielsen E, Yang Z (2008) Rho-GTPase-dependent filamentous actin dynamics coordinate vesicle targeting and exocytosis during tip growth. Journal of Cell Biology **181:** 1155-1168

Lenartowska M, Michalska A (2008) Actin filament organization and polarity in pollen tubes revealed by myosin II subfragment 1 decoration. Planta **228:** 891-896

Li H, Lin Y, Heath RM, Zhu MX, Yang Z (1999) Control of pollen tube tip growth by a Rop GTPase-dependent pathway that leads to tip-localized calcium influx. The Plant cell **11:** 1731-1742

Li H, Wu G, Ware D, Davis KR, Yang Z (1998) Arabidopsis Rho-related GTPases: differential gene expression in pollen and polar localization in fission yeast. Plant physiology **118:** 407-417

Li J-F, Nebenführ A (2007) Organelle targeting of myosin XI is mediated independently by two globular tail subdomains. Journal of Biological Chemistry **282:** 20593-20602

Li J-F, Nebenführ A (2008a) Inter-dependence of dimerization and organelle binding in myosin XI. The Plant Journal **55:** 478-490

Li J-F, Nebenführ A (2008b) The tail that wags the dog: The globular tail domain defines the function of myosin V/XI. Traffic **9:** 290-298

Li JF, Chung HS, Niu Y, Bush J, McCormack M, Sheen J (2013) Comprehensive protein-based artificial microRNA screens for effective gene silencing in plants. The Plant cell **25:** 1507-1522

Li S, Gu Y, Yan A, Lord E, Yang ZB (2008) RIP1 (ROP Interactive Partner 1)/ICR1 marks pollen germination sites and may act in the ROP1 pathway in the control of polarized pollen growth. Molecular plant **1:** 1021-1035

Lin Y, Wang Y, Zhu JK, Yang Z (1996) Localization of a Rho GTPase Implies a Role in Tip Growth and Movement of the Generative Cell in Pollen Tubes. The Plant cell **8:** 293-303

Lin Y, Yang Z (1997) Inhibition of Pollen Tube Elongation by Microinjected Anti-Rop1Ps Antibodies Suggests a Crucial Role for Rho-Type GTPases in the Control of Tip Growth. The Plant cell **9:** 1647-1659

Liu GQ, Cai G, Del Casino C, Tiezzi A, Cresti M (1994) Kinesin-related polypeptide is associated with vesicles from Corylus avellana pollen. Cell motility and the cytoskeleton **29:** 155-166

Lo Presti L, Chang F, Martin SG (2012) Myosin Vs organize actin cables in fission yeast. Molecular biology of the cell **23:** 4579-4591

Lush WM, Grieser F, Wolters-Arts M (1998) Directional guidance of nicotiana alata pollen tubes in vitro and on the stigma. Plant physiology **118:** 733-741

Mascarenhas JP, Lafountain J (1972) Protoplasmic streaming, cytochalasin B, and growth of the pollen tube. Tissue & Cell **4:** 11-14

Mayfield JA, Fiebig A, Johnstone SE, Preuss D (2001) Gene families from the Arabidopsis thaliana pollen coat proteome. Science **292:** 2482-2485

Mayfield JA, Preuss D (2000) Rapid initiation of Arabidopsis pollination requires the oleosin-domain protein GRP17. Nature cell biology **2:** 128-130

Miller DD, Sordilis SP, Hepler PK (1995) Identification and localization of three classes of myosins in pollen tubes of *Lilium longiflorum* and *Nicotiana alata*. Journal of Cell Science **108:** 2549-2563

Mo Y, Nagel C, Taylor LP (1992) Biochemical complementation of chalcone synthase mutants defines a role for flavonols in functional pollen. Proc Natl Acad Sci U S A **89:** 7213-7217

Monaghan J, Li X (2010) The HEAT repeat protein ILITYHIA is required for plant immunity. Plant & cell physiology **51:** 742-753

Mori T, Kuroiwa H, Higashiyama T, Kuroiwa T (2006) GENERATIVE CELL SPECIFIC 1 is essential for angiosperm fertilization. Nature Cell Biology **8:** 64-71

Mouline K, Very AA, Gaymard F, Boucherez J, Pilot G, Devic M, Bouchez D, Thibaud JB, Sentenac H (2002) Pollen tube development and competitive ability are impaired by disruption of a Shaker K(+) channel in Arabidopsis. Genes & development **16:** 339-350

Mühlhausen S, Kollmar M (2013) Whole genome duplication events in plant evolution reconstructed and predicted using myosin motor proteins. BMC Evolutionary Biology **13:** 202

Naqvi AR, Sarwat M, Hasan S, Roychodhury N (2012) Biogenesis, functions and fate of plant microRNAs. Journal of cellular physiology **227:** 3163-3168

Nelson BK, Cai X, Nebenführ A (2007) A multi-color set of *in vivo* organelle markers for colocalization studies in *Arabidopsis* and other plants. Plant Journal **51:** 1126-1136

Odronitz F, Kollmar M (2007) Drawing the tree of eukaryotic life based on the analysis of 2,269 manually annotated myosins from 328 species. Genome Biology **8:** R196

Ojangu E-L, Härve K, Paves H, Truve E (2007) *Arabidopsis thaliana* myosin XIK is involved in root hair as well as trichome morphogenesis on stems and leaves. Protoplasma **230:** 193-202

Ojangu EL, Tanner K, Pata P, Jarve K, Holweg CL, Truve E, Paves H (2012) Myosins XI-K, XI-1, and XI-2 are required for development of pavement cells, trichomes, and stigmatic papillae in *Arabidopsis*. BMC Plant Biology **12:** 81

Park E, Nebenführ A (2013) Myosin XIK of *Arabidopsis thaliana* accumulates at the root hair tip and is required for fast root hair growth. PloS One **8:** e76745

Parton RM, Fischer-Parton S, Trewavas AJ, Watahiki MK (2003) Pollen tubes exhibit regular periodic membrane trafficking events in the absence of apical extension. Journal of cell science **116:** 2707-2719

Parton RM, Fischer-Parton S, Watahiki MK, Trewavas AJ (2001) Dynamics of the apical vesicle accumulation and the rate of growth are related in individual pollen tubes. Journal of Cell Science **114:** 2685-2695

Payne RJ, Grierson CS (2009) A theoretical model for ROP localisation by auxin in Arabidopsis root hair cells. PloS one **4:** e8337

Pearson WR, Lipman DJ (1988) Improved tools for biological sequence comparison. Proceedings of the National Academy of Sciences of the United States of America **85:** 2444-2448

Peremyslov VV, Klocko AL, Fowler JE, Dolja VV (2012) Arabidopsis Myosin XI-K Localizes to the Motile Endomembrane Vesicles Associated with F-actin. Frontiers in plant science **3:** 184

Peremyslov VV, Morgun EA, Kurth EG, Makarova KS, Koonin EV, Dolja VV (2013) Identification of myosin XI receptors in Arabidopsis defines a distinct class of transport vesicles. The Plant cell **25:** 3022-3038

Peremyslov VV, Prokhnevsky AI, Avisar D, Dolja VV (2008) Two class XI myosins function in organelle trafficking and root hair development in *Arabidopsis thaliana*. Plant Physiology **146:** 1109-1116

Peremyslov VV, Prokhnevsky AI, Dolja VV (2010) Class XI myosins are required for development, cell expansion, and F-Actin organization in *Arabidopsis*. Plant Cell **22:** 1883-1897

Peremyslow VV, Mockler TC, Filichkin SA, Fox SE, Jaiswal P, Makarova KS, Koonin EV, Dolja VV (2011) Expression, splicing, and evolution of the myosin gene family in plants. Plant Physiology **155:** 1191-1204

Pierson E, Lichtscheidl I, Derksen J (1990) Structure and behaviour of organelles in living pollen tubes of Lilium longiflorum. Journal of Experimental Botany **41:** 1461-1468

Platt A, Horton M, Huang YS, Li Y, Anastasio AE, Mulyati NW, Agren J, Bossdorf O, Byers D, Donohue K, Dunning M, Holub EB, Hudson A, Le Corre V, Loudet O, Roux F, Warthmann N, Weigel D, Rivero L, Scholl R, Nordborg M, Bergelson J, Borevitz JO (2010) The scale of population structure in Arabidopsis thaliana. PLoS genetics **6:** e1000843

Preuss D, Lemieux B, Yen G, Davis RW (1993) A conditional sterile mutation eliminates surface components from Arabidopsis pollen and disrupts cell signaling during fertilization. Genes & development **7:** 974-985

Preuss ML, Serna J, Falbel TG, Bednarek SY, Nielsen E (2004) The Arabidopsis Rab GTPase RabA4b Localizes to the Tips of Growing Root Hair Cells. Plant Cell **16:** 1589-1603

Prokhnevsky AI, Peremyslov VV, Dolja VV (2008) Overlapping functions of the four class XI myosins in *Arabidopsis* growth, root hair elongation, and organelle motility. Proceedings of the National Academy of Sciences of the United States of America **105:** 19744-19749

Qin Y, Leydon AR, Manziello A, Pandey R, Mount D, Denic S, Vasic B, Johnson MA, Palanivelu R (2009) Penetration of the stigma and style elicits a novel transcriptome in pollen tubes, pointing to genes critical for growth in a pistil. PLoS genetics **5:** e1000621

Qin Y, Wysocki RJ, Somogyi A, Feinstein Y, Franco JY, Tsukamoto T, Dunatunga D, Levy C, Smith S, Simpson R, Gang D, Johnson MA, Palanivelu R (2011) Sulfinylated azadecalins act as functional mimics of a pollen germination stimulant in *Arabidopsis* pistils. The Plant Journal **68:** 800-815

Reddy ANS, Day IS (2001) Analysis of the myosins encoded in the recently completed *Arabidopsis thaliana* genome sequence. Genome Biology **2:** research0024.0021-0024.0017

Reichelt S, Knight AE, Hodge TP, Baluska F, Samaj J, Volkmann D, Kendrick-Jones J (1999) Characterization of the unconventional myosin VIII in plant cells and its localization at the post-cytokinetic cell wall. Plant Journal **19:** 555-567

Reisen D, Hanson MR (2007) Association of six YFP-myosin XI-tail fusions with mobile plant cell organelles. BMC Plant Biology **7:** 6

Ryan E, Grierson CS, Cavell A, Steer M, Dolan L (1998) *TIP1* is required for both tip growth and non-tip growth in *Arabidopsis*. New Phytologist **138:** 49-58

Sabalzarini IF, Koumoutsakos P (2005) Feature point tracking and trajectory analysis for video imaging in cell biology. Journal of Structural Biology **151:** 182-195

Saint-Jore-Dupas C, Nebenführ A, Boulaflous A, Follet-Gueye M-L, Plasson C, Hawes C, Driouich A, Faye L, Gomord V (2006) Plant N-glycan processing enzymes employ different targeting mechanisms for their spatial arrangement along the secretory pathway. Plant Cell **18:** 3182-3200

Samuel MA, Chong YT, Haasen KE, Aldea-Brydges MG, Stone SL, Goring DR (2009) Cellular pathways regulating responses to compatible and self-incompatible pollen in Brassica and Arabidopsis stigmas intersect at Exo70A1, a putative component of the exocyst complex. The Plant cell **21:** 2655-2671

Sanford WW, Bonanos S, Xanthakis A (1964) A preliminary study of orchid pollen germination and the chromatographic isolation of a stimulant for columns. Phytochemistry **3:** 671-676

Sattarzadeh A, Franzen R, Schmelzer E (2008) The *Arabidopsis* class VIII myosin ATM2 is involved in endocytosis. Cell Motility and the Cytoskeleton **65:** 457-468

Sattarzadeh A, Schmelzer E, Hanson MR (2011) Analysis of Organelle Targeting by DIL Domains of the Arabidopsis Myosin XI Family. Frontiers in plant science **2:** 72

Schein M, Yang Z, Mitchell-Olds T, Schmid KJ (2004) Rapid evolution of a pollen-specific oleosin-like gene family from Arabidopsis thaliana and closely related species. Molecular biology and evolution **21:** 659-669

Schwab R, Ossowski S, Riester M, Warthmann N, Weigel D (2006) Highly specific gene silencing by artificial microRNAs in *Arabidopsis*. Plant Cell **18:** 1121-1133

Schwab R, Palatnik JF, Riester M, Schommer C, Schmid M, Weigel D (2005) Specific effects of microRNAs on the plant transcriptome. Developmental cell **8:** 517-527

Shi R, Chiang VL (2005) Facile means for quantifying microRNA expression by real-time PCR. BioTechniques **39:** 519-525

Shimmen T (2007) The sliding theory of cytoplasmic streaming: fifty years of progress. Journal of Plant Research **120:** 31-43

Shimmen T, Yokota E (1994) Physiological and biochemical aspects of cytoplasmic streaming. International Review of Cytology **155:** 97-139

Sirova J, Sedlarova M, Piterkova J, Luhova L, Petrivalsky M (2011) The role of nitric oxide in the germination of plant seeds and pollen. Plant science : an international journal of experimental plant biology **181:** 560-572

Sorek N, Poraty L, Sternberg H, Bar E, Lewinsohn E, Yalovsky S (2007) Activation status-coupled transient S-acylation determines membrane partitioning of a plant Rho-related GTPase. Molecular and Cellular Biology **27:** 2144-2154

Sorek N, Segev O, Gutman O, Bar E, Richter S, Poraty L, Hirsch JA, Henis YI, Lewinsohn E, Jurgens G, Yalovsky S (2010) An S-acylation switch of conserved G domain cysteines is required for polarity signaling by ROP GTPases. Current biology : CB **20:** 914-920

Sparkes I (2011) Recent advances in understanding plant myosin function: life in the fast lane. Molecular Plant **4:** 805-812

Sparkes I, Runions J, Hawes C, Griffing L (2009) Movement and remodeling of the endoplasmic reticulum in nondividing cells of tobacco leaves. The Plant cell **21:** 3937-3949

Sparkes IA, Teanby NA, Hawes C (2008) Truncated myosin XI tail fusions inhibit peroxisome, Golgi, and mitochondrial movement in tobacco leaf epidermal cells: a genetic tool for the next generation. Journal of Experimental Botany **59:** 2499-2512

Staiger CJ, Sheahan MB, Khurana P, Wang X, McCurdy DW, Blanchoin L (2009) Actin filament dynamics are dominated by rapid growth and severing activity in the Arabidopsis cortical array. The Journal of cell biology **184:** 269-280

Szumlanski AL, Nielsen E (2009) The Rab GTPase RabA4d regulates pollen tube tip growth in Arabidopsis thaliana. The Plant cell **21:** 526-544

Takagi H, Ikegami K, Takano M, Ogasawara N (1995) Substance promoting germination and tube growth of Polygonatum odoratum pollen. Acta Horticulturae **390:** 153-160

Tamura K, Iwabuchi K, Fukao Y, Kondo M, Okamoto K, Ueda H, Nishimura M, Hara-Nishimura I (2013) Myosin XI-i links the nuclear membrane to the cytoskeleton to control nuclear movement and shape in Arabidopsis. Current biology : CB **23:** 1776-1781

Tang X, Hepler PK, Scordilis SP (1989) Immunochemical and immunocytochemical identification of a myosin heavy chain polypeptide in *Nicotiana* pollen tubes. Journal of Cell Science **92:** 569-574

Thorsness MK, Kandasamy MK, Nasrallah ME, Nasrallah JB (1993) Genetic Ablation of Floral Cells in Arabidopsis. The Plant cell **5:** 253-261

Tiezzi A, Moscatelli A, Cai G, Bartalesi A, Cresti M (1992) An immunoreactive homolog of mammalian kinesin in Nicotiana tabacum pollen tubes. Cell motility and the cytoskeleton **21:** 132-137

Tirlapur UK, Faleri C, Cresti M (1996) Immunoelectron microscopy of myosin associated with the generative cells in pollen tubes of Nicotiana tabacum L. Sexual plant reproduction **9:** 233-237

Tiwari SC, Polito VS (1990) An analysis of the role of actin during pollen activation leading to germination in pear (Pyrus communis L.): treatment with cytochalasin D. Sexual plant reproduction **3:** 121-129

Tominaga M, Kojima H, Yokota E, Nakamori R, Anson M, Shimmen T, Oiwa K (2012) Calcium-induced mechanical change in the neck domain alters the activity of plant myosin XI. The Journal of Biological Chemistry **287:** 30711-30718

Tominaga M, Kojima H, Yokota E, Orii H, Nakamori R, Katayama E, Nason M, Shimmen T, Oiwa K (2003) Higher plant myosin XI moves processively on actin with 35 nm steps at high velocity. EMBO Journal **22:** 1263-1272

Tominaga M, Yokota E, Sonobe S, Shimmen T (2000) Mechanism of inhibition of cytoplasmic streaming by a myosin inhibitor, 2,3-butanedione monoxime. Protoplasma **213:** 46-54

Toyota M, Gilroy S (2013) Gravitropism and mechanical signaling in plants. American journal of botany **100:** 111-125

Tsukamoto Y, Matsubara S (1968) Studies on germination of chrysanthemum pollen II. occurrence of a germination promoting substance. Plant and Cell Physiology **9:** 237-245

Twell D, Yamaguchi J, McCormick S (1990) Pollen-specific gene expression in transgenic plants: coordinate regulation of two different tomato gene promoters during microsporogenesis. Development **109:** 705-713

Ueda H, Yokota E, Kutsuna N, Shimada T, Tamura K, Shimmen T, Hasezawa S, Dolja VV, Hara-Nishimura I (2010) Myosin-dependent endoplasmic reticulum motility and F-actin organization in plant cells. Proceedings of the National Academy of Sciences of the United States of America **107:** 6894-6899

Updegraff EP, Zhao F, Preuss D (2009) The extracellular lipase EXL4 is required for efficient hydration of Arabidopsis pollen. Sexual plant reproduction **22:** 197-204

Van Damme D, Bouget FY, Van Poucke K, Inze D, Geelen D (2004) Molecular dissection of plant cytokinesis and phragmoplast structure: a survey of GFP-tagged proteins. The Plant Journal **40:** 386-398

Vernoud V, Horton AC, Yang Z, Nielsen E (2003) Analysis of the small GTPase gene superfamily of Arabidopsis. Plant physiology **131:** 1191-1208

Vick JK, Nebenfuhr A (2012) Putting on the breaks: regulating organelle movements in plant cells(f). Journal of integrative plant biology **54:** 868-874

Vidali L, Augustine RC, Fay SN, Franco P, Pattavina KA, Bezanilla M (2009a) Rapid screening for temperature-sensitive alleles in plants. Plant physiology **151:** 506-514

Vidali L, Burkart GM, Augustine RC, Kerdavid E, Tüzel E, Bezanilla M (2010) Myosin XI is essnetial for tip growth in *Physcomitrella patens*. Plant Cell **22:** 1868-1882

Vidali L, McKenna ST, Hepler PK (2001) Actin polymerization is essential for pollen tube growth. Molecular Biology of the Cell **12:** 2534-2545

Vidali L, Rounds CM, Hepler PK, Bezanilla M (2009b) Lifeact-mEGFP reveals a dynamic apical F-actin network in tip growing plant cells. PloS one **4:** e5744

Walter N, Holweg CL (2008) Head-neck domain of Arabidopsis myosin XI, MYA2, fused with GFP produces F-actin patterns that coincide with fast organelle streaming in different plant cells. BMC plant biology **8:** 74

Wang G, Wang F, Zhang X, Zhong M, Zhang J, Lin D, Tang Y, Xu Z, Song R (2012) Opaque1 encodes a myosin XI motor protein that is required for endoplasmic reticulum motility and protein body formation in maize endosperm. The Plant cell **24:** 3447-3462

Wang Q, Kong L, Hao H, Wang X, Lin J, Samaj J, Baluska F (2005) Effects of brefeldin A on pollen germination and tube growth. Antagonistic effects on endocytosis and secretion. Plant physiology **139:** 1692-1703

Wang X, Teng Y, Wang Q, Li X, Sheng X, Zheng M, Samaj J, Baluska F, Lin J (2006) Imaging of dynamic secretory vesicles in living pollen tubes of Picea meyeri using evanescent wave microscopy. Plant physiology **141:** 1591-1603

Wang YF, Fan LM, Zhang WZ, Zhang W, Wu WH (2004) Ca2+-permeable channels in the plasma membrane of Arabidopsis pollen are regulated by actin microfilaments. Plant physiology **136:** 3892-3904

Weigel D, Glazebrook J, eds (2002) *Arabidopsis*: A Laboratory Manual. Cold Spring Harbor Laboratory Press, Cold Spring Harbor, N.Y.

Williams JH (2008) Novelties of the flowering plant pollen tube underlie diversification of a key life history stage. Proceedings of the National Academy of Sciences of the United States of America **105:** 11259-11263

Wilsen KL, Lovy-Wheeler A, Voigt B, Menzel D, Kunkel JG, Hepler PK (2006) Imaging the actin cytoskeleton in growing pollen tubes. Sexual plant reproduction **19:** 51-62

Wilson ZA, Morroll SM, Dawson J, Swarup R, Tighe PJ (2001) The *Arabidopsis MALE STERILITY1* (*MS1*) gene is a transcriptional regulator of male gametogenesis, with homology to the PHD-finger family of transcription factors. The Plant Journal **28:** 27-39

Wolters-Arts M, Lush WM, Mariani C (1998) Lipids are required for directional pollen-tube growth. Nature **392:** 818-821

Wu G, Gu Y, Li S, Yang Z (2001) A genome-wide analysis of Arabidopsis Rop-interactive CRIB motif-containing proteins that act as Rop GTPase targets. The Plant cell **13:** 2841-2856

Wu SZ, Ritchie JA, Pan AH, Quatrano RS, Bezanilla M (2011) Myosin VIII regulates protonemal patterning and developmental timing in the moss Physcomitrella patens. Molecular plant **4:** 909-921

Wu Y, Yan J, Zhang R, Qu X, Ren S, Chen N, Huang S (2010) Arabidopsis FIMBRIN5, an actin bundling factor, is required for pollen germination and pollen tube growth. The Plant cell **22:** 3745-3763

Xia Z, Liu Y (2001) Reliable and global measurement of fluorescence resonance energy transfer using fluorescence microscopes. Biophysical Journal **81:** 2395-2402

Ylstra B, Touraev A, Moreno RM, Stoger E, van Tunen AJ, Vicente O, Mol JN, Heberle-Bors E (1992) Flavonols stimulate development, germination, and tube growth of tobacco pollen. Plant physiology **100:** 902-907

Yokota E, Ueda H, Hashimoto K, Orii H, Shimada T, Hara-Nishimura I, Shimmen T (2011) Myosin XI-dependent formation of tubular structures from endoplasmic reticulum isolated from tobacco cultured BY-2 cells. Plant physiology **156:** 129-143

Yuan Z, Chen H, Chen Q, Omura T, Xie L, Wu Z, Wei T (2011) The early secretory pathway and an actin-myosin VIII motility system are required for plasmodesmatal localization of the NSvc4 protein of Rice stripe virus. Virus Research **159:** 62-68

Zhang H, Qu X, Bao C, Khurana P, Wang Q, Xie Y, Zheng Y, Chen N, Blanchoin L, Staiger CJ, Huang S (2010) Arabidopsis VILLIN5, an actin filament bundling and severing protein, is necessary for normal pollen tube growth. The Plant cell **22:** 2749-2767

Zhang Y, McCormick S (2007) A distinct mechanism regulating a pollen-specific guanine nucleotide exchange factor for the small GTPase Rop in Arabidopsis thaliana. Proceedings of the National Academy of Sciences of the United States of America **104:** 18830-18835

Zinkl GM, Preuss D (2000) Dissecting Arabidopsis Pollen-Stigma Interactions Reveals Novel Mechanisms that Confer Mating Specificity. Annals of Botany **85:** 15-21

Zinkl GM, Zwiebel BI, Grier DG, Preuss D (1999) Pollen-stigma adhesion in Arabidopsis: a species-specific interaction mediated by lipophilic molecules in the pollen exine. Development **126:** 5431-5440

Zonia L, Munnik T (2008) Vesicle trafficking dynamics and visualization of zones of exocytosis and endocytosis in tobacco pollen tubes. Journal of experimental botany **59:** 861-873

Appendix

Golgi Stack Dynamics in Tobacco BY-2 Cells

- *This appendix is revised from a paper published by Stephanie L Madison and Andreas Nebenführ.*

  Madison SL, Nebenführ A (2011) Live-cell imaging of dual-labeled Golgi stacks in tobacco BY-2 cells reveals similar behaviors for different cisternae during movement and brefeldin A treatment. Molecular Plant. 4: 896-908

Andreas Nebenführ performed the experiment and analyzed the results from the brefeldin A treatment on the ST-CFP/ManI-YFP line. He also performed the monensin treatment on the ST-CFP/ManI-YFP line.

A.1: Introduction

The Golgi apparatus is at the heart of the secretory system in both animal and plant cells. It is comprised of stacks of flattened membrane cisternae surrounded by vesicles and has a characteristic *cis*-to-*trans* polarity (reviewed in (Staehelin and Moore, 1995; Polishchuk and Mironov, 2004; Staehelin and Kang, 2008). The Golgi apparatus is responsible for modifying and sorting proteins as well as synthesizing lipids. It plays a crucial role in the processing of N-linked glycans on glycoproteins, which is achieved by multiple glycosidases and glycosyltransferases that are arranged from the *cis* to the *trans* cisternae in the order in which they operate on their substrates (reviewed in (de Graffenried and Bertozzi, 2004; Schoberer and Strasser, 2011). In plants, the Golgi apparatus also produces complex poly-saccharides needed for cell wall synthesis (Driouich et al., 1993). Only a few of the many enzymes predicted to be involved in the synthesis of pectins and hemicelluloses have been isolated to date and their localization within the different cisternae is just beginning to be unraveled (Chevalier et al., 2010). The *cis*-to-*trans* polarity of Golgi cisternae is also reflected in a progressive acidification of the cisternal lumen (Boss et al., 1984). This progressive drop in pH presumably plays a role in sorting of cargo molecules as well as activation of proteolytic enzymes in later Golgi compartments (Jiang and Rogers, 1999). Drugs, such as the cation ionophore monensin, that disrupt the pH gradient across the membrane therefore block secretion and lead to a swelling of the *trans* Golgi network (TGN) and *trans* cisternae (Zhang et al., 1993).

A unique characteristic of the plant Golgi apparatus is that it consists of numerous motile stacks (Boevink et al., 1998; Nebenführ et al., 1999). These stacks are approximately 300 nm thick with a cisternal diameter ~800 nm. Plant Golgi stack movements are dependent on the actin cytoskeleton and myosin motor proteins (Nebenführ et al., 1999; Avisar et al., 2008; Peremyslov et al., 2008; Prokhnevsky et al., 2008; Peremyslov et al., 2010). Even though Golgi stack motility

in plants has been observed for over a decade, there are still unanswered questions surrounding the underlying mechanisms. First, it is not known how myosin motors mediate Golgi movements. It is possible that myosin motors could attach directly to Golgi stacks (Li and Nebenführ, 2007) and thus move them in parallel to but essentially independently of the actin-associated ER network. Alternatively, Golgi stacks could move through the cell by attaching to endoplasmic reticulum export sites (ERES), which, in turn, are part of the motile ER (Runions et al., 2006; Ueda et al., 2010). Second, we have only a very general understanding of how Golgi stack integrity is maintained in the face of the physical shear forces that are likely to act upon stacks during their movement through the cytoplasm. The matrix proteins that surround Golgi cisternae are currently the best candidates for providing the cohesive forces that maintain cisternal association (Latijnhouwers et al., 2005; Renna et al., 2005; Latijnhouwers et al., 2007; Matheson et al., 2007), although the specific interactions that mediate Golgi stack integrity are still unknown.

The structural organization of the Golgi apparatus into cisternae of different protein compositions is dynamically maintained by a complex interplay of anterograde and retrograde transport mechanisms. The anterograde flow of cargo through Golgi stacks is most likely mediated by a cisternal progression/maturation mechanism whereby individual cisternae are being pushed through the stack while their membrane composition is continuously modified by recycling Golgi-resident enzymes back to earlier compartments (Nebenführ, 2003; Schoberer and Strasser, 2011). This retrograde transport has been shown to depend on COPI vesicles (Letourneur et al., 1994). Interestingly, Golgi enzyme recycling reaches as far back as the ER (Brandizzi et al., 2002) so that Golgi stack maintenance also depends on continuous export from the ER. Indeed, Golgi stacks can be disrupted and Golgi enzymes redistributed to the ER by overexpressing a GTP-locked form of Sar1, the small GTPase necessary for COPII vesicle

formation at ERES (Osterrieder et al., 2010; Schoberer et al., 2010).

Curiously, inhibition of the COPI-dependent retrograde recycling pathway with the fungal drug brefeldin A (BFA) also leads to a redistribution of Golgi enzymes into the ER (Boevink et al., 1998; Lee et al., 2002; Ritzenthaler et al., 2002; Saint-Jore et al., 2002; Schoberer et al., 2010). This redistribution most likely depends on direct membrane continuities between Golgi cisternae and the ER (Sciaky et al., 1997; Ritzenthaler et al., 2002), although the mechanism by which these continuities occur is still debated. One model posits that loss of COPI coats during BFA treatment exposes SNARE proteins on the cisternal surface that normally mediate fusion of Golgi-derived vesicles with the ER (Elazar et al., 1994; Nebenführ et al., 2002; Ritzenthaler et al., 2002). Another model assumes that such COPI-independent membrane continuities occur also under normal conditions to mediate recycling of Golgi residents (Schoberer et al., 2010). Interestingly, two independent studies have concluded that the disassembly of Golgi stacks during BFA treatments occurs directionally such that *trans* cisternae fuse with the ER first, while *cis* cisternae fuse last (Ritzenthaler et al., 2002; Schoberer et al., 2010). While the first study was mostly based on the analysis of EM images taken at various time points during the BFA treatment (Ritzenthaler et al., 2002), the second study relied on the observation of fluorescent markers that localized to different Golgi sub-compartments as well as fluorescently labeled Golgi matrix proteins (Schoberer et al., 2010).

In this study, these questions were revisited using tobacco BY-2 suspension-cultured cells that carry dual-labeled Golgi stacks. Individual Golgi stacks were observed during normal movement as well as during BFA and monensin treatments. Analysis of detailed time-lapse imaging revealed both a remarkable stability of Golgi stacks as well as an unexpected equivalence of the *cis* and *trans* sides.

A.2: Methods

A.2.1: Tobacco BY-2 cell culture growth conditions

Tobacco (*Nicotiana tabacum* var. Bright Yellow 2) cells were grown in modified Murashige and Skoog medium under constant shaking (120 rpm) in the dark at 27°C (Nagata et al., 1982). The cells were transferred to fresh medium every week using a 1:200 dilution to maintain them in the log growth phase.

A.2.2: Constructs

Each tobacco BY-2 cell line was transformed with two of the following markers: (1) soybean α-1,2 mannosidase I-YFP, which localizes predominately to the *cis* end of the Golgi (Nebenführ et al., 1999; Saint-Jore-Dupas et al., 2006), (2) *Arabidopsis thaliana* β1,2-xylosyltransferase-YFP, which is used to label medial cisternae (Pagny et al., 2003), and (3) rat α-2,6-sialyltransferase-YFP (or CFP), which primarily localizes to the *trans* half of the Golgi (Boevink et al., 1998). The *cis* marker is based on the full-length protein (Nebenführ et al., 1999). For the medial marker, the coding region corresponding to the first 36 amino acids of XT was amplified from *Arabidopsis* cDNA. The *trans* markers incorporate the first 52 amino acids of ST and was a kind gift by Dr. Chris Hawes (Oxford Brookes University, UK). All markers carry the fluorescent protein at their C-termini in the lumen of the Golgi. Expression of all markers was driven by the double 35S promoter (Nelson et al., 2007). The expression constructs were cloned into binary plasmids (pVKH18, pFGC19, pBIN20) and transformed via *Agrobacterium* into BY-2 cells as described previously (Nebenführ et al., 1999). Selection of transformed cells was achieved by adding 100 μg/ml hygromycin, 10 μg/ml glufosinate, or 50 μg/ml kanamycin, respectively, to the medium.

A.2.3: Microscopy

Tobacco BY-2 cells co-expressing two fluorescent protein fusions were visualized using an Axiovert 200 M microscope (Zeiss) equipped with filters for CFP and YFP fluorescence (C-35520; Chroma Technology). Transgenic cells were observed in their cortical cytoplasm closest to the cover slip with a 63X (1.4 NA) plan-apo oil immersion objective, and images were captured using a digital camera (Orca ER; Hamamatsu Photonics) using OpenLab5 software (Improvision/Perkin Elmer). Most CFP and YFP images were taken sequentially after switching the excitation light with an external DG-4 wavelength switcher (Sutter Instruments). For simultaneous image capture, the excitation wavelengths were rapidly alternated (CFP/YFP/CFP/YFP/CFP) during a single exposure to avoid sequential detection of the two markers. In this case, an image splitter (Dual-View; Optical Insights) was used to separate the emission wavelengths into two images that were projected side by side on the camera chip (dichroic filter 505dcxr; emission filters D465/30 for CFP and HQ535/30 for YFP; Chroma Technology). The CFP and YFP half-images were separated and CFP bleed-through was removed computationally from the YFP image. For all images, background subtraction was used to remove camera noise prior to quantitative analysis. Contrast enhancement was used to increase the signal intensity and decrease background fluorescence for presentation in the figures and movies. To determine the relative position of two cisternae in the same Golgi stack, a peak-finding plug-in (Particle Tracker; http://weeman.inf.ethz.ch/particletracker; (Sabalzarini and Koumoutsakos, 2005) to ImageJ (http://rsb.info.nih.gov/ij/) was used.

A.2.4: Monensin treatment

Three to five-day-old tobacco BY-2 cells were placed in a perfusion chamber and modified Murashige and Skoog medium was perfused at 0.5 ml/min. Sequential time-lapse imaging was started about three minutes before monensin (Acros Chemicals) and latrunculin B

(LatB, Sigma) were added. Images were taken for 60 minutes with 10-second intervals using CFP and YFP filters. Final monensin concentration was 10 μM from a stock solution of 3 mM in ethanol, and LatB had a final concentration of 1 μM from a stock solution of 1 mM in DMSO. Sizes of cisternae were measured in ImageJ after manual selection of the fluorescent areas.

A.2.5: Movement analysis

Six-day-old tobacco BY-2 cells co-expressing ST-CFP and ManI-YFP were observed. Simultaneous image capture was used to capture time-lapse images in 1-second intervals for 1 minute. After separation of the CFP and YFP signals, 20 individual Golgi stacks were tracked over time separately in the CFP and YFP images using OpenLab5 software. X and Y coordinates of the manually selected center points were transformed so that the direction of movement was in the positive X direction, with very little movement in the Y direction. This allowed for progress of the stacks to be followed along this new axis with the new parameter *d*. For each time point, the location of the stack in the YFP image was subtracted from its location in the CFP image to obtain the distance between the *cis* and *trans* cisternae (d_{CFP} - d_{YFP}). Thus, positive values indicate the *trans* cisternae leading, whereas negative values indicate the *cis* cisternae leading. Neither half was considered to be leading when the measured distance between the ST-CFP and ManI-YFP markers was less than 0.14 μm, which is less than half the length of the diagonal of a pixel. For every image, the speed in each frame was calculated by OpenLab5 software. The calculated CFP and YFP image speeds were averaged to obtain the overall speed of the Golgi stack at that time point.

A.2.6: Brefeldin A treatment

Three to six-day-old tobacco BY-2 cells were treated with brefeldin A (BFA, Molecular Probes/Invitrogen) and latrunculin B (LatB, Sigma) while on a large coverslip on the inverted microscope. BFA was used at a final concentration of 10 μg/ml from a stock solution of 5 mg/ml

in ethanol. LatB had a final concentration of 1 μM. Cells were observed for 20 minutes after drugs were added by sequential time-lapse imaging with 5-second intervals between images. Individual Golgi stacks were identified manually, and OpenLab5 software was used to measure the maximal fluorescence intensities of the selected areas for every frame in the image sequence.

A.3: Results

A.3.1: Dual-labeled Golgi stacks reveal different localization of marker proteins

To examine Golgi stack movements and disassembly, fluorescent proteins were fused to the transmembrane domains of Golgi proteins that have been shown to localize to different cisternae with various degrees of overlap. A full-length clone of soybean α-1,2 mannosidase I fused to YFP (ManI-YFP; Nebenführ et al., 1999; Saint-Jore-Dupas et al., 2006) was used as a *cis* marker. The first 36 amino acids of *Arabidopsis thaliana* β1,2-xylosyltransferase fused with YFP (XT-YFP; Pagny et al., 2003) was utilized as a medial marker. Finally, the first 52 amino acids of rat α-2,6-sialyltransferase fused to YFP or CFP (ST-YFP/ST-CFP; Boevink et al., 1998) was employed as a *trans* marker.

Pairs of fusion proteins were examined in the cortical cytoplasm after stable co-expression in tobacco BY-2 cells. Golgi stacks in cell lines expressing either ManI-YFP and ST-CFP or XT-YFP and ST-CFP often appeared tri-colored due to partial overlap (**Figure A.1A, A.1B, A.1D, and A.1E**). This is most noticeable in the side-views shown in the insets of **Figure A.1D and A.1E**. There appeared to be more non-overlapping regions when ST-CFP was co-expressed with ManI-YFP than with XT-YFP. This was confirmed by determining the centers of the labeled cisternae with a peak-finding algorithm. This analysis revealed that ST-CFP cisternae were, on average, slightly closer to XT-YFP cisternae (0.20 ± 0.01 μm; SE, n = 115 from four

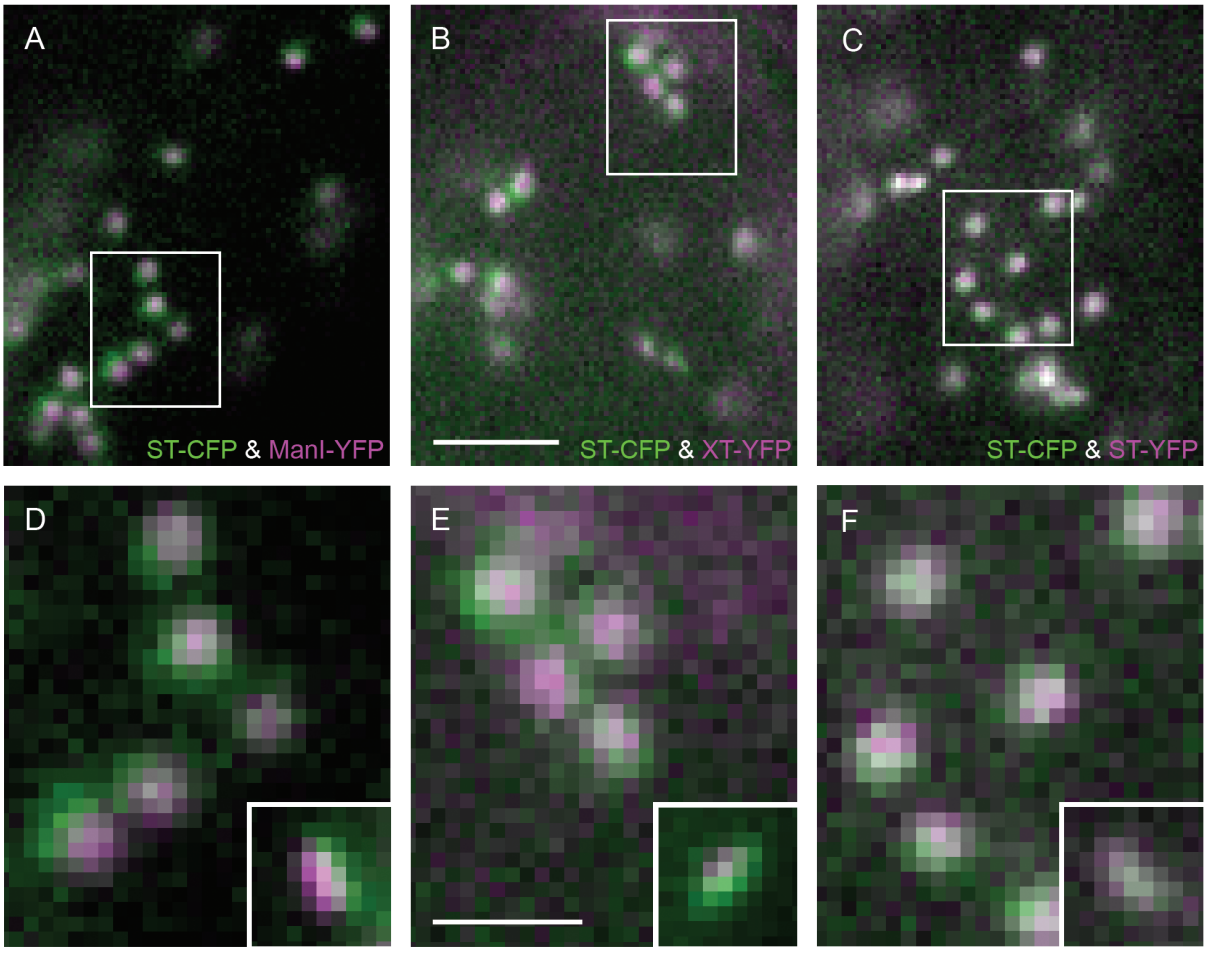

Figure A.1: Differential localization of marker proteins in dual-labeled Golgi stacks

Transgenic tobacco BY-2 cells co-expressing ST-CFP (**A-F**) and ManI-YFP (**A, D**), XT-YFP (**B, E**), or ST-YFP (**C, F**). Outlined regions (**A-C**) are magnified 3X in (**D-F**). Note the different degrees of overlap between ST-CFP (green) and the YFP fusions (magenta). The region of overlap (white) is most notable in the side-views shown for different stacks at the same magnification in the insets (**D-F**). ST-CFP and ST-YFP are almost completely overlapped while ST-CFP and XT-YFP or ManI-YFP have smaller overlapping regions. Scale bar = 5 μm in (**A-C**) and 2 μm in (**D-F**).

cells) than to ManI-YFP cisternae (0.21 ± 0.01 μm; SE, n = 125 from eight cells), although this difference was not statistically significant (Mann-Whitney test, $p > 0.05$). Thus, our observations support previous findings that these proteins localize to different cisternae (Boevink et al., 1998; Nebenführ et al., 1999; Pagny et al., 2003). In contrast, Golgi stacks in cell lines expressing ST-CFP and ST-YFP usually appeared predominately white with no clear separation between the channels because both fusion proteins localized to the *trans* cisternae (**Figure A.1C and A.1F**). Consistent with this impression, the average distance between ST-CFP and ST-YFP cisternae was only about half a pixel (0.09 ± 0.01 μm; SE, n = 137 from five cells). This slight displacement may have been caused by the temporal delay between CFP and YFP image capture, or could simply reflect random noise.

A.3.2: Monensin treatment affects *trans* cisternae more than *cis* and medial cisternae

Previous studies have shown that treating plant cells with monensin, an ionophore that is specific for monovalent cations, ultimately results in the sequential swelling of Golgi cisternae (Zhang et al., 1993), presumably due to the resulting influx into acidic late Golgi compartments (Zhang et al., 1993; Satiat-Jeunemaitre et al., 1994). In electron micrographs, it could beobserved that the *trans* Golgi network is the first to swell followed by the *trans* cisternae. Medial and *cis* cisternae started to swell only later during the treatment.

The rate of swelling of different cisternae was observed by live-cell imaging in BY-2 cells co-expressing ST-CFP and ManI-YFP (**Figure A.2A**) or XT-YFP (**Figure A.2B**). Cells were treated with 10 μM monensin and 1 μM latrunculin B (to prevent movement of the stacks) and observed using sequential time-lapse imaging with 10-second intervals between images. In cells expressing either ST-CFP and ManI-YFP or ST-CFP and XT-YFP, the cisternae labeled with ST-CFP began to swell by 5 minutes and appeared to reach a maximum size by 35 minutes after the addition of monensin (**Figure A.2** and **Movies A.1 and A.2**). Swelling of the *cis* and

Figure A.2: Monensin treatment preferentially affects *trans* cisternae

Transgenic tobacco BY-2 cells co-expressing ST-CFP (green) and ManI-YFP (magenta; **A**) or XT-YFP (magenta; **B**) were observed 0-50 minutes after addition of monensin. Note the increase in fluorescence intensity in **A** beginning at 20 minutes. Also, note that the *trans* cisternae swelled to a greater extent than the *cis* and medial cisternae. Due to the focus shifting during the time lapse, different stacks are shown after 20 minutes. Scale bar = 5 μm.

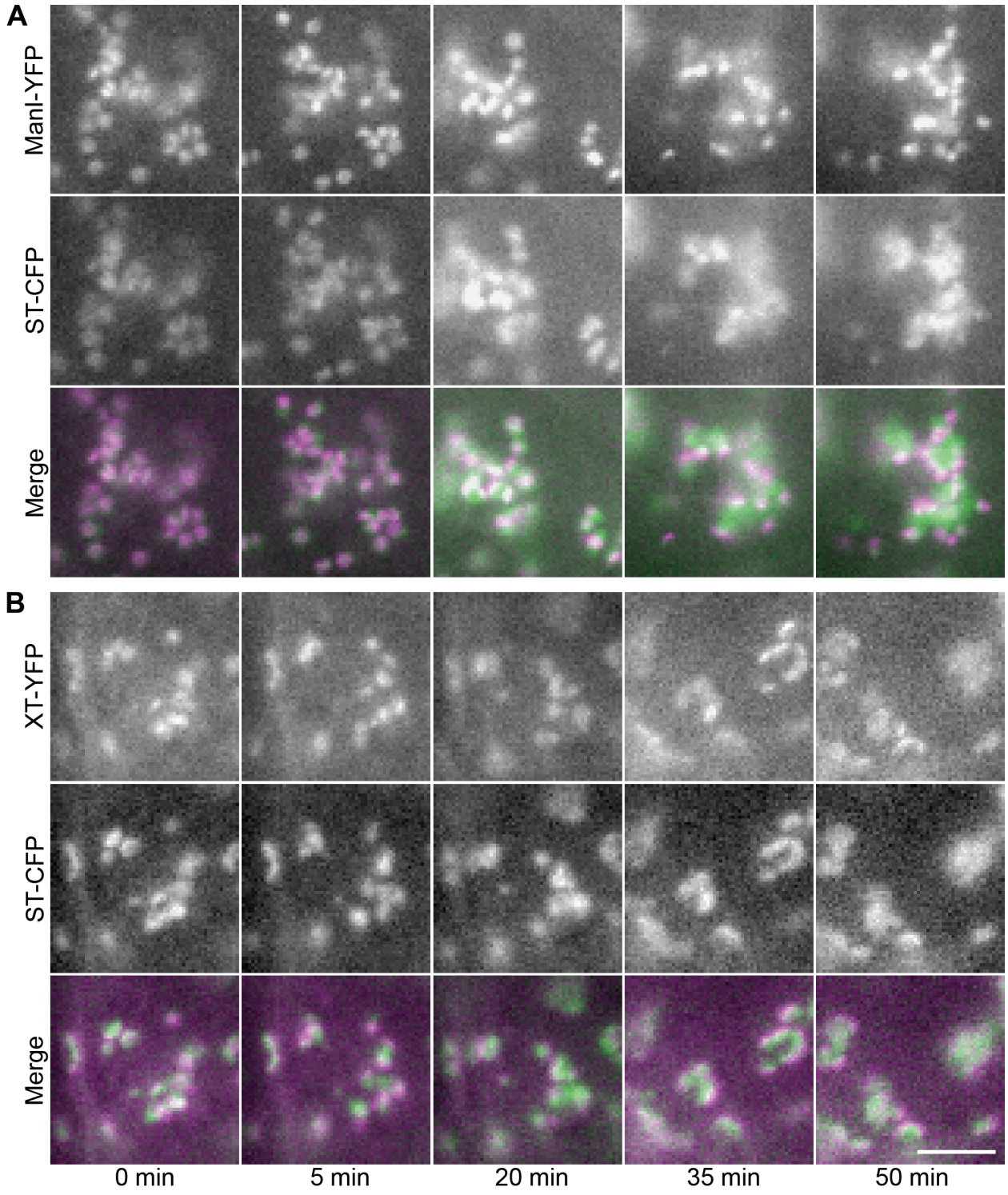
A
ManI-YFP
ST-CFP
Merge
B
XT-YFP
ST-CFP
Merge
0 min
5 min
20 min
35 min
50 min

medial cisternae was less noticeable, but these cisternae appeared to start enlarging by about 30 minutes after the start of the monensin treatment. Quantitative analysis of the apparent cisternal sizes at 0 and 50 minutes in monensin confirmed these impressions and revealed that *trans* cisternae swelled on average by ~ 50% whereas medial and *cis* cisternae increased in size by only ~20% and ~10%, respectively (n = 12-30 in two cells per treatment).

Frequently, swollen cisternae containing the ST-CFP marker surrounded by smaller cisternae labeled with either the ManI-YFP or XT-YFP marker were observed (**Figure A.2**). In some cases, the swelling of the cisternae also coincided with an increase in fluorescence intensities. This increase is clearly visible in **Figure A.2A** (20-50 minutes). Confirming previous studies, the *trans* cisternae were more affected by monensin treatment than the other cisternae.

A.3.3: Golgi stacks move as intact units with a slight preference for the *cis* cisternae to lead

For over a decade, it has been known that plant Golgi stacks are motile and that their movements are dependent on the acto-myosin network (Boevink et al., 1998; Nebenführ et al., 1999). While it is generally assumed that Golgi cisternae remain stacked during these movements, this has not been tested experimentally. Furthermore, it has yet to be determined whether Golgi stacks have a particular orientation while traveling through the cytoplasm.

To address these questions, a BY-2 suspension culture cell line that stably expressed ST-CFP and ManI-YFP was observed. Simultaneous image capture of the two fluorophores was used to observe Golgi stacks at 1-second intervals for 1 minute (**Figure A.3A** and **Movie A.3**). Since there was no delay between the CFP and YFP images, it was possible to calculate the distance between the *cis* and *trans* cisternae in any given frame. Movements of 20 individual Golgi stacks in the video sequences from eight cells were independently tracked in both the CFP and YFP images, and the distance between the two signals in the direction of movement was calculated (d_{CFP} - d_{YFP}). Positive distance values indicate that the *trans* end was moving ahead

Figure A.3: Golgi stacks move as intact units at various speeds and orientations

(**A**) Transgenic tobacco BY-2 cells co-expressing ST-CFP (green) and ManI-YFP (magenta) were imaged at 1-second intervals with simultaneous image capture for CFP and YFP channels. Scale bar = 2 μm.

(**B**) For each Golgi stack, the distance between the *trans* and *cis* cisternae (d_{CFP} - d_{YFP}) was calculated in every frame. Positive values indicate that the *trans* half was ahead while negative values indicate that the *cis* half was ahead. Example 1 shows the distance between cisternae for the stack shown in **A**. Note that stacks can have various orientations while moving.

(**C**) Instantaneous speeds were also calculated for every measurement of 20 different stacks. Note there is no correlation between speed and the distance between cisternae or stack orientation.

(**D**) Summary of Golgi stack orientation in individual frames. A cisterna was counted as leading if the distance between the markers was larger than 0.14 μm.

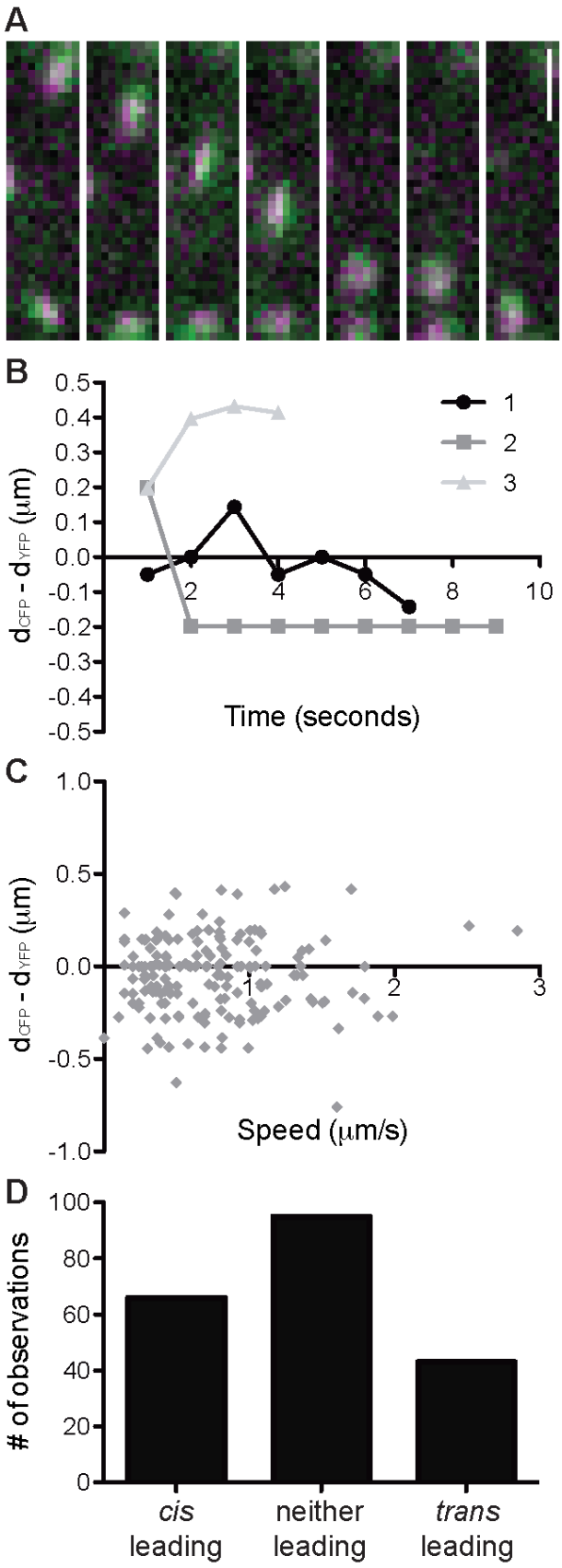
A
B
0.5
0.4
0.3
0.2
0.1
0.0
-0.1
-0.2
-0.3
-0.4
-0.5
dCFP - dYFP (μm)
2
4
6
8
10
1
2
3
Time (seconds)
C
1.0
0.5
0.0
-0.5
-1.0
dCFP - dYFP (μm)
1
2
3
Speed (μm/s)
D
100
80
60
40
20
0
# of observations
cis leading
neither leading
trans leading

for a given frame, while negative distance values suggest that the *cis* half was leading at that time (**Figure A.3B**). In all observed stacks, the *cis* and *trans* markers remained in close proximity during the movements (maximal distance between centers < 0.8 μm), suggesting that Golgi stack integrity was maintained during movements. Of the 20 stacks observed, eight consistently had either the *trans* or *cis* cisternae leading (examples 2 and 3 in **Figure A.3B**), while 12 stacks alternated which end was ahead during the time lapse (**Figure A.3A** and example 1 in **Figure A.3B**).

Since either half of the Golgi stack could lead during movements, the next question asked was whether there was a correlation between orientation and speed of the Golgi stack at different time points. Analysis of a total of 204 time points revealed that orientation of a Golgi stack during movement was not influenced by its speed (**Figure A.3C**). Furthermore, there was also no correlation between the distance between cisternae and speed of the stack (**Figure A.3C**). This suggests that Golgi stacks remain intact and do not show a preferential orientation while moving at speeds of 0-3 μm/s. This was further explored by comparing the number of cases in which the *cis* half, *trans* half, or neither half was leading (**Figure A.3D**). Neither half was considered to be leading when the distance between the ST-CFP and ManI-YFP markers was less than 0.14 μm, which is one half of the diagonal of a pixel. Using this criterion, neither end of the observed stacks was clearly leading in almost half of the time points. In the remaining half of the observations, there was a slight but significant preference for the *cis* cisternae to lead while the stacks were moving (**Figure A.3D**; $\chi^2 = 4.85$, $p = 0.028$).

A.3.4: Golgi stack disassembly can occur in either the *trans*-to-*cis* or *cis*-to-*trans* direction

Brefeldin A (BFA) treatment is known to cause the redistribution of Golgi enzymes to the endoplasmic reticulum (ER; Boevink et al., 1998; Ritzenthaler et al., 2002; Saint-Jore et al., 2002; Schoberer et al., 2010). It has been proposed that this redistribution occurs sequentially,

beginning with the *trans* cisternae and progressing to the *cis* (Ritzenthaler et al., 2002; Schoberer et al., 2010); however, this redistribution has not been observed for individual stacks as it is occurring. To re-examine the order of redistribution of Golgi enzymes, tobacco BY-2 cells co-expressing ManI-YFP and ST-CFP, XT-YFP and ST-CFP, or ST-YFP and ST-CFP were treated with 10 μg/ml brefeldin A (36 μM BFA) and 1 μM latrunculin B (LatB). LatB stopped all Golgi movements (data not shown) and prevented the observed stacks from moving out of the focal plane, thus ensuring that changes in fluorescence intensity were only due to fusion with the ER. It is important to note that BFA-induced redistribution of Golgi enzymes to the ER is not dependent on cytoskeletal networks (Saint-Jore et al., 2002). During the course of BFA treatment, the cells gradually lost distinct Golgi stacks (**Figure A.4A** and **Movie A.4**) while, slowly, an ER-like network appeared (data not shown). This recapitulates results previously obtained by several groups (Boevink et al., 1998; Ritzenthaler et al., 2002; Saint-Jore et al., 2002; Schoberer et al., 2010).

To gain a more detailed view of the events during Golgi-ER fusion, tobacco BY-2 cells were observed during the first 20 minutes following addition of BFA using time-lapse imaging (**Figure A.4A** and **Movie A.4**). Images were taken in 5-second intervals and the CFP and YFP intensities of individual Golgi stacks were measured. Sometimes, multiple Golgi stacks were too close together to analyze separately; these clusters were measured as one unit as long as all included stacks responded to BFA at the same time. The maximal fluorescence intensities of individual stacks were plotted against the treatment time (**Figure A.4B-A.4E**) and used to determine the timing of the loss of Golgi signal for each marker. Several different behaviors of the two markers were observed. Many stacks lost both markers simultaneously (**Figure A.4B and A.4D**). Others lost only the ST-CFP marker while ManI-YFP remained largely unchanged (**Figure A.4C**). Still other Golgi stacks lost only the ManI-YFP marker (**Figure A.4E**).

Figure A.4: Brefeldin A treatment can result in sequential loss of ST-CFP and ManI-YFP

(**A**) Five Golgi stacks from a transgenic tobacco BY-2 cell co-expressing ST-CFP (green) and ManI-YFP (magenta) are shown 12-16 minutes after the addition of brefeldin A. (**B-E**) Maximal fluorescence intensities of individual stacks marked in **A** were plotted as a function of treatment time. Black and gray arrows indicate the start of decrease in fluorescence intensity for ST-CFP and ManI-YFP, respectively. Note that stacks B and D lost both markers simultaneously, while stack C only lost the *trans* marker and stack E lost only the *cis* marker. Scale bar = 2 μm.

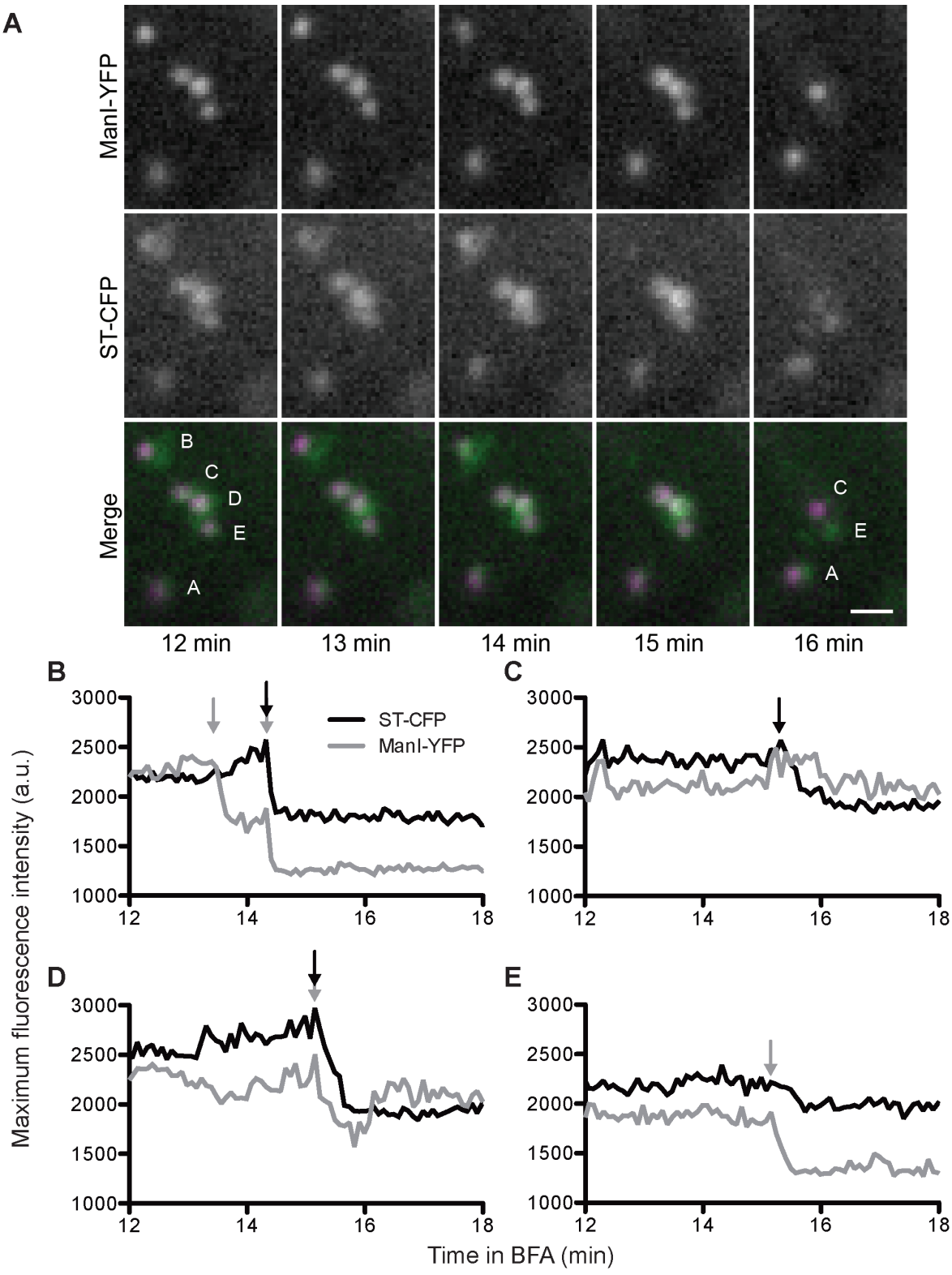
A
ManI-YFP
ST-CFP
Merge
B
C
D
E
A
12 min
13 min
14 min
15 min
16 min
B
C
D
E
ST-CFP
ManI-YFP
3000
2500
2000
1500
1000
12
14
16
18
Maximum fluorescence intensity (a.u.)
Time in BFA (min)

Interestingly, Golgi stacks that lost one of their fluorescent markers in several steps were also observed, suggesting that these events could represent individual cisternae fusing with the ER (ManI-YFP in **Figure A.4B**). In many cases, there was a brief increase in fluorescence intensity immediately preceding the loss of a fluorescent marker from the Golgi stack (e.g. **Figure A.4B and A.4D**).

In those cases in which, initially, only one marker was lost from a Golgi stack, the other marker eventually also disappeared into the ER, thus leaving no trace of the Golgi stack (data not shown). The sequential loss of the two fluorescent markers could occur in close succession or with more delay. Depending on the relative timing of these events, each stack was assigned to one of five categories: those that lost both signals within less than 10 seconds of each other (CFP ≈ YFP), those where the two events occurred within 10-30 seconds of each other (CFP > YFP and CFP < YFP), and those events in which loss of one marker preceded loss of the other one by more than 30 seconds (CFP >> YFP and CFP << YFP). When tobacco BY-2 cells co-expressing ManI-YFP and ST-CFP were treated with BFA, about half of the Golgi stacks lost both markers within 10 seconds of each other. The remaining half was split more or less evenly between those that lost the *trans* marker first (CFP < YFP and CFP << YFP) and those that lost the *cis* marker first (CFP > YFP and CFP >> YFP). Therefore, fusion of *cis* and *trans* cisternae with the ER occurred more or less simultaneously for about half of the stacks, and the sequential cisternal loss of the other stacks did not show a preference for either *cis* or *trans* cisternae to fuse first with the ER (n = 103 from 14 cells; **Figure A.5A**).

Similar results were obtained when tobacco BY-2 cells co-expressing XT-YFP and ST-CFP were treated with BFA (n = 65 from 13 cells; **Figure A.5A**). In about half of the Golgi stacks observed, the YFP and CFP signals were lost simultaneously. The other stacks were distributed more or less evenly between those that lost the *trans* marker first (CFP < YFP and

Figure A.5: Golgi disassembly can occur in either a *trans*-to-*cis* or a *cis*-to-*trans* direction

Transgenic tobacco BY-2 cells co-expressing ST-CFP and ManI-YFP (**A, B**), XT-YFP (**A, C**), or ST-YFP (**A, D**) were treated with brefeldin A and observed for 20 minutes. Individual stacks could have lost both markers within 10 seconds of each other (CFP ≈ YFP), within 10-30 seconds of each other (CFP > YFP, CFP < YFP), or more than 30 seconds apart from each other (CFP >> YFP, CFP << YFP). Gray squares shown in (**B-D**) represent the average ± the standard error of the mean. Note that about half of the events affected the two markers independently when they localized to different cisternae (**A**). There was no apparent preference in timing for simultaneous or sequential events for any of the marker combinations (**B-D**).

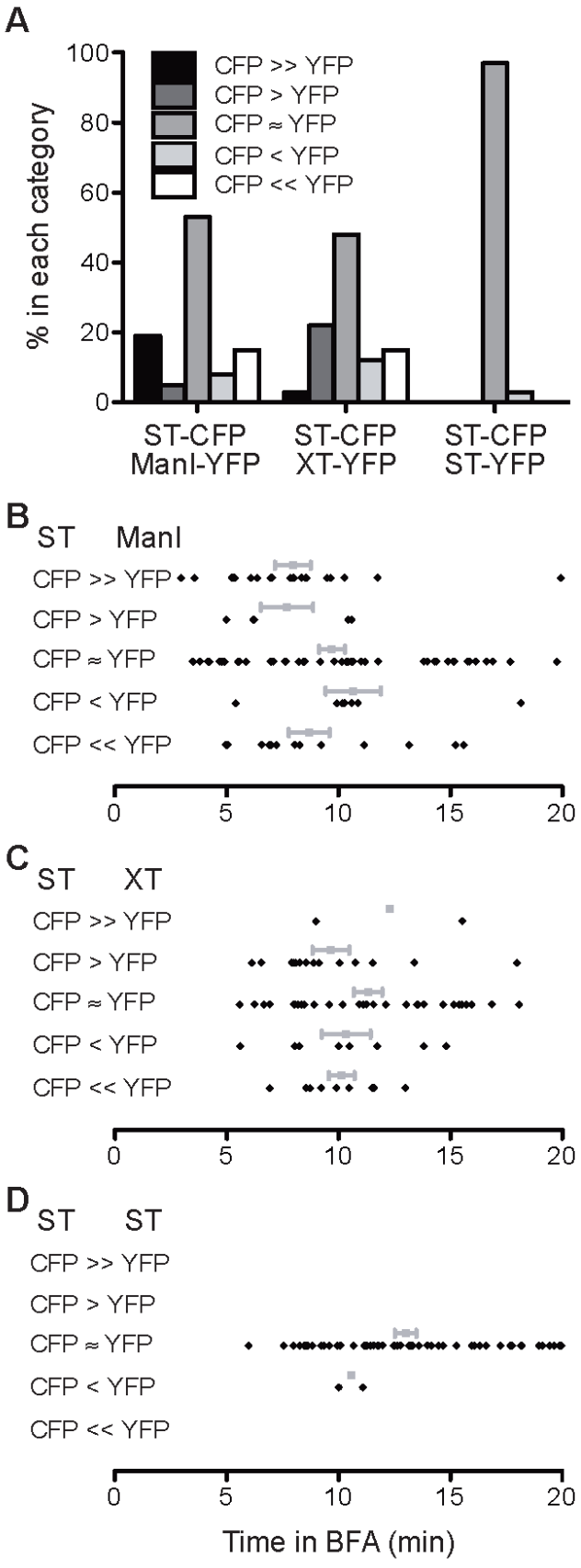
A
100
80
60
40
20
0
% in each category
CFP >> YFP
CFP > YFP
CFP ≈ YFP
CFP < YFP
CFP << YFP
ST-CFP ManI-YFP
ST-CFP XT-YFP
ST-CFP ST-YFP
B
ST ManI
CFP >> YFP
CFP > YFP
CFP ≈ YFP
CFP < YFP
CFP << YFP
0 5 10 15 20
C
ST XT
CFP >> YFP
CFP > YFP
CFP ≈ YFP
CFP < YFP
CFP << YFP
0 5 10 15 20
D
ST ST
CFP >> YFP
CFP > YFP
CFP ≈ YFP
CFP < YFP
CFP << YFP
0 5 10 15 20
Time in BFA (min)

CFP << YFP) and those that lost the medial marker first (CFP > YFP and CFP >> YFP). Interestingly, when the redistribution occurred sequentially, there was, on average, less of a delay between the medial and *trans* markers than between the *cis* and *trans* markers. In particular, the ratio of stacks that lost their markers sequentially within 30 seconds of each other (CFP > YFP and CFP < YFP) to those that lost their markers with a delay of more than 30 seconds (CFP >> YFP and CFP << YFP) was 0.37 for the *cis*-*trans* marker pair and 1.83 for the medial-*trans* marker pair.

As a control, tobacco BY-2 cells co-expressing ST-YFP and ST-CFP were also treated with BFA. Since both markers were localized to the same compartment, sequential fusion with the ER was not expected to be observed. In almost all of the Golgi stacks observed (n = 64 from 18 cells), YFP and CFP signals were lost simultaneously; however, two Golgi stacks showed loss of the CFP signal 10 seconds before the loss of the YFP signal. Thus, as expected, when YFP and CFP were both fused to the same Golgi protein, loss of both markers generally occurred simultaneously (**Figure A.5A**).

The summary of Golgi stack behavior did not reveal a specific pattern for the sequential loss of cisternae (**Figure A.5A**). However, it is possible that condensing the behavior of many stacks over 20 minutes could have masked such patterns. Therefore, the timing of events in different categories was analyzed (**Figure A.5B-A.5D**). No specific preference for *trans* first or *trans* last events was detectable in any of the datasets. The average start time of events in each category ranged from 7 to 13 minutes and none of the categories clearly preceded the others (**Figure A.5B and A.5C**). This suggests that, within the first 20 minutes of treatment, there is no preferential order of fusion.

A.4: Discussion

Among eukaryotic organelles, the Golgi apparatus has attracted considerable attention because of its unusual three-dimensional organization and remarkable dynamic behavior, both of which have defied simple explanations. Despite many decades of intensive research, we still have no detailed explanation of the mechanisms that maintain Golgi cisternae in a stable stacked arrangement with a clear *cis*-to-*trans* polarity while at the same time permitting continuous flow of secretory products through the organelle (Schoberer and Strasser, 2011). The plant cell Golgi introduces an additional layer of complexity by displaying rapid stop and go movements that put additional requirements on Golgi stack coherence and vesicle targeting (Nebenführ and Staehelin, 2001). In this study, we utilized detailed time-lapse observations of dual-labeled Golgi stacks to investigate various aspects of Golgi stack dynamics and integrity.

Different sub-compartments of the Golgi were labeled with fluorescent protein fusions to different Golgi-targeting domains. The transmembrane domains of mannosidase I (ManI), xylosyltransferase (XT), and sialyltransferase (ST) fused to fluorescent proteins have already been shown by immunogold labeling to localize primarily to the *cis*, medial, and *trans* cisternae, respectively (Boevink et al., 1998; Nebenführ et al., 1999; Pagny et al., 2003; Saint-Jore-Dupas et al., 2006). When ST-CFP and ST-YFP were co-expressed, their signals almost completely overlapped. The slight differences of ST-CFP and ST-YFP fluorescence signals may have resulted from the use of sequential time-lapse imaging, which has a delay between the capture of CFP and YFP images. During this delay, the Golgi stacks could have shifted slightly. Importantly, the differences between ST-CFP and ST-YFP signals were always smaller than the differences observed with other marker pairs.

Confirming previous findings from confocal microscopy, we observed with wide-field epifluorescence that ST-CFP fluorescence did not completely overlap with ManI-YFP or XT-

YFP fluorescence, indicating that the fusion proteins are localized to different compartments (Boevink et al., 1998; Nebenführ et al., 1999; Pagny et al., 2003; Saint-Jore-Dupas et al., 2006). Similar results have been obtained previously with combinations of other Golgi markers in tobacco leaf epidermal cells (Saint-Jore-Dupas et al., 2006; Latijnhouwers et al., 2007; Schoberer et al., 2010). Thus, it is possible to distinguish different sub-compartments of the Golgi based on the slight separation of signal distributions of two fluorophores with wide-field-epifluorescence microscopy, even though the small size of Golgi stacks (cisternal diameter ~800 nm, stack thickness ~300 nm) is just slightly over the theoretical resolution limit of visible light microscopy (200-350 nm). The different localization of the two markers was most easily seen when observing side-views of Golgi stacks. We cannot determine whether or not the markers label a single cisterna or several; however, previous immunogold labeling suggests that the markers probably label two or more cisternae (Boevink et al., 1998; Nebenführ et al., 1999; Pagny et al., 2003). Interestingly, ManI-YFP often formed smaller fluorescent spots than the other markers, which is consistent with the observations of a smaller diameter of *cis* cisternae in EM images (Staehelin and Kang, 2008). In summary, the employed markers localize to different sub-compartments of the Golgi, thus allowing us to observe the fate of these different cisternae in living cells.

Monensin preferentially affects the trans cisternae

Using electron microscopy, monensin has been shown to lead to swelling of the *trans*-Golgi network, followed by similar effects on the *trans* cisternae and eventually also on the medial and *cis* cisternae (Zhang et al., 1993). This effect has been interpreted as resulting from an exchange of K^+ ions and protons across the Golgi membranes, hence the stronger effect in the more acidic late Golgi compartments (Zhang et al., 1993; Satiat-Jeunemaitre et al., 1994). We could confirm these findings by using live-cell imaging to compare the rate of swelling between

ST-CFP-labeled cisternae and either ManI-YFP or XT-YFP-labeled cisternae. In both cases, the *trans* cisternae swelled to a greater extent compared to the medial and *cis* cisternae. Frequently, we observed *trans* cisternae from different stacks come in close proximity to each other while the other end of the stacks were pointed away from the cluster. This has not been described before, possibly because such larger-scale rearrangements are difficult to discern in EM thin sections. Alternatively, it is also possible that the clustering effect does not occur in sycamore cells (Zhang et al., 1993; Satiat-Jeunemaitre et al., 1994) but is specific for BY-2 cells. We also occasionally observed an increase in fluorescence intensity that coincided with the cisternal swelling. When observed, the increase in fluorescence intensity was usually greater for the ST-CFP marker (data not shown). This is consistent with the predicted alkalinization effect of monensin on the lumen of Golgi cisternae (Pressman and Fahim, 1982), since fluorescent proteins have reduced fluorescence efficiency at low pH (Tamura et al., 2003).

Golgi stacks move as intact units with various orientations

We used simultaneous imaging of CFP and YFP fluorescence to investigate the orientation and integrity of Golgi stacks while they were moving through the cell. Because of this unique approach, we were able to directly determine the location of each marker at any given moment in order to calculate the distance between *cis* and *trans* cisternae. We did not observe any Golgi stacks with a distance larger than 0.8 μm between the centers of ST-CFP and ManI-YFP signals, even when stacks were moving with speeds of up to 3 μm/s. This suggests that Golgi stacks remain intact while traveling through the cytoplasm. While this has been expected based on the scarcity of stack fragments in electron micrographs, this has not been documented before experimentally.

The observed separation of *cis* and *trans* markers during movements could, in principle, result from two different effects. On the one hand, Golgi cisternae may have shifted relative to

each other, as in a slanted stack of books, such that the front-most cisterna is traveling ahead of the trailing cisterna. For the vast majority of the observed Golgi stacks, this would imply that the *trans* cisternae would be displaced relative to the *cis* cisternae by less than one half of their diameter. Such 'sheared' Golgi stacks are sometimes visible in EM images, although the separation of *cis* and *trans* cisternae may not be as large as the maximum described here (Nebenführ, unpublished observations). On the other hand, Golgi stacks might move perpendicular to the plane of the cisternae. In this case, the separation of the signals would simply represent the distance between *cis* and *trans* cisternae within a stack. Previously, it was suggested that Golgi stack movements preferentially occurred in the plane of the cisternae (Nebenführ et al., 1999), which would rule out the second option. Our images, unfortunately, do not allow us to distinguish between these possibilities, since the relatively long exposure time needed to collect sufficient signal from both fluorophores (500 ms) results in a slight stretching of the shape of the fluorescent spots in the direction of movement. Alternative imaging approaches with higher temporal and spatial resolution will be necessary to resolve this issue.

Previous findings indicated that Golgi stack movements rely on the acto-myosin network (Boevink et al., 1998; Nebenführ et al., 1999). Recently, T-DNA knockout mutants for various class XI myosin isoforms in *Arabidopsis thaliana* supported the involvement of myosin motors, since several single, double, triple, and quadruple mutants showed reduced Golgi stack motility (Peremyslov et al., 2008; Prokhnevsky et al., 2008; Peremyslov et al., 2010). Similarly, overexpression of dominant-negative myosin tail fragments slowed down Golgi stack movements in tobacco and *Arabidopsis* leaf epidermal cells (Avisar et al., 2008; Sparkes et al., 2008; Avisar et al., 2009; Avisar et al., 2012). These results do not establish whether Golgi stacks are moved directly by myosin motors attached to their surface or whether their movement depends on association with another motile organelle such as the ER. Such an association was

proposed when it became evident that Golgi stacks remain in close association with ER export sites (ERES) that were labeled with components of the COPII machinery. More recently, a physical connection between Golgi stacks and ER membranes was supported with results from laser trap experiments (Sparkes et al., 2009). On the other hand, direct binding of myosins to the plant Golgi has been suggested by labeling of stacks with fragments of a myosin organelle-binding domain (Li and Nebenführ, 2007).

The observation that either end of a Golgi stack can move ahead of the other may provide insights into this question of direct versus indirect Golgi propulsion. In particular, it can be expected that the part of the Golgi where a force is applied should move ahead while the other end of the Golgi will be dragged behind. The fact that we have observed both kinds of Golgi stack movements, *cis* side leading or *trans* side leading, is difficult to reconcile with the ERES attachment model that presumably should result in a more uniform orientation, with the *cis* cisternae leading. Direct attachment of the myosin motors to all sides of the Golgi, on the other hand, could explain the observations presented here. In many cases, a moving Golgi stack kept alternating between having the *trans* and *cis* cisternae lead. These alternating polarities could be explained by a continuous change in orientation as a Golgi stack 'rolls' along the actin filament with the aid of multiple motor proteins bound all over its surface. It is also conceivable that the seemingly continuous movements observed by us in 1-second intervals actually consisted of a series of short runs interrupted by release of the actin filament from the Golgi myosin and rebinding on a different surface of the stack. Overall, we did observe a slight bias for the *cis* end of the Golgi stack to lead during movements. This may suggest that the *cis* side of Golgi stacks carries a higher density of myosin motor proteins or that the myosin motors on that half of the Golgi are more active. Further research will be needed to test this hypothesis; in particular, identification of Golgi myosins and their distribution on the Golgi surface will be crucial.

Golgi stack disassembly can occur in either the trans-to-cis or cis-to-trans direction

Previous studies have shown that brefeldin A (BFA) treatment results in the redistribution of Golgi enzymes to the endoplasmic reticulum (ER; Boevink et al., 1998; Ritzenthaler et al., 2002; Saint-Jore et al., 2002; Schoberer et al., 2010). Normal retrograde transport from the Golgi back to the ER requires COPI-coated vesicles (Letourneur et al., 1994). COPI coat proteins are no longer recruited to Golgi stack membranes when plant cells are treated with BFA (Ritzenthaler et al., 2002), consistent with a BFA-induced block of ARF activation by Sec7-type ARF-GEFs (Donaldson et al., 1992). It has been proposed that the resulting redistribution of Golgi proteins to the ER during BFA treatment is a result of Golgi and ER membrane fusion in the absence of vesicle formation (Elazar et al., 1994; Nebenführ et al., 2002). An alternative model postulates that BFA unmasks a COPI-independent retrograde transport pathway of Golgi enzymes into the ER (Schoberer et al., 2010). Furthermore, two independent studies concluded that Golgi enzyme redistribution into the ER occurs sequentially in a *trans*-to-*cis* direction (Ritzenthaler et al., 2002; Schoberer et al., 2010).

To further identify the events and possible mechanisms of BFA-induced Golgi stack disassembly, we performed detailed time-lapse imaging of cells co-expressing ST-CFP and ManI-YFP, ST-CFP and XT-YFP, or ST-CFP and ST-YFP during the first 20 minutes of BFA treatment. The short interval between individual time-lapse images (5 s) allowed us to precisely determine the time at which the fluorescence signal was lost from a Golgi stack as well as the time it took for the fluorescence intensity to reach background levels (typically 15-20 s). The duration of loss of fluorescence signal from individual Golgi stacks in BFA-treated cells was significantly shorter than expected from the normal half-life of Golgi residents measured in FRAP experiments (2-5 min; Brandizzi et al., 2002; Schoberer et al., 2010). This suggests that loss of a Golgi marker into the ER in response to BFA involves processes that do not normally

operate in an untreated cell (Sciaky et al., 1997). Thus, we interpret the loss of fluorescence signal from a stack as indicating a BFA-induced fusion of the labeled cisternae with the ER (Ritzenthaler et al., 2002).

In almost all of the cases in which ST-CFP and ST-YFP were co-expressed, both markers were lost simultaneously. This result supports the idea that proteins localized to the same cisternae will redistribute to the ER simultaneously following treatment with BFA. On the other hand, when either *cis* and *trans* or medial and *trans* markers are co-expressed, about half of the stacks observed lost their fluorescence signals sequentially. This is consistent with the sequential fusion of cisternae with the ER that has been described by Ritzenthaler et al. (2002) based on EM images. It should be noted that the large number of Golgi stacks that lost both fluorescent signals at the same time would not have been detected in the previous study.

Our finding of a random order of fusion for *cis* and *trans* cisternae, on the other hand, contradicts conclusions that BFA-induced Golgi stack disassembly always occurs in the *trans*-to-*cis* direction (Ritzenthaler et al., 2002; Schoberer et al., 2010). Apparently, the interpretation of the EM images as representing *cis* cisternae (Ritzenthaler et al., 2002) was incorrect, and we now assume that about half of the Golgi stack remnants in our earlier study actually represent the *trans* half. It is unclear why the recent study by Schoberer et al. (2010) did not observe the same random distribution of ER-Golgi fusions as described here. In that case, both Golgi membrane proteins and Golgi matrix markers residing in the *trans* half of the stacks were found to be preferentially lost during BFA treatments of tobacco leaf epidermis cells (Schoberer et al., 2010). It is possible that this reflects tissue-specific differences between suspension-cultured BY-2 cells, which have been proposed to be derived from root cells (Winicur et al., 1998), and leaf epidermis cells (Robinson et al., 2008).

Our results indicate that, following BFA treatment, fusion between ER and Golgi membranes can occur anywhere on the Golgi stack. We postulate that the order of cisternal fusion with the ER is determined by the relative proximity of the different cisternae to the ER, such that the cisterna closest to the ER will be the first to fuse with it. This fusion may then lead to a disruption of normal Golgi organization, which results in additional fusion events with the remaining cisternae. Consistent with this model, we observed that the delay between *trans* and medial fusion events tended to be shorter than the delay between *trans* and *cis* fusions.

Drug treatments as useful tools for protein localization within the Golgi

Identification of the precise sub-Golgi localization of a given protein is of great interest, since cargo molecules traverse the cisternae in a predictable *cis*-to-*trans* direction and therefore encounter Golgi-resident enzymes in a particular order. This is already well established for enzymes involved in the modification of N-linked oligosaccharides that are arranged in an assembly-line fashion according to the order in which they operate on their substrates (reviewed in Schoberer and Strasser, 2011). Enzymes involved in the synthesis of cell wall polysaccharides presumably also follow a similar arrangement (Zhang and Staehelin, 1992); however, very little is currently known about their distribution in Golgi stacks (Chevalier et al., 2010).

The most commonly used technique for determining the localization of proteins within the Golgi is using immunogold labeling and electron microscopy (e.g. Saint-Jore-Dupas et al., 2006; Chevalier et al., 2010). While providing the most definitive evidence for cisternal localization, this method is technically challenging and requires suitable antibodies that recognize their epitope in fixed and embedded material. The results presented here, on the other hand, suggest that a relatively simple approach based on three fluorescently labeled markers and two drug treatments can give a good indication as to which section of a Golgi stack (*cis*, medial, or *trans*) the protein resides in. For example, the protein of interest fused to CFP could be co-

expressed in tobacco BY-2 cells with ManI-YFP, XT-YFP, or ST-YFP. Researchers can then compare the localization of their protein to these three standard markers as well as perform BFA and monensin experiments to further confirm the location of the protein within the Golgi. An even simpler 'first-look' experiment might involve only co-expression with a medial marker such as XT-YFP followed by BFA and monensin treatments. Simultaneous loss of CFP and YFP signals in BFA would be interpreted as medial localization of the protein of interest. Sequential loss of signals would suggest *cis* or *trans* localization, which would be easily resolved with monensin treatment. Thus, our observations suggest a simple procedure for the identification of the localization of unknown membrane proteins to specific Golgi sub-compartments.

Conclusions

Golgi stacks display a remarkable stability during rapid intracellular movements, which is probably due to the action of matrix proteins that anchor the cisternae to each other. Although Golgi stacks display a clear *cis*-to-*trans* polarity that is reflected in both cisternal morphology and protein composition, there is little to no difference between cisternae when it comes to myosin-driven movements or BFA responses. The specialization of different cisternae, on the other hand, is detectable by monensin treatment, which presumably is reflective of the higher luminal acidity in *trans* cisternae. We speculate that myosin motor proteins are binding all over the surface of Golgi stacks, which allows them to move in any direction and even change orientation during movements along actin filaments. Finally, we demonstrate that a combination of Golgi markers with known localization and drug treatments is sufficient to predict the sub-Golgi localization of unknown membrane proteins by fluorescence microscopy.

A.5: References for Appendix

Avisar D, Abu-Abied M, Belausov E, Sadot E (2012) Myosin XIK is a major player in cytoplasm dynamics and is regulated by two amino acids in its tail. Journal of experimental botany **63:** 241-249

Avisar D, Abu-Abied M, Belausov E, Sadot E, Hawes C, Sparkes IA (2009) A comparative study of the involvement of 17 Arabidopsis myosin family members on the motility of Golgi and other organellles. Plant Physiology **150:** 700-709

Avisar D, Prokhnevsky AI, Makarova KS, Koonin EV, Dolja VV (2008) Myosin XI-K Is required for rapid trafficking of Golgi stacks, peroxisomes, and mitochondria in leaf cells of Nicotiana benthamiana. Plant Physiol **146:** 1098-1108

Boevink P, Oparka K, Sant Cruz S, Martin B, Betteridge A, Hawes C (1998) Stacks on tracks: the plant Golgi apparatus traffics on an actin/ER network. Plant Journal **15:** 441-447

Boss WF, Morre DJ, Mollenhauer HH (1984) Monensin-induced swelling of Golgi apparatus cisternae mediated by a proton gradient. Eur J Cell Biol **34:** 1-8

Brandizzi F, Snapp E, Roberts A, Lippincott-Schwartz J, Hawes C (2002) Membrane protein transport between the ER and Golgi in tobacco leaves is energy dependent but cytoskeleton independent: Evidence from selective photobleaching. Plant Cell **14:** 1293-1309

Chevalier L, Bernard S, Ramdani Y, Lamour R, Bardor M, Lerouge P, Follet-Gueye M-L, Driouich A (2010) Subcompartment localization of the side chain xyloglucan-synthesizing enzymes within Golgi stacks of tobacco suspsension-cultured cells. Plant Journal **64:** 977-989

de Graffenried CL, Bertozzi CR (2004) The roles of enzyme localisation and complex formation in glycan assembly within the Golgi apparatus. Curr Opin Cell Biol **16:** 356-363

Donaldson JG, Finazzi D, Klausner RD (1992) Brefeldin A inhibits Golgi-membrane catalysed exchange of guanine nucleotide onto ARF protein. Nature **360:** 350-352

Driouich A, Faye L, Staehelin LA (1993) The plant Golgi apparatus: a factory for complex polysaccharides and glycoproteins. Trends in Biochemical Sciences **18:** 210-214

Elazar Z, Orci L, Ostermann J, Amherdt M, Tanigawa G, Rothman JE (1994) ADP-ribosylation factor and coatomer couple fusion to vesicle budding. Journal of Cell Biology **124:** 415-424

Jiang L, Rogers JC (1999) Sorting of membrane proteins to vacuoles in plants. Plant Science **146:** 55-67

Latijnhouwers M, Gillespie T, Boevink P, Kriechbaumer V, Hawes C, Carvalho CM (2007) Localization and domain characterization of Arabidopsis golgin candidates. J Exp Bot **58:** 4373-4386

Latijnhouwers M, Hawes C, Carvalho C (2005) Holding it all together? Candidate proteins for the plant Golgi matrix. Curr Opin Plant Biol **8:** 632-639

Lee MH, Min MK, Lee YJ, Jin JB, Shin DH, Kim DH, Lee KH, Hwang I (2002) ADP-ribosylation factor 1 of Arabidopsis plays a critical role in intracellular trafficking and maintenance of endoplasmic reticulum morphology in Arabidopsis. Plant Physiol **129:** 1507-1520

Letourneur F, Gaynor EC, Hennecke S, Demolliere C, Duden R, Emr SD, Riezman H, Cosson P (1994) Coatomer is essential for retrieval of dilysine-tagged proteins to the endoplasmic reticulum. Cell **79:** 1199-1207.

Li J-F, Nebenführ A (2007) Organelle targeting of myosin XI is mediated independently by two globular tail subdomains. Journal of Biological Chemistry **282:** 20593-20602

Matheson LA, Hanton SL, Rossi M, Latijnhouwers M, Stefano G, Renna L, Brandizzi F (2007) Multiple roles of ADP-ribosylation factor 1 in plant cells include spatially regulated recruitment of coatomer and elements of the Golgi matrix. Plant Physiol **143:** 1615-1627

Nagata T, Nemoto Y, Hasezawa S (1982) Tobacco BY-2 cell line as the "HeLa" cell in the cell biology of higher plants. International Review of Cytology **132:** 1-30

Nebenführ A (2003) Intra-Golgi transport: escalator or bucket brigade? *In* DG Robinson, ed, The Golgi apparatus and the plant secretory pathway. Blackwell, Oxford, pp 76-89

Nebenführ A, Gallagher L, Dunahay TG, Frohlick JA, Masurkiewicz AM, Meehl JB, Staehelin LA (1999) Stop-and-go movements of plant Golgi stacks are mediated by the acto-myosin system. Plant Physiology **121:** 1127-1141

Nebenführ A, Ritzenthaler C, Robinson DG (2002) Brefeldin A: Deciphering an enigmatic inhibitor of secretion. Plant Physiology **130:** 1102-1108

Nebenführ A, Staehelin LA (2001) Mobile factories: Golgi dynamics in plant cells. Trends in Plant Science **6:** 160-167

Nelson BK, Cai X, Nebenführ A (2007) A multi-color set of *in vivo* organelle markers for colocalization studies in *Arabidopsis* and other plants. Plant Journal **51:** 1126-1136

Osterrieder A, Hummel E, Carvalho CM, Hawes C (2010) Golgi membrane dynamics after induction of a dominant-negative mutant Sar1 GTPase in tobacco. J Exp Bot **61:** 405-422

Pagny S, Bouissonnie F, Sarkar M, Follet-Gueye ML, Driouich A, Schachter H, Faye L, Gomord V (2003) Structural requirements for Arabidopsis beta1,2-xylosyltransferase activity and targeting to the Golgi. Plant J **33:** 189-203

Peremyslov VV, Prokhnevsky AI, Avisar D, Dolja VV (2008) Two class XI myosins function in organelle trafficking and root hair development in *Arabidopsis thaliana*. Plant Physiology **146:** 1109-1116

Peremyslov VV, Prokhnevsky AI, Dolja VV (2010) Class XI myosins are required for development, cell expansion, and F-Actin organization in *Arabidopsis*. Plant Cell **22:** 1883-1897

Polishchuk RS, Mironov AA (2004) Structural aspects of Golgi function. Cell Mol Life Sci **61:** 146-158

Pressman BC, Fahim M (1982) Pharmacology and toxicology of the monovalent carboxylic ionophores. Annu Rev Pharmacol Toxicol **22:** 465-490

Prokhnevsky AI, Peremyslov VV, Dolja VV (2008) Overlapping functions of the four class XI myosins in *Arabidopsis* growth, root hair elongation, and organelle motility. Proceedings of the National Academy of Sciences of the United States of America **105:** 19744-19749

Renna L, Hanton SL, Stefano G, Bortolotti L, Misra V, Brandizzi F (2005) Identification and characterization of AtCASP, a plant transmembrane Golgi matrix protein. Plant Mol Biol **58:** 109-122

Ritzenthaler C, Nebenführ A, Movafeghi A, Stussi-Garaud C, Behnia L, Pimpl P, Staehelin LA, Robinson DG (2002) Reevaluation of the effects of brefeldin A on plant cells using tobacco bright yellow 2 cells expressing Golgi-targeted green fluorescent protein and COPI antisera. Plant Cell **14:** 237-261.

Robinson DG, Langhans M, Saint-Jore-Dupas C, Hawes C (2008) BFA effects are tissue and not just plant specific. Trends in Plant Science **13:** 405-408

Runions J, Brach T, Kuhner S, Hawes C (2006) Photoactivation of GFP reveals protein dynamics within the endoplasmic reticulum membrane. J Exp Bot **57:** 43-50

Sabalzarini IF, Koumoutsakos P (2005) Feature point tracking and trajectory analysis for video imaging in cell biology. Journal of Structural Biology **151:** 182-195

Saint-Jore CM, Evins J, Batoko H, Brandizzi F, Moore I, Hawes C (2002) Redistribution of membrane proteins between the Golgi apparatus and endoplasmic reticulum in plants is reversible and not dependent on cytoskeletal networks. Plant Journal **29:** 661-678

Saint-Jore-Dupas C, Nebenführ A, Boulaflous A, Follet-Gueye M-L, Plasson C, Hawes C, Driouich A, Faye L, Gomord V (2006) Plant N-glycan processing enzymes employ different targeting mechanisms for their spatial arrangement along the secretory pathway. Plant Cell **18:** 3182-3200

Satiat-Jeunemaitre B, Fitchette-Lainé A-C, Alabouvette J, Marty-Mazars D, Hawes C, Faye L, Marty F (1994) Differential effects of monensin on the plant secretory pathway. Journal of Experimental Botany **45:** 685-698

Schoberer J, Runions J, Steinkellner H, Strasser R, Hawes C, Osterrieder A (2010) Sequential depletion and acquisition of proteins during Golgi stack disassembly and reformation. Traffic **11:** 1429-1444

Schoberer J, Strasser R (2011) Sub-compartmental organization of Golgi-resident N-glycan processing enzymes in plants. Mol Plant **4:** 220-228

Sciaky N, Presley J, Smith C, Zaal KJM, Cole N, Moreira JE, Terasaki M, Siggia E, Lippincott-Schwartz J (1997) Golgi tubule traffic and the effects of brefeldin A visualized in living cells. Journal of Cell Biology **139:** 1137-1155

Sparkes IA, Ketelaar T, de Ruijter NCA, Hawes C (2009) Grab a Golgi: Laser trapping of Golgi bodies reveals *in vivo* interactions with the endoplasmic reticulum. Traffic **10:** 567-571

Sparkes IA, Teanby NA, Hawes C (2008) Truncated myosin XI tail fusions inhibit peroxisome, Golgi, and mitochondrial movement in tobacco leaf epidermal cells: a genetic tool for the next generation. Journal of Experimental Botany **59:** 2499-2512

Staehelin LA, Kang BH (2008) Nanoscale architecture of endoplasmic reticulum export sites and of Golgi membranes as determined by electron tomography. Plant Physiol **147:** 1454-1468

Staehelin LA, Moore I (1995) The plant Golgi apparatus: Structure, functional organization and trafficking mechanisms. Annual Review of Plant Physiology and Plant Molecular Biology **46:** 261-288

Tamura K, Shimada T, Ono E, Tanaka Y, Nagatani A, Higashi S-i, Watanabe M, Nishimura M, Hara-Nishimura I (2003) Why green fluorescent fusion proteins have not been observed in the vacuoles of higher plants. Plant Journal **35:** 545-555

Ueda H, Yokota E, Kutsuna N, Shimada T, Tamura K, Shimmen T, Hasezawa S, Dolja VV, Hara-Nishimura I (2010) Myosin-dependent endoplasmic reticulum motility and F-actin organization in plant cells. Proceedings of the National Academy of Sciences of the United States of America **107:** 6894-6899

Winicur ZM, Zhang GF, Staehelin LA (1998) Auxin deprivation induces synchronous Golgi differentiation in suspension-cultured tobacco BY-2 cells. Plant Physiology **117:** 501-513

Zhang GF, Driouich A, Staehelin LA (1993) Effect of monensin on plant Golgi: re-examination of the monensin-induced swelling in cisternal architecture and functional

activities of the Golgi apparatus of sycamore suspension-cultured cells. Journal of Cell Science **104:** 819-831

Zhang GF, Staehelin LA (1992) Functional compartmentation of the Golgi apparatus of plant cells. Immunocytochemical analysis of high-pressure frozen- and freeze-substituted sycamore maple suspension culture cells. Plant Physiology **99:** 1070-1083

Vita

Stephanie Lin Madison was born in West Chester, Pennsylvania on July 2, 1985. She received her B.S. degree in Biology from Lock Haven University of Pennsylvania in May 2007. She moved to Knoxville and started her Ph.D. program in the department of Biochemistry and Cellular and Molecular Biology at the University of Tennessee in August 2007. She joined Dr. Andreas Nebenführ's lab in May 2008. Stephanie officially received her Ph.D. in July 2014.